The Investigation and Implementation of Electrical Impedance Tomography Hardware System

Jieqiu Yang

Thesis submitted to De Montfort University

for the Degree of Doctor of Philosophy

May 2006

ABSTRACT

Electrical impedance tomography (EIT) is a medical imaging technology that provides a tomographic representation of the distribution of electrical impedance within the body. As the electrical impedance varies for different body tissues, it is possible to characterize tissues from the images and to detect physiological events.

EIT systems have been developed from applying a single signal frequency to a range of frequencies. Imaging at multiple frequencies significantly improves the ability to characterize and differentiate heterogeneity within the region of interest. Applications of EIT are limited by its poor resolution as a consequence of limited number of electrodes and lack of independently published measurements.

In a practical EIT system design the parallel structure is normally adopted as it provides a real time monitoring structure. However, there is a difficulty in expanding to a 2-dimensitional or 3-dimensitional high resolution imaging system, as the number of electrodes increase.

In this thesis, a serial structure spectrum EIT system has been investigated and developed. Modelling of the electrical circuit has shown that the system bandwidth is degraded primarily by the signal transmission in the coaxial cable and multiplexer. To remove the capacitive effect of these components, a distribute system concept has been developed. The concept uses active electrodes in which a current source and a front end amplifier are embedded in the electrode which makes direct contact with the tissue being measured.

The active electrode is based on the Howland current source. The required high output impedance of Howland current source can be realised by matching the two resistor arms. However, from the electrical equivalent circuit analysis the actual output impedance of this circuit was found to be degraded by the op-amp's limited open loop gain, especially at higher frequencies. To solve the problem, the author describes in detail a novel method of compensating for the above effects. Subsequent circuit tests showed significant improvement after the compensation. Further, to improve the small signal noise ratio a programmable gain amplifier to adapt the frame data measurement was developed. These developments have led to the feasibility of active electrodes. The thesis

describes in detail the development, of the MK2 EIT system which is presented as the output of this research.

ACKNOWLEDGEMENTS

I would like to take this opportunity to acknowledge everyone for the assistance given to me throughout my period at De Montfort University.

First of all, I would like to thank my first supervisor Dr Wei Wang for giving me this opportunity to study in De Montfort University, and the discussion and suggestion during this period.

I would like to thank my second supervisor Prof. Malcolm McCormick for his patient in my English and his invaluable contribution to the manuscript.

I am very grateful to Mr Dilip Chauhan, Dr Brian Bramer and the members in my group for the help provided during my studies.

Special thanks to my wife Huiyan for her constituent support and encouragement and my daughter Shan for her happiness given to me.

DECLARATION

The work presented within this thesis is the exclusive work of the author, Jieqiu Yang, except where otherwise acknowledged. Furthermore, the work presented has not been published or otherwise distributed by any person other than the author.

Jieqiu Yang

May 2006

CONTENTS

LIST OF FIGURES

LIST OF TABLES

Introduction

This thesis is a part of research project of the EIT/EIM group of De Montfort University. The main research interest is applying EIT technology into early stage breast cancer diagnosis.

1. Breast cancer

Each year more than 41,700 women in the UK are diagnosed with breast cancer, and it causes more than 12,400 deaths. Worldwide, more than a million women are diagnosed with breast cancer every year, accounting for a tenth of all new cancers and 23% of all female cancer cases [1].

The breast is a gland designed to make milk. The lobules in the breast make the milk, which then drains through the ducts to the nipple. Like all parts of the human body, the cells in the breasts usually grow and then rest in cycles. The periods of growth and rest in each cell are controlled by genes in the cell's nucleus. When the genes are in normal working order, they keep cell growth under control. However, when the genes develop an abnormality, they sometimes lose their ability to control the cycle of cell growth and rest. This uncontrolled growth of breast cells is breast cancer [2].

Early diagnosis of breast cancer is vital to save patient life. At this stage, the uncontrolled growth of cells hasn't started to break through normal tissue, which means it is not life-threatening. Finding breast cancers early has also meant that many more women being treated for breast cancer are able to keep their breasts. When caught early, localized cancers can be removed without resorting to breast removal.

2. Medical imaging technologies

Mammograms are probably the most popular diagnosis method of breast cancer disease. It is a photograph system showing the absorption rate of different tissue to penetration X-ray. Mammograms in the breast screening can detect breast cancer at a very early stage. However, the X-ray is a radiation source even though only a very low dose required, so that it has to be controlled and regulated carefully. The mammogram

taking need to compress the breast carefully and most women find it uncomfortable and a few find it painful. The absorption rates of different breast tissue are the crucial parameters to distinguish them and identify the abnormal tissue. The poor sensitivity causing false negative or false positive diagnosis is its main technical drawback [3].

X-ray scanner can provide a high resolution computed axial tomographic image. During the imaging process, the X-ray slice data is generated using an X-ray source that rotates around the human body with X-ray detectors positioned on the opposite side of the circle from the x-ray source. The collected data set is then sent to a powerful computer to reconstruct and display an anatomy image of this scanned slice. Pixels in an image obtained by CT scanning are displayed in terms of relative radiodensity. CT is regarded as a moderate to high radiation diagnostic technique.

Magnetic Resonance Imaging (MRI) is a new powerful diagnostic technique, which uses magnetic fields, not radiation to create images of human body. When taking the image, the patient has to be placed into a strong magnetic field which is created by permanent magnet or super conductor coil. The magnetic field aligns the protons of hydrogen atoms in the human tissue, which are then exposed to a beam of radio waves. This spins the various protons of the body, and they produce a faint signal that is detected by the receiver portion of the MRI scanner. And using these collected data, the computer then reconstructs the body image.

Contrast-enhanced MRI has been shown to detect cancer earlier than mammography in high-risk women, but it also increases the rate of false-positive tests and has not been shown to reduce the breast cancer death rate. In addition, MRI screening for breast cancer is at least 10 times more costly than mammography screening [4].

Ultrasonic imaging is similar to radar in that pulses are propagated through the body, causing reflected waves to occur at various discontinuities throughout the path of the beam. In the doses used for imaging, it appears that ultrasound does not have any harmful effect on body cells. Ultrasound imaging instruments are cheaper than X-ray CT or MRI scanners and are able to image soft tissues which cannot be seen on plain X-ray. For these reasons it is replacing X-rays as an imaging modality in many areas, especially in obstetrics.

Ultrasound imaging is sensitive to certain state of breast cancer. These techniques' value to breast cancer diagnosis is still unproven and need more evaluation [5].

2. EIT/EIM

Differences in electrical impedance properties between normal/benign and malignant tissue were identified in the 1920's [6]. Malignant tissue differs from normal breast tissue in electrical properties because of differences in water and electrolyte content, changes in membrane permeability, orientation and packing density of cells [7]. The potential for these electrical differences to be used in cancer detection was widely recognized and investigated in vitro and in vivo [8].

Application of EIT in breast cancer detection is called electrical impedance mammography (EIM). Electrical impedance measurement reflects the physical changes of breast tissues in terms of capacitance and resistance on special electrical frequency, so that any early physiological change or pathology change of cells will be found. EIM is a non-invasive, no radiation technique, which is more suitable for routine breast cancer screening. The electrical impedance scanning (EIS) system has been developed and preliminary results of a clinical trial showed promise for early detection of breast cancer and identification of young women at increased risk of having the disease at time of screening [9].

The resolution of EIM image is limited by the number of applied electrodes and the signal to noise level of measurement [10]. Cherepenin et al (2001) [11] and other groups including 3D Image Group of De Montfort university has worked on 3-dimentional EIM system implementation [12].

De Montfort group has developed first generation electrical impedance measurement system MK1 for breast tissue electrical property research. This thesis is part of current project aiming to develop MK2 electrical impedance tomography system, which can also be used as EIM research and development platform. The detail research activities of this group will be introduced in Chapter 2 of the thesis.

3 The outline of the thesis

The thesis includes author's research work on the EIT system structure. Chapter 1 introduces the basic concepts about the bio-impedance, the measurement methods, the application on the electrical impedance tomography and the development of EIT

hardware system and reconstruction algorithm. The primary EIT research work at the 3D Imaging Group in De Montfort University is given in Chapter 2, which is the starting point of this research work. Chapter 3, 4 and 5 present the detailed electric circuit analysis. simulation and physical electronics implementation on constant current source, front-end amplifier and programmable gain amplifier, and signal demodulation. These three function blocks are the foundation of the EIT hardware system design. The factors affecting on the measurement bandwidth, accuracy and data acquisition strategy for image reconstruction are discussed in Chapter 6. As always research issue, the electrode material and test tool implementation, such as saline tank and electronic phantom, is described in Chapter 7. As a main output of the thesis, the MK2 EIT system's performance is presented in Chapter 8.The conclusion and future work is given in Chapter 9.

Chapter 1 Review

1.1 Electrical impedance of biological tissue

All biological tissues are made of cells which are membrane-bounded compartments filled with a concentrated solution of chemicals and salts. Groups of cells perform specialized functions and are linked by an intricate communications system. The cell membrane maintains an ion concentration gradient between the intracellular and extra cellular spaces.

Due to the different compositions of biological tissues some can be treated as conductors (e.g. blood, muscle, intracellular and extra cellular fluid etc) and some are insulators (e.g. fat, bone etc). In the case of conductors, the resistivity or its inverse, conductivity is used to represent the tissue's electrical characteristic, while in the case of insulators, the permittivity or dielectric constant, is used. The electrical properties of biological tissues, especially *in vivo*, are still a valid subject of research.

As a conductor, when a voltage E is applied across a biological tissue, a current I will tend to traverse the tissue, the electrical impedance Z_B that is mathematically described by the complex relation between the voltage and current, is shown in Figure 1.1

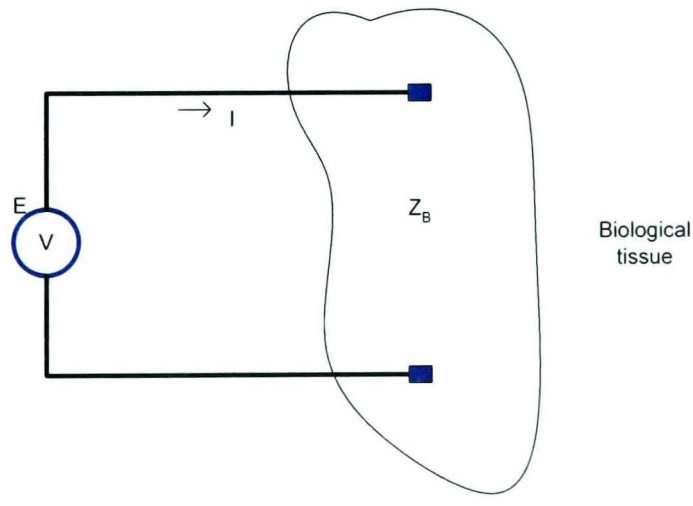

Figure 1.1 Biological tissue impedance measurement

E is applied voltage, I is measured current, then the biological impedance is the ratio of voltage to current [13]. This impedance varies with time, the geometrical shape of the tissue, temperature, its biochemistry and others, like physiological and pathological

changes. In addition, impedance is sensitive to the frequency of applied voltage, so it is also a function of frequency. Mathematically the impedance is a complex number $Z_B=R+jX$.

A basic equivalent electric circuit describing any biological impedance Z_B is shown in Figure 1.2. It is seen that, as frequency increases, the parallel resistance, R_M, loses significance to the point where only the purely resistive path Ra is left. At lower frequencies, the element C_M may be neglected, and once more, the circuit behaves in a purely resistive manner with the value (R_a+R_M). The behaviour of tissue impedance can be illustrated as a function of frequency, or Cole-Cole plot [14].

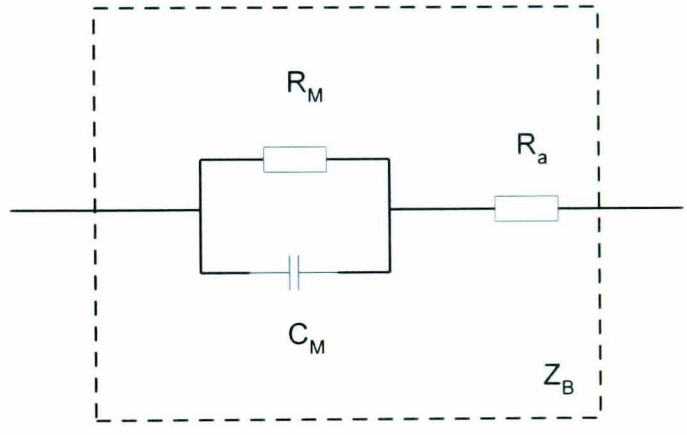

Figure 1.2 The basic 3-element equivalent electric circuit of biological impedance Z_B

In this presentation, the real component R is plotted versus the imaginary component X in the complex plane with the frequency as the variable parameter. The three-element equivalent circuit shown in Figure 1.2 above can be described by the expression

$$Z_B = R_a + \frac{R_M}{1+\omega^2\cdot\tau^2} - j\frac{\omega\tau R_M}{1+\omega^2\cdot\tau^2} \qquad \text{Eq1.1}$$

where ω is the applied frequency and $\tau = R_M \cdot C_M$ is the time constant. The real part R_e and the imaginary part I_m of Z_B are described by the follow relationship:

$$\left(R_e - R_a - \frac{R_M}{2}\right)^2 + I_m^2 = \left(\frac{R_M}{2}\right)^2 \qquad \text{Eq1.2}$$

it describes a circle equation with central point at $(R_a + \frac{R_M}{2}, 0)$ and radius of $\frac{R_M}{2}$. Therefore, the Cole-Cole plot of equivalent circuit is a half circle, as shown in Figure 1.3. This result is derived from the three-element model and obviously, with a complicated

circuit model of biological tissue impedance, the central point of circle is not necessary on the real axis, but is located beneath it.

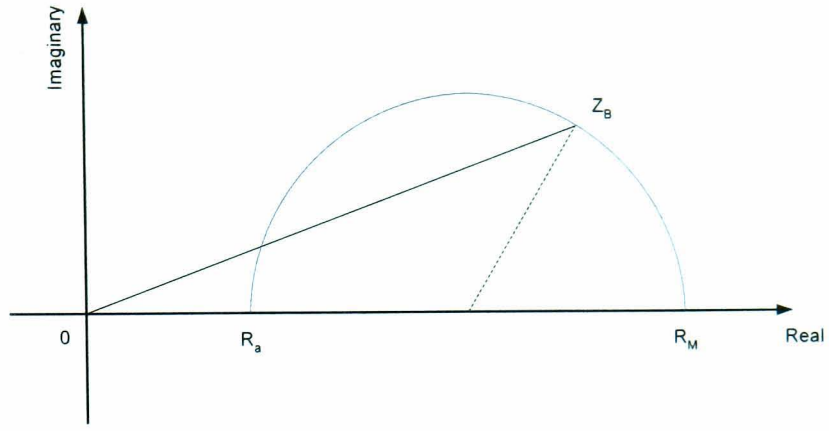

Figure 1.3 The Cole-Cole plot of three-component equivalent circuit of biological tissue

The capacitive behaviour of biological tissue is due to the contribution made by the cell membrane which has a complex structure and dielectric properties [15]. At high frequencies, the electric current traverses easily through the cell membrane, while at low frequencies, the membrane presents a high impedance pathway and most of the current flow through the electrolytic solution.

1.2 Electrical impedance measurement

Many methods are used for electrical impedance measurement, from which the modulus and phase information of biological tissue are obtained to be physiologically or clinically interpreted. In the past, the modulus, because it is easier to obtain, has been popularly used in impedance image reconstruction.

The first circuit used in the biological impedance measurement is classical resistive Wheatstone bridge, which is widely applied in the research laboratories. In this method, the biological tissue forms one of its four branches, operating over a wide frequency range from dc to hundreds MHz. This measurement method can give high accuracy and precision, but relatively slow measurement speed due to the need to balance the bridge, especially at high driving frequency. Therefore, this method is unsuitable for the monitoring purposes.

In physiological practice, the simplest method to measure biological impedance is through the measurement of voltage and current. Two basic configurations are employed:

the two-electrode method and four-electrode method. Here the electrodes are used to apply current or sense voltage.

The two-electrode measurement method uses two electrodes to apply current to the tissue being measured and sense the voltage presented, as shown in Figure 1.4a. The current generated from voltage source (V) is injected into the measured tissue (Z_B) from the electrodes A and B, with a serial connected resistor R. The voltage value V_o can also be read on these two electrodes A and B. The measured information Z_B, therefore, can be calculated from these known electric values as:

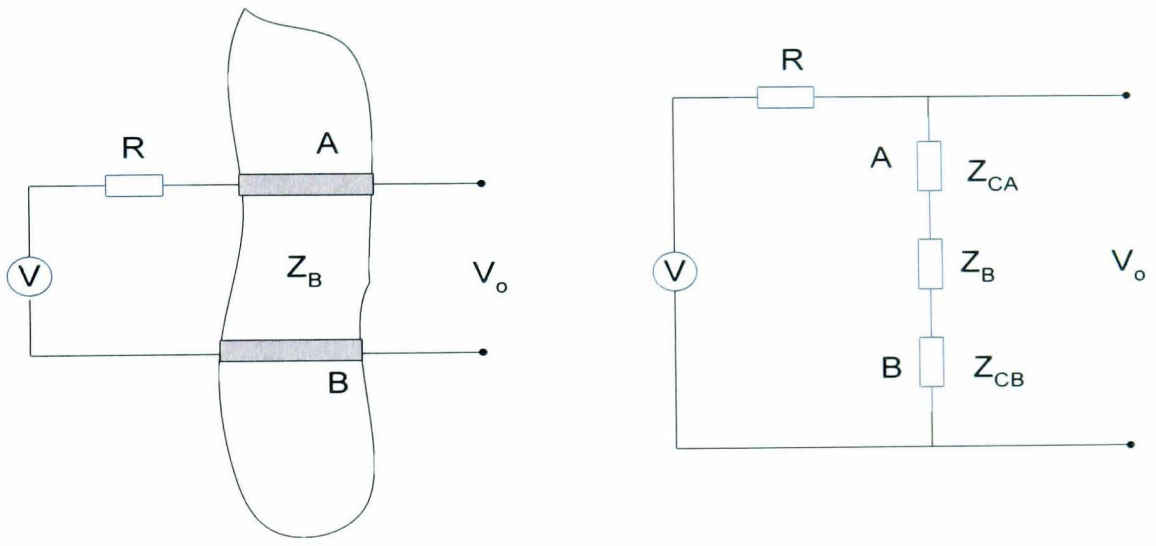

Figure 1.4 Two-electrode impedance measurement

a) The illustration of measurement circuit. b) The illustration of equivalent circuit of measurement with electrode contract impedance Z_{CA} and Z_{CB}

$$Z_B = \frac{V_o \cdot R}{V - V_o} \qquad \text{Eq1.3}$$

Because the read voltage is not proportional to the impedance to be measured, in practice, the serial connected resistor R is adopted with very large value, or it can be seen using current source I to replace the voltage source. Therefore, the read voltage is linearly related to the measured biological impedance, as

$$V_o = I \cdot Z_B \qquad \text{Eq1.4}$$

If the applied voltage or current is an AC signal with frequency under study, the read voltage V_o is modulated with this carrier. The measured biological impedance must be recovered from read voltage after demodulation process.

Two-electrode measurement uses the same electrode pair to apply current and sense voltage. When it is applied to biological impedance measurement, the contact between the electrode and electrolyte will introduce polarization impedance to the total measured impedance as shown in Figure 1.4b. The effect of polarization impedance is also reflected in the voltage reading, and the voltage must be calibrated. In addition, as the current is injected into the tissue, the current field around the electrodes is normally not distributed homogenously. It is dependent on the electrode shape, contact area and tissue's structure.

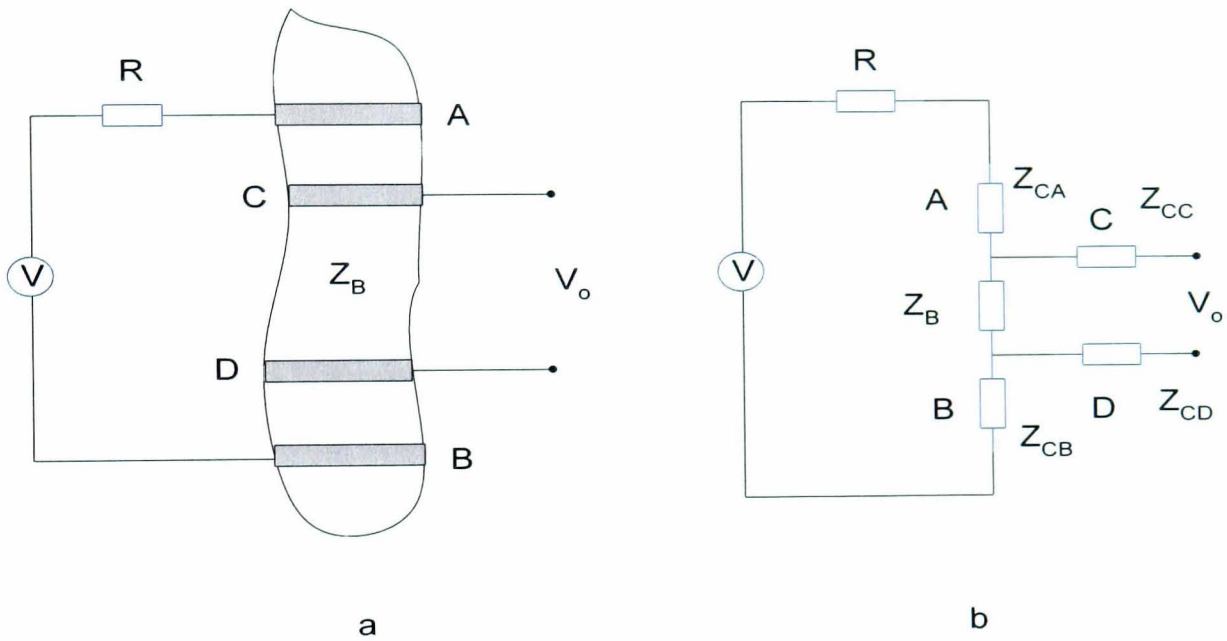

Figure 1.5 The four-electrode impedance measurement

a) The illustration of the measurement circuit. b) The illustration of the measurement equivalent circuit with electrode contact impedance Z_{CA}, Z_{CB} Z_{CC}, and Z_{CD}

Separating the current injecting electrodes and voltage sensing electrodes, results in four-electrode measurement method [13]. As Figure 1.5 shows, the constant current is injected into the biological tissue to be measured on the electrode pair (A and B), and the voltage is read on the electrode pair (C and D). It can be seen that the injected current is independent of the electrode/electrolyte interface impedance, and this condition is best satisfied when the current source output-impedance is large when compared to the sum of the interface and tissue impedance. In addition, if the current electrodes are located further away from the voltage electrodes, the two latter detect a signal in a region with uniform distribution of current lines, thus favouring an output/input linear relationship. In practice, real current field distribution in the tissue to be measurement is limited by both

anatomical shape and physiological conditions. The voltage electrodes still experience the polarization impedance problem but this can be minimized by using high input-impedance measurement amplifier. The shape, material and contact area of electrodes are still a subject under investigation in biological impedance measurement.

In EIT research work, the biological impedance measurement is carried out over a wide frequency bandwidth and the result constitutes impedance spectrometry in the frequency domain. Some research [16] uses the impedance analyzer, which is based on the four-electrode measurement method. In practice, the instrument is often connected to the impedance cell by means of leads, whose stray capacitance is liable to introduce measurement errors [17, 18].

Alternatively, biological impedance spectrometry can be performed in the time domain. Here a Step-response method is applied to measure the relative permittivity of insulating materials over a wide frequency range (0.1Hz to 1MHz) [19]. This method simultaneously applies two voltage steps of equal amplitude but opposite polarity to the impedance to be measured, and uses the Fourier transform to obtain the complex relative permittivity in the frequency domain.

There is still an argument here about the influence of skin effect due to the high frequency current passing through the biological tissue, when the spectrum scanning is used [20]. Skin effect is obvious as high frequency current passing through good conduction material. However, some biological tissues like blood and muscle are good electric conductors, and the others like skin and fat are not good conductors. This situation makes it difficult to distinguish the skin effect on the mixed tissue impedance measurement.

1.3 Impedance frequency characteristics of biological tissues

Knowledge of biological tissue impedance is very important to determining tissue type using measured electric data. If the impedance distribution in a body part can be reckoned by the outside impedance measurements, the pixel obtained in the 2-D plane or 3-D space will represent the local tissue impedance situation, then with which an impedance image is achieved. The impedance characteristic of biological tissue can also provide useful information to identify the normal or abnormal type of tissue in the diagnosis using the impedance method.

Figure 1.6 shows the complex impedance spectrum of tissues calculated from the mean values of data measured on all samples of each type of tissues [21]. It can be seen that some tissues such as transversal muscle and lung tissue can be identified over the low frequency band A (100Hz – 10KHz), using impedance modulus measurement. However, the modulus impedance of longitudinal muscle and lung tissue do not have significantly different impedance in this frequency range, even though a significant difference can be found over the higher frequency range B (10 KHz – 1MHz). This different impedance characteristic is also reflected on the phase angle chart.

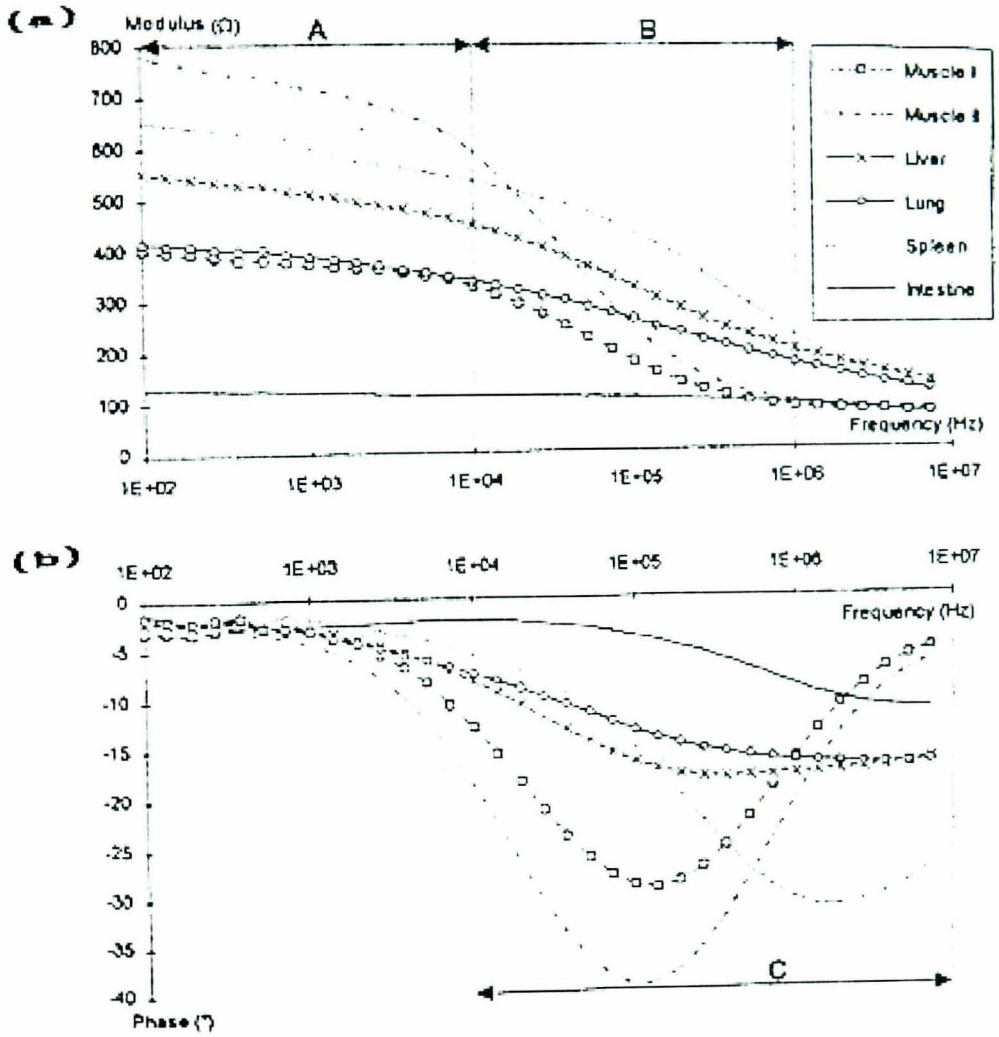

Figure 1.6 The complex impedance spectrum of tissues [9]

It has been shown that it is possible to characterize tissue *in vitro* and to identify them in frequency range that depends on the tissue type. A posterior identification of tissue anisotropy is also possible from the measurement of electrical impedance spectrum [22]. The investigation of tissues impedance performance in the frequency domain has established the feasibility of impedance imaging system development, especially when employs wider frequency range measurements of impedance distribution. However, the

systematic measurement errors are significant in the imaginary component at frequencies above 100 KHz, compared to the measurements made on the real component of impedance [23]. It must be mentioned here, that a distinction should be made between *in vitro* and *in vivo* application, because the electrical properties of living tissues and excised tissues of the same type differ and also because in vivo measurements are subjected to experimental constraints that are particularly difficult to solve [24].

Obviously, the characterization of cancerous tissue is an important field of electrical bio-impedance spectrometry. It is well known that cancerous and normal tissues differ morphologically, and it can be assumed that these differences induce changes in the electrical properties. Since breast cancer is the most frequent form of cancer in women, it arouses great interest in terms of the levels of screening and therapy. The current imaging technique proposed for diagnosis, as x-ray mammography is not sensitive to some kinds of tissues and it is difficult to distinguish the regions of interest. Therefore, using the electrical impedance method it is hoped to identify the difference between cancerous and normal tissues based on the permittivity and conductivity properties.

1.4 EIT reconstruction

Electrical impedance tomography is a technique that produces images of the impedance distribution in a slice through a body by means of non-invasive electrical measurements and a reconstruction algorithm. Since different tissues have different impedances, it is possible to characterize tissues from the images and to detect physiological events.

1.4.1 The principle of image reconstruction

When the current is injected into the imaged object, the current distributes in the whole area and forms a current field that can be described by the Maxwell equation in Eq1.5:

$$\nabla \cdot (C \cdot \nabla V) = 0 \text{ in } \Omega \qquad \text{Eq1.5}$$

where C is the conductivity distribution in domain Ω and V is the potential. With boundary conditions, the conductivity of internal object can be calculated and displayed as an impedance or conductivity image of the slice of the object.

Given the voltage and the current density distributions on the boundary or internally, solving for the conductivity distribution, is termed inverse problem. EIT image reconstruction algorithms are the process for solving the inverse problem. However, because the inverse problem is a nonlinear problem that is ill posed, very often, the solution of the inverse problem involves transforming the nonlinear equation to linear equation, and then obtaining a solution by an iterative process based on the numerical techniques. The process for setting up a linear mathematical model of the imaged object is called as forward problem, and the model is often realized using finite-element method (FEM). FEM can model very complicated material structures of special physical characteristics with support of digital computing technology.

Electrical impedance tomography uses given boundary current density and boundary voltage distribution to reckon the internal conductivity or current or voltage distribution inside the imaged object. The image reconstruction algorithms are mainly divided into two categories: the non-iterative method, represented by the back-projection method, and the iterative method, represented by the Newton-Raphson method.

1.4.2 Back-projection image reconstruction algorithm

The back-projection reconstruction algorithm in EIT is transplanted from the method used for imaging in x-ray computer-aided tomography. It was proposed by Barber and Brown of Sheffield University (UK) [25]. This method is based on the assumption that conductivity does not differ very much from a constant, and the inverse problem is simplified as a linear description.

Sensitivity matrix

If Ω is the domain to be imaged and Γ is the surface of Ω, as shown in Figure 1.7, the electrode pair (A_1, A_2) is noted as A, and the electrode pair (B_1, B_2) is noted as B, then letting V_A be the potential distribution when a unit current is injected into the electrode pair A, the whole domain satisfies the Maxwell equation as shown in Eq1.5. Therefore, at the electrode pair A on the surface of the domain, the potential responses to the injected unit current on the local conductivity:

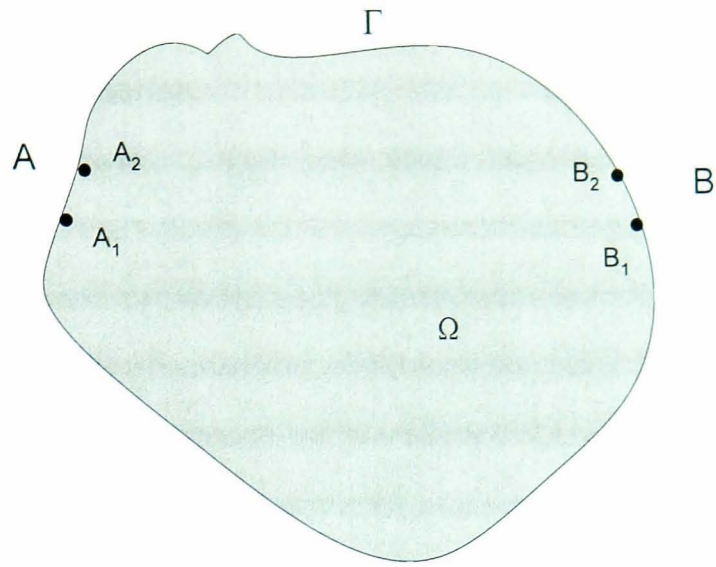

Figure 1.7 The domain to be imaged with two pairs of electrodes A and B on the boundary

$$C\frac{\partial V_A}{\partial n} = \pm 1 \qquad \text{Eq1.6}$$

and outside the domain, the potential and conductivity have no relationship that is:

$$C\frac{\partial V_A}{\partial n} = 0 \qquad \text{Eq1.7}$$

At electrode pair B, the potential also satisfies these equations.

By using the Gauss formula, the sensitivity relationship, V_{AB} potential difference on electrode pair B when a unit current is injected into the electrode pair A, can be represented as

$$V_{AB} = V_A(B_1) - V_A(B_2) = \int_\Omega C\nabla V_A \cdot \nabla V_B d\Omega \qquad \text{Eq1.8}$$

Considering the general conductivity distribution and associated voltage measurement in terms of uniform and perturbed conductivity distributions, such that

$$C = C + \delta C \qquad \text{Eq1.9}$$

$$V_A = V_A + \delta V_A \qquad \text{Eq1.10}$$

$$V_B = V_B + \delta V_B \qquad \text{Eq1.11}$$

Then, the equation Eq 1.8 can be rewritten as:

$$V_{AB} = \int_\Omega (C + \delta C)\cdot\nabla(V_A + \delta V_A)\cdot\nabla(V_B + \delta V_B)\cdot d\Omega \qquad \text{Eq1.12}$$

This equation shows a nonlinear relationship between changes of conductivity and changes of potentials in the domain. If it is assumed that the gradient of changes of

voltage is much smaller than the gradient of voltage in the domain, then equation Eq1.12 can be simplified to a linear equation:

$$\delta V_{AB} = \int_{\Omega} \delta C \cdot \nabla V_A \cdot \nabla V_B \cdot d\Omega \qquad \text{Eq1.13}$$

which is known as the literalized sensitivity relationship [26]. If the domain Ω is split into a number of discrete elements of uniform conductivity, then equation Eq1.13 can be represented as a set of linear equations. In matrix form, this can be written as

$$\delta V = S \cdot \delta C \qquad \text{Eq1.14}$$

where S is called sensitivity matrix. In order to determine δC, it is therefore necessary to solve this linear system.

Back projection

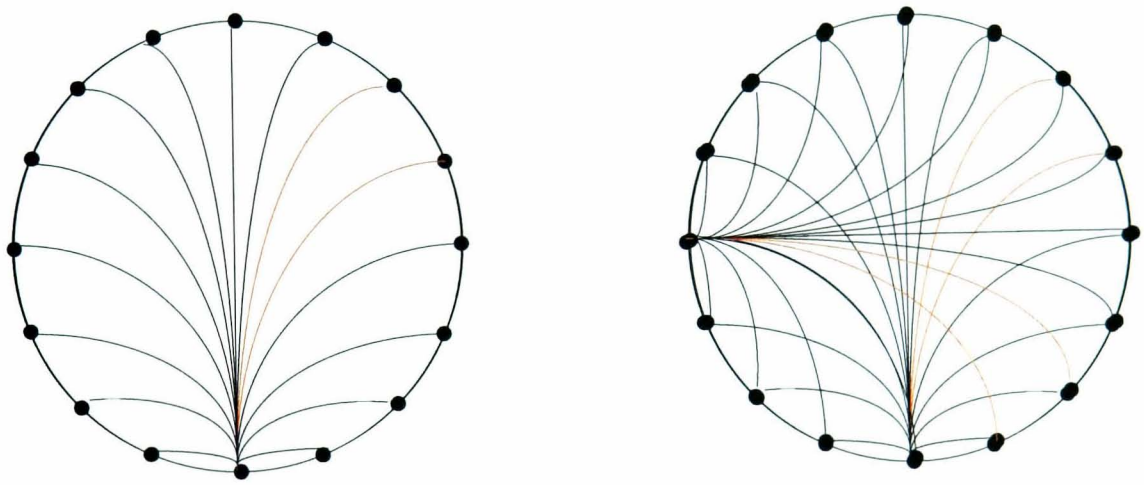

a b

Figure 1.8 The principle of the back projection along equipotential line algorithm

(a) Back projection of this normalized variation in the zone defined by the equipotential

(b) Superposition of two back projections to form the reconstruction image

If the measurement is performed for all the independent injections on the uniform conductivity distribution, $C = C_u$, the equation Eq1.8 becomes:

$$V_{AB} = C_u \cdot \int_{\Omega} \nabla V_A \cdot \nabla_B \cdot d\Omega \qquad \text{Eq1.15}$$

By normalizing the sensitivity relation Eq1.14 with respect to this equation, the Eq1.15 can be written as:

$$\delta V_n = S_n \cdot \delta C_n \qquad \text{Eq1.16}$$

where $\delta V_n = \frac{\delta V_{AB}}{V_{AB}}$, $\delta C = \frac{\delta C}{C_u}$ and $S_n = \frac{S}{\int_\Omega \nabla V_A \cdot \nabla V_B \cdot d\Omega}$.

If the two injection electrodes are sufficiently close, they can be assimilated to a dipole and it is possible to determine the equal potential lines in Ω for all the independent injections for the uniform conductivity C_u, as shown in Figure 1.8a. When the conductivity passes from C_u to $C_u+\delta C$, the variation of the potential difference between two measuring electrodes is due only to the variation of δC in the zone comprised between the two equal potential lines passing through the two measuring electrodes. Therefore, this variation in the potential difference can be back projected in the corresponding zone, and the reconstructed image is obtained by superposing the results of back projection for all the independent injections, as illustrated in Figure 1.8b. In this algorithm, the matrix S is constructed in which the row corresponds to one pixel in the image, and each column to a region between two equal potential lines that can provide a voltage measurement, as Figure 1.9 shown [27].

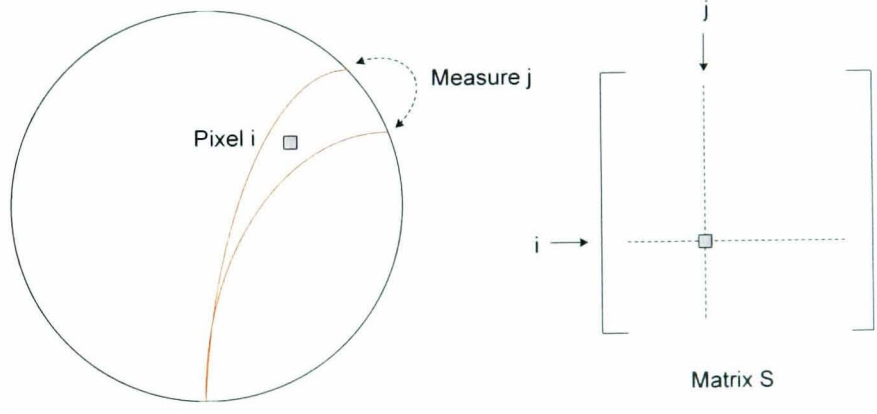

Figure 1.9 The definition of sensitivity matrix S

The back projection algorithm is popular in EIT image system implementation due to the insensitivity to system noise in the measurement. Research has been carried out using filtering methods to solve the distortion and blur problems [28,29]. The reconstructed image shows the relative change of conductivity comparing the uniformed background C_u, which is not easy available in most occasions. With the development of electrical impedance spectrum imaging technologies, the idea is to use different

frequency measurements on the same object to be imaged for EIT image reconstruction. This can eliminate the relay on the uniformed background measurements, with availability of wide bandwidth image frequency measurements [30].

1.4.3 Newton-Raphson algorithm

This algorithm is a numerical approach that iteratively solves the forward problem. The obtained reconstructed image is a static image, which normally involves both longer running time and greater computing complexity.

1.4.3.1 Finite-element modeling for forward problem solving

The imaged object resistivity or conductivity distribution is modelled using finite-element mesh, which is also a basis for transforming the partial differential equation electric field into a linear algebra description. The elements of the two-dimensional problem can be triangular or quadrilateral in shape. Triangular elements are the simplest of the available two-dimensional forms and can be directly used to model both structural and diffusion problems. The simplicity of the triangular element generally demands that a large number be used to accurately approximate a solution; this is particularly true when using the linear basis triangular element.

The finite-element mesh is set up by discretization of a solution domain, which is usually achieved by first subdividing it into one or more relatively large regions called macro domains. Then, each macro domain is subdivided into triangular elements to form a finite-element mesh. A quadrilateral element always contains two triangular elements, as obtained by connecting the nodes from diagonally opposite corners of each quad. The general rule is that triangular elements, which approximate an equilateral shape, are preferred over those that are long and narrow. Figure 1.10 below shows a circular shape 2-dimensional domain finite-element mesh with uniform conductivity distribution and the voltage distribution calculated when an electric current is injected as a boundary condition.

Finite-element methods can be applied to complicated domain contours. Accuracy is dependent on the number of elements and order of the base function used. Increasing number and order are accompanied by massive increase in computing work. The finite-

element method is also suitable for modelling objects by 3-dimensional meshes, which obviously would lead to more accurate simulations of the real current field distribution in real internal human bodies due to the actual 3-dimensional distribution.

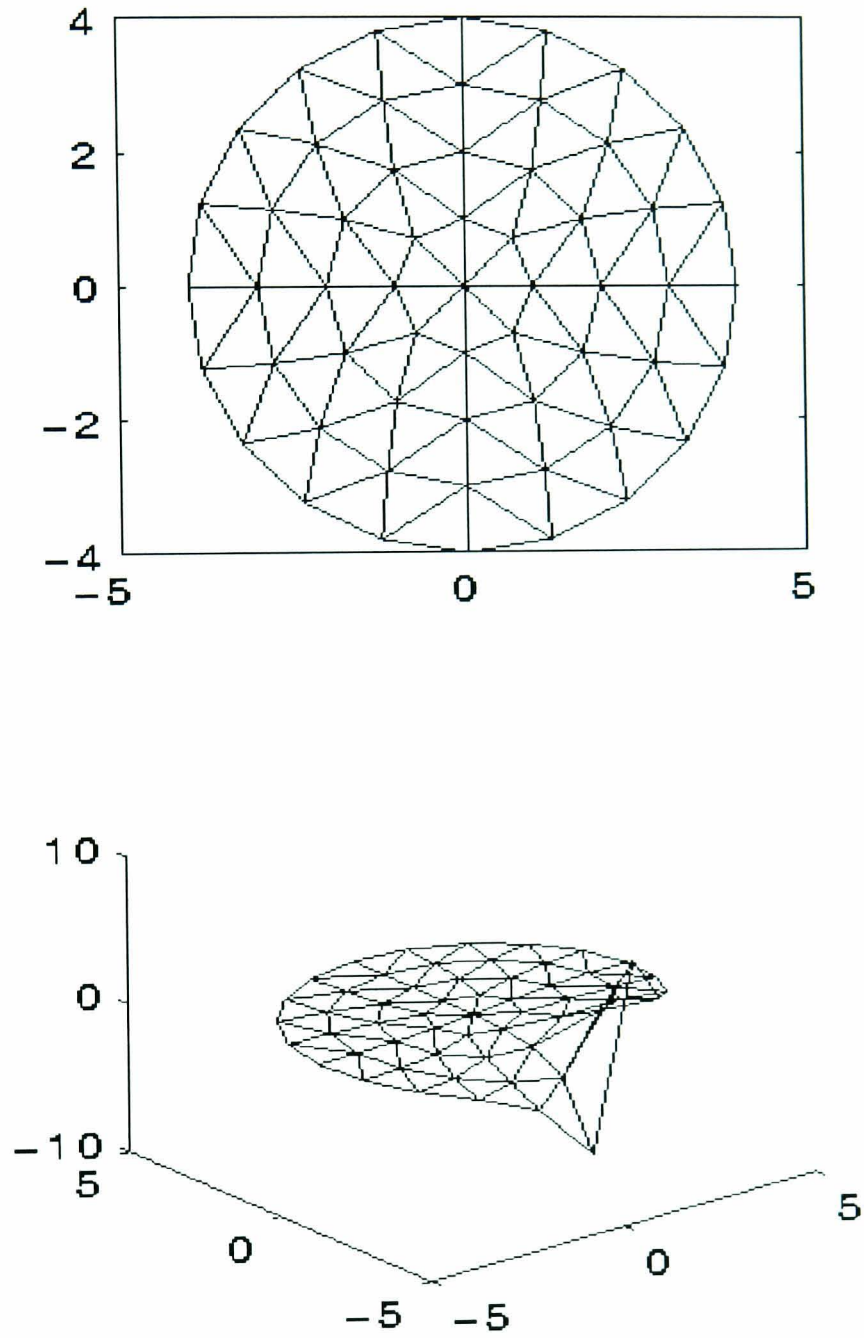

Figure 1.10 2-dimension finite element model

Applying the finite-element basic function, the partial differential equation problem is transformed into a linear problem, and the voltage distribution on the nodes of mesh can be solved. From different resistivity or conductivity setting on the finite-element model, the boundary voltage distribution on the object to be imaged can be calculated out

as measurement reference. It is called forward problem solving on the electrical impedance tomography reconstruction.

1.4.3.2 Newton-Raphson algorithm implementation

As mentioned earlier, the forward problem gives the estimated value of the voltage that can be measured on the surface electrode. The difference between the estimated value and real measured value of surface voltage reflects that the conductivity setting is not matched with the real internal conductivity distribution. The Newton-Raphson algorithm is iteratively modifies the finite-element conductivity distribution to compare the calculated voltage with the measured voltage until their error is within an acceptable value. Then, the final modified conductivity distribution matrix is displayed as the wanted EIT reconstructed image.

This method is modified by Yorkey [31], who suggested that the Marquardt regularization method should be used to improve the matrix's conditioning. It is claimed that this makes computation more stable and ensures better convergence.

Compared to the back projection method, the Newton-Raphson method gives an absolute value of the internal conductivity distribution. This method has strict demand on the quality of measured boundary voltage data.

1.5 EIT hardware system

To achieve a high quality electrical impedance tomography, the data acquisition system is an essential device to image reconstruction. The first generation of EIT systems is represented by the Sheffield MK1, which is designed with 16 electrodes and applied current at a single frequency, usually below 100 kHz [32]. The MK2 led to a real time data acquisition system with 25 frames per second measurement speed subsequently [33]. The MK3a and MK3b were the multi-frequency, Electrical Impedance Tomography Spectroscopy (EITS) systems [34]. In Table 1.1 a brief summary of the main performance characteristics for these devices is given [35].

The major limit to the application of EIT is poor spatial resolution, which is related to the number of independent data available on the boundary of the object for image reconstruction. This problem directly indicates that more electrodes should be used [36]. However, it is not a simple case of increasing the number of electrodes to overcome this problem. Comparing the surface of the object being imaged, the large number of

electrodes, the complexity of electrode itself and difficulties of processing of massive data are interrelated and pose a complex problem. Because of this reason, most EIT data acquisition system today still use 8/16 electrodes configuration.

Table 1.1 Typical performance characteristics of the Sheffield data collection systems

	MK1	MK2	MK3a	Mk3b
Operating frequency (kHz)	50	20	9.6-1220	9.6-1220
Applied current (mA)	5	5	0.25-2	0.25-2
Frame rate (s^{-1})	10/24	25	33.4(66.8)	16.7
Reconstruction time(s)	1-5	0.04	0.1	0.2
Electrode configuration	16 adjacent	16 adjacent	16 interleaved	64 interleaved
Independent measurements	104	104	49	784(3D)
Signal to noise ratio (dB)	51	68	61	43
			@9.6kHz	@9.6kHz

1.5.1 EIT data acquisition system structure

The first generation EIT hardware system was achieved in serial structure, using a single current source and voltage measurement circuit for each four-electrode combination measurement in turn using a digitally controlled multiplexer [37,38]. For some real time imaging purposes, a serial structure system cannot provide enough data acquisition speed for 25 frames per second display. Therefore, some systems began using a parallel system, which use a separated current sources and voltage measurement circuits to each configured data acquisition electrode combinations [39]. Due to the expense of the electronic devices and the size of the circuits patched into a very limited space, a parallel structure system cannot be achieved on high-density electrodes arrangements. Therefore, in practice a semi parallel system is normally built to satisfy the imaging speed requirements [40].

Both serial and parallel structure systems have to use the cable or multiplexer for current or voltage signal transmission. The stray capacitance of these devices will perform a low-pass filtering to the signal passing through. Therefore, the data system is difficult to operate over 1MHz and simultaneously satisfy the demand on measurement

accuracy. This represents a bottleneck of development of multi-frequency EIT systems in the radio frequency band.

As mentioned earlier, the current field in the imaged object is distributed in 3-dimensional space. Therefore, an improvement of the reconstructed image may be possible if 3-D image reconstruction is achieved. Obviously, the parallel system is not an ideal structure for this purpose design. However, the serial system can offer much more channels, but cannot give credit on high frequency data measurement due to the using of multiplexer and coaxial cable. In order to improve measurement accuracy and simplify the connection between the system and electrodes, it may be necessary to move part of the measurement system closer to the electrodes, that is to say, distribute the measurement system around the electrodes. This distributed system would need to be embedded the front-end circuit (current source and preamplifier) into the body of the electrodes [41]. Achievement of this kind of active electrodes is dependant on the development of integrated circuit processing.

1.5.2 Constant current source

In most of EIT data acquisition systems, the current is injected at a given moment by means of two electrodes only, and during the data acquisition time, the amplitude is maintained constant. However, some systems use a current injection strategy known as the "optimal current strategy" [42, 43]. This method consists of applying several currents with different amplitudes, through several electrodes and simultaneously measuring the voltages on all the electrodes. This "optimal" current makes it possible to maximize the distinguish ability between two distributions of different conductivities.

Whatever the current driving strategy used for data acquisition, a voltage controlled current source is the basic building block for EIT hardware system design. The first system used the isolated negative-feedback current source [33], as Figure 1.11 shows. The main limitation stems from the properties of the transformer resulting in stray capacitance and limited transinductivity. Although it is still used in single frequency systems, many other types of current source have been made to achieve multi-frequency measurements.

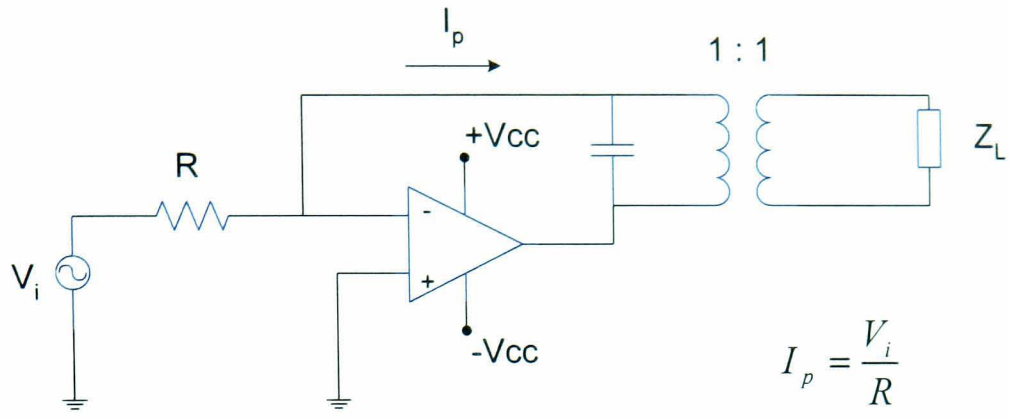

Figure 1.11 The isolated negative-feedback current source used in early EIT system

Most of the voltage controlled current sources (VCCS) used in EIT systems are based on the Howland circuit. The basic structure of the Howland current source is shown in Figure1.12. In theory, if the two feedbacks are identical, the output impedance will be infinite. In practice, mismatches in the resistors making up the feedback loops, the presence of stray capacitances and the frequency limits of the operational amplifier result in the output impedance being limited. Franco [44] demonstrated that with 0.1% resistors, if resistance mismatched correspond to the worst case, the output impedance can be as low as 375kΩ. This type of current source was applied to EIT at the University of Wisconsin [45] in a single frequency system.

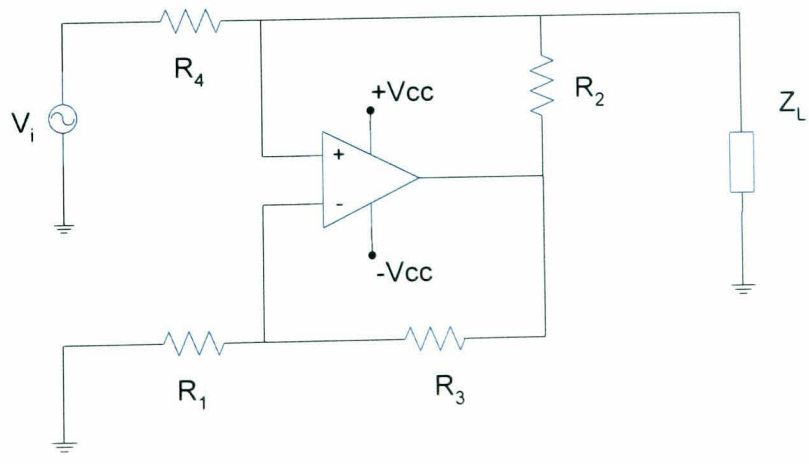

Figure1.12 Basic circuit structure of Howland current source

Another type current source is the current mirror circuit. This current generator is fully described by Bragos et al [46], in which the AD844 is a current feedback amplifier

and output is defined by the first stage, a transconductance amplifier MAX435 as shown in Figure 1.13. The output impedance of this current source can reach 100kΩ for frequency up to 100 kHz.

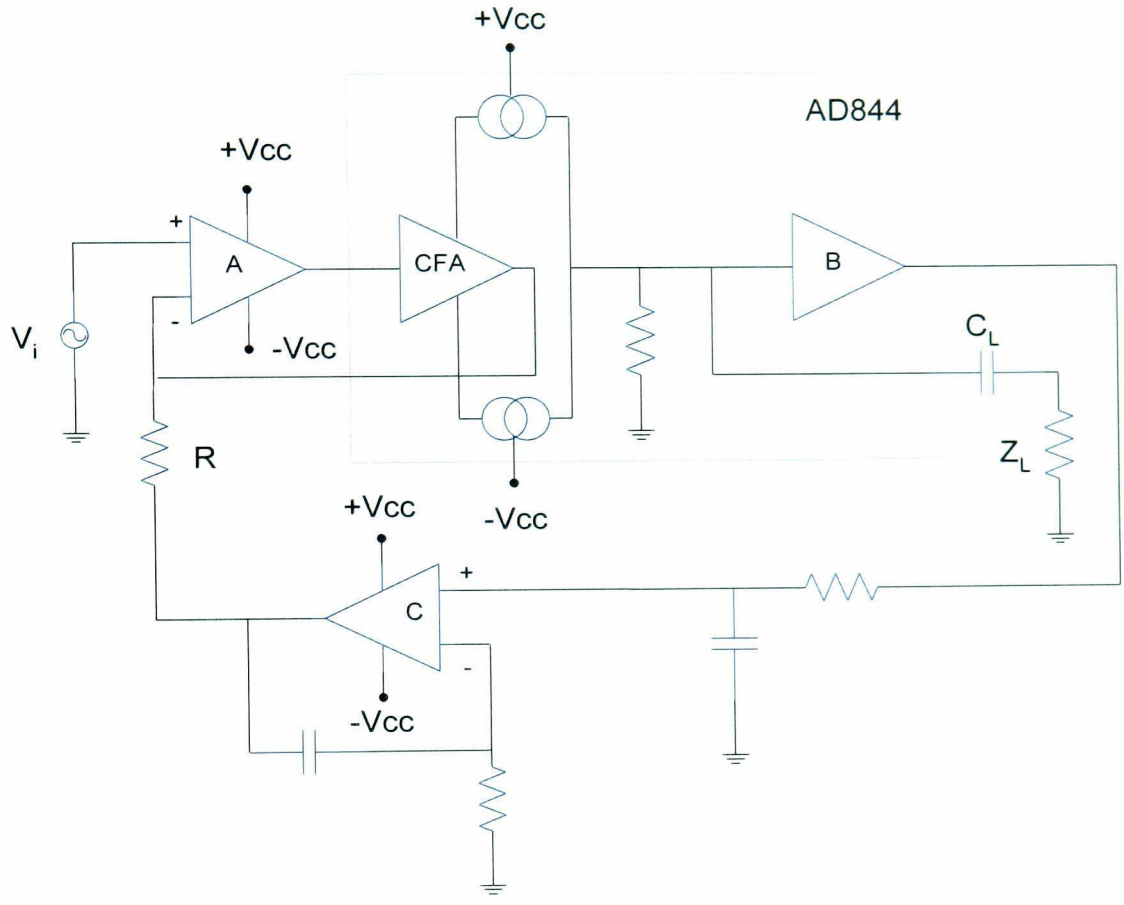

Figure 1.13 Integrated current-feedback amplifier (CFA) used as voltage controlled current source

For wide band EIT system design, the performance of current source is dominated by the bandwidth of electronic device. In addition, it is also affected by the system connections with electrodes, such as multiplexer and cable.

1.5.3 Voltage signal measurement

In an impedance-imaging system, the key points of the voltage measurement system are high input impedance voltage buffer and high common-mode rejection ratio (CMRR) amplifier.

In most of EIT systems, voltage buffers are used as a preamplifier stage in the differential path. In early single-frequency device, the ac-coupled bootstrapped buffer is a structure that is commonly used [47, 48], which is shown in Figure 1.14. The AC coupling by capacitance C_2 is required to avoid saturation of the measurement channel

by the electrode-skin interface polarization voltage and to prevent the operational amplifier's bias current from circulating in the measurement electrodes. It is also required to avoid the accidental circulation of any DC current from the measurement system, and the transient electrode polarization voltage that arises after a current has been passed through a DC-coupling electrode. At the imaging frequency, the reactance of capacitance C_1 can be ignored. It can be shown that by bootstrapping resistance R_1, it is possible to obtain an input resistance:

$$R_i = R_1 \cdot \frac{1}{1 - A_v} \qquad \text{Eq1.17}$$

here A_v is the buffer's gain. In practice, as pointed out by Rosell et al [49], the buffer's input capacitance limits the circuit's input impedance. According to these authors, the input impedance reaches its maximum value:

$$R_{in} = 2\pi \cdot R_1 R_2 C_1 \qquad \text{Eq1.18}$$

at the resonance frequency:

$$f = \frac{1}{2\pi\sqrt{R_1 R_2 C_1 C_2}} \qquad \text{Eq1.19}$$

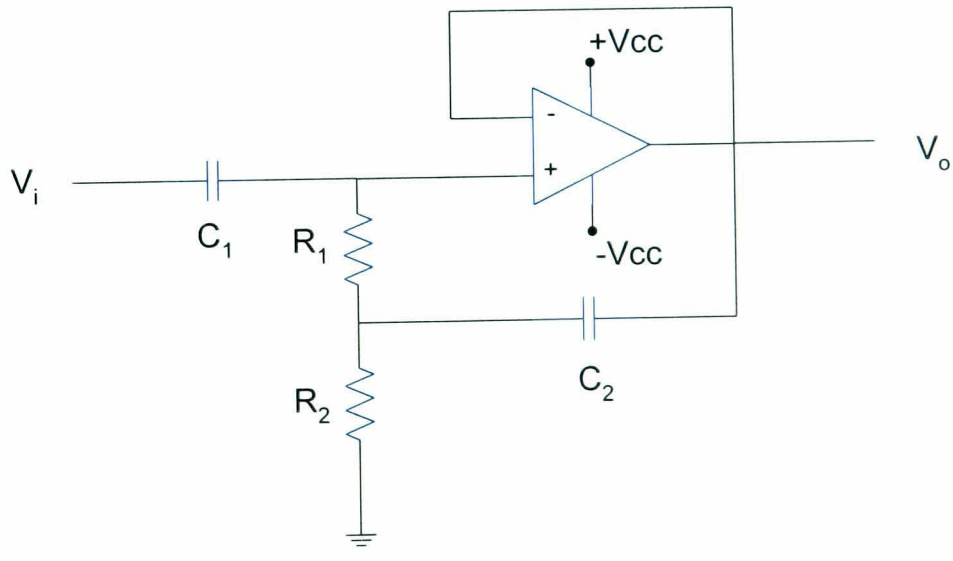

Figure 1.14 The AC-coupled bootstrapped buffer as front-end of voltage measurement circuit

The typical instrumentation amplifiers used in impedance imaging have the classic two-stage three op-amps structure, which has been extensively analyzed in biomedical applications by Webster [50]. To obtain a high CMRR in the differential amplifier,

working with a high differential gain and therefore using broad bandwidth operational amplifiers is recommended. This simplest design is to introduce correction RC networks that make it possible to adjust the CMRR at low and high frequency (see Figure 1.15), by compensating the imbalances in the transfer functions of the two differential branches. Smith [40] has given a solution that consists of dedicating one instrumentation amplifier to each electrode pair and connecting 16 monolithic instrumentation amplifiers to each electrode pair (16 pairs) by coaxial cables via DC blocking capacitors.

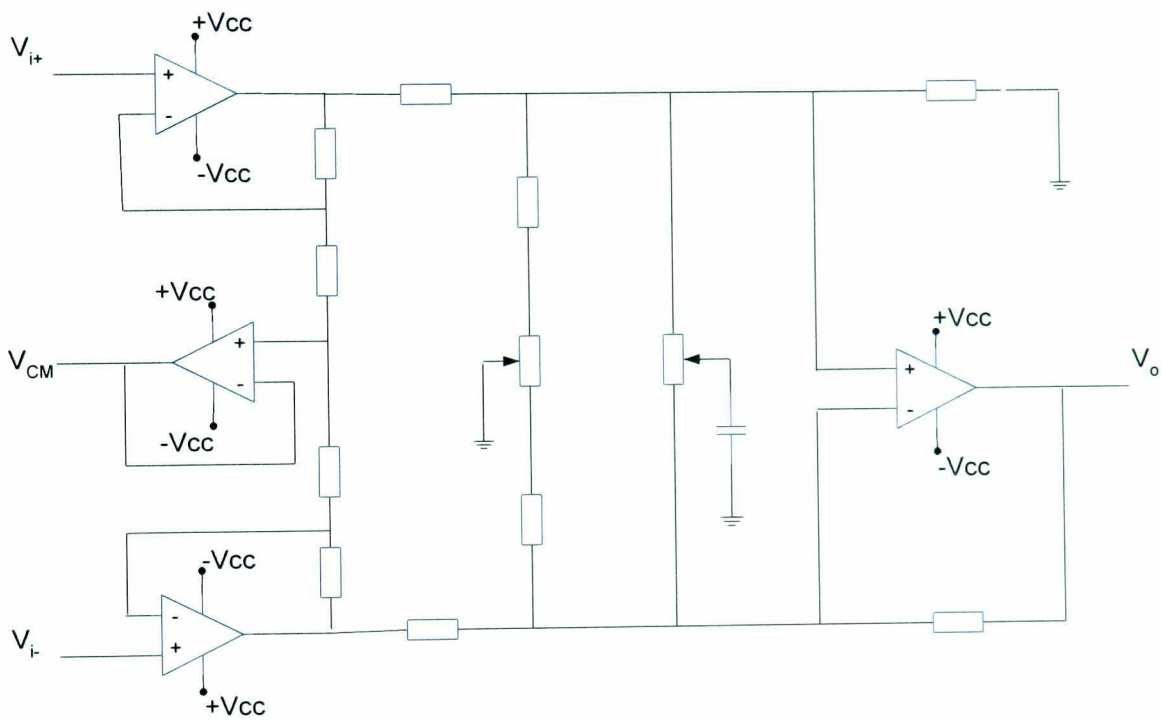

Figure 1.15 The instrumentation amplifier used as differential signal measurement can provides high common mode rejection ratio

The group at Oxford Brooks University [51] developed an alternative approach, shown in Figure 1.16, based on a differential-input voltage-controlled current sources structure. The front-end of this instrumentation amplifier is similar to that of the typical structure, except for the power supplies. The two input buffers have separate power supplies. Current sources are inserted in the supply lines of one buffer, and its power supplies are clamped by Zener diodes so that any supply current change caused by a differential-input voltage results in an output current, which is measured by the third operational amplifier. The author indicated that a bench prototype exhibited a CMRR of 80dB at 10 kHz and of 60dB at 100 kHz, measured at unit gain.

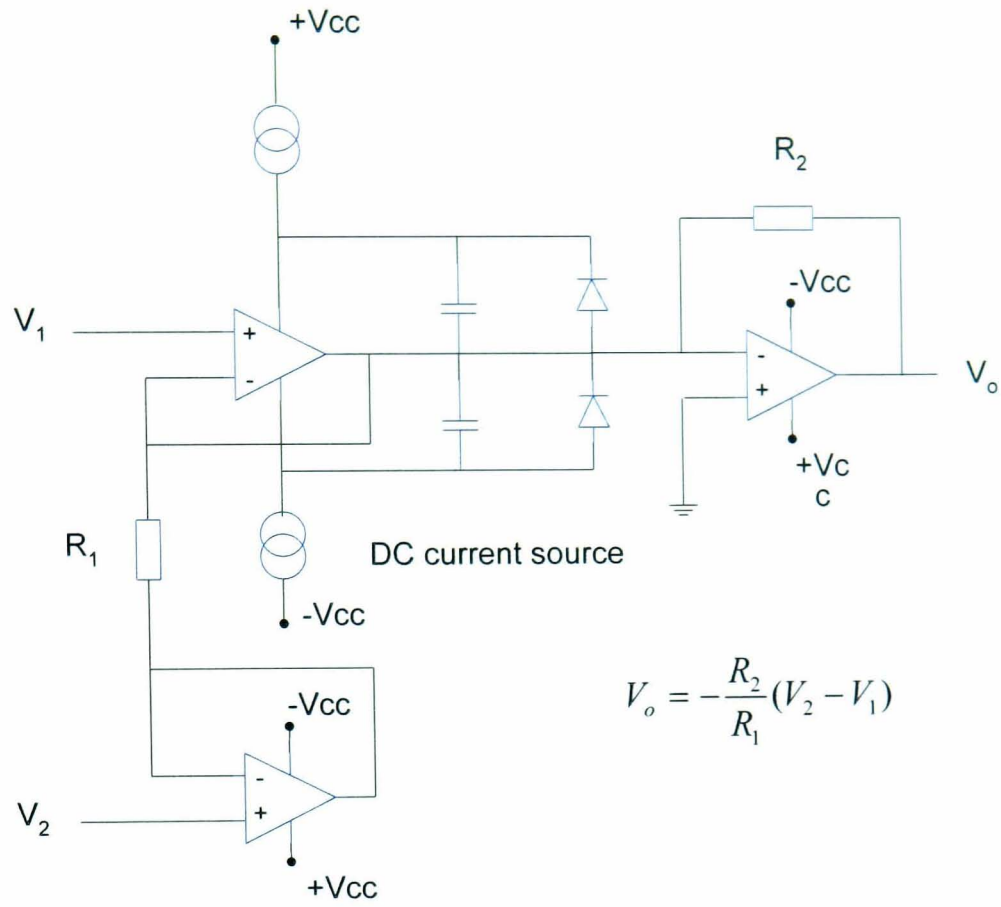

Figure 1.16 The differential-input voltage-controlled current sources structure front-end amplifier used in Oxford Brooks system design

1.5.4 Voltage signal demodulation

The frequency range of the bio-impedance variation in a human is considered to limit to 50 Hz so that bio-impedance signals are amplitude-modulated signals with a carrier frequency equal to the injected current frequency and a bandwidth of 100Hz [52]. Since the information of interest is contained in this low frequency bandwidth, some form of demodulation that shifts the signal frequency down is required.

The amplitude demodulation or RMS-to-DC conversion techniques are employed into the measurement in low frequency imaging systems for which phase information is not of importance because tissues behave almost resistively. Skidmore et al used a monolithic true RMS-to-DC converter in a 16-electrode system. Another similar demodulation is peak detection. It is used by the Catholic University of Leuven [53] and they have developed a high-precision amplitude detection system that includes a two half-wave rectifier followed by an integrator. A disadvantage of these techniques is that the signal frequency noise present at other frequencies is also rectified and this can lead to errors [54].

It is well established that phase-sensitive demodulation (PSD) techniques exhibit better performances, in terms of error and signal-to-noise ratio, than the previous solutions. Therefore, most of the demodulation techniques used in EIT is PSD. The principle of PSD consists of shifting the measured signal down to a low-frequency band by multiplying it with a reference signal synchronized with the injected current and by filtering the high-frequency harmonics generated by this process. The practical implementation determines that two types of phase-sensitive demodulators: coherent synchronous demodulators use four-quadrant linear multipliers; phase-sensitive synchronous detectors consist of an amplifier whose gain is switched between +1 and –1 by the reference signal, and both devices are followed by a low-pass filter.

Phase-sensitive detectors are popular being used for analogue demodulation. perhaps because of the relative simplicity of their structure. However, the major drawback of this method is that odd harmonics components of the signal fundamental are translated down to the output and lead to errors [55]. Band-pass filtering of the input signal prior to demodulation would eliminate this problem, but this it difficult to achieve with sufficient accuracy in multi-frequency system.

The low-pass filter required to extract the DC component and eliminate the high-frequency components is a crucial part that must be carefully designed in real time EIT system. The narrower the filter bandwidth, the better the signal-to-noise ratio is, but the settling time will be longer [54]. By using an integrator rather than a filter, the measurement time can be cut as short as one period of the driving function, although usually a few tenths of periods are used to reduce noise [56]. Since the output signal that will be considered for obtaining the real and imaginary parts of the impedance is a DC voltage, any offset will introduce errors. These can be compensated for in a calibration procedure, but the design of the whole system must ensure that the offset drift is kept within acceptable limits.

Owing to the limits inherent to analogue modulators, description of digital demodulators suited to EIT have been published as a new demodulation technique in single-frequency system and in multi-frequency systems [42, 33, 57, 58]. Due to using a lookup table stored in the DSP memory as the reference signal, the result of demodulation has less noise component than its analogue type coherent demodulation.

In addition, the demodulation is not DC offset sensitive. Normally, an anti-aliasing filter is required prior to input of analogue-to-digital converter.

1.6 Summary

Electrical impedance characteristic of biological tissue can provide internal information about structure and shape inside the body. Using computer-aid image reconstruction technique, the electrical impedance tomography is acquired for medical diagnostic purpose.

The resolution of the reconstructed image is limited by the data set collected on the boundary of imaged object, in which the number of independent data relies on the number of electrodes. In addition, the current injected into the object is distributed in 3-dimensional space. Therefore, more electrodes are needed to obtain high-resolution image reconstruction. This is the hot point for EIT research and development.

As the tissue performs more complex impedance property, EIT hardware systems need to be designed for wideband electrical impedance measurement or spectrum measurement, particularly having frequencies over 1MHz. This places high demands on the constant current source and front-end amplifier designs.

The performance of EIT data acquisition hardware is related to the electrodes connection and signal path to the system. Therefore, the system structure is crucial, and is a balance between measurement accuracy and building expense. This thesis concentrates on research into the system structure and key function blocks necessary to develop a new generation of De Montfort EIT systems that outperform existing designs.

Chapter 2 De Montfort MK1 System Review and MK2 System Development

2.1 De Montfort MK1 system review

The De Montfort MK1 system is a single channel measurement device designed for body tissue bioelectric property test, as pictured in Figure 2.1. It applied four-electrode measurement with two electrodes for current injection and the other two electrodes for voltage sensing. The current source in MK1 could provide constant current in the bandwidth from 1 KHz to 1MHz. The sine wave for current control is generated from an oscillator circuit. In practice, the precision of the signal frequency from this simple structure circuit was hard to satisfy the demand of spectrum scanning. In each sample measurement, the spectrum character of the tissue has to be formed by stacking all the single frequency measurements manually due to the lack of automatic timing control and analogue-to-digital conversion. The result of the measurement was read by means of digital oscilloscope.

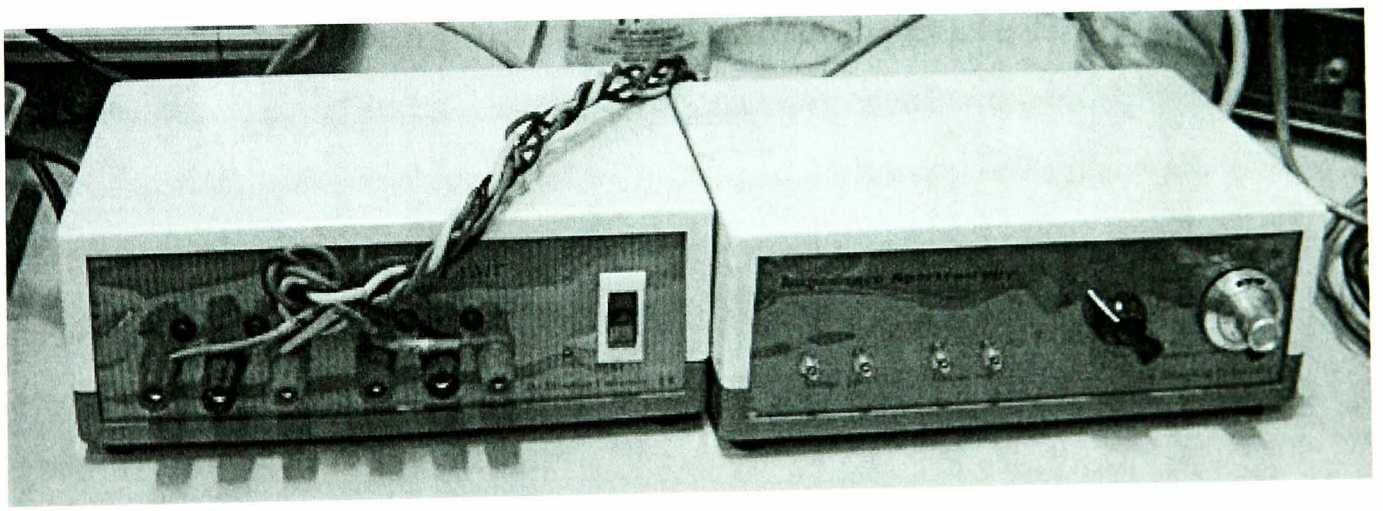

Figure 2.1 The De Montfort MK1 system

The MK1 system was used in the body tissue bioelectrical impedance investigation. It was also used as a development platform for two-dimensional electrical impedance

measurement, especially for electrode leads design and electrode material selection. In clinical research, the four-electrode electrical impedance measurement device was also used in the impedance plethysmography for determination of cardiac stroke volume.

The MK1 system was based on analogue technology, so its measurement accuracy was affected by the harmonic frequency of injected current wave and loss of transmission of signal by long cabling. Without digital control timing and analogue-to-digital conversion function, the MK1 system could not be applied in any continuous impedance measurement function.

2.2 Breast tissue bioelectric property investigation in DMU

From 1995, the EIT research group in De Montfort University has been involved in breast cancer imaging research, especially in breast tissue bioelectric property investigation in collaboration with Glenfield General Hospital, Leicester, UK. The hospital's Department of Histopathology provided the pathological findings that allowed comparison, and clinical validation, of the readings taken.

The bioelectric properties of different breast tissues were tested in a specially designed chamber, in which the size and position of electrodes is calibrated by using saline in controlled conditions. The chamber is pictured in Figure 2.2. The current injection electrodes are made of stainless steel, and are placed at two terminals of cylinder chamber, in which one of them has the function of a stopper. The two electrodes measuring the difference in potentials are plugged into the chamber from the top holes, which ensure the same distance of the two measuring electrodes for all impedance measurements. The measurements are taken by means of the De Montfort MK1 system and HP 4194 impedance analyzer.

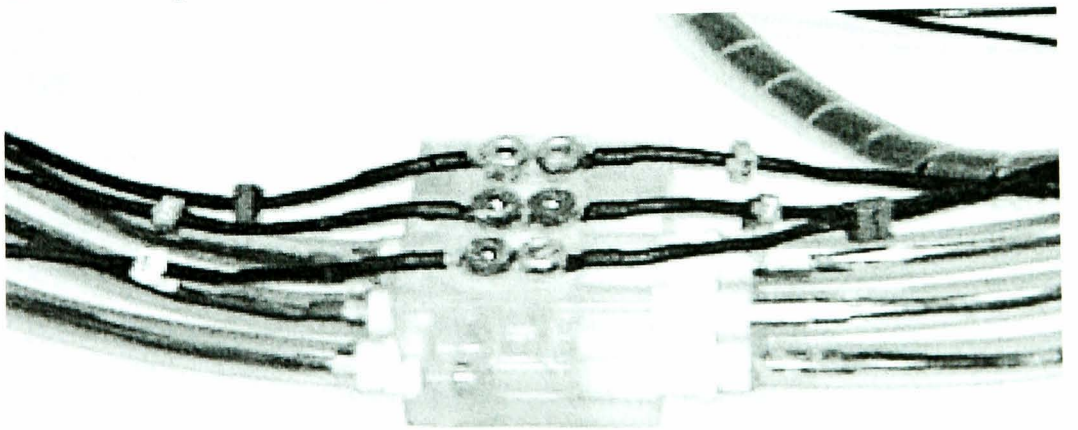

Figure 2.2 The chamber with the cables used in the tissue bioelectric property research

The *in vitro* study results were collected from more than 60 patients. Using the magnitude measurement, fat tissue was found to be significantly distinguished from other tissue types. The stroma and malignant tissues show stable impedance performance at measurement frequency less than 100 KHz, but there is significant differentiation between these two biologically similar tissues, as shown in Figure 2.3 [8]. This result reveals the possibility of image reconstruction between two differential frequencies to distinguish the normal and abnormal biological tissue.

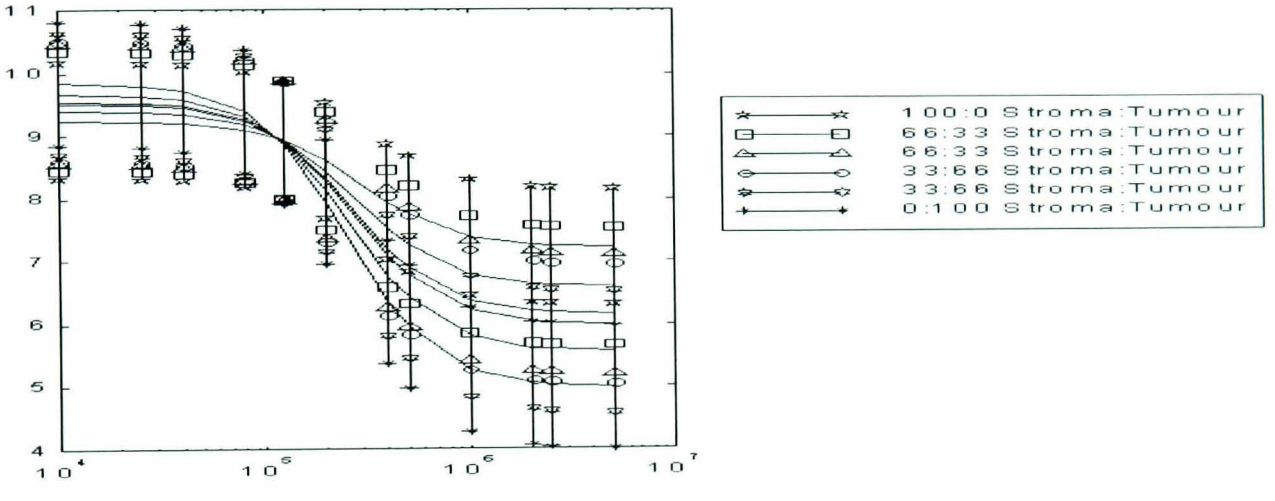

Figure 2.3 Stroma and tumour tissues electrical property at wide frequency bandwidth.

2.3 De Montfort MK2 system development

The MK1 system has provided a good platform for further development of an electrical impedance measurement device. Based on the result of clinical study, the new MK2 system is planned for taking two-dimensional impedance measurement, which means that the system has electrical impedance tomography function with a wide imaging frequency bandwidth. The system is to have at least a 16/32 electrodes configuration with flexible drive/ receive pattern programmable system timing.

The voltage controlled current source is the most important part in the four-electrode impedance measurement circuit design. The sine wave voltage generator is to use digital synthesis technique, which can provide a good quality single frequency sine wave with minimum harmonic components, and flexible frequency and phase selection/settings. The voltage-to-current converter provides constant current to inject into

the imaged object, so that the output impedance should be large enough for keeping the current source accuracy.

The voltage signal is picked up by the front-end amplifier on the receiving electrode pairs. As the measured object is equivalent to a signal source with high output impedance, the front-end amplifier is a challenge with respect of the input impedance and common-mode rejection circuit parameters. Due to the complex mode of bio-impedance of tissue, the measurement should have the ability to produce the magnitude and phase information of each measurement, or real part and imaginary part of each measurement. The dynamic range of measurement for two-dimensional electrical impedance tomography varies from the driving and receiving electrode positions. Increasing the signal-to-noise ratio is essential for high accuracy measurement to be achieved, and a programmable gain amplifier is the better choice to match the measurement dynamic range.

The data acquisition speed for imaging reconstruction is crucial for the physiological activity monitoring. However, for the breast electrical impedance image reconstruction, the real-time image is not necessary due to the property of breast tissue and organ. Therefore, the MK2 development will focus on the accuracy of measurement and the extension of number of measurement channel.

In EIM research, the imaging frequency of interest is in the wide range from DC to high frequency over 100K Hz or even over 1MHz. The MK2 research and development target is to concentrate on the factors effecting measurement bandwidth, explore potential solutions, analyze the circuitry and study the methodology of the system implementation.

The critical feature in image reconstruction from bio-impedance analysis is that the internal impedance of the imaged object is calculated from injected current and measured boundary voltage. This inverse solving process relies upon the number of independent data being measured. High resolution reconstructed impedance distribution from very limited number of data will have some uncertainty. In image reconstruction practice, this problem is solved by modelling the imaged object to limit the range of convergence in the reconstruction algorithm. The MK2 data acquisition system will also act as a platform for measuring parameters of the modelling matched to the real imaged object output.

2.4 The aims of the thesis

This thesis aims to investigate the electrical impedance measurement method and possible extended hardware implementation. In addition, based on these research results, the MK2 data acquisition system plays a key role for providing accurate data for the image reconstruction algorithm implementation and further hardware development.

- Give a basic electric circuit analysis on the serial EIT system, and find its limits on the high frequency impedance measurements.
- Investigate the popular used Howland topology current source to find the best way to improve its output-impedance. If it is possible, try to give a solution on matching of resistors in the manufacturing process.
- High CMRR front-end amplifier design and embedded active electrode design as a potential solution for wider bandwidth EIT system implementation.
- With all electrodes combination voltage measurement, design a program controlled gain amplifier to enhance small voltage signal measurements in terms of signal-to-noise ratio.
- Investigate the all data acquisition methods and electrode configurations for high-speed data collection system design.
- Design and implementation of Multi-channel EIT system is the main output of this project. It will be achieved from the prototype designs from above investigations.

2.5 Summary

The De Montfort MK1 impedance analyzer has been successfully used for clinical tissue bioelectrical properties investigation. The results demonstrate the feasibility of using the electrical impedance imaging technology on breast cancer early detection in that tissue specificity has been shown in Figure 2.3.

As the first electrical impedance imaging system, devoted to breast cancer research, the MK2 data acquisition system development will focus on the accuracy of measurement; extend system bandwidth, and the possibility of multi-channel extension. The MK2 system is the hardware platform for further hardware developments and inverse problem solving.

Chapter 3 Wide Band Howland Current Source

3.1 Introduction

Electrical impedance tomography requires the application of electrodes onto the surface of the body, around the region of interest. Like most EIT systems, the MK2 uses 16 electrodes for two-dimensional data collection. For breast cancer imaging purposes, the arrangement of these electrodes is critical and any positional errors and contact problems make the acquired data distorted and non-reproducible.

Many methods [40, 50, and 51] have been used in the data acquisition strategy; they can be divided into two categories: current drive and voltage drive. Current drive is the classic four-electrode method [13] used in EIT systems, and in the MK2 system design. The accuracy of data will directly depend on the quality of constant current source. As the measured impedance is in the range of 100Ω to 2KΩ, the output impedance of current source should have at least 200KΩ to ensure its 1% accuracy. In addition, if the contact impedance is considered, the equivalent output impedance of the current source should be much higher. In the multi-frequency EIT data acquisition system, the output impedance of the current source will be even worse at the high imaging frequency. The performance of current source in the system can be affected by other peripheral connections, which includes electrodes, cable and multiplexer.

The Howland topology is the most popular design in current source constructions, as reviewed in the section of 1.5.2 in Chapter 1. In 2003, A S Ross [76] also suggested a tuning method based on GIC circuit to resolve the effect of stray capacitance on this current source and they reported an improvement of output impedance at a tuned frequency. Due to the complexity of the implementation and the limitation of bandwidth, this method is still in the early stage of development.

In this chapter, the Howland topology circuit is investigated using electric circuit analysis and PSPICE simulation. An optimized design method is provided for practical circuit design and prototyping.

3.2 Howland current source

In multi-frequency EIT data acquisition system, the performance of the constant current source is degraded by the application of cables and multiplexer. The stray capacitance of these devices shunts the high frequency signal path. In the MK2 system, using separate driving and receiving electrodes reduces the effect of this problem, as 16 electrodes apply current and 16 electrodes take voltage measurement. However, a more efficient solution would be to distribute the front-end circuit around the imaging area, thereby removing most of the cable and multiplexer connections. In addition, the electronic circuit needs to be optimized to achieve highest possible output impedance in its simplest structure.

Howland current source has simple circuit layout and could be implemented into a small package, which shows a potential for an active electrode application.

3.2.1 Basic Structure of Howland Circuit

The circuit in Howland topology involves one operational amplifier and a resistor network, as shown in Figure 3.1. For the ideal operational amplifier, the gain is infinite and the input impedance is infinite, so

$$I = -\frac{R_2}{R_1 \cdot R_4} \cdot V_i + \left[\frac{R_2}{R_1 \cdot R_4} - \frac{1}{R_3} \right] \cdot V \qquad \text{Eq3.1}$$

When

$$\frac{R_2}{R_1} = \frac{R_4}{R_3} \qquad \text{Eq3.2}$$

then

$$I = -\frac{1}{R_3} \cdot V_i \qquad \text{Eq3.3}$$

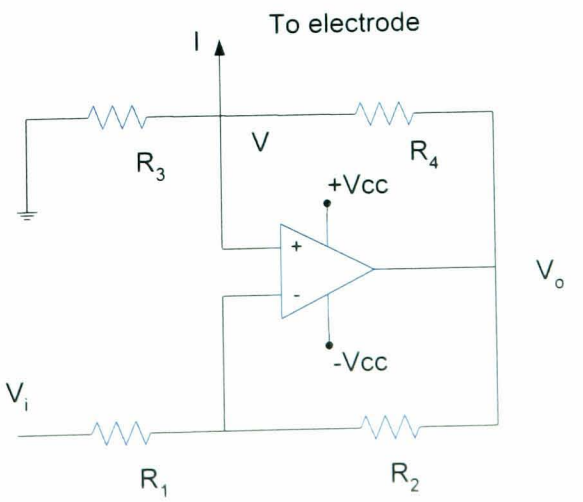

Figure 3.1 The basic structure of Howland current source

From Eq3.3 it can be seen that the output current is dominated by the input voltage and R3, and this circuit is ideally a constant current source under the condition $\frac{R_2}{R_1} = \frac{R_4}{R_3}$.

If the resistors were perfectly matched, the output impedance of the circuit would be infinite. The common mode voltage V is the loading voltage, which follows the change of load impedance. When the current is designed large or load is large, this common mode voltage drives the operational amplifier into saturation. Consequently, the loading voltage directly limits the compliance of the basic Howland circuit.

3.2.2 *The improved Howland current source*

To improve the compliance of this constant current source, a resistor R_5 is inserted between the non-inverting input and output of current source, as shown in Figure 3.2.

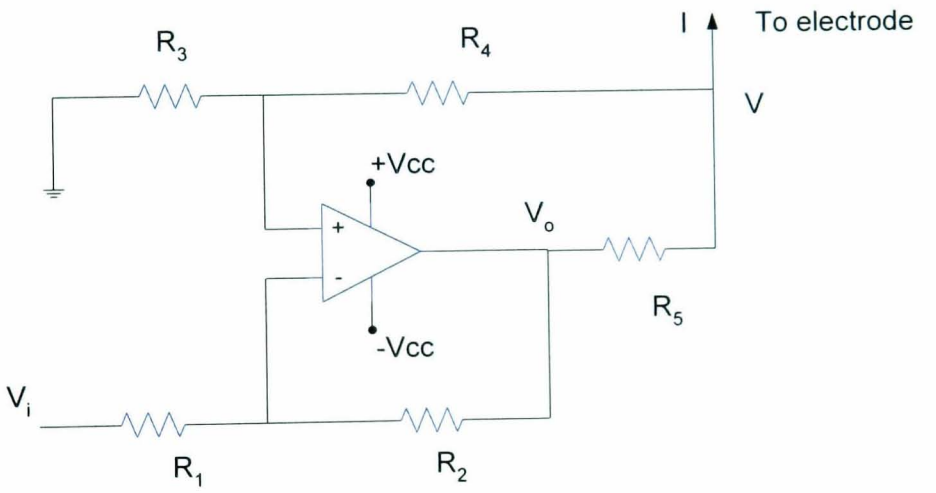

Figure 3.2 The improved Howland current source circuit

If Op-amp A is considered as an ideal operational amplifier, the output current of the circuit can be described as

$$I = -V_i \cdot \frac{R_2}{R_5 \cdot R_1} + \frac{R_3}{R_5 \cdot (R_3 + R_4)} \left(\frac{R_2}{R_1} - \frac{R_4 + R_5}{R_3} \right) \cdot V \qquad \text{Eq3.4}$$

When

$$\frac{R_2}{R_1} = \frac{R_4 + R_5}{R_3} \qquad \text{Eq3.5}$$

then Eq3.4 will be simplified to:

$$I = -V_i \cdot \frac{1}{R_5} \cdot \frac{R_2}{R_1} \qquad \text{Eq3.6}$$

According to Eq3.6, the improved Howland circuit output current is dominated by the input voltage *Vi* and value of resistors R_1, R_2 and R_5. It forms an ideal constant current source under these conditions. *Vi* can also be connected to the non-inverting input terminal of op-amp. Under the same conditions as above, the output current is

$$I = V_i \cdot \frac{1}{R_5} \cdot \frac{R_2}{R_1} \qquad \text{Eq3.7}$$

The output impedance of the improved circuit could be found by the following procedure. Assume $V_i = 0$, then

$$I = V\left[\frac{1}{R_5} \cdot \frac{R_3}{R_3 + R_4} \cdot (1 + \frac{R_2}{R_1}) - (\frac{1}{R_3 + R_4} + \frac{1}{R_5})\right] \qquad \text{Eq3.8}$$

Therefore the output impedance of the circuit is

$$Z_O = \frac{V}{I} = \frac{R_5\left(1 + \frac{R_4}{R_3}\right)}{\frac{R_2}{R_1} - \frac{R_5 + R_4}{R_3}} \qquad \text{Eq3.9}$$

When the condition $\frac{R_2}{R_1} = \frac{R_4 + R_5}{R_3}$ is satisfied, the circuit will perform as an ideal current source and the output impedance is infinite.

The analysis is based on the ideal operational amplifier. In practice, the dynamic range, gain bandwidth production, and open-loop gain are limited, especially at high frequency. Due to the introduction of R_4, the voltage over the load impedance is divided by R_3 and R_4, and is presented to the non-inverting input of amplifier. Therefore, the compliance of this Howland circuit is improved.

3.3 The problems on matching Howland circuit resistors

In the implementation of the current source, infinite output impedance is unachievable due to the tolerance of resistors and the imperfection of operational amplifier.

3.3.1 The effect of unmatched resistors in Howland circuit

With unmatched resistors, Z_0 will be degraded to a limiting level. If $\frac{R_2}{R_1} = \frac{R_4 + R_5}{R_3} = k$ and the tolerance of commercial product R_1 to R_5 is α, then in the worst case situation:

$$Z_{worst\_case} = \frac{R_5(1+\frac{R_4}{R_3})(1-\alpha)^3}{4k\alpha} \qquad \text{Eq3.10}$$

It can be seen in Eq3.10 that three factors affect the output impedance of the circuit.

(1) Tight tolerant resistors will directly ensure high output impedance. The current source using *0.1%* tolerance resistors have ten times larger output impedance than one using *1%* tolerance resistors.

(2) The ratio $\frac{R_5}{k}$ can be worked out using Eq3.6, in which V_i is limited in the dynamic range of operational amplifier and I is the amplitude of constant current being required.

(3) The ratio of $\frac{R_4}{R_3}$ is smaller than the close-loop gain of the operational amplifier, which is designed with respect to the stability of the operational amplifier and the working bandwidth.

Table 3.1 gives the calculated minimum output impedance using the above analysis using different resistor settings:

Table 3.1 The expected output impedance of Howland current source with an ideal op-amp

Resistor setting values (kΩ)				Output impedance of current source with different resistor Tolerance (kΩ)		
R_5	R_4	R_3	k	5%	1%	0.1%
2	1	1	3	5.72	32.3	332.3
2	5	1	7	7.35	41.6	427.3
2	10	1	12	7.86	44.5	457

In addition, with unmatched resistors, the largest amplitude deviation of the constant current can be estimated from Eq3.6

$$\Delta I_{\max} = \frac{R_2}{R_1 \cdot R_5} \cdot V_i \cdot \frac{6 \cdot \alpha + 2 \cdot \alpha^3}{(1-\alpha^2)^2} \qquad \text{Eq3.11}$$

Here, the tolerance of resistor is α. Therefore, for the prototyping circuit, the current could have as large as a 0.6% deviation with using of 0.1% tolerance resistors. This design error does not take into account the effects of the operational amplifier and input voltage. Consequently, the deviation will be even greater.

3.3.2 *The effect of non ideal operational amplifier in Howland circuit*

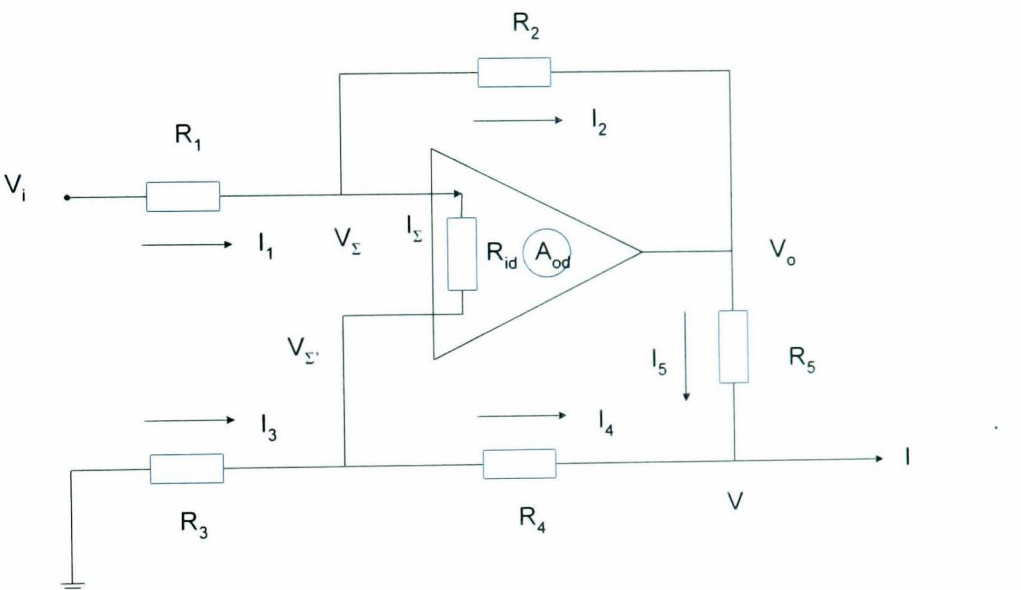

Figure 3.3 The operational amplifier internal electric model given in Howland current source which is presented with limited input-impedance R_{id} and limited open-loop gain A_{od}

The results in the previous section were acquired using resistors connected to an ideal operational amplifier. Actually, the operational amplifier is not perfect as assumed having infinite open-loop differential amplify gain and infinite input impedance. All the derived equations assume that the operational amplifier does not absorb any current, which is not true in bipolar operational amplifiers, especially those for high-speed use. Figure 3.3 depicts an operational amplifier model with finite differential gain A_{od} and input impedance R_{id}. The current absorbed by the operational amplifier is I_Σ; V_Σ and $V_{\Sigma'}$ are the input voltages at the inverting and non-inverting terminals respectively, and V_o is the output voltage of the operational amplifier. Therefore, the basic equations are given as:

$$V_{E'} - V_E = \frac{V_o}{A_{od}} \qquad \text{Eq3.12}$$

$$I_E = \frac{V_E - V_{E'}}{R_{id}} \qquad \text{Eq3.13}$$

If the loading current is I and the loading voltage is V, at the circuit nodes V_Σ, $V_{\Sigma'}$ and V, the current sum is zero:

$$I_1 - I_2 - I_E = 0 \qquad \text{Eq3.14}$$

$$I_4 - I_3 - I_E = 0 \qquad \text{Eq3.15}$$

$$I - I_5 - I_4 = 0 \qquad \text{Eq3.16}$$

Here, I_1 to I_5 denote the current passing through the resistors R_1 to R_5.

Combining the equations Eq3.12 to Eq3.16, the loading current can be described as:

$$I = -\frac{\dfrac{R_2}{R_1 + R_2}\left(\dfrac{1}{R_5} + \dfrac{R_3}{R_3 + R_4} \cdot \dfrac{1}{A_{od} \cdot R_{id}}\right)}{\dfrac{1}{A_{od}} + \left(\dfrac{R_1 \cdot R_2}{R_1 + R_2} - \dfrac{R_3 \cdot R_4}{R_3 + R_4}\right) \cdot \dfrac{1}{A_{od} \cdot R_{id}} + \dfrac{R_1}{R_1 + R_2}} \cdot V_i$$

$$+ \left[\frac{\dfrac{R_3}{R_3 + R_4}\left(\dfrac{1}{R_5} + \dfrac{R_3}{R_3 + R_4} \cdot \dfrac{1}{A_{od} \cdot R_{id}}\right)}{\dfrac{1}{A_{od}} + \left(\dfrac{R_1 \cdot R_2}{R_1 + R_2} - \dfrac{R_3 \cdot R_4}{R_3 + R_4}\right) \cdot \dfrac{1}{A_{od} \cdot R_{id}} + \dfrac{R_1}{R_1 + R_2}} - \frac{R_3 + R_4 + R_5}{R_5 \cdot (R_3 + R_4)} \right] \cdot V \qquad \text{Eq3.17}$$

According to this equation, the current will be dominated by input voltage V_i, if the second part of equation is forced to equal to zero. If input voltage $V_i = 0$, the output impedance is $Z_o = V / I$, that is

$$Z_0 = \frac{R_5 \cdot (R_3 + R_4)}{R_3} \cdot \frac{\dfrac{R_1}{R_1 + R_2} + \dfrac{1}{A_{od}} + \left(\dfrac{R_1 \cdot R_2}{R_1 + R_2} \dfrac{R_3 \cdot R_4}{R_3 + R_4}\right) \cdot \dfrac{1}{A_{od} \cdot R_{id}}}{\dfrac{R_3 \cdot R_2 - R_1 \cdot (R_4 + R_5)}{R_3 \cdot (R_1 + R_2)} \dfrac{R_3 + R_4 + R_5}{R_3} \cdot \dfrac{1}{A_{od}} + \left(R_4 + R_5 - \dfrac{R_1 \cdot R_2 \cdot (R_3 + R_4 + R_5)}{R_3}\right) \cdot \dfrac{1}{A_{od} \cdot R_{id}}} \qquad \text{Eq3.18}$$

Because normally the value of open-loop gain and the input impedance of an operational

amplifier are relatively large, it can be seen that $\frac{1}{A_{od} \cdot R_{id}}$ is relatively unimportant and can be ignored. Hence, the effect of $\frac{1}{A_{od}}$ is the main error source of the Howland circuit and the output impedance can be given as

$$Z_0 = \frac{R_5 \cdot (R_3 + R_4)}{R_3} \cdot \frac{\frac{R_1}{R_1 + R_2} + \frac{1}{A_{od}}}{\frac{R_3 \cdot R_2 - R_1 \cdot (R_4 + R_5)}{R_3 \cdot (R_1 + R_2)} - \frac{R_3 + R_4 + R_5}{R_3} \cdot \frac{1}{A_{od}}} \qquad \text{Eq3.19}$$

When the constant current source condition $\frac{R_2}{R_1} = \frac{R_4 + R_5}{R_3}$ is applied, the output impedance of the circuit is dominated by A_{od}. The output impedance Z_0 can reach infinity, when

$$\frac{R_3 \cdot R_2 - R_1 \cdot (R_4 + R_5)}{R_3 \cdot (R_1 + R_2)} - \frac{R_3 + R_4 + R_5}{R_3} \cdot \frac{1}{A_{od}} = 0 \qquad \text{Eq3.20}$$

or

$$\frac{R_2}{R_1} = \frac{R_4 + R_5}{R_3} + \left(1 + \frac{R_4 + R_5}{R_3}\right) \cdot \left(1 + \frac{R_2}{R_1}\right) \cdot \frac{1}{A_{od}} \qquad \text{Eq3.21}$$

From the foregoing description, it can be seen that the effect of finite open-loop gain is magnified by the square of non-inverting input gain. In addition, in practice, the gain of negative feedback of amplifier should be kept to a smaller value to make it easy to match. The output impedance could be described as

$$Z_o = \frac{R_5 \cdot (R_3 + R_4)}{R_3} \cdot \frac{1 + \frac{1}{A_{od}}\left(1 + \frac{R_2}{R_1}\right)}{\frac{R_2}{R_1} - \frac{R_4 + R_5}{R_3} - \left(1 + \frac{R_2}{R_1}\right) \cdot \left(1 + \frac{R_4 + R_5}{R_3}\right) \cdot \frac{1}{A_{od}}} \qquad \text{Eq3.22}$$

And the output current is

$$I = \frac{V_i}{R_5} \cdot \frac{R_2}{R_1 + \frac{R_1 + R_2}{A_{od}}} \qquad \text{Eq3.23}$$

The output current is also affected by the finite open-loop gain of the amplifier and this effect works with the sum of the value of the negative feedback loop resistors ($R_1 + R_2$).

3.4 The solution to improve Howland Circuit performance

As analyzed in last section, in equation Eq3.22, when the resistors are matched as $\frac{R_2}{R_1} = \frac{R_4 + R_5}{R_3} = k$, which k is the negative feedback gain of the circuit. The output impedance of the Howland circuit is

$$Z_o = \frac{R_5 \cdot (R_3 + R_4)}{R_3} \cdot \frac{1 + \frac{1}{A_{od}} \cdot (1 + k)}{(1 + k)^2 \cdot \frac{1}{A_{od}}} \qquad \text{Eq3.24}$$

From the equation Eq3.21, the matching of resistors $\frac{R_2}{R_1} = \frac{R_4 + R_5}{R_3}$ does not produce the desired high output impedance of the current source due to the effect of the finite open-loop gain of the op-amp. However, an infinite output impedance of the current source can still be reached by slightly adjusting one of the balanced resistors, such as R_3 which will satisfy the equation Eq3.21. Assuming ΔR is needed for the adjustment, and then equation Eq3.221 can be written as

$$k = \frac{k \cdot R_3}{R_3 + \Delta R} + \left(1 + \frac{k \cdot R_3}{R_3 + \Delta R}\right) \cdot (1 + k) \cdot \frac{1}{A_{od}} \qquad \text{Eq3.25}$$

and the adjustment for R_3 could be made as

$$\frac{\Delta R}{R_3} = \frac{(1 + k)^2 \cdot \frac{1}{A_{od}}}{k - (1 + k) \cdot \frac{1}{A_{od}}} \approx \frac{(1 + k)^2}{k} \cdot \frac{1}{A_{od}} \qquad \text{Eq3.26}$$

The adjustment of the resistor depends on the open-loop gain of op-amp used in the circuit, and the circuit's close loop gain.

After the adjustment of R_3, the amplitude of output current is not changed and only affected by the open loop gain:

$$I = \left[\frac{V_i \cdot R_2}{R_5 \cdot R_1}\right] \cdot \frac{1}{1 + \frac{1}{A_{od}} \cdot (1+k)} \qquad \text{Eq3.27}$$

The adjustment of R_3 provides a compensation for the imperfection of operational amplifier to balance Howland circuit. This method does not increase the complexity of circuit and easy to achieve. As this compensation does not affect the designed output current, it will extremely simplify the circuit manufacturing when this circuit is applied into active electrode application where hundreds of active electrodes are demanded for uniformed output current.

3.5 PSPICE simulation

The previous analysis is based on an ideal operational amplifier with different tolerance resistors. In fact, the operational amplifier itself is far from the perfect, especially at high working frequencies. In the manufacture's datasheet, the gain bandwidth product or unit gain bandwidth is provided as a design reference. This parameter indicates if the working frequency is too close to the higher end of bandwidth, the operational amplifier cannot provide a high open loop gain and the phase shift will increase dramatically. Some manufactures give this bandwidth parameter with compensated gain, which allows users to design the devices into the circuit without a special compensation network, which is needed for the operation stability and accuracy. However, normally this compensated bandwidth is much narrower than the natural bandwidth. Care must be taken when an uncompensated operation amplifier is used in the circuit design, as this kind of amplifier has a wider gain bandwidth product in the datasheet than in practice. Basically, without any compensation components they cannot work properly. The compensation network cancels oscillation, drift and other unwanted amplifier behaviour. However, they certainly adversely reduce the circuit working bandwidth. In addition, with amplifier working in different power output, it also has the bandwidth change.

The operational amplifier compensation capacitance and small internal drive currents act together to limit the rate, at which the output can change, even when a large input unbalance occurs. This limiting speed is usually specified as slew rate (SR). The slew rate limits the amplitude of an undistorted sine wave output swing above the frequency at which the full supply swing requires the maximum slew rate of the operational amplifier. A sine wave of frequency f hertz and amplitude A volts requires a minimum slew rate of $2\pi fA$ volts per second. For externally compensated operational amplifier the slew rate depends on the compensation network used.

For internally compensated operational amplifiers the open loop gain as a function of frequency is simply a 6dB/octave roll-off beginning at some fairly low frequency, an intentional characteristic necessary for stability. This roll-off results in a constant 90° lagging phase shift from input to output (open-loop) at all frequencies above the beginning of the roll-off, increasing to 120° to 160° as the open-loop gain approaches unity. Since a 180° phase shift at a frequency where the voltage gain equals 1 will result in positive feedback as oscillation, the phase margin that specifies the difference between the phase shift at f_T and 180° must be checked in the circuit design.

For high-speed operation, in general, bipolar transistor operational amplifiers have higher bias currents. In addition, some operational amplifiers have asymmetrical output drive capability, with the ability to sink more current than they can source or *vice versa*. Therefore, in selection of the operational amplifier a symmetrical structure amplifier will be a better choice. Nowadays integrated circuit manufacture process has adopted a laser trimming technology to reduce the bias current and draft voltage problems.

Table 3.2 The frequency response of a non-ideal op-amp (from OPA620 datasheet, Burr-Brown)

Closed-Loop Bandwidth (–3dB)		Gain = +1V/V	300MHz
		Gain = +2V/V	100MHz
		Gain = +5V/V	40MHz
		Gain = +10V/V	20MHz
Gain-Bandwidth Product		Gain ≥ +5V/V	200MHz
Full Power Bandwidth	V O = 5Vp-p	Gain = +1V/V	11MHz
	V O = 2Vp-p	Gain = +1V/V	27MHz

Having considered most market available operational amplifiers, the *OPA620KU* is chosen as the current source design. Its bandwidth parameters are shown in Table 3.2. The *OPA620* is a precision wideband monolithic operational amplifier featuring very fast settling time, low differential gain and phase error, and high output current drive capability. The *OPA620* is internally compensated for stability. It has a very low offset, fully symmetrical differential input due to the "classical" operational amplifier circuit architecture, as Figure 3.4 shown. The *OPA620* may be used in all operational amplifier applications requiring high speed and precision. Low noise and distortion, wide bandwidth, and high linearity make this amplifier suitable for radio frequency applications. Short-circuit protection is provided by an internal current-limiting circuit.

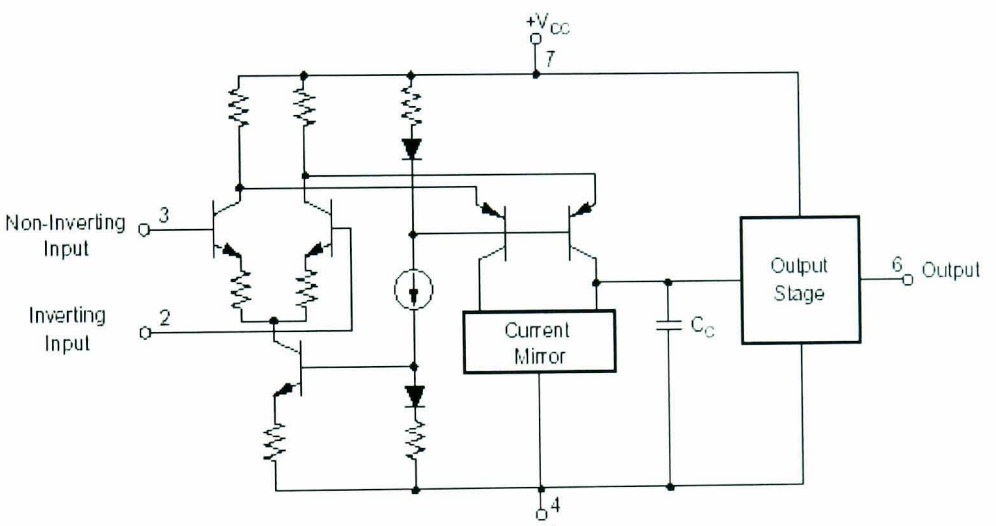

Figure 3.4 Fully symmetrical differential input stage of operational amplifier OPA620

The PSPICE model of the *OPA620* is the commercial model from Burr-Brown, Inc, which is useful when analyzing the performance of analogue circuits and systems using computer simulation. This model is particularly true for Video and RF amplifier circuits where parasitic capacitance and inductance can have a major effect on circuit performance. Simulation is performed to demonstrate the performance of the operational amplifier in the Howland topology circuit over the working bandwidth and designed constant current amplitude. The power supply and voltage source used in the simulation is set to the ideal situation without noise or other limitations.

3.5.1 Simulation 1: Howland circuit with a non-ideal op-amp

According to the product datasheet, the *OPA620* has ±3V input voltage range for accurate operation, and it is compensated for stability. With a desired output current 2mA maximum, two sets of simulations are carried out with the resistor values as Table 3.3.

Table 3.3 The resistor value settings in the Howland circuit simulation with different gain

	Gain	R1	R2	R3	R4	R5
Resistor setting 1	1.5	2kΩ	3kΩ	2kΩ	2kΩ	1kΩ
Resistor setting 2	3	1kΩ	3kΩ	1kΩ	2kΩ	1kΩ

Figure 3.5 is the Howland circuit for the simulation. The power rails for the operational amplifier are ±5V dc source without any wave frequency or noise included. The resistors *R1* to *R5* values are the nominal value in the Table 3.3. The simulation is applied with a frequency scanning from 1 kHz to 10MHz and with the resistance load changing from 200Ω to 2000Ω by a step of 200Ω. The simulation results are shown in Figure 3.6 and Figure 3.7, which show the output current changing versus loading and frequency.

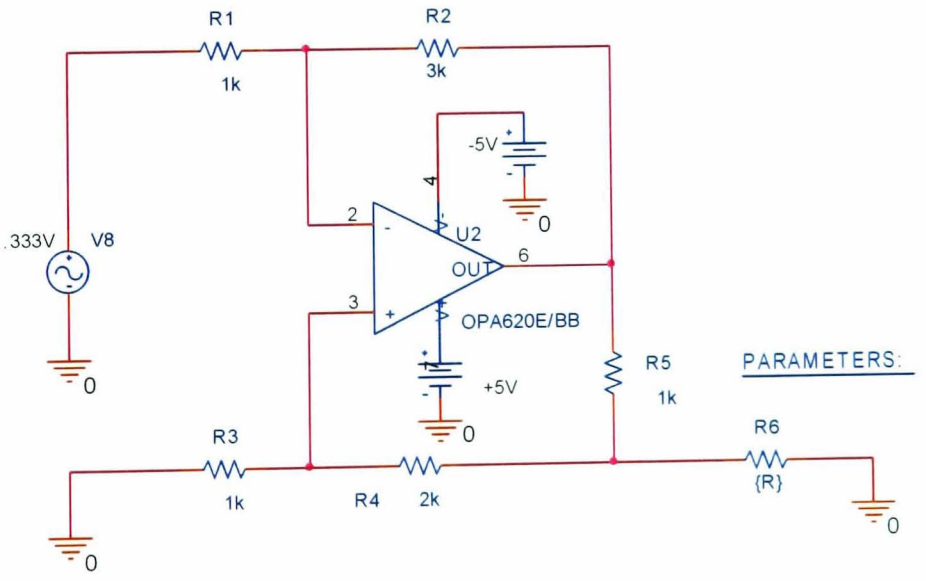

Figure 3.5 The Howland circuit in PSPICE simulation

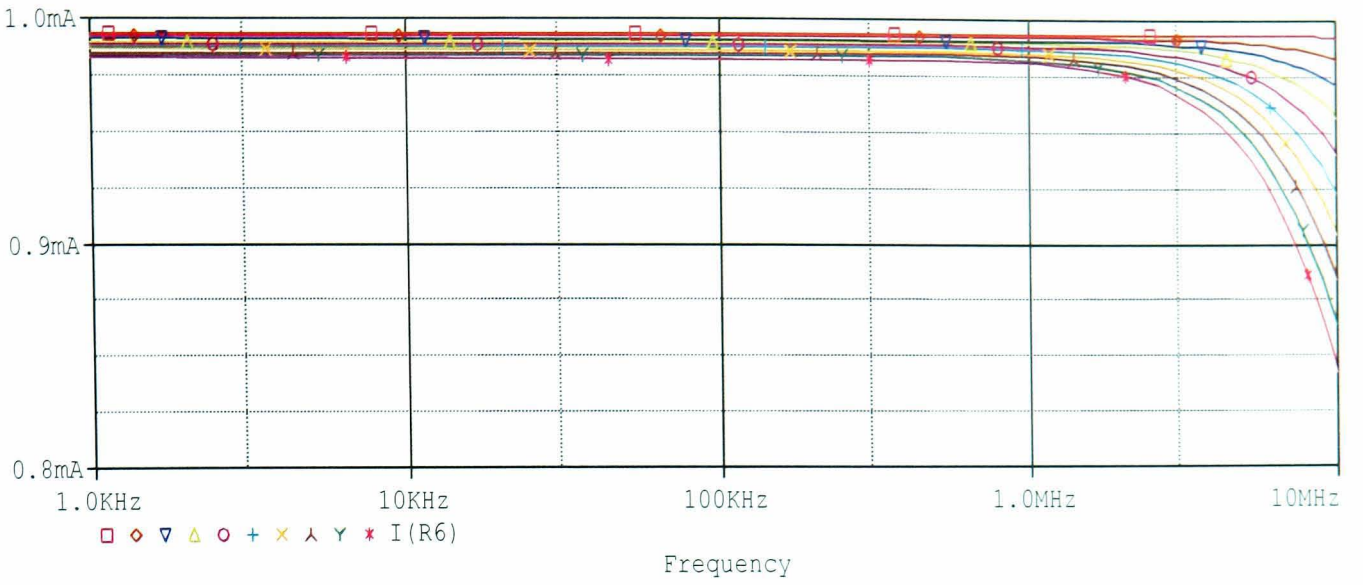

Figure 3.6 The Howland current source simulation: the current output versus the frequency with the resistor network setting 1 (loading is changed from 200Ω □ to 2000Ω · by a step of 200Ω)

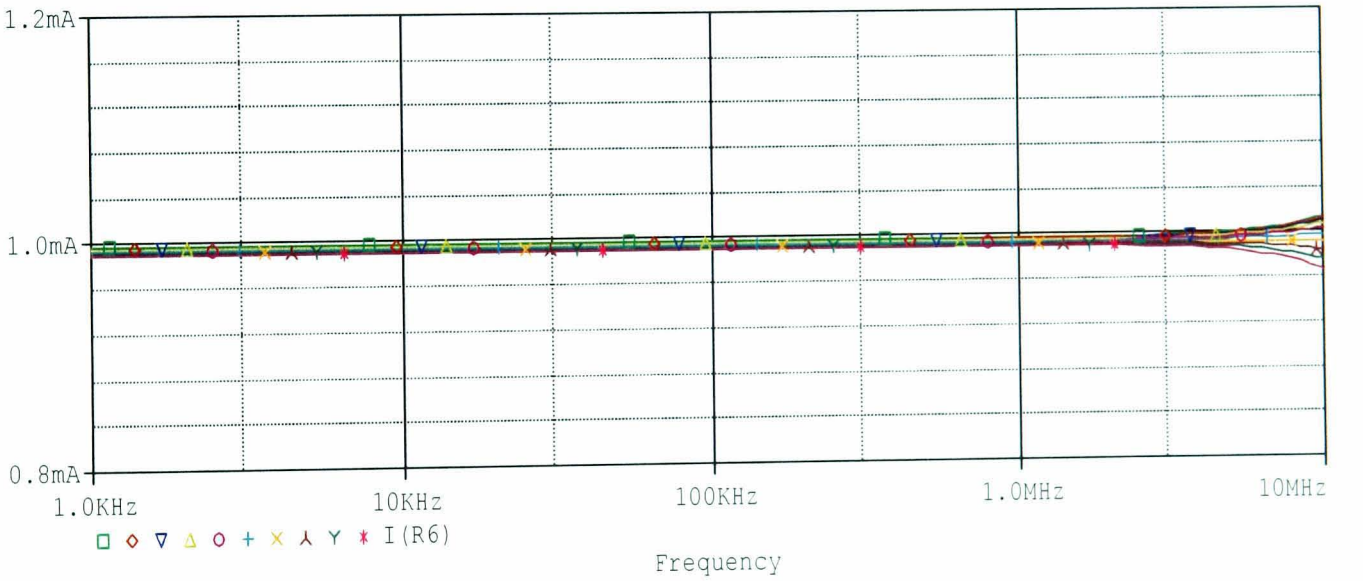

Figure 3.7 The Howland current source simulation: the current output versus the frequency with the resistor network setting 2 (loading is changed from 200Ω □ to 2000Ω · by a step of 200Ω)

Table 3.4 is the output impedance of the current source with two different resistor settings. The output impedance of setting 1 is smaller than the value of setting 2, and both of them are far away from desired value of the output impedance, as discussed in section 3.3.1, even though in this simulation the resistors are using their nominal values.

Table 3.4 The equivalent output impedance of the Howland circuit with different gain settings versus frequency

Frequency (Hz)	Circuit Setting 1 R1=2KΩ; R2=3KΩ; R3=2KΩ; R4=2KΩ; R5=1KΩ	Circuit Setting 2 R1=1KΩ; R2=3KΩ; R3=1KΩ; R4=2KΩ; R5=1KΩ
1K	162.19KΩ	254.33KΩ
10K	159.36KΩ	253.38KΩ
100K	156.64KΩ	254.33KΩ
1M	137.28KΩ	237.65KΩ
2M	95.10KΩ	201.62KΩ
5M	30.52KΩ	96.97KΩ

3.5.2 Simulation 2: compensated the Howland circuit

According to Eq3.26, with op-amp OPA620 (about 800 open-loop-gain at 250 kHz), the adjustment of resistor value can be worked out as shown in Table 3.5.

Table 3.5 Resistor R_3 value adjusted according to the limited open-loop gain at high frequency in the Howland circuit simulation

	Gain	R1	R2	R3	R4	R5
Resistor setting 1	1.5	2kΩ	3kΩ	**2010Ω**	2kΩ	1kΩ
Resistor setting 2	3	1kΩ	3kΩ	**1006Ω**	2kΩ	1kΩ

This simulation still uses the circuit as Figure 3.5 shown. The power rails for the operational amplifier is +/-5V DC source without any other waved frequency or noise included. The values of the resistors are kept as the nominal values in the

Table 3.5. The simulation is applied over 1kHz to 10MHz and with the resistance load changing from 200Ω to 2000Ω by a step of 200Ω. The simulation results are shown in Figure 3.8 and Figure 3.9, which show the output current changing versus load and frequency.

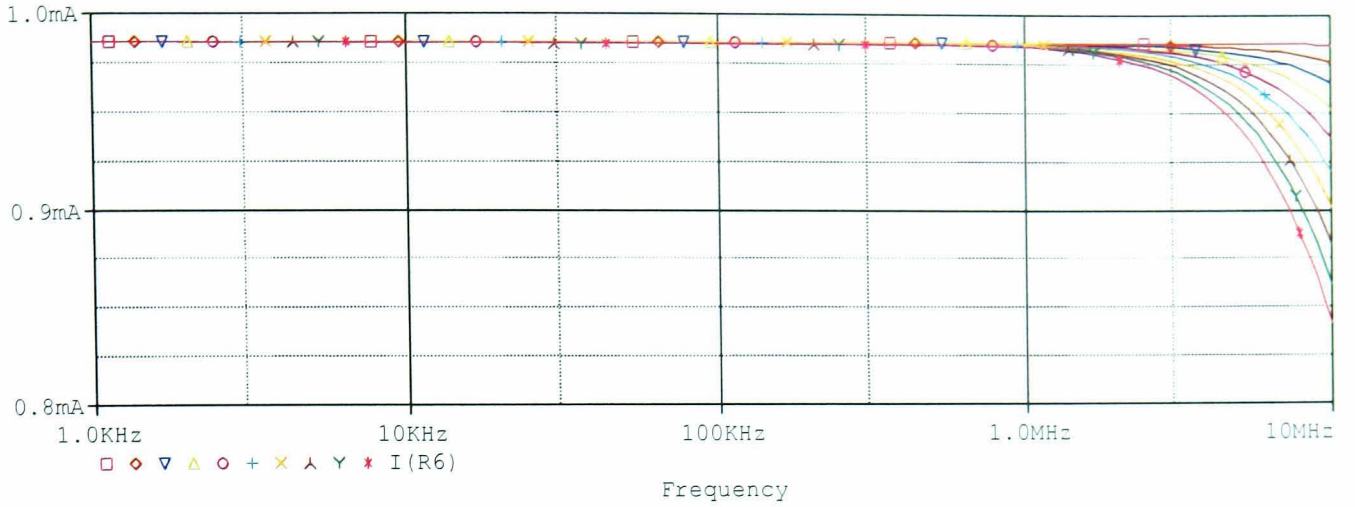

Figure 3.8 The Howland circuit simulation result with resistor setting 1 plus resistor value adjustment (loading is changed from 200Ω □ to 2000Ω · by a step of 200Ω)

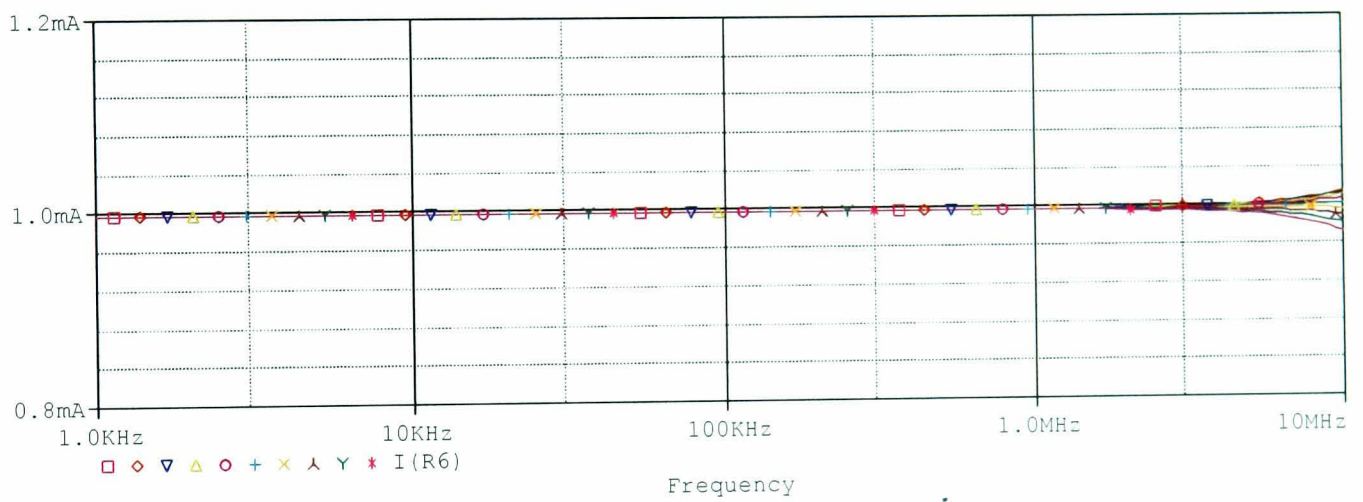

Figure 3.9 The Howland circuit simulation result with resistor setting 2 plus resistor value adjustment (loading is changed from 200Ω □ to 2000Ω · by a step of 200Ω)

Table 3.6 The improved equivalent output impedance of the Howland circuit with the consideration of the limited open-loop gain

Frequency (Hz)	Circuit Setting 1 R1=2KΩ; R2=3KΩ; **R3=2010Ω**; R4=2KΩ; R5=1KΩ	Circuit Setting 2 R1=1KΩ; R2=3KΩ; **R3=1006Ω**; R4=2KΩ; R5=1KΩ
1K	4.89MΩ	5.32MΩ
10K	3.17MΩ	3.99MΩ
100K	2.35MΩ	3.89MΩ
1M	717.66KΩ	2.28MΩ
2M	216.16KΩ	796.56KΩ
5M	30.52KΩ	149.41KΩ

Table 3.6 lists the calculated output impedance of the two circuit settings at the investigated frequency bandwidth. It can be seen that at the low frequency, the calculated output impedance have been improved comparing with the circuit settings without compensation. Still the circuit setting with high close-loop gain keeps larger output impedance as expected.

3.5.3 Simulation conclusions

In this section, two simulations using high-speed operational amplifier OPA620 commercial PSPICE model, have been carried out for the Howland circuit simulation. It shows that the simulation results agree to the previous mathematical/physical analysis on the operational amplifier. The new compensation method could be used in the practical circuit design and easy to be implemented.

1. According to the simulation results, it is seen that using the tight tolerance resistors in the circuit design, the main difficult is to match the resistor network.
2. In practice, the open-loop gain of an operational amplifier is limited, especially at high frequency. In this situation, to improve the output impedance further, it would be necessary to give certain compensation to the effect of limited gain.
3. Using tight tolerance resistors is an easy solution in the circuit implementation. If it is available, laser-trimming technique is more applicable.
4. For multi-channel current source design, it must consider not only the output impedances, but also the uniformity of the output current values. Otherwise, it has to use certain complicated calibration procedure to correct.
5. The performance of the current source also depends on the load being driven. The large load will cause the op-amp saturation if the load voltage is high.
6. At higher frequency, the performance of current source is significantly degraded by the stray capacitance of electronic components, such as op-amp and other passive devices. If the current is delivered by cable and multiplexers, the situation will become worse. Solving this problem has to be reply on the distributed system design and the active electrodes application, which will be discussed in the following chapters.

The results form basic guiding for the practical circuit design and are applied to the differential voltage controlled current source research.

3.6 The current source PCB design and test

3.6.1 The design of the printed circuit board of the current source

A differential current generator is built into a printed circuit board as Figure 3.10 shown. The package of the amplifier is small, surface-mount to ensure the smallest size of the physical circuit, to offer the best ac performance. In addition, all peripheral components are chosen as surface-mount package, which has low lead inductance.

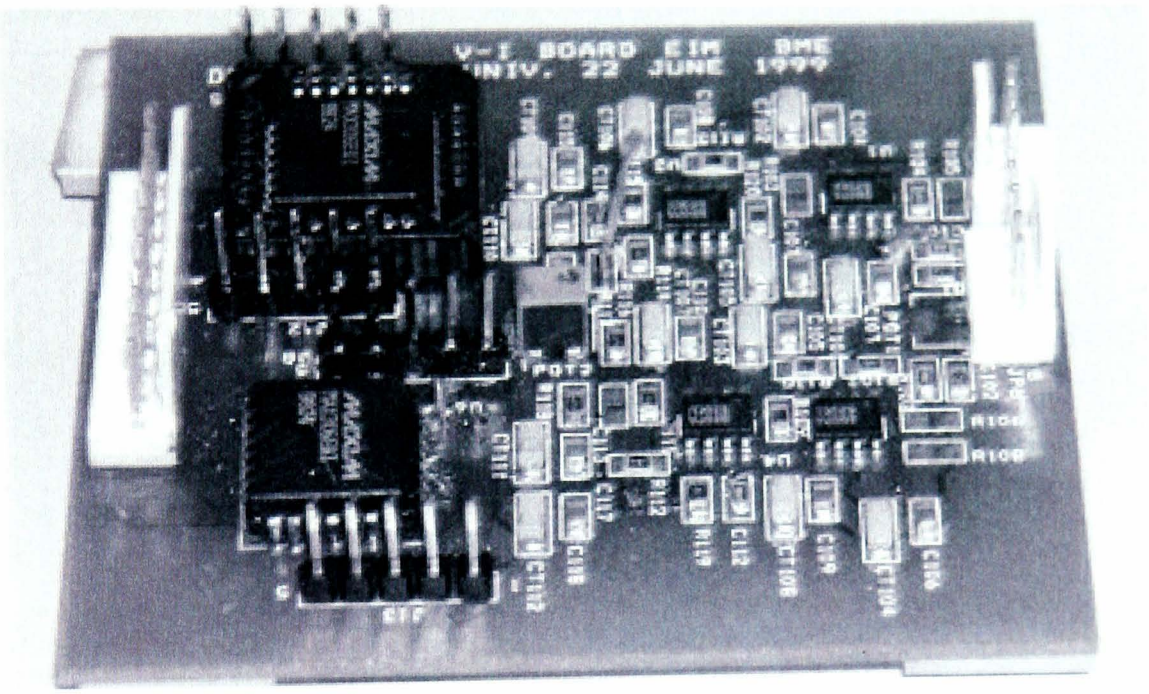

Figure 3.10 The current source

All printed circuit board tracks are laid as short as possible so that the current signal can be connected to the ground at the nearest place. Stray capacitances should be minimized, especially at high impedance nodes, such as the amplifier's input terminals. Stray signal coupling from the output or power supplies to the inputs should be minimized. All circuit element leads should be no longer than ¼ inch to minimize lead inductance. It will minimize the electromagnetic interference to the nearby circuit.

Power supply bypassing is extremely critical and must always be used, especially when driving high current loads. In the circuit, Tantalum capacitor 1μF and parallel ceramic 0.1μF are added to the power supply pins of the amplifier. The voltage signal transmitted from sine wave generator is terminated at 50Ω, matching the characteristic impedance of the transmission line.

Metal film resistors are chosen to improve the frequency and noise responses and matching of resistors is done manually using an ohmmeter.

The op-amp OPA620KU is the small outline and surface mount chip, which has internal laser trimmed compensation. This benefits the matching of two current circuits, which are built into the differential structure current source. In addition, it is a good pioneer work for distribute-system design.

3.6.2 *Test of the printed circuit board of the current source*

The output impedance of the current source can be determined using a measurement of the voltage on the different loads. In the diagram as shown in Figure 3.11, the voltages on the two load R and R' are measured as V and V' using a voltage meter. In addition, the output current I from the current source has the relationship with the output impedance of the circuit and the load resistance as

$$I = \frac{V}{Z_o // R} = \frac{V'}{Z_o // R'} \qquad \text{Eq3.28}$$

therefore, the output impedance Z_o can be derived from this equation:

$$Z_o = \frac{V' - V}{\frac{V}{R} - \frac{V'}{R'}} \qquad \text{Eq3.29}$$

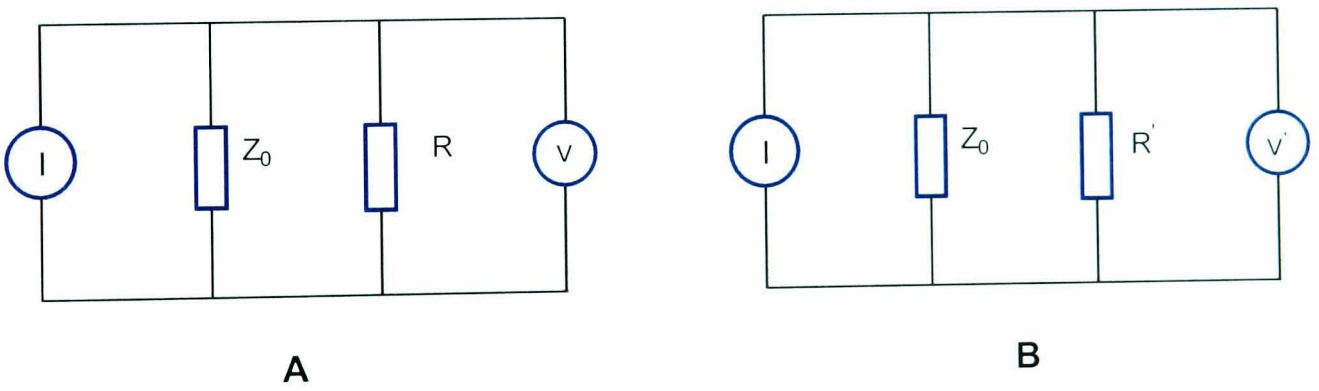

Figure 3.11 The current source equivalent output-impedance measurement

A digital oscilloscope (DSO 1604) is used to measure the voltage on the load resistor, which is connected in parallel with the load. The load resistance is changed from 100Ω to 1000Ω and the current frequency is chosen being measured at 20 KHz, 100 KHz, and 500 KHz, 1 MHz and 2 MHz.

The equivalent output impedance is shown in Figure 3.13. The resistor values are set as table 3.3 and table 3.5 respectively. Comparing the experimental result, as shown in Figure 3.13, with the simulation result, as shown in Figure 3.12, the adjustment on the resistor R_3 has improved the output impedance of the current source as expected, but the

change is smaller than expected. This is due to lack of fine adjustment on the resistor value, and accuracy of measurement tools.

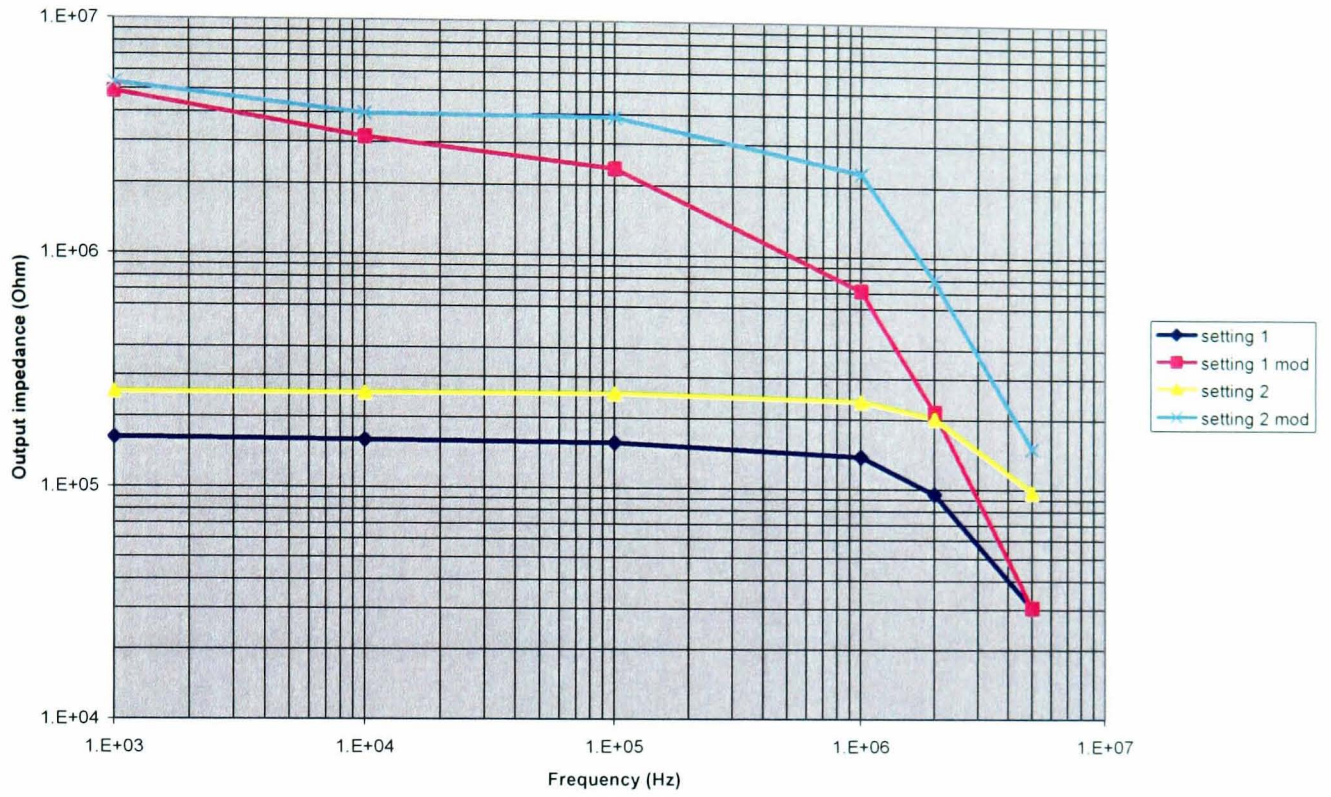

Figure 3.12 The Howland current source simulation: the output impedance versus frequency

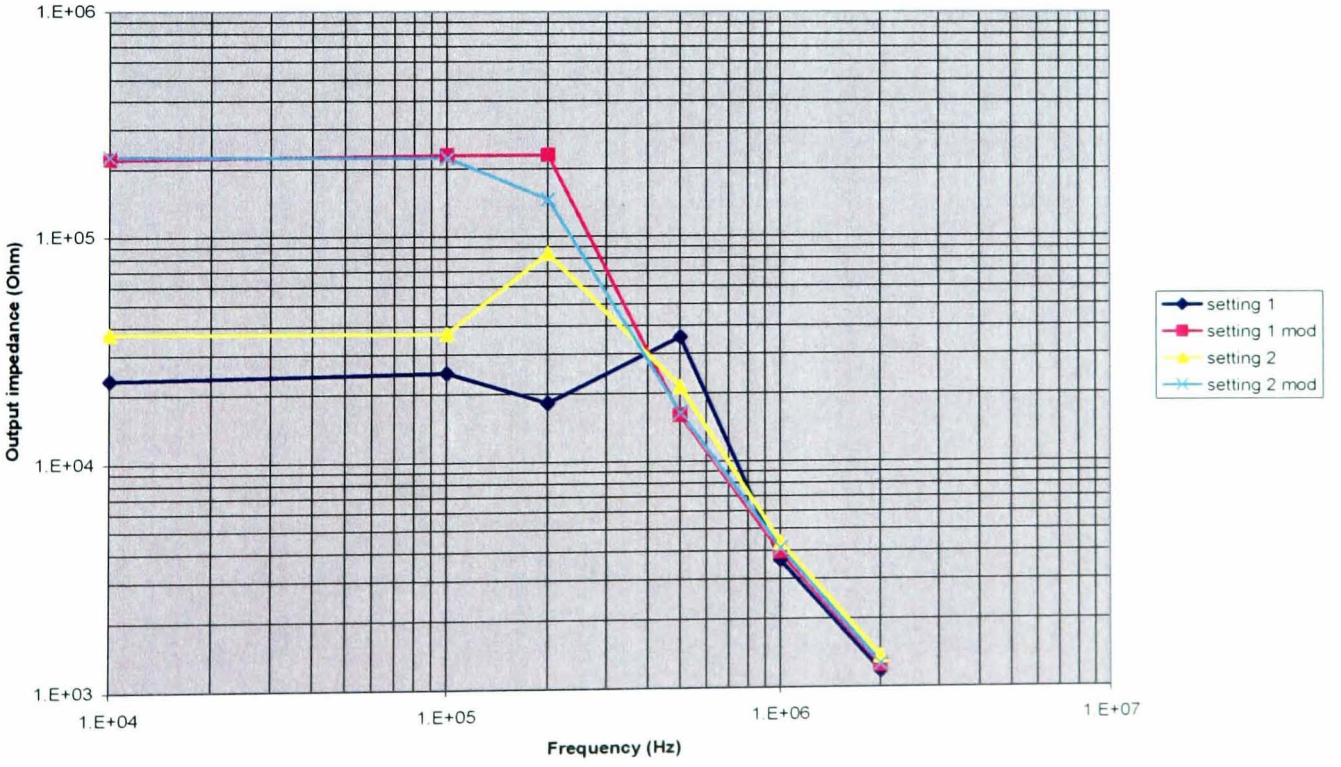

Figure 3.13 The Howland current source PCB circuit test: the output impedance versus frequency

Significantly, at frequency about 1 MHz, the performance of current source becomes worse, which can be seen from either experimental result or simulation result. Firstly, the working bandwidth of the op-amp has reached the limit, and over this frequency the phase shift will increase. As it has been mentioned earlier in this thesis, the high performance bandwidth is far smaller than the one provided in the datasheet. Secondly, the stray capacitance of printed circuit board played a critical role to demolish the performance of this circuit at high frequency. The output impedance of current source at higher frequency is still an issue in the future EIT system research and development.

3.7 Differential current source

If the current source is referenced to the ground, as shown in Figure 3.14, the voltage drops across the grounded electrode and the tissue. It induces a common mode voltage at the input terminal of the front-end amplifier. This common mode signal has several orders of magnitude higher than the differential signal to be measured. In order to limit its effect, a differential current source is used in most of EIT systems to inject a current into the conducting region. In this case, for a given injection configuration as shown in Figure 3.15, the common mode voltage is minimal for the pair of measurement electrodes opposed to the injection pair, that is, the pair corresponding to the weakest differential signal. In the absence of a common mode feedback, the closer one gets to the injection pair, the more the common mode voltage increases.

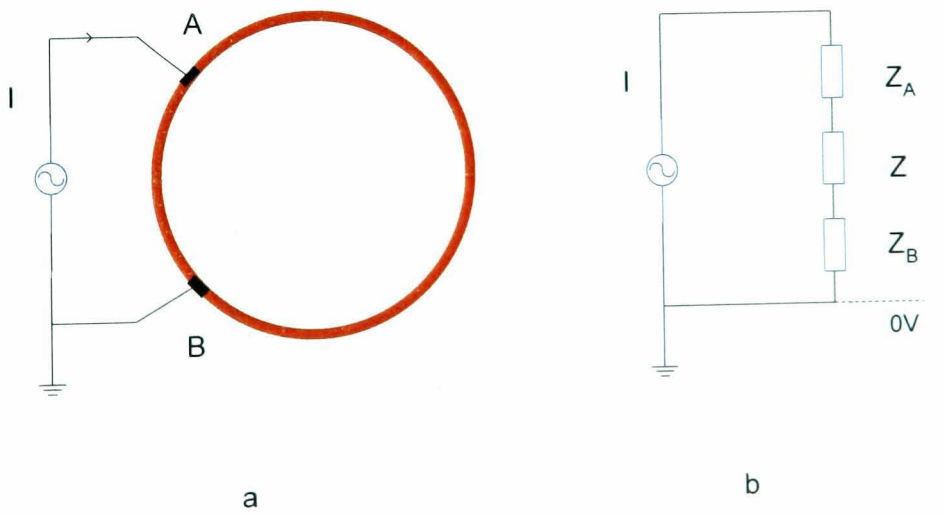

Figure 3.14 The single current source injection mode in electrical impedance measurement.

a) The current source is connected to the electrode pair (A and B) at the boundary of an object. b) The simplified circuit model of impedance measurement.

This design method is applicable to adjacent or diametric drive or any other method that involves the use of a pair of electrodes that inject current with equal amplitude and opposite phases.

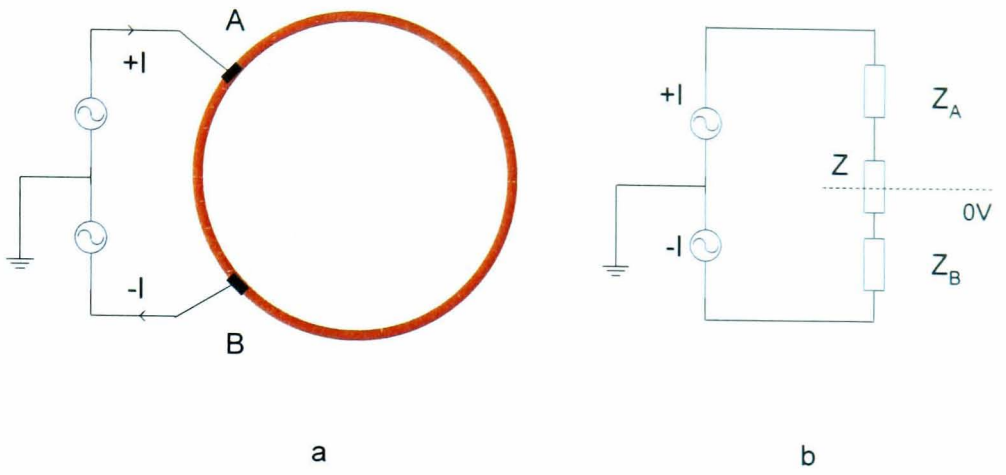

Figure 3.15 The differential current source injection mode in electrical impedance measurement

a) The current source is connected to the electrode pair (A and B) at the boundary of an object.
b) The simplified circuit model of impedance measurement

The equations giving the magnitude of the voltage-to-current conversion factor of a current source implicitly assume that the actual component values are identical to their nominal values and hence that the output impedance is infinite. In practice, however, the actual values of the resistors used always differ from their nominal values. This results in a value of current that differs from that calculated one. These approximations are generally acceptable if a single generator sourcing to earth via the load is used. When two generators are used to form a differential source, to deviation form the nominal current and output impedance values for each generator can have a marked influence on the overall circuit performance. The design of current sources for symmetrical drive in EIT must therefore take into account the tolerances of the components used.

The serial connection of two current sources would result in a conflict if the two sources have different output currents and infinite output impedance. In practice, however, two manufactured circuits always have different and finite output impedance values. The simplified electrical circuit model of the differential current source is shown in Figure 3.16. Z_1 and Z_2 are the output impedance of two current sources and I_1 and I_2 are the delivered currents. Z is the object impedance being measured. From the circuit

configuration, the current applied to the load can be derived

$$I = \frac{Z_1 \cdot I_1 + Z_2 \cdot I_2}{Z_1 + Z_2 + Z} \qquad \text{Eq3.30}$$

And the common mode voltage is

$$V_{com} = \frac{V_1 + V_2}{2} = \frac{Z_1 \cdot Z_2 \cdot (I_1 - I_2)}{Z_1 + Z_2 + Z} + \frac{Z \cdot (Z_1 \cdot I_1 - Z_2 \cdot I_2)}{2 \cdot (Z_1 + Z_2 + Z)} \qquad \text{Eq3.31}$$

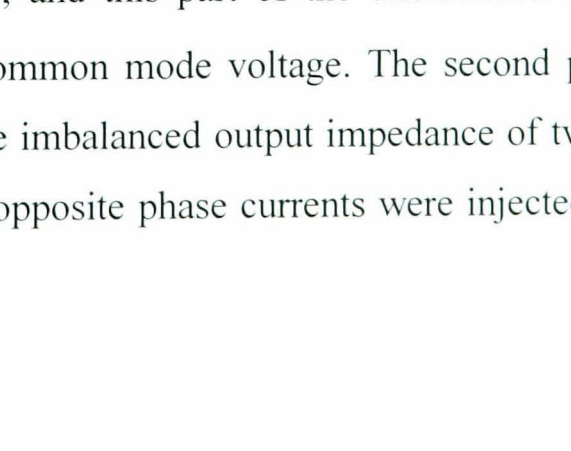

Figure 3.16 The differential current source equivalent electric model

From the equation Eq3.30, it can be seen that the injected current is slightly drifted away from the calculated value, which is to be used in the object impedance measurement. However, if each single current generator is designed with high enough output impedance, comparing with the load impedance being measured, the current drift can be ignored in the measurement and this imbalance will not be a large error source, even if these two current sources are not matched that well.

In the common mode voltage description Eq3.31, this imbalance induces some level of the common mode voltage to the front-end amplifier. It can be seen that the common mode voltage consists of two parts. One part is proportional with the different of two current amplitudes $I_1 - I_2$, and this part of the unbalanced current by-pass the output impedance to form the common mode voltage. The second part of the common mode voltage is produced by the imbalanced output impedance of two current sources, even if two equal amplitude and opposite phase currents were injected into the object. It can be seen, when $I_1 = I_2$

$$V_{com} = \frac{Z \cdot (Z_1 - Z_2) \cdot I_1}{2 \cdot (Z_1 + Z_2 + Z)} \qquad \text{Eq3.32}$$

Using the Howland circuit to build a differential current source, the output currents are still dominated by the resistor-network in Eq3.4. V_i and $V_i^{'}$ are two input voltages to the differential circuit. R_1 to R_5 and $R_1^{'}$ to $R_5^{'}$ are the resistors in respective position in the Howland topology, which form the differential current source. Z_o and $Z_o^{'}$ are the output impedance of these two circuits. Then V and $V^{'}$ are output voltages of two current generators.

$$-\frac{V_i \cdot R_2}{R_5 \cdot R_1} - \frac{V}{Z_o} = -\left(-\frac{V_i^{'} \cdot R_2^{'}}{R_5^{'} \cdot R_1^{'}} - \frac{V^{'}}{Z_o^{'}}\right) \qquad \text{Eq3.33}$$

Because Z_o and $Z_o^{'}$ are relatively large, the performance of this differential current source is relied on the matching of these two resistor networks. In addition, the voltage value of the differential inputs must have the same amplitude and 180° phase shift.

3.8 Voltage controlled current source (VCCS)

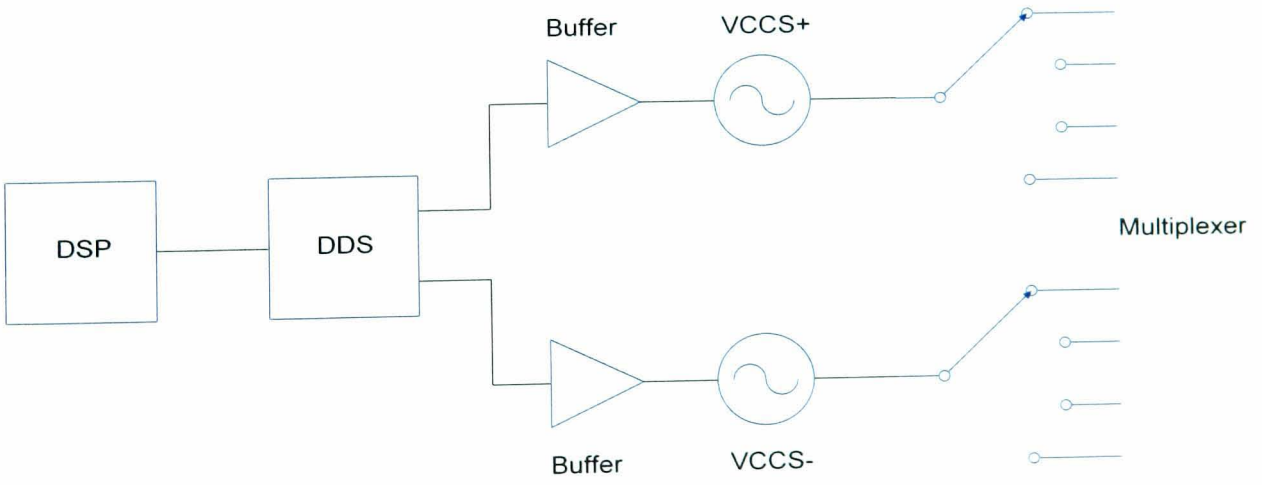

Figure 3.17 The direct digital synthesis VCCS block diagram and the current distribution

As discussed, the value of the Howland circuit output current is proportional to the input voltage, whether it is an inverting input or non-inverting input. In practice, the DSP can provide sine waveform to current generator by digital synthesizer. Therefore, the

applied current value can be adjusted flexibly in some circumstance according to the measured voltage signals on the electrodes. This function could give adaptive current value to improving signal-to-noise ratio. The diagram is shown in Figure 3.17.

The digital solution for a sine wave generator is a direct digital synthesizer, which using fast digital-to-analogue conversion technique can form any frequency and phase shift sine wave in its working bandwidth. Moreover, its amplitude of synthesized sine wave could be set freely with higher digital resolution.

In the MK2 system, the chip AD7008 (Analog Devices, Inc) is adopted for building the digital sine wave generator. The AD7008 direct digital synthesis chip is a numerically controlled oscillator employing a 32-bit phase accumulator, sine and cosine look-up tables, and a 10-bit D/A converter integrated on a single CMOS chip. Clock rates up to 20 MHz and 50 MHz are supported. Frequency accuracy can be controlled to one part in four billion [73]. The AD7008 is easy to interface to the DSP by serial or parallel mode. In addition, the DSP is able to control the signal amplitude directly programming the register on the chip.

The output of the digital-to-analogue converter is configured to be a single power supply, which simplifies the digital circuit power rails. However, it has to be transferred to a pure AC mode before it applies to the current generators.

3.9 Summary

In this chapter, the Howland circuit is discussed in detail in term of electrical circuit analysis, PSPICE simulation, and the printed circuit board experiments. The equivalent output impedance of the current source is the crucial parameter to ensure accuracy for four-electrode measurement. From the analysis, it is seen that the precision of peripheral resistors and the open-loop gain of the op-amp are the key issues to improve the output impedance of the circuit.

The tolerance of the peripheral resistor plays the first role in the development of Howland current source. However, it is still unbalanced by the open-loop gain of the op-amp. Manually adjusted resistors can be used for making a single high output impedance current source. However, as a manufacture operation, it makes this process more difficult to achieve.

Using higher negative feedback gain is shown to give the higher output impedance of the circuit, as seen in equation Eq3.10. This has been linked with the op-amp's gain-bandwidth product. The internal compensation inside the op-amp will also affect the bandwidth of performance.

At high frequency, the output impedance of current source is also degraded by the stray capacitance of the circuit. This situation can be improved by using multi-layer printed circuit board, small outline components and proper track connection or signal isolation.

The compensation method this chapter provided can improve the output impedance effectively, which just need an adjustment on R3 using formula Eq3.26. The designed output current value is not affected by this compensation and no extra component is need. This method makes the Howland circuit current source extremely applicable in the active electrode design.

The result of the Howland topology current source has been applied into the MK2 EIT system design. The generated current is multiplexed to the electrodes by means of connection cable.

Chapter 4 Voltage Measurement

4.1 Introduction

In the current drive configuration EIT system, a differential amplifier is used in the boundary signal collection. It is based on the four-electrode measurement principle, where two electrodes apply constant current into the object and the other two electrodes sense the differential voltage signal across it. Because no earth point is connected to the object being imaged, the method is called floating measurement. With some measurement configurations, the measured differential voltage is often much smaller than the common mode voltage that exists on each receiving electrode pair. Any mismatch of signal path converts the common mode voltage into the differential mode. This can cause large measurement error to the data set. Therefore, the front-end amplifier facing the receiving electrodes must have the ability to reject this common mode voltage to an acceptable level. This is known as common mode rejection. Especially at high imaging frequency, the stray capacitance of electronic components reduces the circuits' performance.

In electrical impedance measurements, the contact impedance due to improper contact between electrodes and the surface of object is time varying and may have a large value. This makes the measured object like a high output impedance signal source. Therefore, the front-end amplifier is required to have sufficient input impedance to cope with this situation.

Another problem existing in the EIT data acquisition systems is that the boundary voltage distributed on the object surface has a large dynamic range, especially when the adjacent electrode measurement configuration applies. It demands that the measurement circuit, including analogue-to-digital conversion, have a very high resolution with good signal-to-noise ratio.

In this chapter, the task focuses on design high input impedance and high common-mode rejection instrument amplifier, and a programmable gain amplifier to achieve precision voltage measurement.

4.2 Voltage Measurement on the Body Surface

In electrical impedance measurement, the four-electrode configuration can minimize the effect of the contact impedance of electrodes by using high output impedance current source. However, the voltage measurement electrodes still raise some issues on the circuit design with the consideration of the contact impedance, polarization potential and common mode voltage rejection etc.

4.2.1 Input impedance of the front-end amplifier

In the EIT data acquisition system, the voltage measurement is the crucial part of the circuit. This is affected by the time-varying tissue impedance, electrode/tissue contact impedance, and mismatch of the differential signal path. It is illustrated in Figure 4.1.

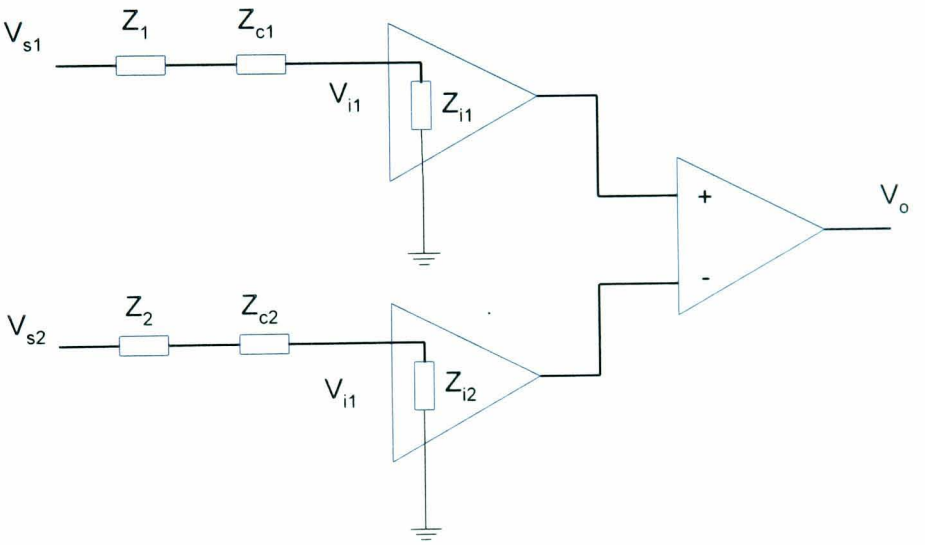

Figure 4.1 The equivalent electrical circuit model of the input stage of the front-end amplifier

In Figure 4.1, Z_1 and Z_2 are the trans-impedance on the measured points of the object surface; Z_{c1} and Z_{c2} are the contact impedance of electrode 1 and 2; and Z_{i1} and Z_{i2} are the input impedance of the front-end amplifier or voltage buffer. Here the effect of the co-axial cable and other connections are ignored and it will be discussed in the Chapter 5. So the voltages onto the input terminal of amplifier V_{i1} and V_{i2} are the values of resistor dividers at V_{s1} and V_{s2}, that is

$$V_{i1} = \frac{Z_{i1}}{Z_1 + Z_{c1} + Z_{i1}} \cdot V_{s1} \qquad \text{Eq4.1}$$

and $$V_{i2} = \frac{Z_{i2}}{Z_2 + Z_{c2} + Z_{i2}} \cdot V_{s2} \qquad \text{Eq4.2}$$

Because of the uncertainty of electrode/tissue contact impedance, the value may be changed between tens to hundreds ohms depending on the electrode material. Contact impedance is produced by connection of two different materials and obviously is complex impedance having capacitance. Consequently, the contact impedance is a function of frequency. At low frequency, the capacitance of the contact impedance will induce phase shift imbalance to the differential input signal paths. It can be seen that the input voltage onto the front-end amplifier is varied by the sum of the source impedance and contact impedance; therefore, the front-end amplifier must have a large input impedance to minimize this unwanted change of voltage on the sensing electrodes.

4.2.2 *Common mode voltage rejection*

Using a floating current source will induce large common mode voltage to the object to be imaged due to no common reference point. The differential Howland topology current source, which is discussed in Chapter 3, is not a floating current source and provides a ground plane somewhere in the imaging area between the two current electrodes. In the homogeneous impedance distribution of the imaged object, this ground plane nearly cuts the area into two equal parts, as shown in Figure 4.2. It may not be at the diameter position due to the imbalance of the differential current source. In this design configuration, the largest common mode voltage encountered on the object is the voltage on the electrode that is injecting current into the imaging area. Other researchers [33] reported the value of this common mode voltage at around $1.7V_{P\text{-}P}$ for an injected current of 1mA. Actually, the common mode voltages on the other receiving electrodes are much smaller than this value.

However, the differential voltage on the receiving electrodes changes with position and voltage measurement strategy. For some imaging algorithms, the interesting part of the measurement is the part changing with physiological activity, which does not concern the absolute value of the voltage on the electrode, or on the imaging point of view, the absolute value of impedance of imaging area, but the relative change with physiological activity. In this case, it is essential that the differential measurement being used to acquire the differential voltage on the electrode pair must be designed with a high common-mode voltage rejection capability.

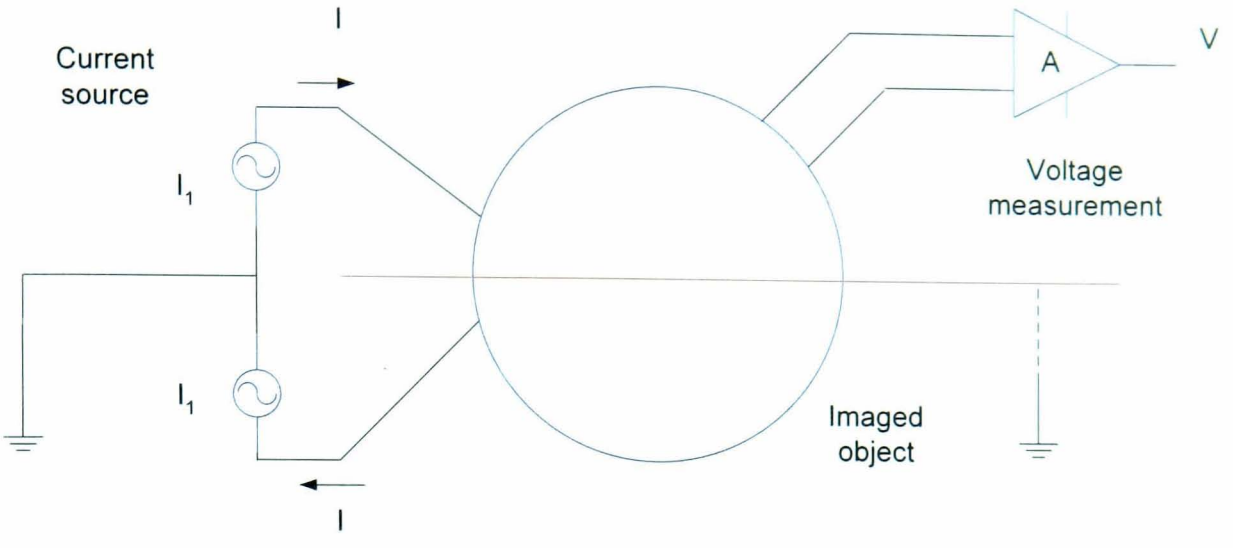

Figure 4.2 The differential voltage measurement with the grounded differential current source driving

In the practical electronic measurement, any imbalance of differential circuit converts a common mode voltage to a differential signal and brings errors to the measurement. Common mode rejection ratio (CMRR) defines the ability of a measurement system to accurately resolve difference measurements in the presence of common-mode voltages. It is shown in Eq4.3, where A_d is the differential gain of a system and A_c is the common gain of a system.

$$CMRR = 20\log\left|\frac{A_d}{A_c}\right| \qquad \text{Eq4.3}$$

Figure 4.3 shows the electric resistance mesh made in the PSPICE simulation software. This mesh is used to simulate 2-dimentional imaging object. The building block is resistor or resistor with parallel-connected capacitor, which could be given the value near the bio-impedance - complex impedance as a substitute of body tissue. This approach was first used by the Cardiff group for electronic circuit test purpose [74]. Here it is used to find the amplitude of common mode voltage and differential mode voltages on each receiving electrode pair with adjacent driving and receiving strategy. From this simulation result, it is possible to derive the dynamic range of voltage measurement and common mode rejection demand for taking an accurate measurement.

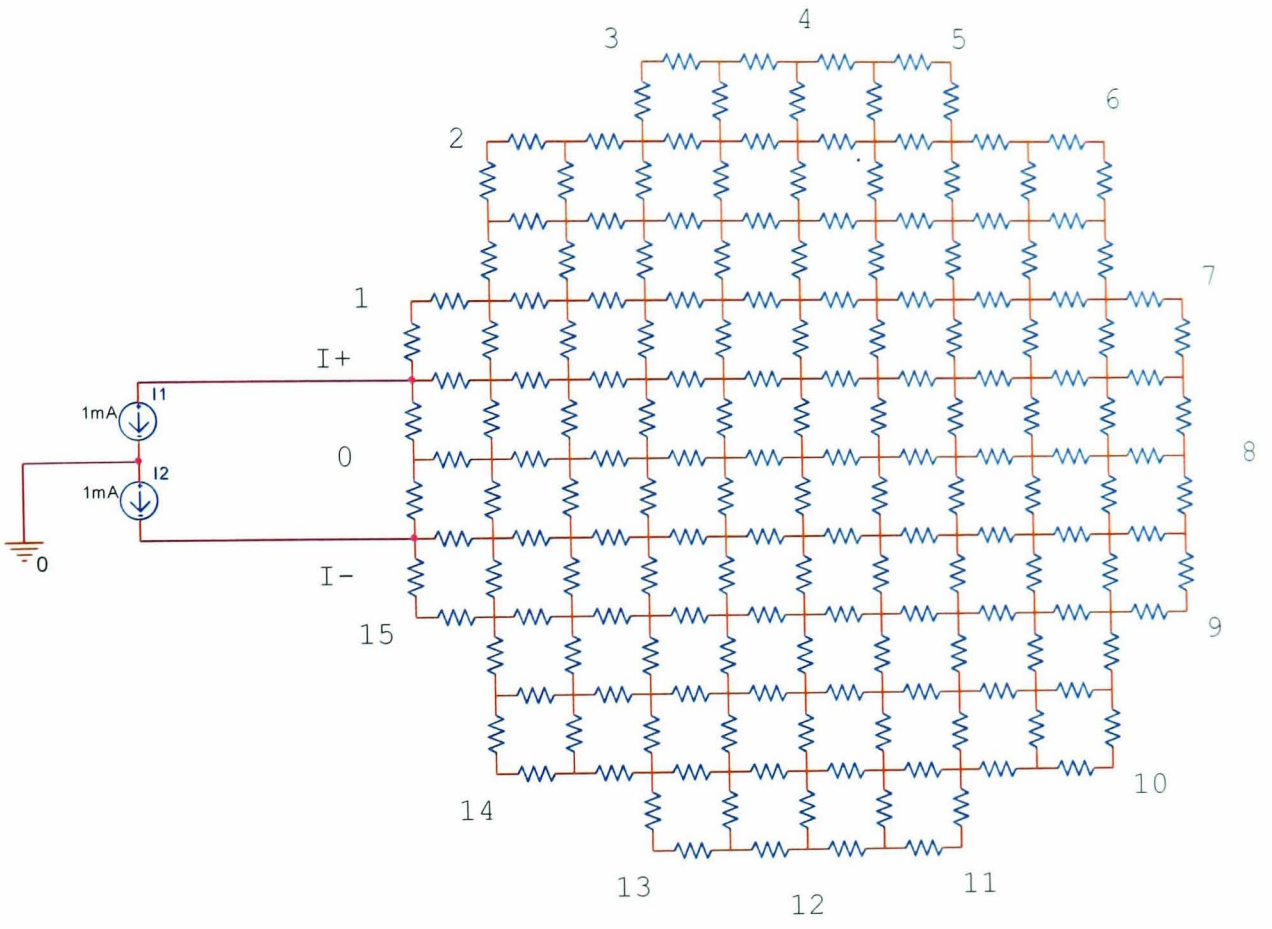

Figure 4.3 The electrical resistance phantom (the electrodes position are marked by numbers)

On this physical mesh, all the values of resistors are made uniform to represent a homogenous distribute impedance object. The ratio of common mode voltage to differential mode voltage is not affected by resistor values and the amplitude of injected current due to the properties of two-port electric network. If the accuracy of measurement is α, then the ratio of A_d and A_c should satisfy the condition Eq4.4, in which V_c is common mode voltage and V_d is differential mode voltage.

$$\frac{A_d}{A_c} > \frac{V_c}{\alpha \cdot V_d} \qquad \text{Eq4.4}$$

Figure 4.4 shows the common mode voltage on the electrodes (red) and the differential voltage (green) on the neighbour receiving electrode pairs. It can be seen that the receiving electrodes, positioned away from the current injecting electrodes, have a smaller voltage signal and the largest common mode voltage is located on the receiving

electrode that is near the current injecting electrode. Obviously, the more electrodes that are arranged on the surface of the object, the larger the CMRR needed to maintain the accuracy of differential measurement. In practice, this is very difficult to ensure, because under certain conditions tissues with different conductivity can dramatically change the current field distribution inside the object and present a small differential voltage on the boundary electrode pair. Figure 4.5 shows the CMRR needed for the differential measurement in 16 channels based on the homogenous distribution of impedance inside the object.

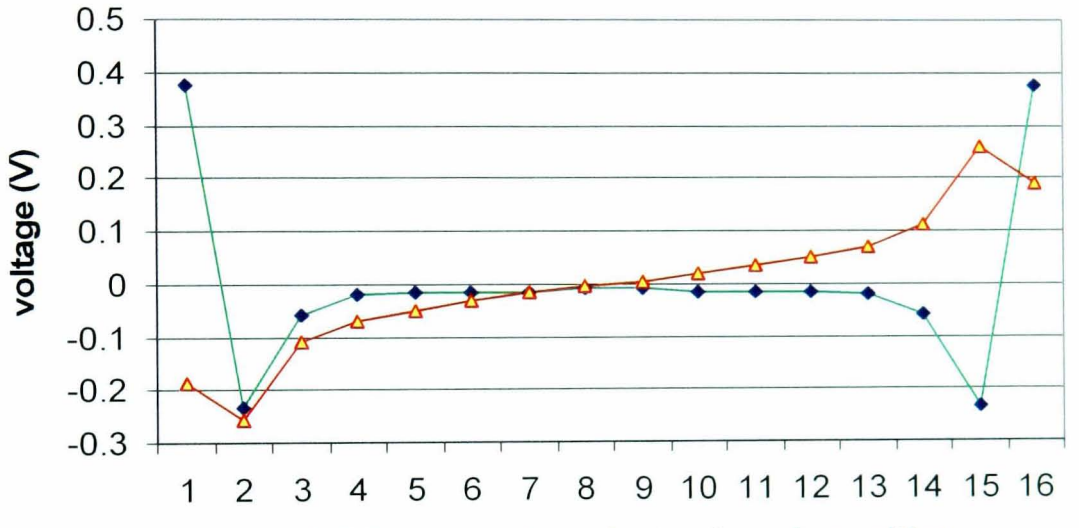

Figure 4.4 Neighbour receiving electrode pair: differential voltage (green) and common mode voltage (red) in 16 electrodes configuration

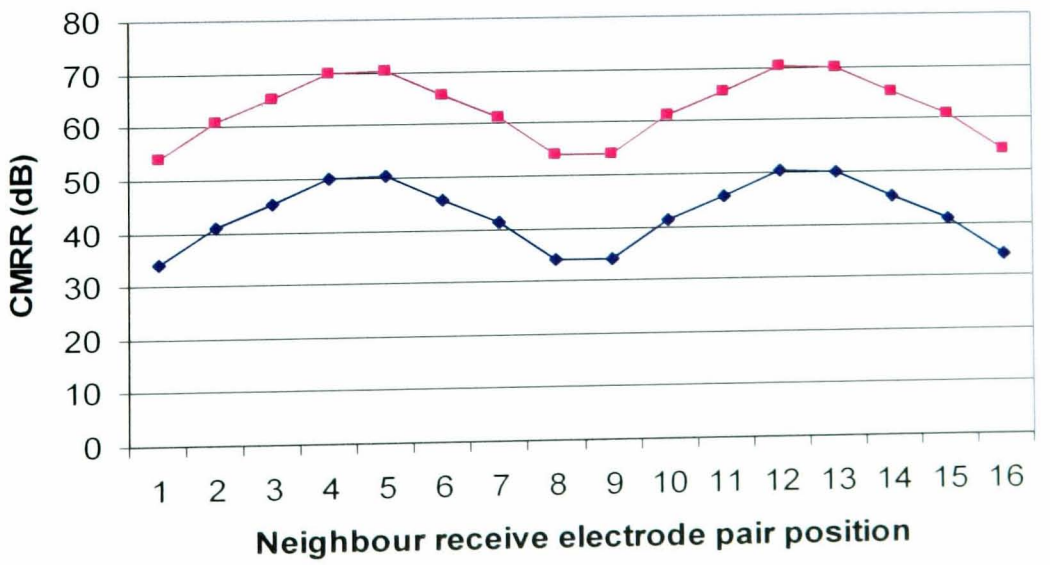

Figure 4.5 The CMRR of front-end amplifier needed for restrain common voltage error less than 1% (black) or 0.1% (pink)

The above analysis provides a relative error of data and the error value is proportional to the measured voltage. However, actual measurement error is also introduced by several other circuit factors like noise level and quantization error, etc. The quantization error is dominated by the sampling resolution of analogue-to-digital converter. For 12-bit analogue-to-digital converter, the resolution of measurement system is 2.44mV in ±5V voltage swing range. It can be calculated that, if the common mode voltage is 5V, the CMRR of the front-end amplifier is required to 66dB to keep the common mode signal error less than the quantization error. Using a programmable gain amplifier could minimize the quantization error when the voltage signal is small and simultaneously provides more detail information in the middle part of the imaged object.

The imaging reconstruction algorithm actually should identify the needed CMRR of the front-end amplifier, which is sensitive to the measurement error. Because this common mode voltage is not a random signal, the effect on the computing process cannot be removed by signal processing.

4.2.3 Electric potential of polarization on the receiving electrodes

The receiving electrodes sense the voltage on the boundary of the imaged object. However, at same time, they also generate slowly changing electric potential to the front-end amplifier due to the chemical reaction between two different contact materials. In frequency domain, this slow changing potential includes the frequencies from dc to tens of hertz and it is obviously different from the imaging frequency used in the EIT data acquisition system, which is from 1 KHz to 2 MHz. For this reason in the principle of signal process, it will be easy to be removed from the signal path before the voltage being measured.

The amplitude of polarization potential on the electrodes could be as high as hundreds millivolt that depends on the material of electrodes. This large value of potential would saturate the signal path easily if no high-pass filtering stage existed.

The position of the high-pass filtering in the signal path is designed under the considerations as:

1. The high-pass filtering will not affect the input impedance of the front-end amplifier, which is crucial to reject the common mode voltage from the signal path.

2. The polarized voltage could saturate the amplifier due to its relatively large amplitude. Therefore, it must be taken into account at designing the gain of amplifier.

3. The polarization potential is a high amplitude and slow changed voltage. In the frequency domain, this signal is very separated from imaging frequencies.

4. The RC constant of high-pass filtering stage will dominate the system time constant and makes the data acquisition system need longer time for signal settling, which will slow down the sampling speed of data acquisition system.

4.3 Design of Front-End Amplifier

The structure of the front-end amplifier has many options in the wide band imaging system. In the measurement system, the front-end amplifier plays two roles: a) achieve the impedance transform from the high impedance signal source to low impedance, b) amplify the signal to proper measurable amplitude and improve the signal-to-noise ratio. The benefit of using buffer structure is that the circuit can be built into electrode body as active electrode without the effect of co-axial cable connection between electrodes and front-end amplifier. It means the capacitance effect from the cable and multiplexer will be eliminated and it makes the measurement near the ideal situation, as illustrated in Figure 4.6

The common mode voltage rejection of op-amp is achieved in the integrated circuit manufacturing process using laser trim technique to match the differential signal path. In wide band measurement system design, it is a challenge at high frequency band due to the complex impedance performance of physical devices.

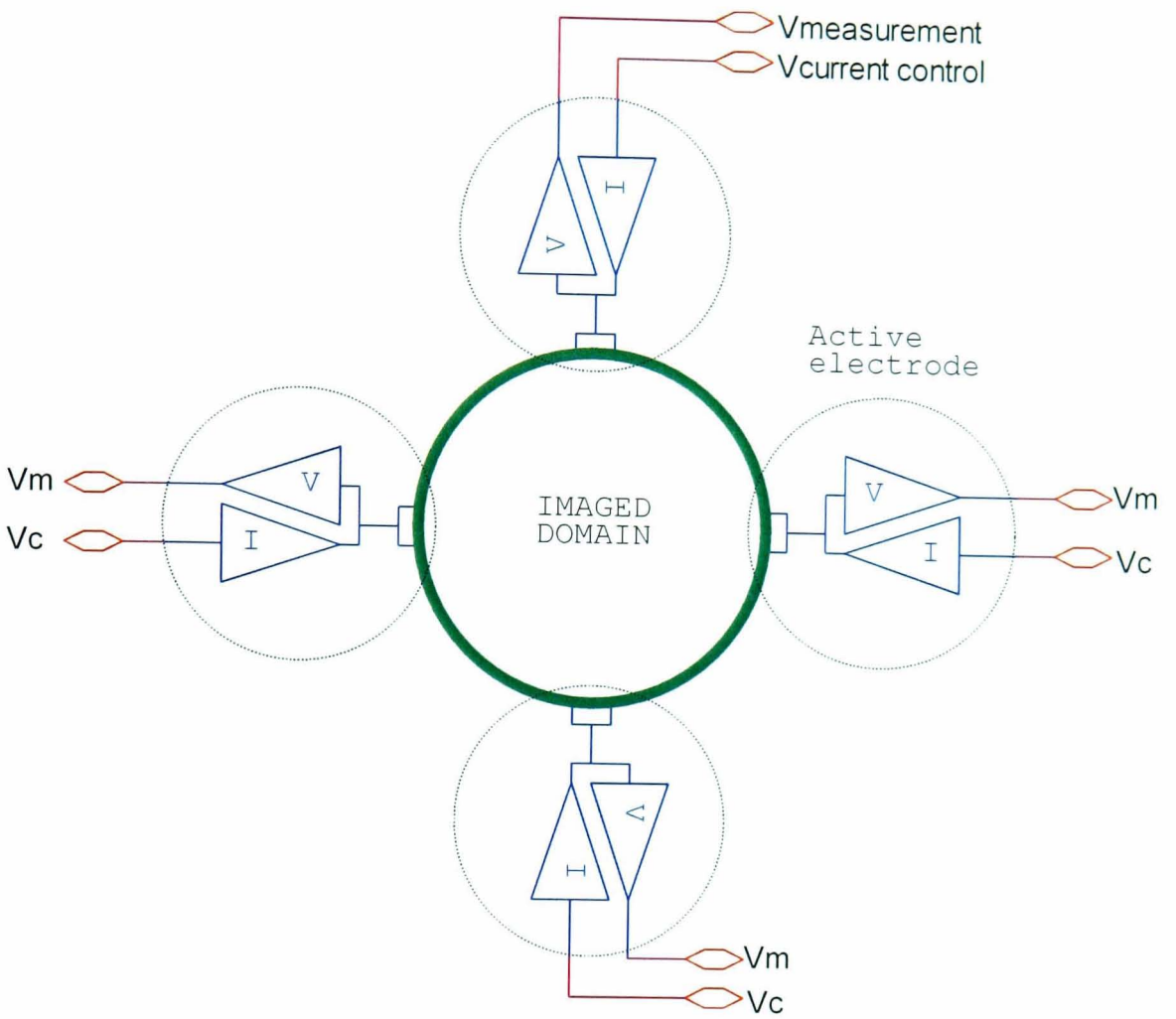

Figure 4.6 The block diagram of the active electrode configuration

4.3.1 High CMRR Instrument Amplifier

Instrument amplifier implemented in a three-op-amp topology is normally used in the four-electrode measurement to achieve the signal source impedance transform. Its structure is shown in Figure 4.7. Op-amp *A1* and *A2* are the differential amplifier pair served as first stage of instrument amplifier, and A3 transforms the differential signal into the single end mode. The signals V_{s1} and V_{s2}, are in differential mode to the differential amplifier inputs, and V_{sc} is common mode signal that V_{s1} and V_{s2} ride on. Therefore, after the differential stage of the instrument amplifier, the output V_{o1} and V_{o2} are:

$$V_{o1} = V_{s1} \cdot \left(1 + \frac{R_2}{R_1}\right) - V_{s2} \cdot \frac{R_2}{R_1} + V_{sc} \qquad \text{Eq4.5}$$

and

$$V_{o2} = V_{s2} \cdot \left(1 + \frac{R_3}{R_1}\right) - V_{s1} \cdot \frac{R_3}{R_1} + V_{sc} \qquad \text{Eq4.6}$$

In the description of the outputs of first stage, the differential mode voltage is amplified by the gain of the amplifier, but the common mode voltage is still kept as the input amplitude. As a result, the CMRR of differential amplifier will increase with increasing of differential gain. However, in practice when the input gain is high, the common mode input voltage affects the bias point on the instrument amplifier's input transistors, and inherent mismatches in the input circuitry cause changes in the output voltage. The CMRR increasing stops at too high gain settings because of these mismatching and bias-point changes.

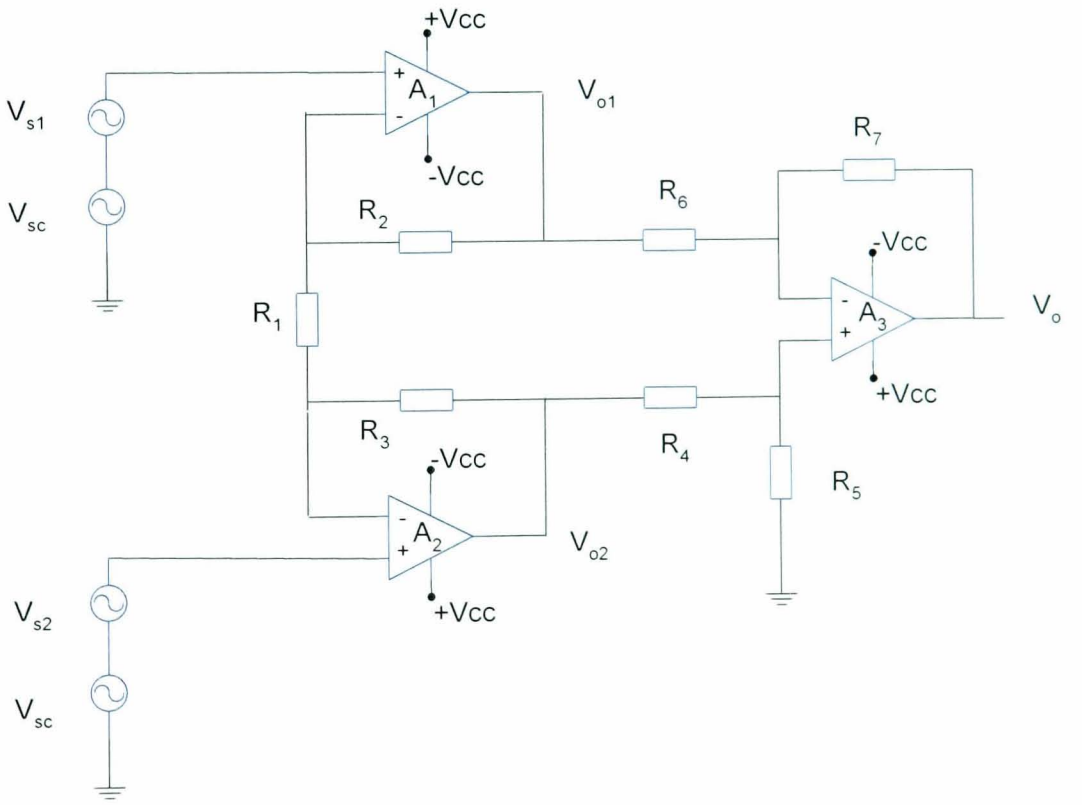

Figure 4.7 The circuit analysis of instrument amplifier

At the output stage of the differential amplifier, combining the two equations Eq4.5 and Eq4.6, the op-amp A3 eliminates the common mode voltage V_{sc} when $\frac{R_{-}}{R_6} = \frac{R_5}{R_4} = k_o$ and $\frac{R_2 + R_3}{R_1} = k_i$

$$V_o = (V_{s2} - V_{s1}) \cdot (1 + k_i) \cdot k_o \qquad \text{Eq 4.7}$$

If the differential gain of the instrument amplifier is A_d

$$A_d = (1 + k_i) \cdot k_o \qquad \text{Eq 4.8}$$

For well-designed instrument amplifier, the output voltage just includes the differential mode voltage from the receiving electrode pair. In practice, the mismatch of resistor network induces certain amount of common mode voltage into the output signal. This common mode error voltage V_{oc} can be described as

$$V_{oc} = V_{sc} \cdot \left(1 + \frac{R_7}{R_6}\right) \cdot \left(\frac{R_5}{R_4 + R_5} - \frac{R_7}{R_6 + R_7}\right) \qquad \text{Eq4.9}$$

If the tolerance of resistors used in the network is α, the maximum common mode gain of instrument amplifier will be $A_{c\max}$ in worst case as

$$A_{c\max} = \left(1 + k_o \cdot \frac{1+\alpha}{1-\alpha}\right) \cdot \frac{k_o}{1 + k_o} \cdot \left(\frac{4 \cdot \alpha}{1 - \alpha^2}\right) \qquad \text{Eq4.10}$$

It will approximately equal to

$$A_{c\max} \approx 4 \cdot k_o \cdot \alpha \qquad \text{Eq4.11}$$

when $(1-\alpha)^2 \approx 1$ as α normally quite small. Combining descriptions of A_d in Eq 4.8 and $A_{c\max}$ in Eq4.11 with definition of the CMRR of the instrument amplifier in Eq4.3, the minimum CMRR with the different input stage gain k_i and the tolerance of resistor α can be worked out as

$$CMRR > 20 \cdot \log \frac{1 + k_i}{4 \cdot \alpha} \qquad \text{Eq4.12}$$

It is deprived with the assumption of using ideal op-amp. From Eq4.12, the gain of second stage amplifier does not affect the common mode rejection of the whole circuit. Table 4.1 calculates some examples using above analysis.

Table 4.1 CMRR of Instrumentation Amplifier with different tolerance resistors

CMRR		Precision of resistors 5%	1%	0.1%
Input stage Gain k_i	1	20dB	34dB	54dB
	4	28dB	42dB	62dB
	8	33dB	47dB	67dB

The increasing of CMRR of the instrument amplifier can be derived using high precision resistors and larger gain settings on input stage. However, the large input gain setting causes an op-amp to saturate due to the large amplitude of common mode signal.

In the case of EIT application, this common mode signal mainly comes from polarization potential on the receiving electrodes. To remove the effect of this slow changed voltage from front-end amplifier, the high-pass filtering stage has to be used into the practical design and the values of resistor and capacitor need to be calculated carefully to avoid damaging the common mode rejection and the high input impedance of the instrument amplifier. At high imaging frequency, the instrument amplifier circuit needs matching not only the resistance of the peripheral components, but also the stray capacitance.

4.3.2 High-pass filtering and the input impedance of the instrument amplifier

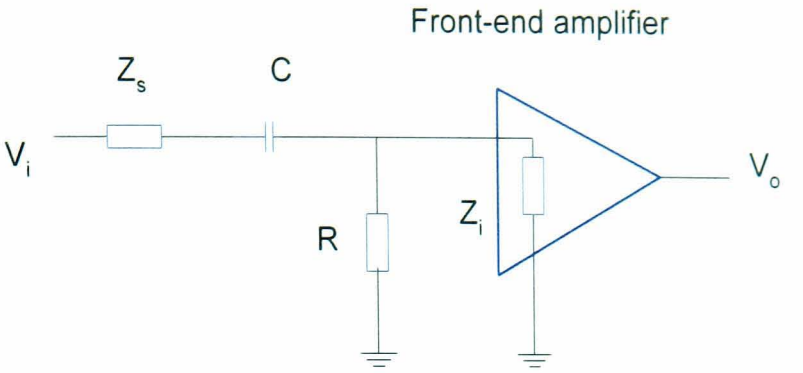

Figure 4.8 The front-end amplifier with limit input-impedance Z_i and a high-pass filtering

Figure 4.8 is the equivalent electric circuit of signal input path, in which Z_S is the summation of source impedance and contact impedance and Z_i is the input impedance of the amplifier. Resistor R and capacitor C is the high-pass stage to stop the slow varying draft voltage. As it is analyzed in section 4.2.1, the effect of uncertainty due to Z_s in the measurement has to satisfy the condition Eq4.13 if the desired measurement accuracy is given as β,

$$\left| \frac{Z_s}{Z_s + R // Z_i + \frac{1}{j\omega C}} \right| < \beta \qquad \text{Eq4.13}$$

in which ω is the applied current frequency. The cut-off frequency of this high-pass filtering ω_{cutoff} is assigned in the system design, which is far less than the applied current frequency. The value of capacitor C and resistor R are chosen according to

$$CR = \frac{1}{\omega_{cutoff}} \qquad \text{Eq 4.14}$$

and the value of R should satisfy the condition:

$$R > \frac{Z_s}{\beta} \qquad \text{Eq 4.15}$$

Some commercially available op-amps are integrated with field-effect transistor (FET) as input stage, which can provide input impedance as high as $10^{12}\Omega$ with input capacitance 1pF. As the imaging frequency is less than 1MHz, the op-amp performs with large input impedance that makes Eq 4.14 and Eq 4.15 true. However, at high frequency the effect of the input capacitance of the op-amp cannot be ignored. Accordingly, the input impedance of op-amp decreases with the applied current frequency increasing.

Fortunately, the contact impedance is also a function of frequency and it decreases with increasing imaging frequency. Above RC setting can still be used at the high frequency imaging.

To maintain the high CMRR of the differential amplifier, the matching of the differential signal path is crucial and high precision components have to be chosen.

4.3.3 *Building of the printed circuit board*

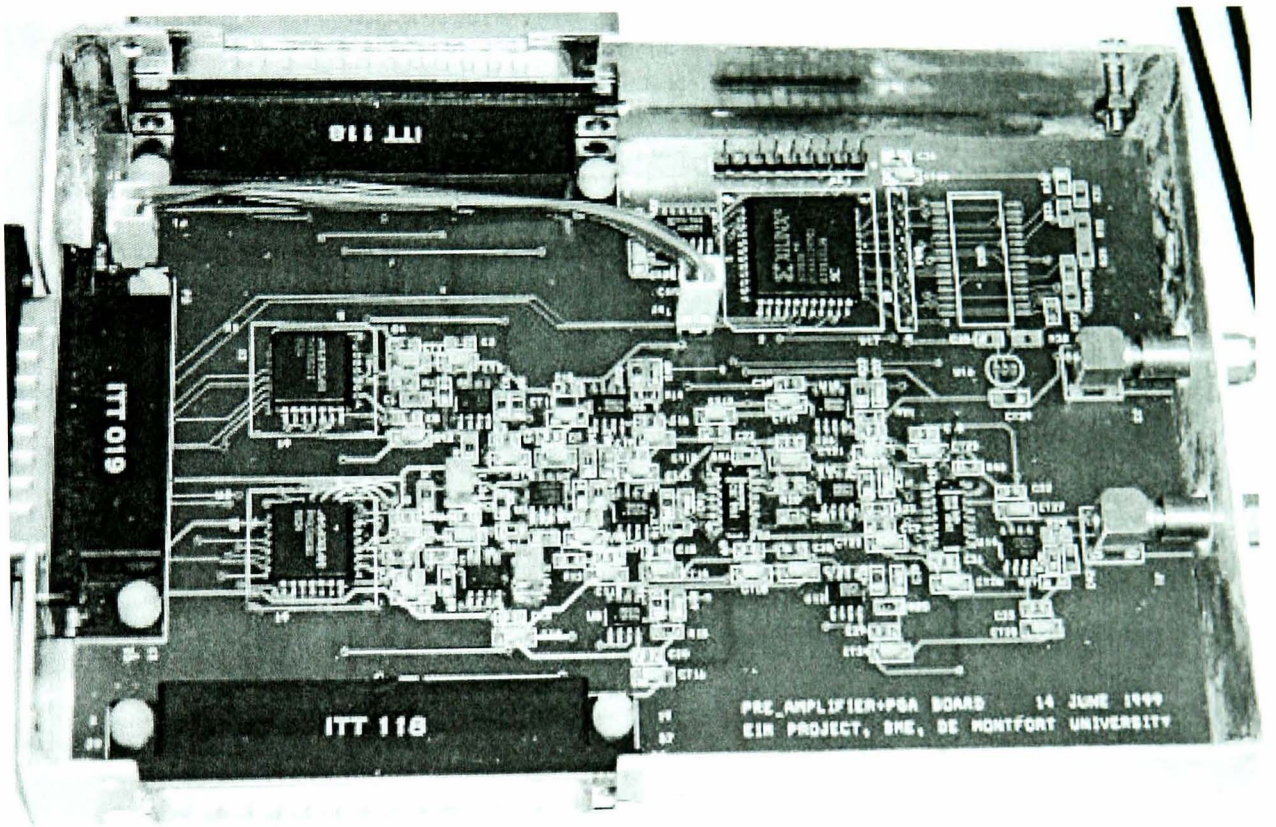

Figure 4.9 The voltage measurement board

According to the analysis of measurement circuit, the printed circuit board is built and tested, as shown in

Figure 4.9. The signal measurement circuit is layout as one part of the analogue module. In EIT hardware system, the multi-channel signals are multiplexed to this differential amplifier to achieve the data acquisition task.

The op-amp, OPA655 (from Bur-Brown, Inc), is chosen as the input stage of the instrument amplifier. The OPA655 combines a wideband and voltage feedback op-amp with a FET input stage to offer an ultra high dynamic range for buffering and trans-

impedance. It provides $10^{12}\Omega$//1.2pF input impedance for the differential mode and $10^{12}\Omega$//1.0pF input impedance for the common mode. In addition, it can achieve 70dB CMRR and 65dB PSRR. Moreover, the gain bandwidth product is 240MHz. The output stage of the instrument amplifier is an OPA620 (from Bur-Brown, Inc), which is internally compensated with 300MHz –3dB bandwidth. It has 75dB CMRR and 60dB PSRR. All these op-amps are integrated in the small-outline surface mount package to ensure better high-speed performance.

The network resistors are metal film resistors with 0.1% precision in surface mount package 0805. The input stage gain is set at 4 to improve CMRR with the same configuration for both input op-amps. The output stage gain is set at 1 to transform the differential signal to a single-end signal. The small value adjustable capacitors are used in the two differential signal paths to balance the symmetric structure in order to achieve better common mode rejection at high imaging frequency. The performance of the first stage of the instrument amplifier is not affected by the precision of the network resistors theoretically. However, for unifying all boards' parameters to achieve the software calibration, high precision resistors are used in whole design.

In the printed circuit board layout, the tracks are made as short as possible and the whole physical board area is kept small to minimize stray effects and interference. The power rails to the op-amp power pin are all de-coupled using 2.2μF Tantalum and 0.1μF ceramic capacitors in parallel.

4.3.4 CMRR test of the front-end amplifier on the printed circuit board

The CMRR of the instrument amplifier is measured using the method shown in Figure 4.10. The common mode voltage V_{cm} is lead to both inputs of the differential amplifier and the output of the instrument amplifier is measured as V_o. With the designed differential gain A_d, the CMRR of the circuit can be calculated as

$$CMRR = 20 \cdot \log\left(A_d \cdot \frac{V_o}{V_{cm}} \right) \qquad \text{Eq4.16}$$

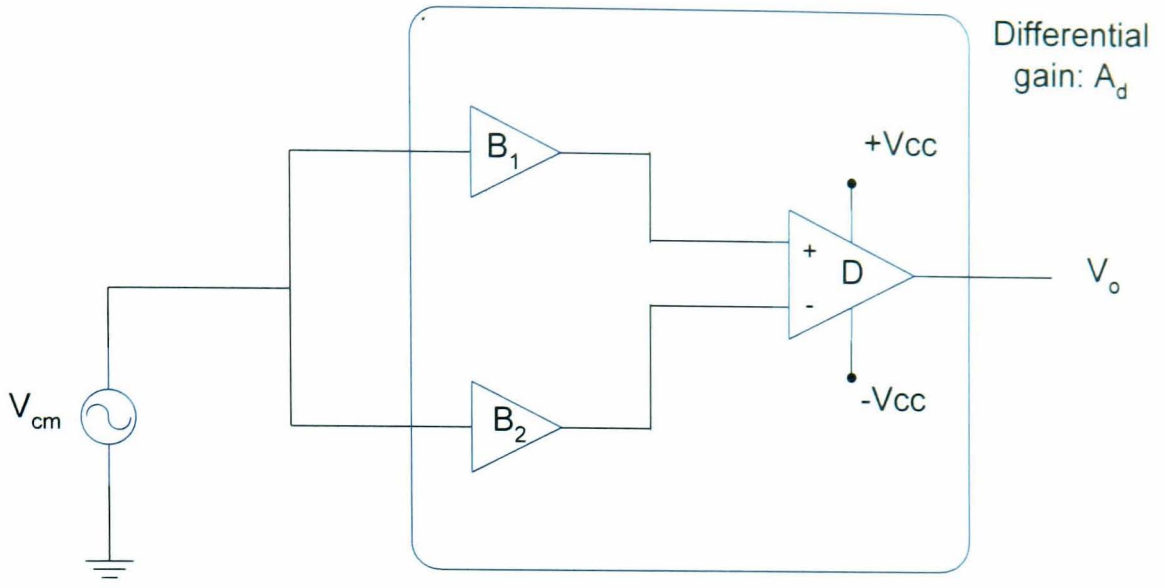

Figure 4.10 The CMRR measurement of the instrumentation amplifier

A programmable function generator (HP4194A) is used to generate wide-band common mode signal and the output amplitude is monitored during the measurement by the same measurement device. The digital oscilloscope (DSO1604) is used for voltage measurement.

The frequency of the common mode voltage added to the circuit is scanned from 1 KHz to 10 MHz. The test result of common mode rejection ratio versus signal frequency is shown in Figure 4.11. It can be seen that at lower frequency (less than 2MHz), the

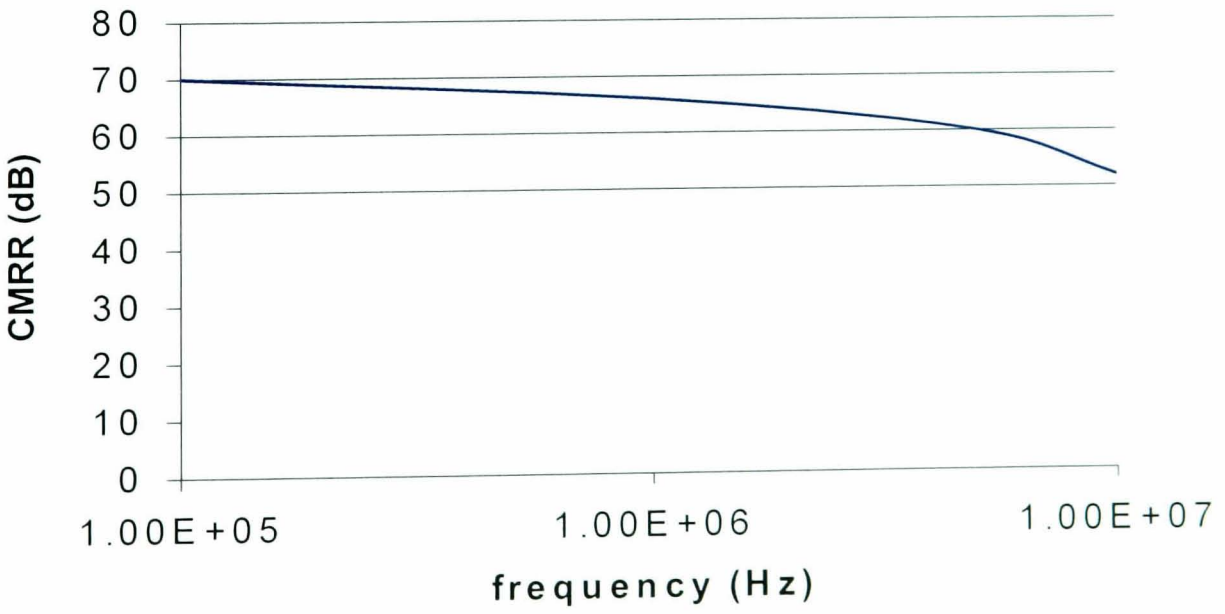

Figure 4.11 The CMRR of the front-end amplifier versus frequency

CMRR of the circuit remains over 60dB. However, at the frequency higher than 2MHz, the CMRR decreases very sharply. This is due to the stray capacitance and inductance effect at radio frequency.

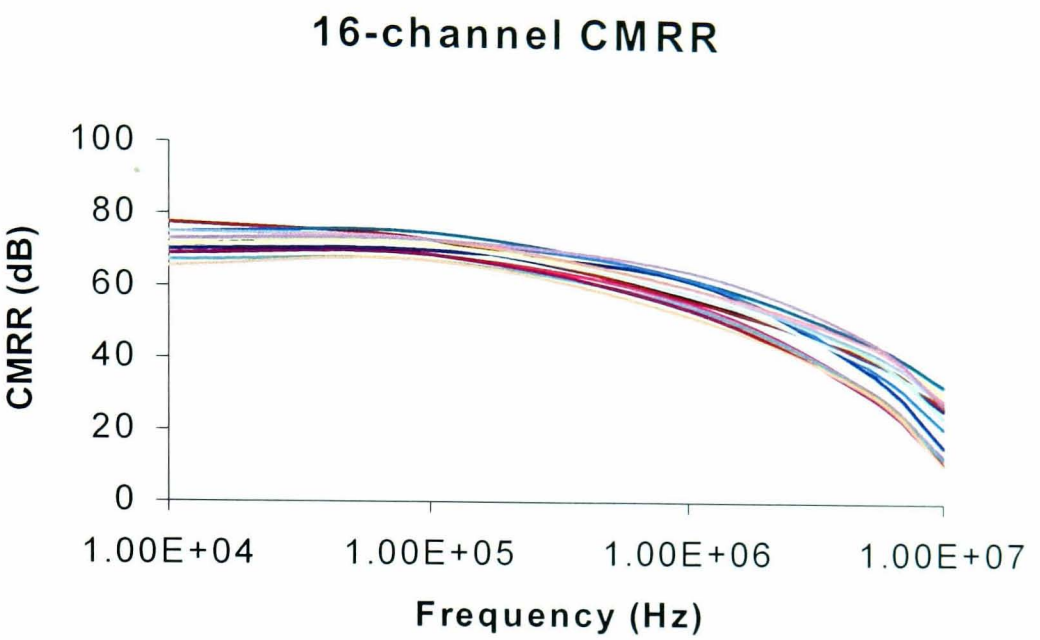

Figure 4.12 The 16-channel CMRR of the front-end circuit in wide frequency band

However, with the common mode voltage added onto the electrode, the CMRR of the complete front-end circuit drops dramatically as shown in Figure 4.12. In this test, the circuit includes the electrodes, the coaxial cable connection and the multiplexer. The CMRR among the channels has different performance. It is due to the imbalance of signal paths from the electrode to the amplifier interface, which is caused by the co-axial cable and the multiplexer. The effect of these connections to the system is discussed in detail in Chapter 6

4.3.5 Conclusions

The differential amplifier is the crucial part in the EIT data acquisition system design. Improvement of common mode rejection of the instrument amplifier is discussed by using electric circuit analysis. The practical printed circuit board of the front-end amplifier is also implemented and tested in two cases, the instrument amplifier itself and multi-channel electrode pairs. The conclusions are:

1. The bio-impedance signal to be measured should be treated as a large output impedance signal source with a serial connected uncertain contact impedance of the electrode.
2. The high input impedance of the front-end amplifier is necessary for the signal measurement and can be achieved by using the op-amp with FET as the input stage.
3. The instrument amplifier can provide the high CMRR due to the typical three-op-amp structure with the input stage setting at higher gain. However, the matching of network resistors around the output amplifier is essential.
4. The common mode voltage affects the op-amp's bias point at the input transistors. Therefore, increasing of the CMRR by increasing of the gain of the differential amplifier can cause the op-amp saturation.
5. The increasing mismatching of the circuit at high frequency makes it difficult to achieve high CMRR in a wide frequency bandwidth. The mismatch of the connections, such as cables and multiplexers, makes it even worse.
6. A high-pass filtering stage is needed to remove the polarization potential induced by the electrode material. However, it may affect the input impedance of the differential amplifier.

4.4 Programmable Gain Amplifier (PGA)

In the electrical impedance measurement, the amplitude of the boundary voltage on the receiving electrodes depends on not only the electrical characteristic of the object, but also the distance from its position to the current injection electrode pair. The shorter the distance is, the larger the amplitude of the boundary voltage. The reason is that the current distribution is attenuated in 2D plane or 3D space. At the opposite position of the current electrodes, the received signal is significantly small. The boundary voltage has a dynamic range of more than 40:1 when considered a 2D circular object with a 32-electrode adjacent driving and receiving configuration. It makes it necessary to use programmable gain amplifier to improve the quality of small signal, especially in terms of signal-to-noise ratio.

4.4.1 Design of programmable gain amplifier

The function block diagram of PGA is shown in the Figure 4.13. When the initial measurement is finished, the demodulation result (signal amplitude) is feedback to the

comparator network. The comparator network sorts the amplitude of the signal into the ladder windows and the outputs of the comparator windows indicate the level that the amplitude of the signal has reached. This amplitude code is then sent to the logic circuit and is encoded into the 4-bit binary format. The logic programme contains all possible corresponding gain control codes, which is applied to the combination of the amplifier group for properly gain settings. This operation is manipulated by the timing control of data acquisition system.

The electronic circuit is shown in Figure 4.14. The measured voltage is a bipolar signal within ±5V dynamic range. After demodulation, the amplitude of the signal is a single polar signal in the range from 0V to 5V. This amplitude signal is feedback to the comparator network. In comparator network, the resistor divider R_1 to R_8 divides the range from 0 to 5V into 8 comparator thresholds. The comparators using 5V power rail give a 5V output when the input is higher than the threshold voltage; otherwise, it maintains the output at ground potential. The values of these resistors are calculated using the designed PGA gain setting.

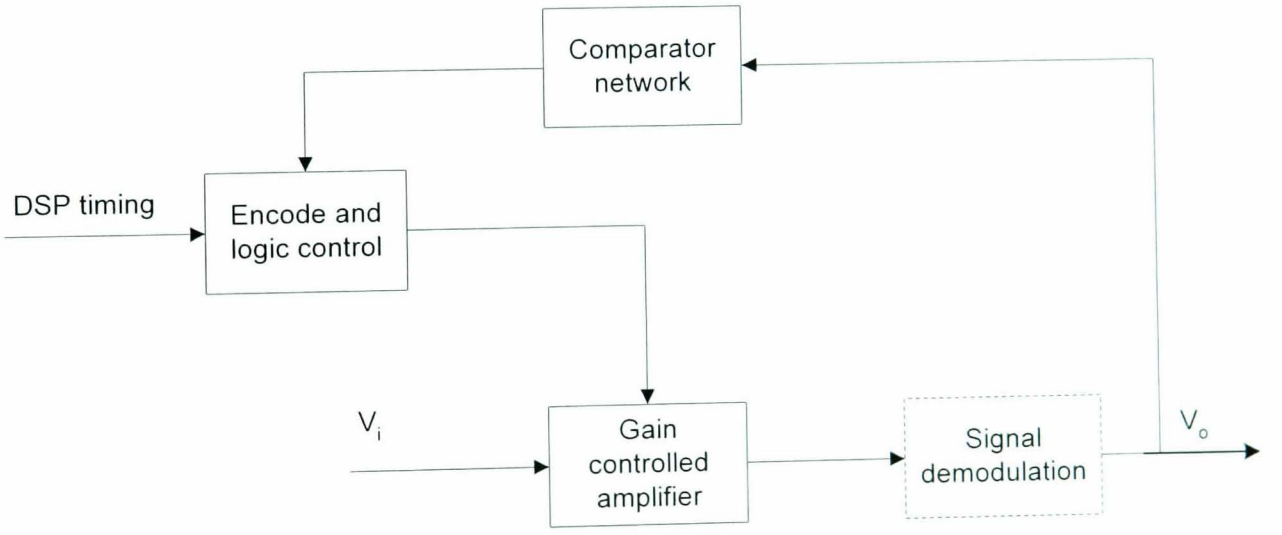

Figure 4.13 The function block diagram of Programmable Gain Amplifier

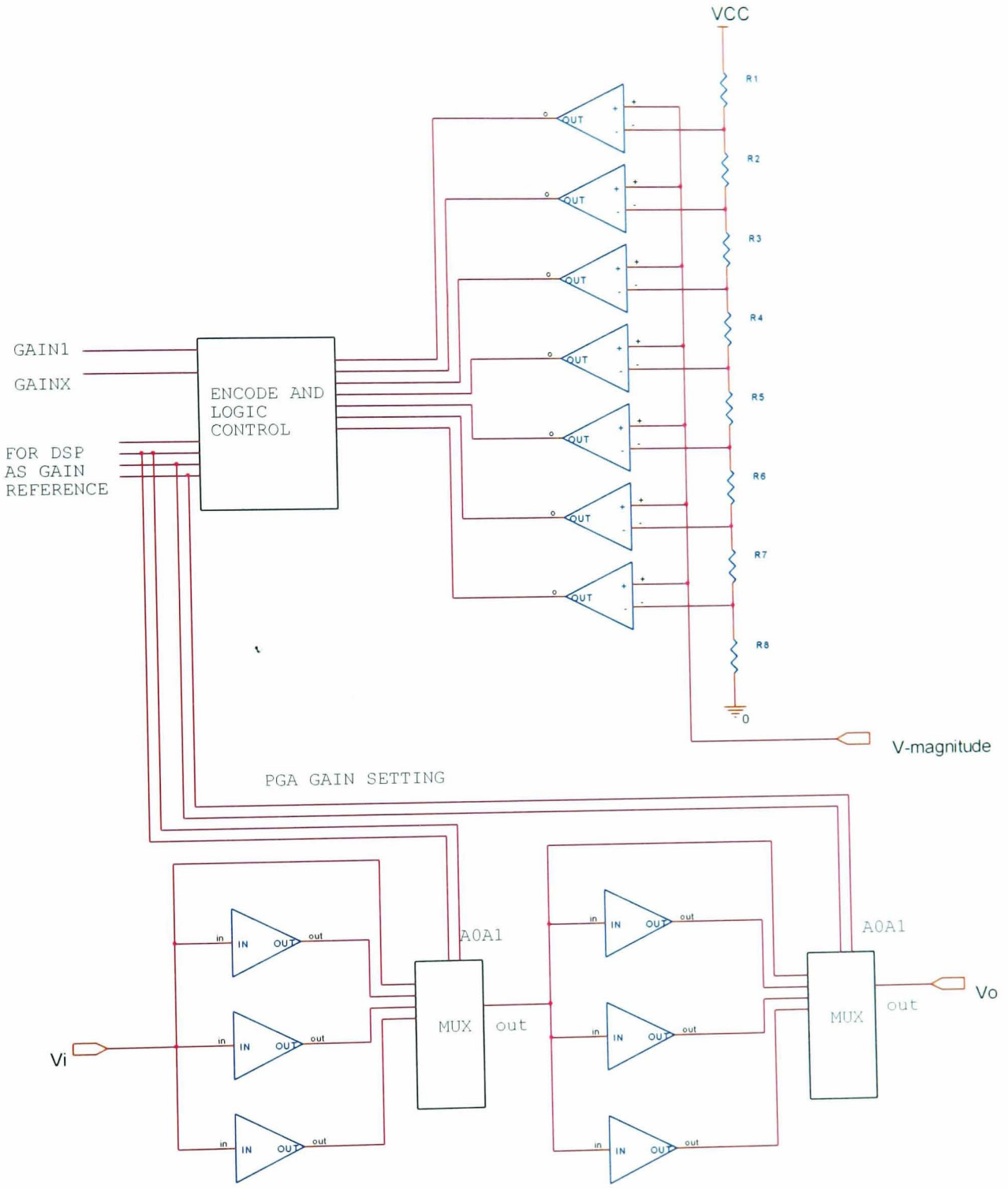

Figure 4.14 Designed programmable gain amplifier with two-stage amplifier structure

The programmable logic chip XC9536 (Xilinx Inc) is used to transform the amplitude information from the comparators output and send out the amplifier gain control signal. Selecting more gain settings results in more complicated gain and phase calibration. However, in practice, using a programmable logic chip will bring flexibility to the system adjustment. The logic chip also sets unity gain to the amplifier when unreasonable amplitude code occurs at the output of the comparators that correspond to

the occasions when interference or electric spark etc appear. The logic chip is controlled by the system timing.

The gain settings of the PGA are designed as a two-stage amplifier array. in which each of them has three amplifiers having gains of 5, 10 and 15. Two multiplexers are used to combine these two stages to form desired gain settings. Unity gain is obtained by directly connecting the original signal to the signal path and no op-amp is involved for this setting. Table 4.2 shows the relationship between the amplitude feedback and the PGA gain setting combination.

Table 4.2 PGA gain control setting table

Output of comparators	Amplifiers gain control signal	Stage 1	Stage 2	PGA gain
1111111	0000	1	1	1
0111111	0100	5	1	5
0011111	1000	10	1	10
0001111	0001	5	5	25
0000111	1001	10	5	50
0000011	1010	10	10	100
0000001	1110	15	10	150
0000000	1111	15	15	225

Actually high gain setting is sensitive to small signal, which is normally mixed with noise, interference and dc draft of the analogue circuit. Therefore, the gain decision mechanism should have enough tolerance to ensure that the signal passing through the PGA does not saturate the op-amp. Furthermore, using high gain setting at high imaging frequency is limited by the op-amp's gain-bandwidth product. It will create more signal distortion and phase shift.

Gain selection is based on the demodulated amplitude of the measured voltage. However, due to the phase shift of the analogue system, the demodulated signal is the real part of the measured voltage. In this case, the PGA may be misled by this untrue signal amplitude and apply an unsuitable higher gain setting to a large signal. This problem can be solved by phase compensation for the demodulation reference signal. According to

this, in practice, the PGA has been designed with adaptive controlled gain setting mechanism.

4.4.2 *Timing control of PGA*

The system logic timing control sends two digital signals to PGA and synchronizes the measurement function during the data acquisition period, which is shown in Figure 4.15. When the system starts the selected channel measurement, the PGA is forced to unity gain by the control signal GAIN1 and the voltage signal with basic system gain amplification is demodulated to an amplitude signal. This demodulated amplitude signal is sent to the analogue-to-digital converter and is feedback to the PGA as well. After the measurement is finished, the PGA control circuit processes this feedback voltage and finds the proper gain setting for the signal path, which will be latched by the control signal GAINX until the system finishes measuring amplitude and phase. The gain decision mechanism requires extra time for PGA gain finding and this affects the data acquisition speed of the system.

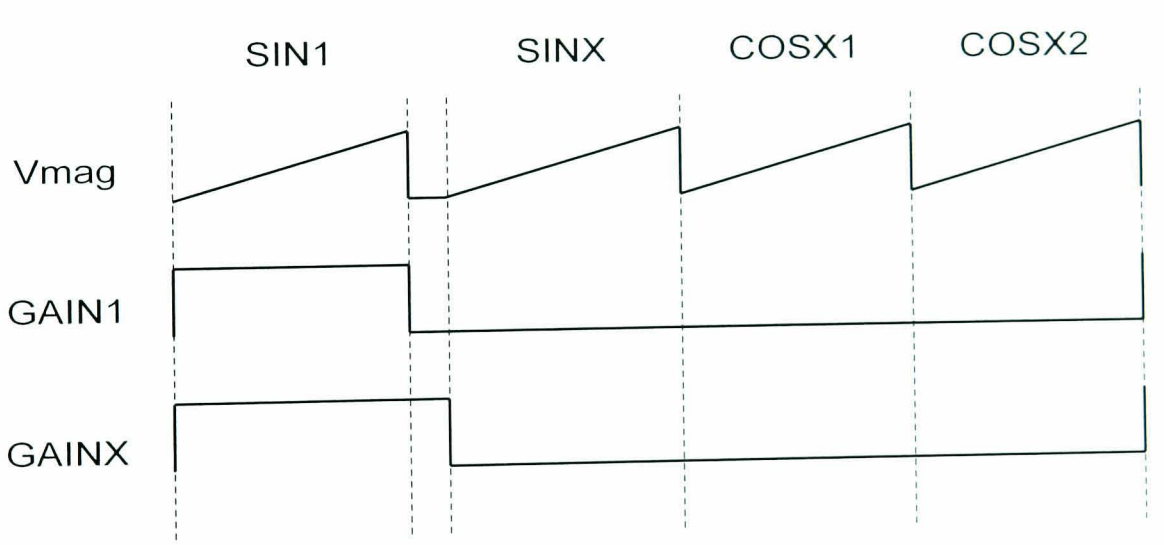

Figure 4.15 PGA gains control timing

The system also receives the gain setting signals during the quantification process of measurement, which is used for the data recovery to remove the effect of different measurement gain. It should be noticed that when repeating the measurement by using

the same driving and receiving pattern, the PGA gain applied to the signal path might be different due to random noise on the demodulated amplitude signal.

4.4.3 *The calibration of amplifier for gain error and phase shift*

The amplifier with different gain has different gain error and phase shift as the signal frequency changing. This has to be taken into account when large PGA gain is applied to the signal path at wide bandwidth measurement. Figure 4.16 shows the changing of gain and phase of amplifier verses the gain settings and frequency, which is simulated with op-amp OPA620 PSPICE model. In this simulation, the gain is set at 1, 5, 10 and 15, and the signal frequency is scanned from 1 kHz to 10MHz. In practice, all these effects are measured in the data acquisition system and used for online or offline correction in data processing.

From the simulation, it can be seen that due to the limit of gain-bandwidth product of op-amp, the op-amp performs badly at high gain setting and this is the reason why the PGA is designed to a two-stage structure. If the imaging frequency is not a pure single frequency signal as presumed, some harmonic frequencies of this signal will be given

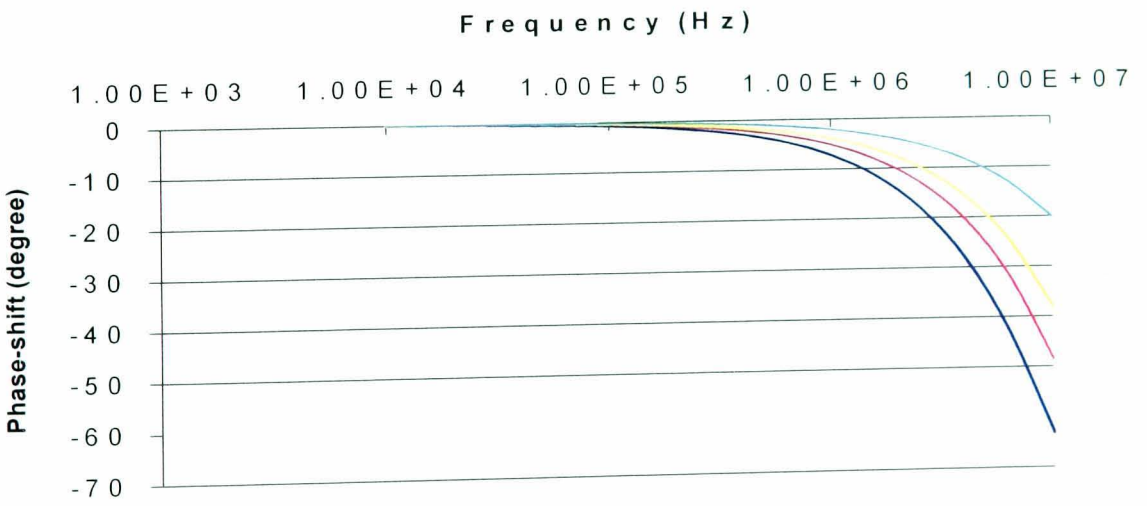

Figure 4.16 One stage PGA phase-shift (blue: gain=1; yellow: gain=5; red: gain=10; black: gain=15)

certain phase shift by the carelessly designed signal path and would cause system oscillation.

The data is recovered in online or offline process to their original level. Actually, the real part and imaginary part of the signal are mixed into the signal amplitude and phase. Therefore, the recovery of data from PGA should consider both gain and phase shift effect, especially at higher imaging frequency.

Each stage of the signal path will give phase shift to the output signal, so the phase shift calibration is not only for the PGA but also for the whole signal path. This is discussed in the Chapter 8.

4.4.4 *Prototype of PGA circuit and its performance*

The PGA circuit is embedded into the amplifier board, which is sealed in the EMC metal case to protect the circuit from outside interference. The components of the circuit are selected with small outline and surface mount package to improve the radio frequency performance.

Figure 4.17 Signal-to-Noise ratio measured on a fixed receiving pair with 16 pairs driving scanning (Red: SNR without PGA, Blue: SNR with PGA)

The PGA has performed well on the signal-to-noise ratio, as shown in Figure 4.17. The data is collected around the boundary on the adjacent receiving electrode pair configuration with a fixed current injection electrode pair, as illustrated in

Figure 4.18. It is obvious that the quality of the signal on the receiving electrode pair at the opposite of the current injection electrodes has been improved by the application of PGA. This effect will also be shown in more detail in the later system test for whole frame data acquisition.

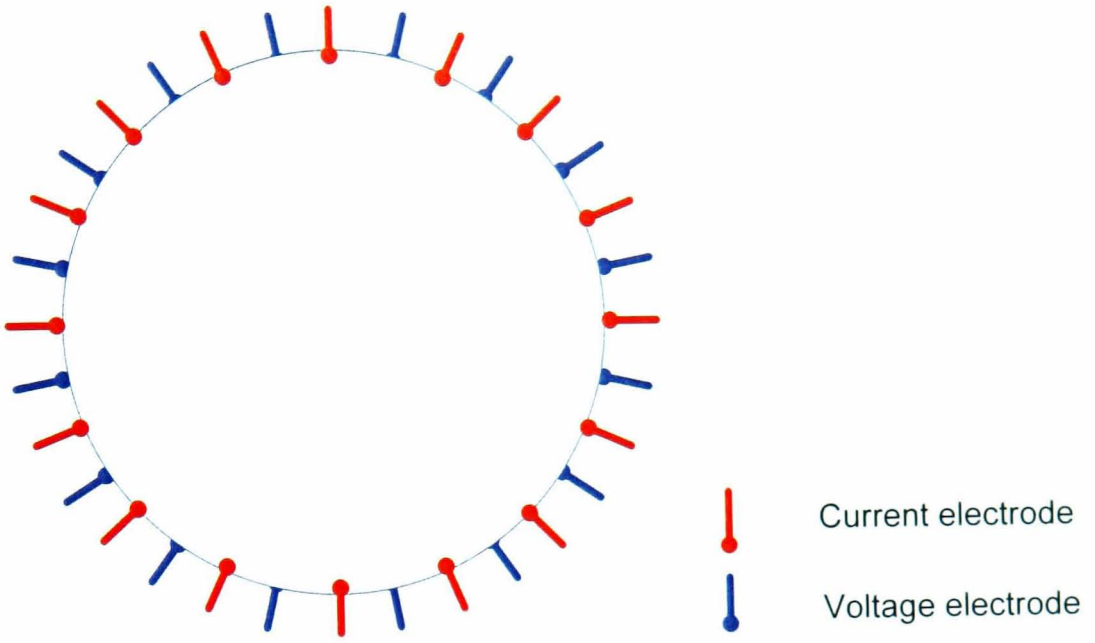

Figure 4.18 The electrode pairs configuration

4.4.5 *Conclusions*

A programmable gain amplifier (PGA) has been used to improve the quality of small signal in the design of data acquisition system. The PGA has the ability to adapt signal amplitude information and apply a suitable gain to the signal path with synchronized timing.

In this section, an eight-gain-setting PGA from unity to gain 225 is designed as an independent function block of the analogue circuit. Due to the limitation of gain-bandwidth product of the op-amp, the PGA consists of two-stage amplifier combination connected by multiplexers to minimize the gain error and phase shift effect.

The system timing handles the PGA control signal to make first signal amplitude measurement on unity gain and then by fixing the suitable PGA gain setting for following measurements. The system also reads the gain setting signals for data recovery purposes.

In addition, the PGA shows the improvement of the quality of signal with the cost of slowing down the speed of data acquisition.

4.5 Summaries

In this chapter, the voltage measurement methodology for electrical impedance tomography is discussed and physical circuit design is implemented. The voltage signal on the electrode is treated as high output impedance signal source, and therefore the front-end amplifier must have a high input impedance and high common mode rejection ability for differential measurement.

To improve the signal quality, the PGA is designed as a part of the analogue circuit and it has shown that good performance can be obtained. Using an op-amp with large gain setting results in the large gain error and phase shift due to the finite gain-bandwidth product. This has been successfully avoided in MK2 design.

The two function blocks reported have been built into an analogue printed circuit board as the voltage measurement unit in the data acquisition system. The performance of the circuit has been tested and meets the requirement of image reconstruction.

Chapter 5 Demodulation

5.1 Introduction

The variation of bio-impedance reflects the position or shape changes of tissue in the measured object corresponding to physiological activity in applied electrical field. The bio-impedance is a time-vary signal and is a function of the frequency. The frequency range of the bio-impedance variation in human is considered to limit to 50Hz so that the bio-impedance signals are amplitude modulated signals with a carrier frequency equal to the injected current frequency and have a base bandwidth of 100Hz [50]. In a real time imaging system, the data acquisition speed needs to be satisfied to display 25-frame per second. For the electrical impedance mammography purpose, it is not required, but high speed data acquisition would definitely be helpful to cancel the effect of contact problem induced by body activity.

The demodulation process is the technique to recover the bio-impedance signal to their base band frequencies. In the early stage of EIT system design, some approaches for measuring the amplitude or the modulus of the impedance like RMS-to-DC conversion [59] and peak detection [60] were used for lower frequency imaging in which the phase data was not of prime importance because tissues behave almost resistively at low frequencies. With the development of the bio-impedance properties research, it has been seen that some abnormal tissue shows more imaginary impedance change due to the capacitive effect at higher frequencies and this makes it possible to distinguish these tissues when using high frequency EIT image, especially for cancer research purpose [75].

To extract the information, phase-sensitive demodulation, a synchronous demodulation method, can be implemented in analogue circuit or digital signal process firmware. Employing reference signal with different phase shift, phase-sensitive demodulation can provide both real part and imaginary part of the complex measured voltage.

5.2 Coherent phase sensitive demodulation

Coherent demodulation is a widely used phase sensitive demodulation technique, which can synchronously provide the real or imaginary part of the measured voltage, depending on the phase difference between it and the reference voltage. The reference voltage has exactly the same frequency as the carrier frequency of the signal being measured. Within the wide band EIT system design, the measured voltage is induced by the injected current that is generated from a voltage controlled current source (VCCS), and so the carrier frequency is programmed in the computer by means of a direct digital synthesizer. The reference voltage can use the same digital function as the wave generator to maintain a waveform, which is the same as the applied frequency of the current source.

Coherent demodulation can also be implemented in the digital signal processor firmware and embedded in the hardware system. Using digital technologies in the signal processing can remove offset and the drift effect of physical device, which is varied with environment and temperature changes. Its accuracy of process is depending on the accuracy of quantization and computing.

5.2.1 *Principle of coherent demodulation*

The principle of coherent demodulation is illustrated in Figure 5.1. The measured

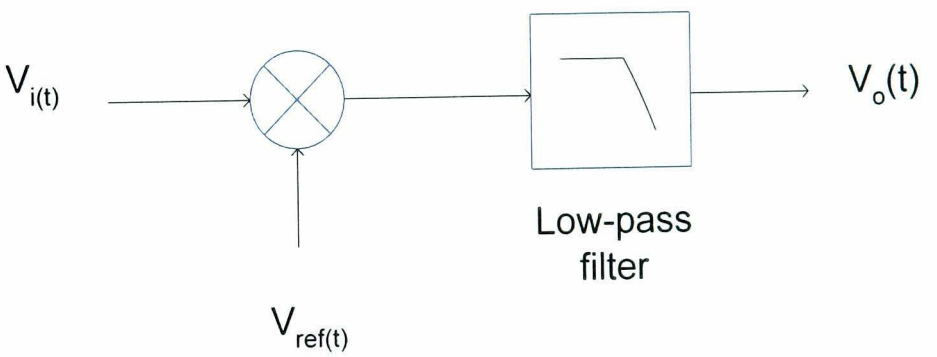

Figure 5.1 Coherent demodulation block diagram

voltage V_i (t) is multiplied by a reference voltage V_{ref} (t) in phase with the driving signal. Provided the measured voltage is

$$V_i(t) = V \cdot \sin(\omega \cdot t + \varphi) \qquad \text{Eq5.1}$$

where ω is the imaging frequency, φ is the phase shift due to the tissue's complex impedance. The reference voltage is

$$V_{ref}(t) = A \cdot \sin(\omega \cdot t) \qquad \text{Eq 5.2}$$

The multiplier output voltage is the product of these two input signals

$$V_x = \frac{A \cdot V}{2} \cdot [\cos(\varphi) - \cos(2\omega t + \varphi)] \qquad \text{Eq5.3}$$

Here A is the magnitude of the reference voltage, and V is the magnitude of the measured voltage. After passing the followed low-pass filtering, the final output removes the high-frequency component that has doubled imaging frequency as

$$V_o = \frac{A \cdot V}{2} \cdot \cos(\varphi) \qquad \text{Eq5.4}$$

It can be seen that this process gives the dc output that is proportional to the real part of the measured voltage. In the same way, if the reference voltage is shifted by 90°, that is, if $V_{ref}(t) = A \cdot \sin\left(\omega \cdot t + \frac{\pi}{2}\right)$, the output voltage will be proportional to the imaginary part of measured voltage:

$$V_o = \frac{A \cdot V}{2} \cdot \sin(\varphi) \qquad \text{Eq 5.5}$$

Therefore, with different 90° phase-different reference voltage applied to the multiplier, the Eq5.3 and Eq5.4 give the real part and imaginary part of measured voltage, in which the magnitude of reference voltage A is just a constant value setting in the computer software.

The magnitude of the measured voltage V is also a function of time, and it will vary with both body physiological activity and movement. The data acquisition system catches a modulated output as tissue impedance on that time point. In addition, from the imaging reconstruction point of view, the acquired data set for one frame image should responds this vary on all boundary electrodes at same time point.

5.2.2 Improvement of low-pass filtering for fast data acquisition

If the demodulated signal is used in continuous monitoring, after a transient time for signal settling, the real component or imaginary component of the measured signal is available for further processing.

However, in the EIT data acquisition system, especially in the serial structure machine, multi-channels are multiplexed to the measurement circuit. The frame rate of the image display therefore depends on the summation of the data acquisition time of

each channel. The low-pass filtering RC time constant occupies relatively large percentage of the sampling time of the system. If the tolerance of the voltage being charged on the capacitor for sampling is α, the low-pass stage needs at least duration t to let the output reach this accuracy,

$$e^{-\frac{t}{RC}} < \alpha \qquad \text{Eq 5.6}$$

Or

$$t > RC \cdot \ln \alpha \qquad \text{Eq 5.7}$$

According to Eq 5.7 the time needed for precise measurement is calculated and shown in Table 5.1. It can be seen that the more accurate measurement the longer circuit settling time is needed. The cutoff frequency of low-pass filtering f_{cutoff}, also related to the time constant RC, should be lower than the imaging frequency f_{image} as shown in Eq 5.8:

$$f_{cutoff} = \frac{1}{2\pi \cdot RC} << f_{image} \qquad \text{Eq 5.8}$$

Table 5.1 Time constant and system measurement accuracy

Measurement Accuracy	Settling Time
10%	2.303RC
1%	4.605RC
0.1%	6.908RC

In the high-frequency image system design, smaller time constant RC can be applied to increase the data acquisition speed. However, for a wide band system, the cut-off frequency is dominated by the lowest imaging frequency. As a consequence, the data acquisition will be extremely slow due to the long settling time. Alternatively, there is another solution for removing of high frequency components, using integrator instead of low-pass filtering, as shown in Figure 5.2.

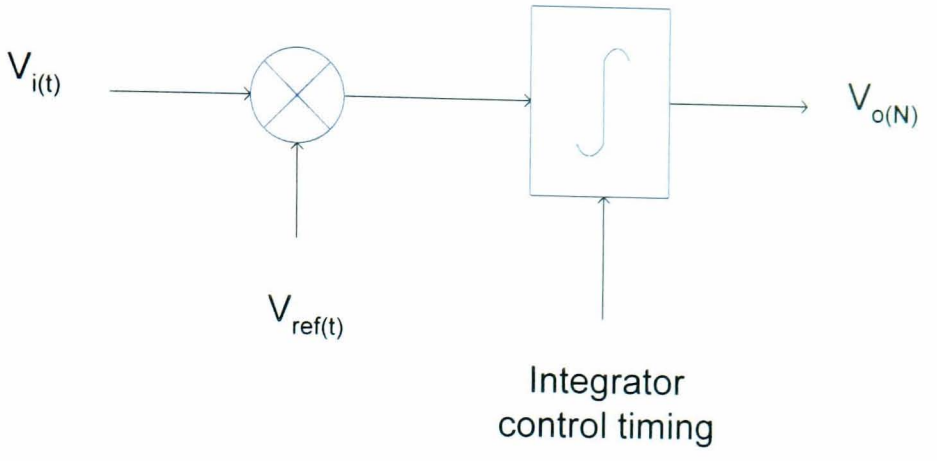

Figure 5.2 Coherent demodulation block with integrator replacing low-pass filter

With integration time T, the equation Eq5.3 is integrated as

$$V_o = \frac{A \cdot V}{2} \cdot \cos(\varphi) \cdot T - \frac{A \cdot V}{2} \cdot \int_0^T \cos(2\omega t + \varphi) dt \qquad \text{Eq 5.9}$$

If the integration time is chosen as the integer times of the signal period, the second term of the output voltage will be zero, and therefore the output of the integrator is still proportional to the real part of the measured voltage:

$$V_o = \frac{A \cdot V}{2} \cdot \cos(\varphi) \cdot T \qquad \text{Eq 5.10.}$$

In the same way, the imaginary part of the measured voltage can be obtained as

$$V_o = \frac{A \cdot V}{2} \cdot \sin(\varphi) \cdot T \qquad \text{Eq 5.11.}$$

In theory, the integration time can be any integer times of the period of signal. The data acquisition time for each channel can be short as single signal period. Consequently, at high imaging frequency, it is possible to make the sampling speed fast. However, in practice, the integration time should be longer than the minimum demanded to remove mixed random noise and interference. In this process some of harmonic frequencies of the imaging signal caused by nonlinear devices are also integrated to zero.

Replacing the low-pass filtering with an integrator minimizes the data acquisition time, but the demodulation is no longer a continuous synchronous demodulation. In EIT imaging system design, it has to be compensated with fast frame data acquisition speed. Moreover, if the sampling is fast enough, the image still can respond to the real time body physiological activity and function changes.

During each interval of data acquisition time, the integrator should have time to discharge the capacitor to zero voltage for the next integration operation. After integration is finished, it should be able to keep the integrated result for sampling by an analogue-to-digital converter. This will delay the data acquisition operation and affect the frame rate of display in the image system.

5.2.3 *Effect of dc offset on demodulation*

If a dc offset or a drift voltage is accumulated into the signal to be demodulated, it will be mixed into the output real part or imaginary part of the measured voltage by the demodulation process to introduce errors to the measurement. Provided the voltage to be demodulated *Vi* (t) has dc component *Ds* and the reference voltage *Vref(t)* has dc component *Dref*, then Eq5.3 becomes

$$V_x = \frac{A \cdot V}{2} \cdot [\cos(\varphi) - \cos(2\omega t + \varphi)] + D_s \cdot A \sin(\omega t) + D_{ref} \cdot V \sin(\omega t + \varphi) + D_s \cdot D_{ref} \quad \text{Eq 5.12}$$

After the low-pass filtering, the ac signal is removed, and therefore the output voltage is the real part of the measured voltage mixed with an error $D_s \cdot D_{ref}$, that is

$$V_o = \frac{A \cdot V}{2} \cdot \cos(\varphi) + D_s \cdot D_{ref} \quad \text{Eq5.13}$$

and the imaginary part of the measured voltage is

$$V_o = \frac{A \cdot V}{2} \cdot \sin(\varphi) + D_s \cdot D_{ref} \quad \text{Eq 5.14}$$

The dc component of the *input voltage Vi*, D_s normally is formed by the op-amp's bias current and offset voltage. The value may be relatively large compared to the amplitude of the measured voltage. Fortunately, the weight to generate this error to the demodulated dc voltage is limited by the value of dc component D_{ref} in the reference voltage, which is usually small due to the high resolution of digital synthesized signal source. For the real part of signal demodulation, the signal-to noise ratio can be derived from Eq5.13 as

$$SNR_{real} = \frac{1}{2} \cdot \frac{V \cdot \cos(\varphi)}{D_s} \cdot \frac{A}{D_{ref}} \quad \text{Eq 5.15}$$

It can be seen that the demodulation output signal-to-noise ratio is dominated by the reference voltage signal-to-noise ratio and the demodulated voltage to the original dc offset ratio. The signal-to-noise ratio of the reference voltage is well controlled, because the magnitude of the reference voltage is at volt level and the dc offset is at millivolt level. However, the ratio of the demodulated real part voltage $V \cdot cos(\varphi)$ to the original signal dc offset D_s is unconvinced. If the measured voltage is from the electrode pair near the current injection electrodes, the signal-to-noise ratio is large.

Eq5.16 gives the signal-to-noise ratio in the imaginary part of signal demodulation. Normally, the phase shift is relatively small, then $V \cdot sin(\varphi)$ is small. Accordingly, $SNR_{imaginary}$ is small comparing with SNR_{real}.

$$SNR_{imaginary} = \frac{1}{2} \cdot \frac{V \cdot \sin(\varphi)}{D_s} \cdot \frac{A}{D_{ref}} \qquad \text{Eq5.16}$$

Other error sources, such as heat noise that is random with zero time-average value, will be minimized in the integration operation. In addition, the value of the demodulated dc signal is proportionally scaled with integration time and the periodic unwanted signals are maintained at the same level.

In analogue circuit implementation, the multiplier itself will also contribute to the dc offset at the output stage and this offset is integrated into the demodulated signal to become another error source. In practice, if this offset affects the accuracy of the measurement, an external offset adjustment has to be added to remove it.

Additional offset errors can also be introduced by the amplifier's input bias currents. To reduce the bias current, it is necessary to match the impedance of the network seen by both inverting and non-inverting input terminals of the amplifier.

Using digital implementation of coherent demodulation can minimize the dc offset in two aspects. Firstly, the signal used for demodulation can be filtered by digital signal processing to remove the effect of the dc offset. Secondly, it can directly use the look-up table of waveform data as a reference signal for the demodulation purpose and consequently no generated dc voltage is included. The accuracy of digital demodulation is only depending on the sampling rate, the resolution of the analogue-to-digital converter and the accumulated error of processing algorithm.

5.2.4 *Effect of polarization potential on demodulation*

The polarization potential is a slowly varying signal coming from electric chemical reaction between an electrode and the contacted imaging object. In the frequency domain, it is separated from the measured voltage that rides on the carrier wave. The value is randomly changed and can be of the order of tens to hundreds millivolt depending on the contact materials being used. Therefore, this voltage signal has to be removed before it saturates the amplifiers in the signal path. Using a high-pass filtering stage can achieve this purpose, but also imposes longer time for signal settling. If the polarization potential is P, and the time constant of the high-pass filtering is τ, then the impact of the polarization potential to the signal path can be described as

$$V(t) = P \cdot e^{-\frac{t}{\tau}} \qquad \text{Eq5.17}$$

Obviously, the amplitude of $V(t)$ attenuates with time t and becomes zero if the settling time is long enough. Furthermore, if a nonzero signal exits, it will be amplified by the amplifiers cascaded with this high-pass filtering stage. Mixed with the measured signal described in Eq5.1, the input signal to the multiplier is

$$V_i(t) = V \cdot \sin(\omega \cdot t + \varphi) + P \cdot e^{-\frac{t}{\tau}} \qquad \text{Eq5.18}$$

Therefore, the output of the multiplier is the product of Eq 5.2 and Eq5.18, that is

$$V_x = \frac{A \cdot V}{2} \cdot [\cos(\varphi) - \cos(2\omega t + \varphi)] + A \cdot P \cdot e^{-\frac{t}{\tau}} \sin(\omega t) \qquad \text{Eq5.19}$$

In Eq5.19, the polarization potential is modulated by the reference voltage signal at the carrier frequency. This modulated signal can easily be removed by low-pass filtering, which normally forms the last stage of demodulation block. However, for the demodulation with integrator as the last stage, this effect cannot be removed from the output because it is not a periodic signal. Therefore, the system must be allowed enough settling time to minimize the impact and consequently longer sampling time slows down the data acquisition speed.

After integration, the second term of Eq5.19 is the error source added to the demodulated signal. As Eq5.20 shows the error $N_{e\text{-}real}(t)$ with an integration period T

starting from arbitrary time t is

$$N_{e-real} = \int^{+T} A \cdot P \cdot e^{-\frac{t}{\tau}} \sin(\omega t) dt \qquad \text{Eq5.20}$$

If the integration time T is considered as integer times of the signal period, the result of integrating Eq5.20 will be

$$N_{e-real} = AP \cdot \frac{\tau}{\omega^2 \cdot \tau^2 + 1} \cdot \left(1 - e^{-\frac{T}{\tau}}\right) \cdot e^{-\frac{t}{\tau}} \cdot \left[\sin(\omega t) + \omega \cdot \tau \cdot \cos(\omega t)\right] \qquad \text{Eq5.21}$$

The time constant τ is calculated by the cut-off frequency, which is far smaller than the inverse of the imaging frequency ω or it is $\tau\omega >> 1$, so, the error induced by the impact of polarization potential can be simplified as:

$$N_{e-real} = AP \cdot \frac{1}{\omega} \cdot \left(1 - e^{-\frac{T}{\tau}}\right) \cdot e^{-\frac{t}{\tau}} \cdot \left[\frac{1}{\omega \cdot \tau} \sin(\omega t) + \cos(\omega t)\right] \qquad \text{Eq5.22}$$

The error is proportional to the magnitude of the polarization voltage, but deceases with increasing of imaging frequency. This implies that the higher imaging frequency, the smaller the impact of the polarization effect. The error is also attenuated exponentially with time and the longer the settling time, the smaller the error. In addition, the large high-pass filtering time constant dominates the effect of this impact. All these factors also make the data acquisition speed slow.

According to Eq5.22, if these effects are to be minimized, the carrier part of the signal must be forced to equal to zero, that is

$$\frac{1}{\omega \cdot \tau} \sin(\omega t) + \cos(\omega t) = 0 \qquad \text{Eq5.23}$$

The impact effect of polarization potential within the integration time will be cancelled from the final output of demodulation. To do this, the integration has to start at time

$$t = k \cdot \frac{\pi}{\omega} - \frac{1}{\omega} \arctan(\omega \cdot \tau) \qquad \text{Eq5.24}$$

Here k is an arbitrary positive integer. It can be seen that allowing a tiny delay to the integration operation will dramatically reduce the effect of polarization potential and decrease the settling time for the analogue system. This will improve the data acquisition system to achieve the fast sampling rate, especially effective at lower imaging frequencies.

In the same way, the error in the imaginary part of the measured signal will be induced by the reference voltage that has 90° phase shift. Therefore, the error $N_{e\text{-}imaginary}$ is

output after the integration operation at arbitrary time point t with integration time T. which is set as an integer times of the modulated signal period of, as

$$N_{e-imaginary} = AP \cdot \frac{\tau}{\omega^2 \cdot \tau^2 + 1} \cdot \left(1 - e^{-\frac{T}{\tau}}\right) \cdot e^{-\frac{t}{\tau}} \cdot \left[\cos(\omega t) - \omega \cdot \tau \cdot \sin(\omega t)\right] \quad \text{Eq5.25}$$

with the same condition, the product of imaging frequency and high-pass filtering time constant is far larger than one, as $\tau\omega >> 1$. Therefore, the error can be simplified as follow

$$N_{e-imaginary} = AP \cdot \frac{1}{\omega} \cdot \left(1 - e^{-\frac{T}{\tau}}\right) \cdot e^{-\frac{t}{\tau}} \cdot \left[\frac{1}{\omega \cdot \tau}\cos(\omega t) - \sin(\omega t)\right] \quad \text{Eq5.26}$$

It can be seen that $N_{e\text{-}imaginary}$ has the same property as $N_{e\text{-}real}(t)$ in frequency and time domains. In addition, $N_{e\text{-}imaginary}$ will be zero, if the integration time starts at

$$t = k \cdot \frac{\pi}{\omega} + \frac{1}{\omega}\arctan\left(\frac{1}{\omega \cdot \tau}\right) \quad \text{Eq5.27}$$

Here k is an arbitrary positive integer. Therefore, to minimize the error, the integration is started after with longer delay.

5.3 Implementation of analogue coherent demodulation

Coherent demodulation can be implemented using analogue devices with digital timing control. In the electrical impedance tomography system, the reference voltage can be generated from the same sine wave synthesizer that feeds the current source. The phase related to the measured voltage can be controlled precisely by the software settings. The analogue demodulation transforms the signal frequency to the original base band, and thereby the sampling rate of the analogue-to-digital converter is reduced. This electronic circuit simply includes a multiplier and an integrator, and therefore, it is very suitable for low cost applications and distributed system designs.

5.3.1 Multiplier

The integrated circuit multiplier chip AD835 (Analog Devices, Inc) is adopted in the analogue coherent demodulation design. It is a four-quadrant, voltage-output, analogue multiplier fabricated on an advanced, dielectrically isolated, complementary bipolar process. In basic mode, it provides the linear product of the X and Y voltage inputs, as shown in function block diagram Figure 5.3.

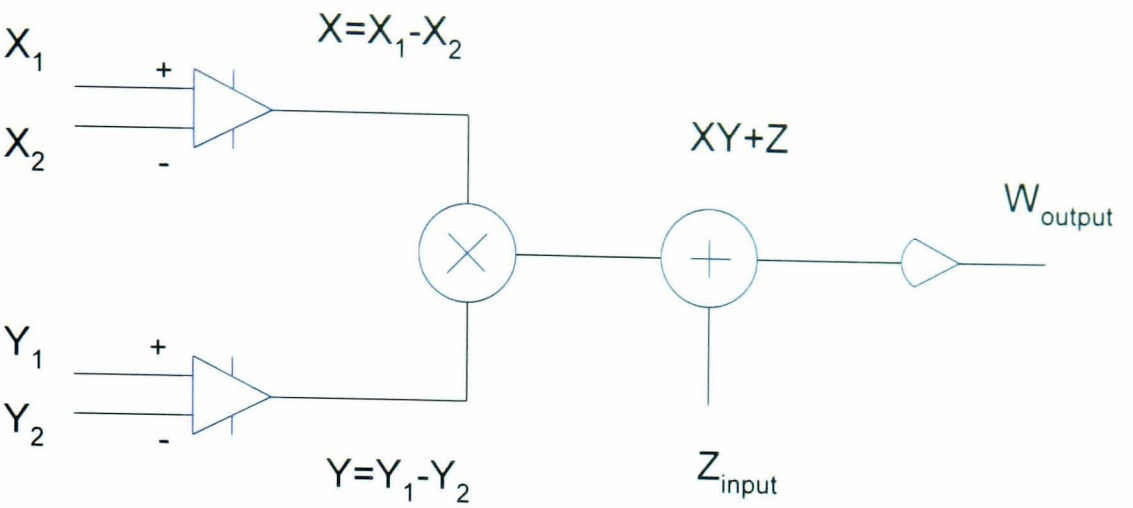

Figure 5.3 The internal function blocks of a differential input analogue multiplier AD835

The Z_{input} provides summing to the product of multiplier, which can be used as an offset voltage adjustment. The output of the multiplier W_{output} provides the functional operation

$$W_{output} = (X_1 - X_2) \cdot (Y_1 - Y_2) + Z_{input} \qquad \text{Eq5.28}$$

where the X_1, X_2 and Y_1, Y_2 are differential input terminals to X and Y inputs.

Table 5.2 AD835 main parameters (Analog Devices, Inc)

Parameters	Conditions	Typical value
Linearity (Relative Error)	T=25°C	±0.5% FS
Offset voltage	T=25°C	±25mV
Bias current	T=25°C	<20μA
Feed through, X Feed through, Y	X=±1V, Y=0V Y=±1V, X=0V	<–46dB <–60dB
–3dB Small Signal Bandwidth	T=25°C	250MHz
–0.1dB Gain Flatness Frequency	T=25°C	15MHz

Table 5.2 lists main parameters related to this demodulation design. The drawback of this chip is the large offset voltage, which can be cancelled by means of an adjustable potentiometer applied to the Z_{input}.

5.3.2 Integrator

The integrator is another important part of the demodulation block. Its performance directly affects the accuracy of the measured data and the sampling speed of real time imaging applications.

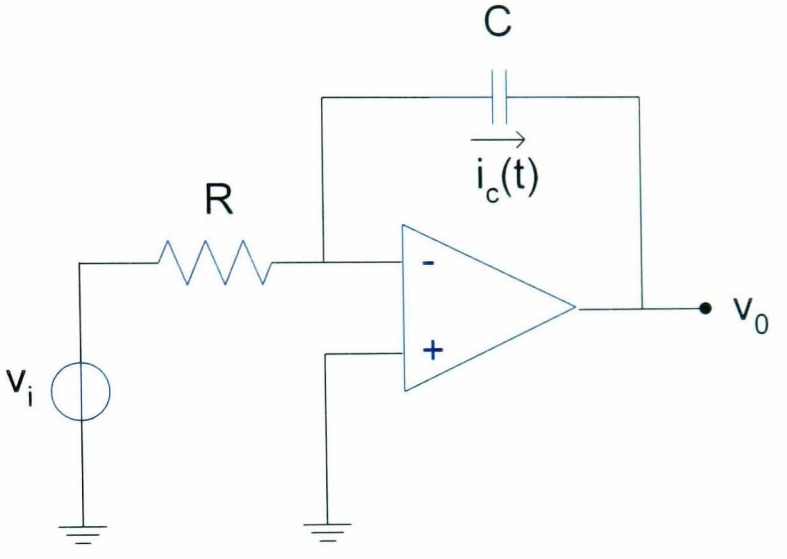

Figure 5.4 The analogue integrator

The analogue integrator is the circuit that performs the mathematical processes of integration, using the charging characteristic of a capacitor. It can be seen that in Figure 5.4, the instantaneous voltage across it is related to the instantaneous current flow into the capacitor by

$$v_c(t) = \frac{1}{C}\int_0^t i_c(t)\cdot dt + v_c(0) \qquad \text{Eq5.29}$$

where $v_c(0)$ is the initial value on the capacitor. The voltage across the capacitor is thus proportional to the integral of the current. Because the capacitor is positioned as a feedback element in an op-amp circuit, with the form of a voltage-controlled current source, the input voltage $v_i(t)$ controls the capacitor current $i_c(t)$ as given by

$$i_c = \frac{v_i(t)}{R} \qquad \text{Eq5.30}$$

This value of $i_c(t)$ can then be substituted in Eq5.29, in which case $v_c(t)$ is expressed directly in terms of $v_i(t)$. However since the positive reference terminal of $v_c(t)$ is on the left, the output voltage is inversed. Note also that the initial voltage on the capacitor is the

initial output. The net result for the output voltage is then

$$v_o = -\frac{1}{RC} \cdot \int_0^t v_i(t)dt + v_o(0) \qquad \text{Eq5.31}$$

The output voltage is proportional to the integral of the input voltage with presence of the inversion sign and the constant $\frac{1}{RC}$. The inversion sign can be adjusted after analogue-to-digital conversion in the data processing. However, the constant RC needs to be selected carefully to ensure that the integrated output just reaches the largest dynamic range of signal path and does not cause the op-amp to saturate.

The transfer function of this integrator is

$$H(j\omega) = -\frac{1}{j\omega RC} \qquad \text{Eq5.32}$$

where ω is the signal frequency. The amplitude response $M(\omega)$ for the integrator is readily determined from the magnitude of Eq5.32 as

$$M(\omega) = \frac{1}{\omega RC} \qquad \text{Eq5.33}$$

It is large at low frequencies but decreases as the frequency increases. Therefore, this circuit is a true dc integrator and suitable for coherent demodulation uses.

The op-amp used in the integrator circuits must have very low dc offset voltage and bias current. They are the crucial parameters in the circuit design.

In the MK2 EIT system, op-amp AD8610 is chosen for the circuit implementation. The AD 8610 is a very high precision JFET input amplifier featuring ultra low offset voltage and drift, very low input bias current and wide bandwidth, as shown in Table 5.3. Unlike many JFET amplifiers, the AD8610 input bias current is low over the entire operating temperature range. In addition, this op-amp is stable with capacitive loads of over 1000pF in non-inverting unity gain mode; much larger capacitive loads can be easily driven at higher noise gains without any external compensation. Its outputs slew at 50V/μs in either inverting or non-inverting gain configurations, and settle to 0.01% accuracy in less than 600ns. All these characteristics make the AD8610 suitable for the integrator circuit design.

Table 5.3 AD8610 main parameters (from Analog Devices, Inc)

Parameters	Conditions	Typical value
Offset Voltage	+25°C<T<+125°C	90μV
Input Bias Current	-40°C<T<+85°C	+20 pA
Offset Voltage Drift	-40°C<T<+125°C	0.5μV/°C
Voltage Noise Density	f=1kHz	6 nV/$\sqrt{Hz}$
Current Noise Density	f=1kHz	5 fA/$\sqrt{Hz}$

Obviously, the capacitor used in the circuit for integration operation must be a high quality capacitor with high insulation resistance to ensure that the leakage current on the capacitor is in the tolerance. Both capacitors and resistors must also have low temperature coefficient.

5.3.3 *Circuit design and control timing*

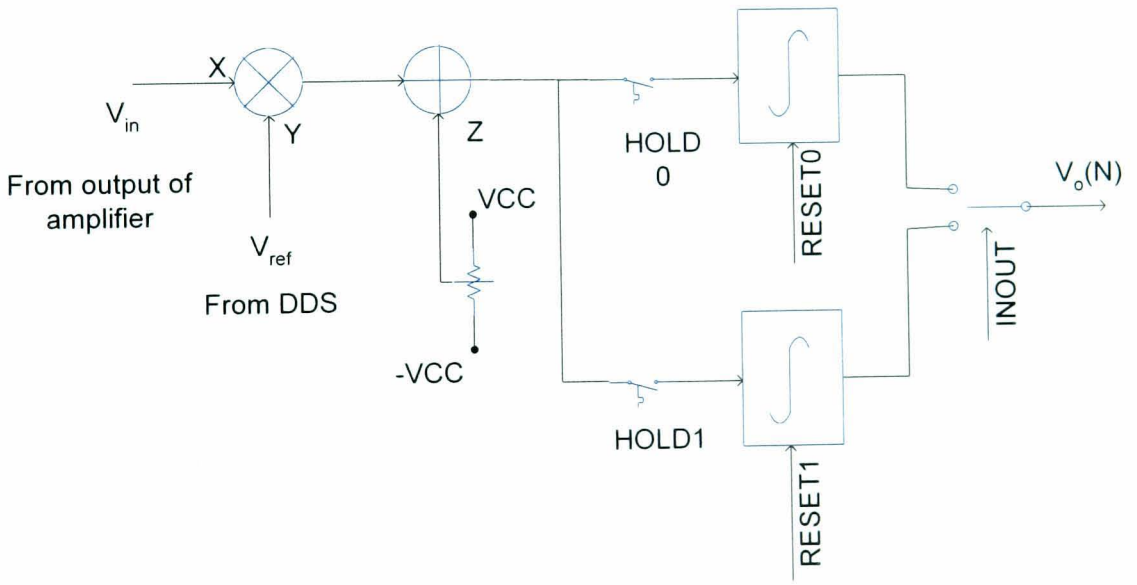

Figure 5.5 Illustration of the demodulation block

The demodulation function block is designed as shown in Figure 5.5. The received signal from the electrodes after amplification is sent to the X input of the multiplier, and the reference voltage is directly sent to the Y input of the multiplier from the DDS output. The measured signal and the reference signal both ride on identical frequency, as they are all generated from the same synthesizer. Both these signals are single-end signals and the

other terminals of differential inputs are connected to the ground. A multi-turn potentiometer is used to adjust offset voltage of the multiplier in the range of positive to negative voltage. Due to the fact that the demodulation on each electrode pair is independent from the others, the integrator has to be discharged to zero before the new demodulation starts. In addition, after demodulation is finished, the integrator is allowed a short time to hold the result for analogue-to-digital conversion and PGA gain adaptive control process. This is achieved by using two analogue switches (MAX301, MAXIM, Inc), one for discharging and the other for result holding operation.

To improve the speed of data acquisition further, two integrators are designed into the circuit, one working for integration, the other holding the result and discharging. These two integrators should have matched RC constants to provide the same scale demodulated signal as Eq5.31 shown. However, in practice, this is difficult to implement. Therefore, in MK2 this work is done by a software calibration after data acquisition finished. The integration results, of both integrators, are sent to the analogue-to digital converter in turn for quantization.

The demodulation control timing and integrator operation is shown in Figure 5.6. Before the data acquisition starts, the integrators are in the discharge state as the control signal RESET0=0, which means the integration capacitor is shunted by switches. When the signal demodulation starts, the signal and the reference voltage are multiplied. The product is sent to integrator 0. Integrator 0 will wait a short time T_s for analogue settling. This time duration is calculated using the equation Eq5.24 or Eq5.27 for the real part or the imaginary demodulated part. Then the control sets RESET0=1 and HOLD0=0. Integrator 0 starts integration operation. It will present the integer times the period of the carrier wave to cancel high frequencies as a result of the integration result. After that, the signal sets HOLD0=1 to break the input of integrator 0 and hold the integration result for the analogue-to-digital conversion. Once the data sampling is finished, integrator 0 is discharged again by the control signal RESET0=0 and HOLD0=0. When integrator 0 is working on result holding and then discharging, integrator 1 is working on another measurement in turn. These operations are carried on until all configured channels have been measured. The integration results from the two integrators are multiplexed to the analogue-to-digital converter by the control signal INTOUT. When

INTOUT=0, the result from integrator 0 is presented and when INTOT=1, the result from integrator 1 is presented.

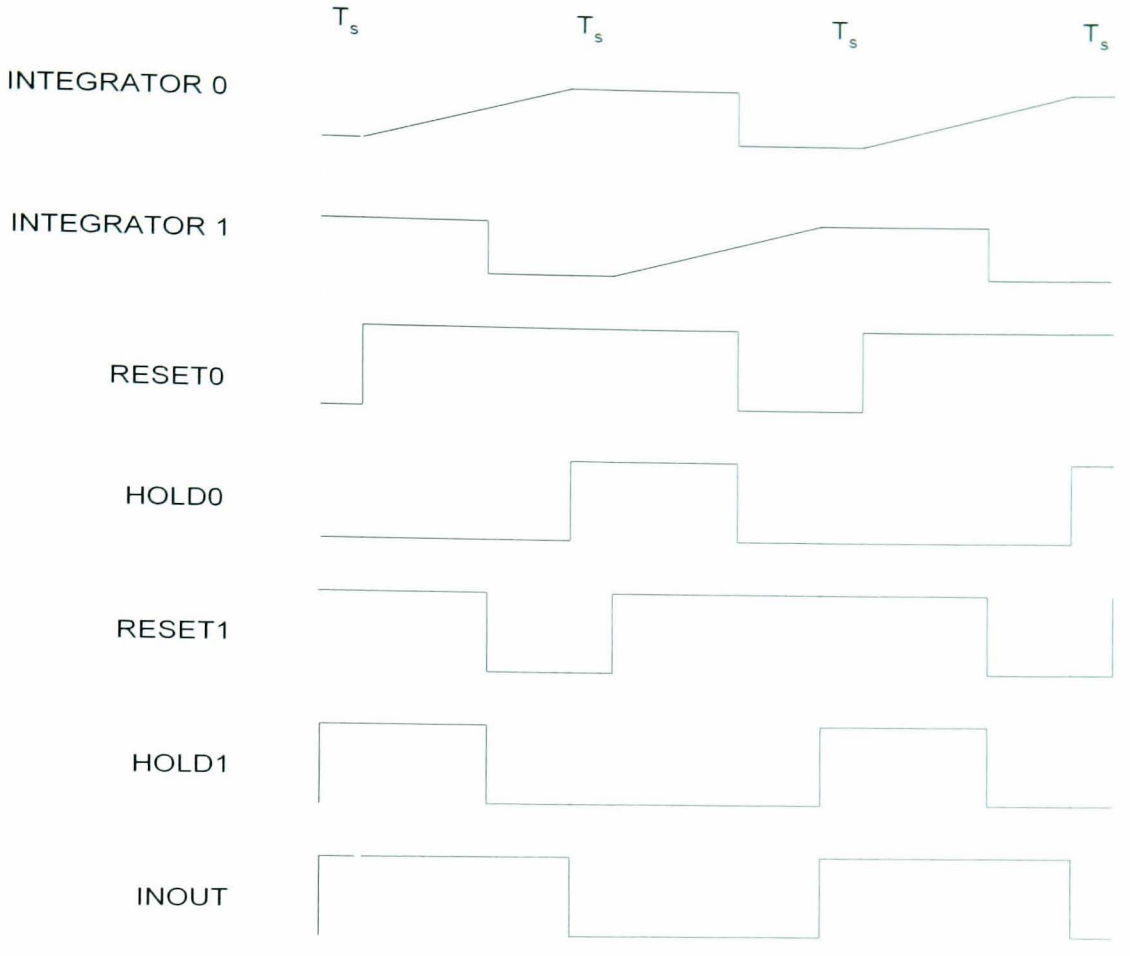

Figure 5.6 Signal demodulation operation and control timing

The demodulation output is also used as the gain control signal for the programmable gain amplifier. Once the measured channel is addressed, the system measures the real part of the signal on the receiving electrode pair with the basic signal path gain controlled by the system timing, and then set new PGA gain and make real measurements.

The printed circuit board for coherent demodulation design is shown in Figure 5.7. The board is mounted into the mainframe machine, and the RF interference isolation is considered during board layout.

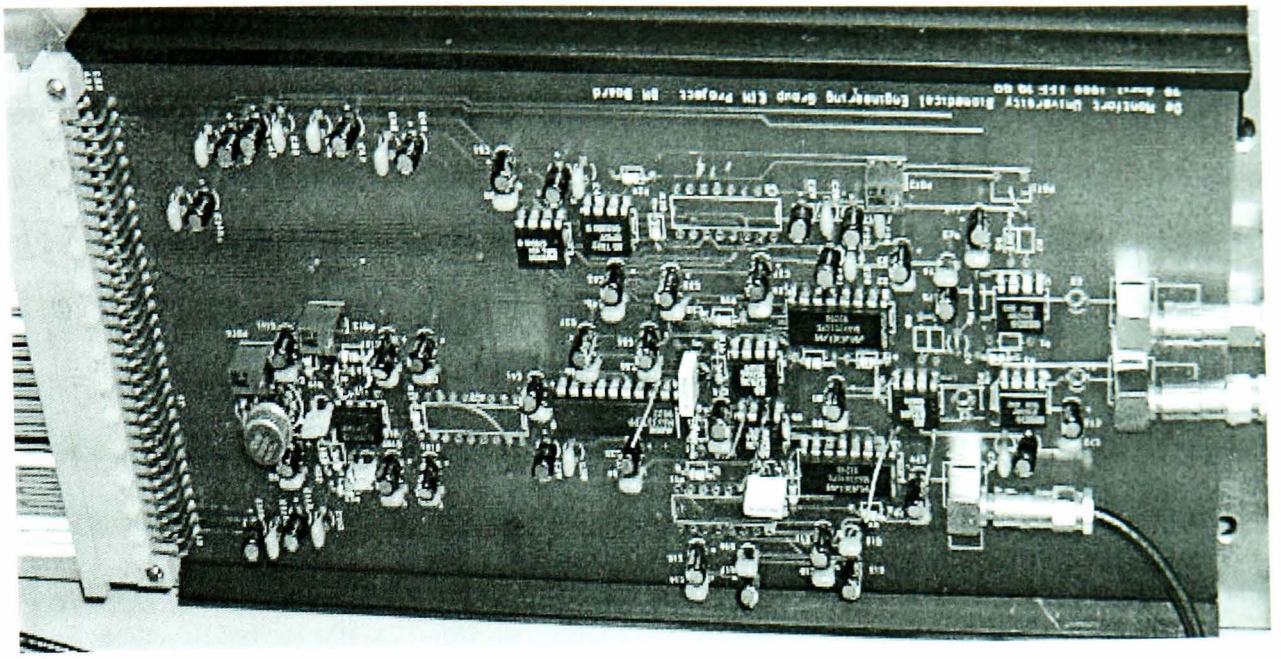

Figure 5.7 The modulation board

5.4 Implementation of digital coherent demodulation

With the development of digital electronic technologies, more complex signal processing algorithms have been used in the electronic data acquisition system. Using high-resolution analogue-to-digital conversion techniques, the original analogue signal can be transformed into the digital format. This minimizes the effects of imperfect parameters of physical devices such as drift voltage, bias current and temperature concerned variations. In addition, the data transmission using digital techniques also reduces the design difficulties in terms of amplitude attenuation, phase shifting and interference.

Digital implementation of demodulation is based on the digitalized signal by means of the analogue-to-digital converter. The accuracy of the demodulation algorithm is dominated by the converter resolution and the algorithm computing error.

The measured signal from the receiving electrode pair is a physiological varying signal riding on the carrier wave that is applied at imaging frequency. Therefore, in the frequency domain, it is a narrow band signal. If it is measured in relatively short period, it could be treated as constant signal riding on the carrier.

With sampling interval T, the analogue signal $v_i(t) = V \cdot \sin(\omega \cdot t + \varphi)$ .is converted into digital format as

$$v_s = \sum_{n=-\infty}^{\infty} V_i \cdot \sin(n\omega T + \varphi) \cdot \delta(t - nT) \qquad \text{Eq5.34}$$

Here $\delta(t)$ is a unit impulse function and n is an arbitrary integer. In the Fourier transform, it is the convolution of two functions in the frequency domain as

$$V_s = \frac{1}{T}\sum_{k=-\infty}^{\infty}\delta(j\omega - kj\omega_s) \qquad \text{Eq5.35}$$

Here $\omega_s = \frac{2\pi}{T}$ is the sampling frequency in radians/second and k is arbitrary integer. It can be seen that the measured signal is modulated by the sampling frequency.

When $\omega_s > 2\omega$, the Nyquist condition is satisfied and the sampled digital signal can be recovered to the original analogue signal after low-pass filtering. In the demodulation process, two signal data sets are multiplied in software operation, following the same principle as it does in the analogue demodulation. The reference voltage is actually a lookup table generated from computing and stored in the memory.

However, when $\omega_s < 2\omega$, the sampled digital signal is aliased, and the lower frequency signal is represented as

$$v_a(t) = V \cdot \sin[(\omega_s - \omega)\cdot t - \varphi] \qquad \text{Eq5.36}$$

If proper low-pass filtering is applied, the signal is shifted to a lower frequency by the sampling frequency and the result is still the same amplitude and phase information as before. This solution can be found in the normal narrow band DSP algorithm.

If the lookup table as demodulation reference is calculated at frequency $\omega - \omega_s$, using the coherent demodulation method the real and imaginary part of measured signal can still be obtained. However, for high imaging frequency data acquisition uses, the sampling frequency is reduced and this makes it possible to use low sampling rate analogue-to-digital conversion.

$$V = \frac{1}{N}\sum_{n=k}^{k+N} v(n)\cdot v_{ref}(n) \qquad \text{Eq5.37}$$

Eq5.37 is used for demodulation of real or imaginary part of the measured signals, in which N is the sample number in integer times period of the signal. The front 0 to k-1 samples are discarded due to the signal settling.

In practice, the considerations on the implementation include quantization of the output samples, linearity, the need for sample-and-hold circuits, and limitations on the sampling rate. In addition, the analogue-to-digital converter needs to be accompanied with a high-speed digital signal processor for further computing processing and. Using a

lower sampling rate converter can dramatically reduce the cost of the data acquisition system.

Obviously digital implementation of coherent demodulation does not need the real reference voltage, and the problem caused by the dc drift and offset on the measured signal is completely removed.

5.5 Summary

In this chapter, the coherent demodulation method has been discussed and the implementation by analogue and digital techniques is described. With two 90° phase-different reference voltages that are at the same frequency as carrier is, the real and imaginary part of the measured signal can be demodulated.

Using low-pass filtering to separate the biomedical signal is common process and provides a continuous output, which is suitable for physiological monitoring purpose. However, in the EIT data acquisition system, because the signal measurements are multiplexed among the receiving electrode combinations, it is not acceptable to take long time to let signal settling, from the real time imaging or physiological measurement points of view. In EIT practice, the integrator is used to replace the low-pass filtering for removing high frequency component. In theory, the integration time can be as short as one period of the signal and this makes the data acquisition much faster.

The effect of dc offset to the demodulation is minimized by the high quality of reference voltage, but for the imaginary part demodulation, it should be taken into account that the imaginary part of voltage is extremely small due to small phase shift induced by the bio-impedance.

Polarization potentials must be removed from signal path because of their large and random amplitude, and then the high-pass filtering has to be adopted. However, the high-pass filtering stage RC time constant does apply side effect on the integration results. By choosing a proper starting time for integration, the impact can be minimized.

This phase sensitive demodulation technique is implemented in analogue circuit technology with integrated circuit multiplier in MK2 data acquisition system. To increase the data acquisition speed, two integrators are used in turn, as one is integrating, the other is holding the result and discharging.

A scheme for digital demodulation, based on high resolution, high sampling rate analogue-to-digital converter and high performance digital signal processor is also presented. Because the measured signal is a narrow band signal, it makes it possible to use a sampling frequency lower than Nyquist rate to demodulate the real and imaginary part of the measured signal.

Chapter 6 System Structure and System Timing

6.1 Introduction

The electrical impedance tomography is a computer aided imaging technology, which collects boundary voltages from the surface electrodes to reconstruct the internal impedance distribution. The boundary voltage is generated when an ac current is injected into the imaged object, and with constant current, this voltage is proportional to the transfer impedance if this measurement is treated as a two-port electric network. However, as the low frequency current is very "soft", the injected current disperses all around the field and does not display a planar propagation property. Impedance change in the medium of interest affects the current field distribution in all directions within the volume. Even with this imperfect situation the capability of extracting useful data, though impaired is still considered practical. Therefore, the accurate measurement of the voltages on the boundary are very important in order to recover the inside impedance distribution as well as possible. The impedance distribution is solved from the boundary conditions by formulating an inverse problem for solution.

The resolution of the impedance image reconstruction depends on the number of independent data being measured on the surface of the object, and applying the four-electrode method, it will rely on the number of electrodes and the measurement strategy adopted in the data acquisition. However, the number of electrodes mounted on the surface of the imaged object is limited by the size of the electrode and the difficulties of the contact to the surface. Therefore, the quality of the reconstructed image is poor when considered for potential clinical applications. To overcome the problems previously encountered, proper data acquisition strategy is very important in the EIT system design.

The data acquisition system collects the voltage signals on all possible combinations of electrodes at the same time or in sequence depending on the hardware resources. Obviously, real time imaging is essential for monitoring physiological phenomena and activities in body rhythm. Here real time means that imaging should be at least 25 frames per second for continuous display of the image. However for the electrical impedance

mammography purpose, real time is not strictly required, even though the data acquisition still need to be at a fast rate to avoid physiological effects.

According to the clinical research [8], abnormal breast tissue has larger admittance than the normal tissue has due to the shape and status change of the cell in the pathological conditions, especially at high frequency around 1MHz. Therefore, there is a need to extend the bandwidth of existing EIT systems to cover this frequency range. Of course, high measurement accuracy is essential. This improvement and migration of EIT system from single frequency to wide band measurement introduces many problems in term of the hardware structure, layout, and solving or minimizing radio frequency problems during the physical implementation.

Considering the analogue circuit tolerance and the measurement methodology demand, the system timing is organized into a programmable logic device to ensure it can be modified for any purpose of experiments during the research and clinical trial. In addition, the firmware design should be flexible to suit applying any possible electrode combinations and configurations for imaging reconstruction algorithm development.

The system hardware should be suitable for potential future technology updates, and therefore to be designed as a development platform for software test with a suitable electrode lead interface to fit both saline phantom test and clinical research.

6.2 Structure of EIT data acquisition system

The data acquisition system design of electrical impedance tomography is focused on achieving high accuracy, fast speed and wide frequency bandwidth. According to whether the multi-channel data acquisition is multiplex operated or not, the hardware system is divided into parallel and serial system structure catalogues. The parallel structure system uses fixed current driving and voltage receiving circuit on each electrode combination pairs. It measures all the boundary voltages at the same time when an injection current is applied onto a driving electrode pair. The parallel structure system provides full speed of the data acquisition, and makes it possible to put the measurement circuit near the electrode amounting space. It significantly benefits the high frequency performance of the analogue circuit due to shorter cabling connection. Parallel system operation is used in most of real time imaging systems with 16 or 32 electrodes configuration for physiological monitoring purpose.

As discussed earlier, the resolution of EIT is limited by the number of electrodes involved into the data acquisition; however increasing the number of electrodes to improve the quality of image is difficult in practical system due to cost, manufacturing and difficulty of calibration. Therefore, the serial structure system using multiplexer to address multi-channels in turn is still a practical choice.

In addition, with the development of integrated circuit manufacturing, complex and high-speed circuits can now be built into a single small outline package. It makes it possible to integrate the current generation or measurement circuit into the electrode to form an active electrode. Using active electrodes cancels the need for coaxial cable connection and makes fundamental improvements to high frequency image reconstruction.

6.2.1 Serial structure EIT system

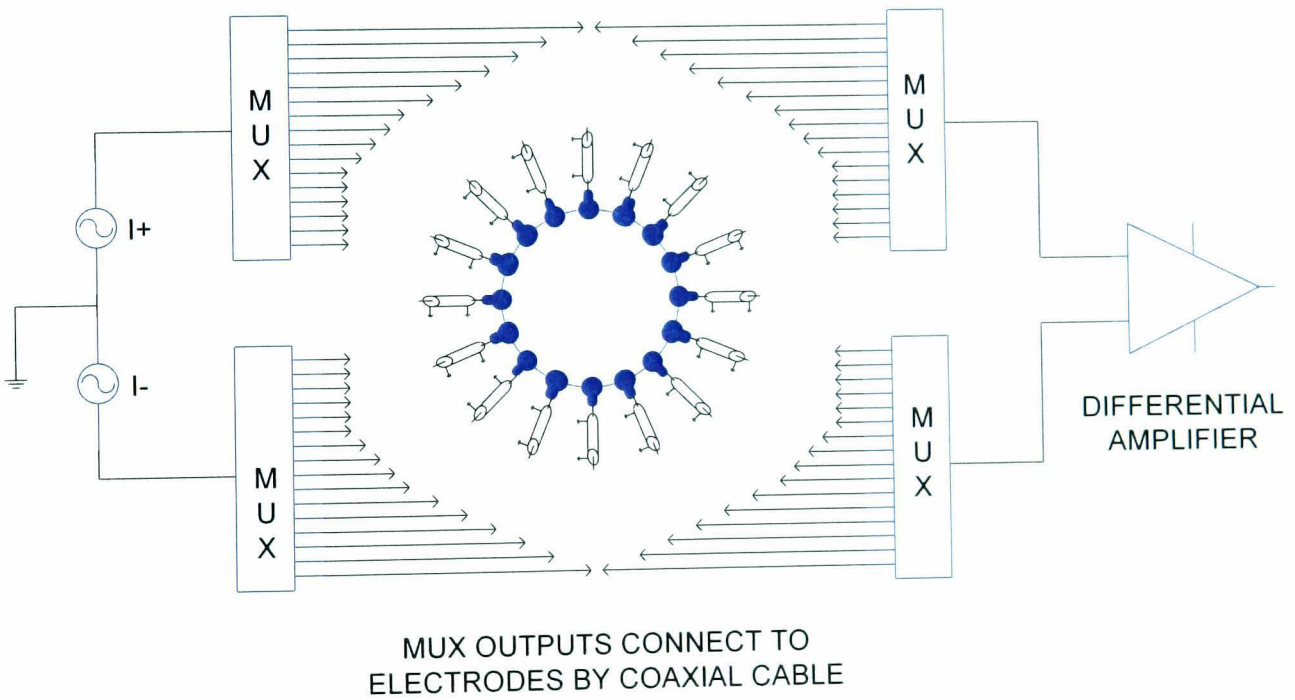

Figure 6.1Illustration of serial Structure EIT System

In serial structure EIT data acquisition system, all electrode combinations share one current source and one voltage measurement circuit. The system diagram is shown in Figure 6.1. The electrodes and measurement instrument is connected by means of coaxial cable. Due to the low data acquisition speed, the serial structure cannot be used in the real time system, and suffers the problem of narrow bandwidth. However, for mammography

(cancer detection) purposes, the abnormal breast tissue's pathological condition is in a stable process, without strong disturbance from other physiological rhythms, such as blood flow and breathing. Therefore, the real time imaging is not a necessary demand in the data acquisition system design for EIM. The difficulties are focused on producing a wide band measurement and data accuracy.

The measurement model of the EIT system is shown in Figure 6.2 in which, the coaxial cable and multiplexer are described with their equivalent electric circuits. As discussed in the measurement circuit design, the common-mode signal rejection ability of the measurement circuit depends on the matching of the differential signal input paths to the front-end amplifier. In addition, the input impedance of the front-end amplifier has to be large enough to constrain the effect of the high output impedance signal and the contact impedance of electrodes. However, as the signal passing through the multiplexers and coaxial cable connections, the performance of the designed circuit can be seriously degraded by stray capacitance and the on-resistance of these components, especially at high frequencies.

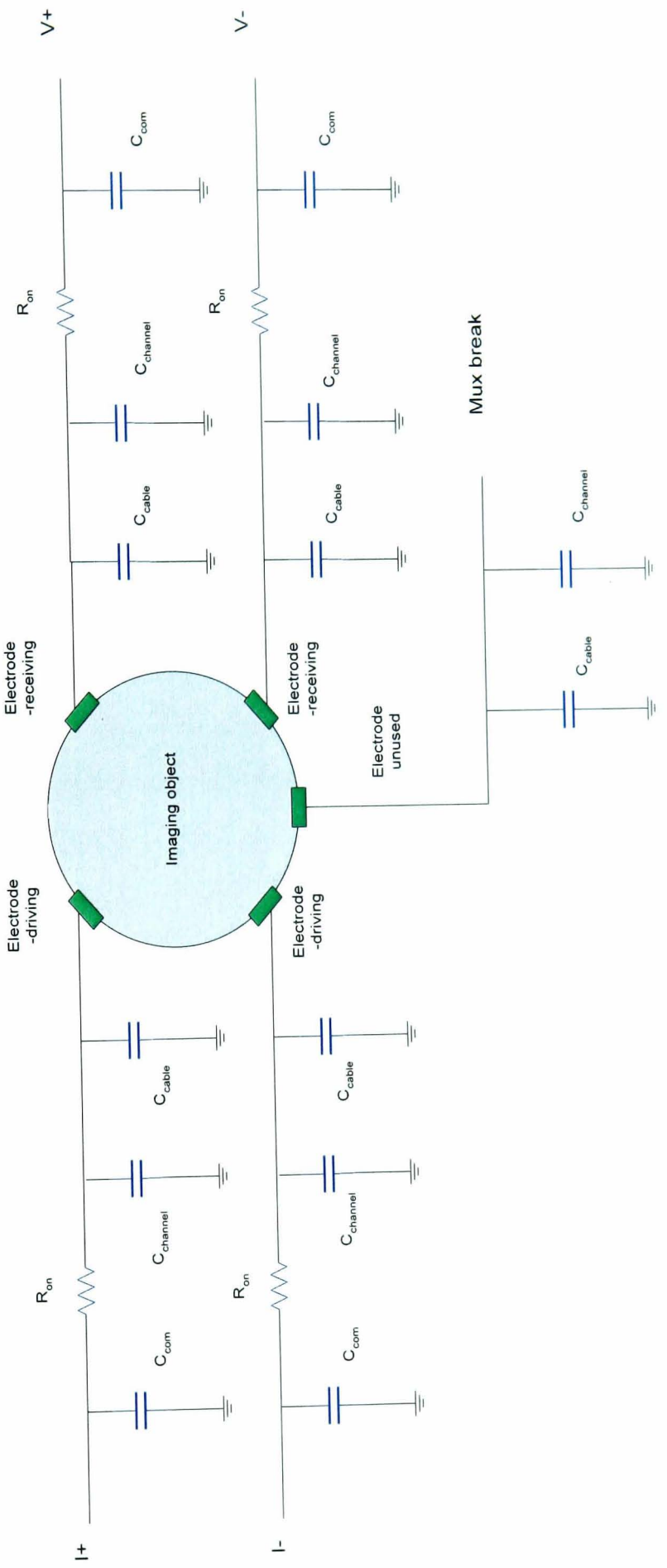

Figure 6.2 The measurement model of EIT system

6.2.2 Multiplexer performance

The multiplexer consists of field-effect transistors (FET). Basically the FET switch is a bi-directional device, and therefore signals can go either way through it. In the EIT data acquisition system, the multiplexer devices can be used either as de-multiplexing for current injection or as multiplexing for voltage channel measurements.

In the low frequency imaging data acquisition applications, the multiplexer on-resistance, which varies over the input signal swing, is a significant factor. Normally it induces undesired non-linearity to the measurement. However, as it is discussed in the current source and the front-end amplifier design, this effect can be minimized by high output impedance of current source and high input impedance of front-end amplifier.

At high imaging frequency, the limitation of the multiplexer appears due to the combination of substrate and stray capacitances which forms low-pass filtering to voltage signal or feed-through effect to current injection. The simplified equivalent electric circuit model of the multiplexer is shown in Figure 6.3, in which Cin is the input capacitance; Ccom is the output capacitance; and Ron is the on-resistance. The typical values of these parameters from commercial products are shown in Table 6.1.

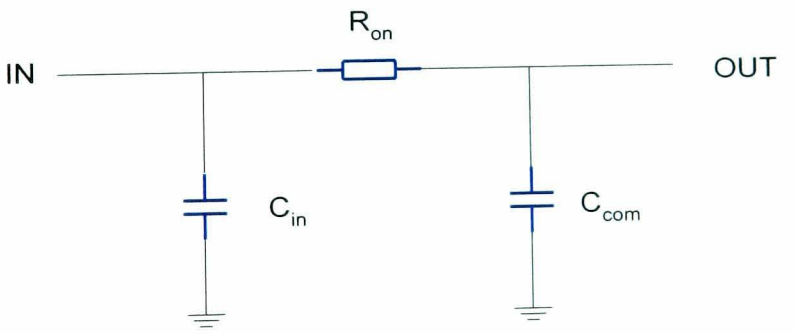

Figure 6.3 The simplified equivalent electric circuit model of the multiplexer

Table 6.1 Key parameters of main commercial multiplexers

Product	MUX	Manufacture	C_{in}	R_{on}	C_{com}
MM74HC4051	8×1	Fairchild	15pF	30±5Ω	90pF
4052	4×2				45pF
4053	2×4				30pF
MAX4581	8×1	MAXIM	4pF	50±1Ω	25pF
4582	4×2				17pF
4583	2×4				12.5pF
MAX308	8×1	MAXIM	3pF	60±1.5Ω	37pF
MAX309	4×2				25pF
ADG408	8×1	Analog Devices	11pF	40±15Ω	54pF
ADG409	4×2				34pF
MAX306	16×1	MAXIM	8pF	60±1.5Ω	140pF
MAX307	8×2				70pF
ADG406	16×1	Analog Devices	5pF	80±4Ω	60pF
ADG407	8×2				40pF

When a multiplexer is used in the current injection, the output impedance of the current source is degraded by the stray capacitance of the multiplexer, which is parallel connected to the output impedance of the current source as shown in Figure 6.4. This situation becomes worse as imaging frequency increasing. In the same way, when a multiplexer is connected to the front-end amplifier for measurement channel selected, the input impedance of the differential amplifier is also degraded by the stray capacitance of the multiplexer.

Obviously, FETs with lower on-resistance tend to have larger capacitance. The choice of multiplexer is a trade-off between the on-resistance and the stray capacitance. In addition, it should be mentioned that much of the bandwidth lose is due to the protection components, for example, current limiting series resistance and capacitance of clamping diodes. A higher-speed switch is achievable by eliminating some of these protections. However, because an over range signal would easily destroy the gate isolation of CMOS transistor, the amplitude of input signal has to be considered carefully.

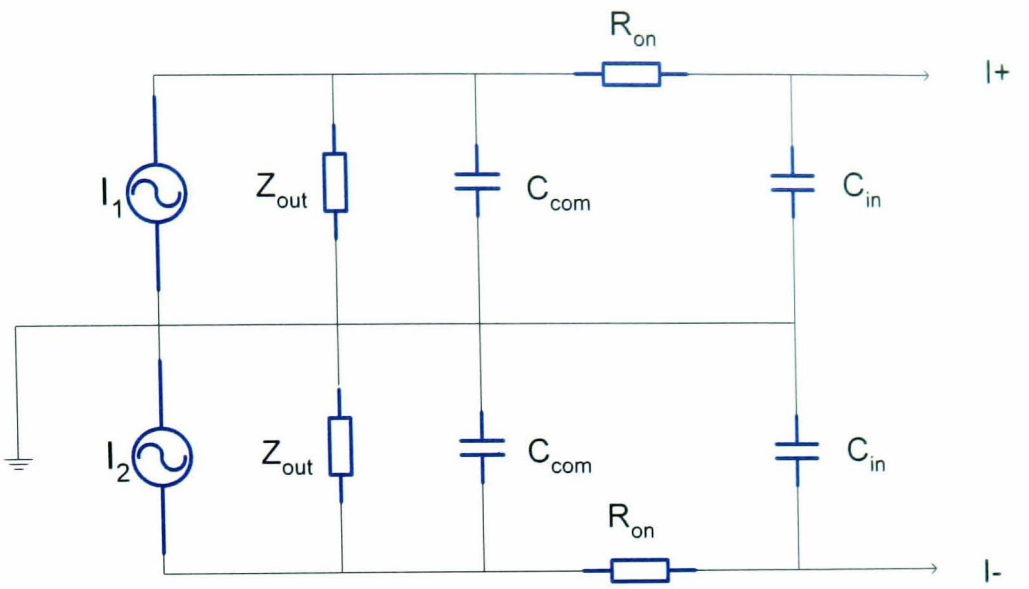

Figure 6.4 The output impedance of a current source degraded by the stray capacitance of a multiplexer

Figure 6.5 shows the performance of the multiplexer over a frequency range from 10k to100MHz. The simulation circuit used is shown in Figure 6.6, in which multiplexer ADG406 (Analog Devices, Inc) is tested with constant current source and the load impedance changed from 100Ω to 2000Ω by a step of 100Ω. It can be seen that with 2000Ω loading impedance, 1% accuracy is maintained over a bandwidth of about 100 kHz.

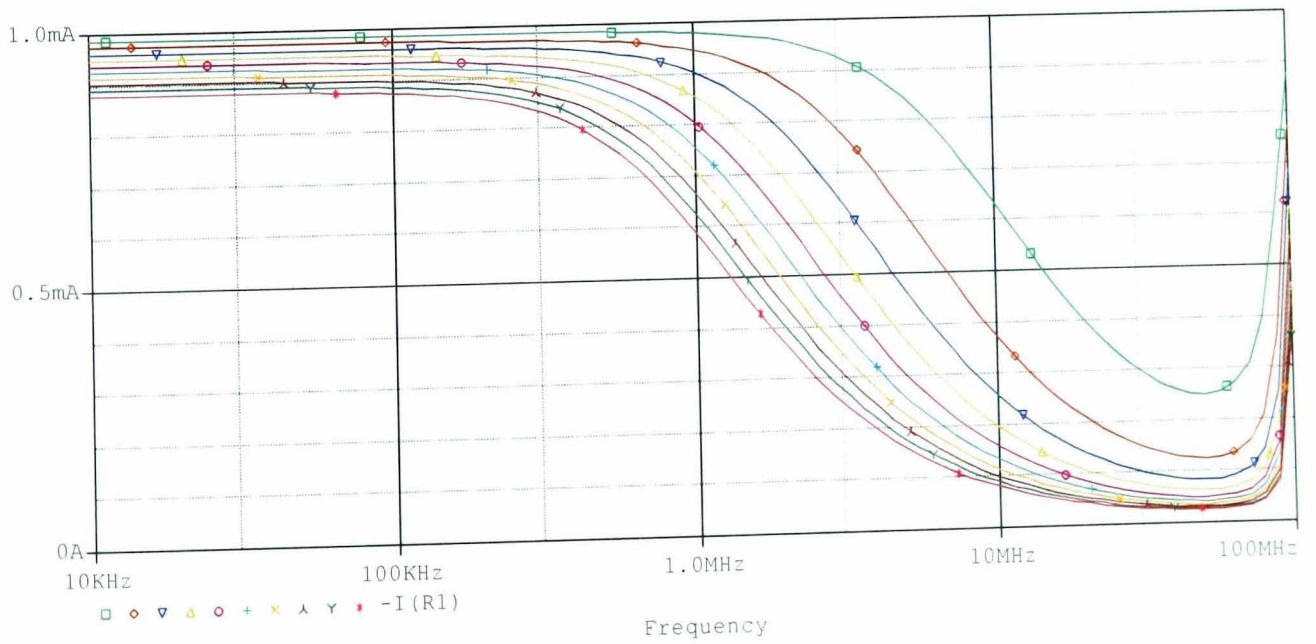

Figure 6.5 The multiplexer performance: current versus frequency (loading is changed from 200Ω □ to 2000Ω · by a step of 200Ω)

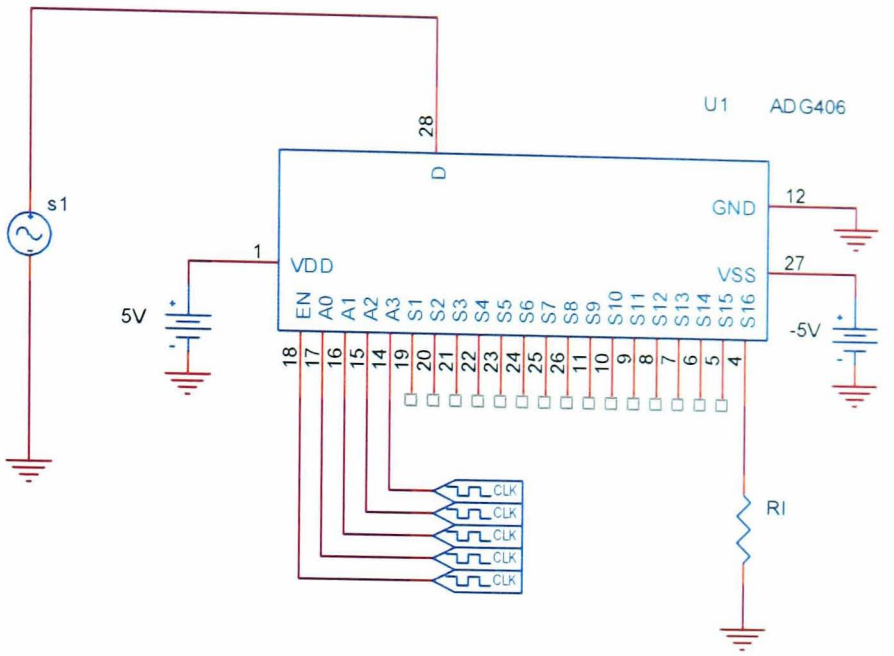

Figure 6.6 The simulation circuit of the connection of the multiplexer for PSPICE

According to Table 6.2, the roll-off of frequency response of the multiplexer is mainly introduced by the common output capacitance, which increases as the number of switches in the multiplexer increasing. The bandwidth of the measurement system can be improved by using cascaded multiplexers instead of multi-inputs multiplexer. However, care needs to be taken when using cascaded switches, as the on line resistors will be increased.

6.2.3 The coaxial cable effects

Coaxial cable is used as signal transmission lines for current injection and voltage collection. The measured object is by the side of the measurement system, and relatively long cable connections are needed between the mainframe machine and electrodes mounted on the surface of the object, whether the system has a parallel or serial structure. The coaxial cable used normally has a characteristic impedance of 50Ω. In addition, the high frequency signal path is impedance matched during the design procedure to ensure the minimum reflection and oscillation of signal occurs.

6.2.3.1 Capacitance of coaxial cable

Coaxial cable has the advantage of being completely shielded, i.e., there is no radiation or pickup of external signals. It is necessary for the multi-channel EIT system to eliminate the cross talk between channels.

Figure 6.7 PSPICE model of the coaxial cable

However, coaxial cable has capacitance between the centre conductor and the shield conductor surrounding it. According to the manufacture's datasheet, the capacitance of the cable is about 30pF/foot (RG174U). The effect on the constant current transmission can be simulated by the PSPICE circuit shown in Figure 6.7. Coaxial cable RG174U is used in the simulation, which has characteristic impedance 50Ω for RF signal transmission. The constant current source is set at 1mA amplitude and the load

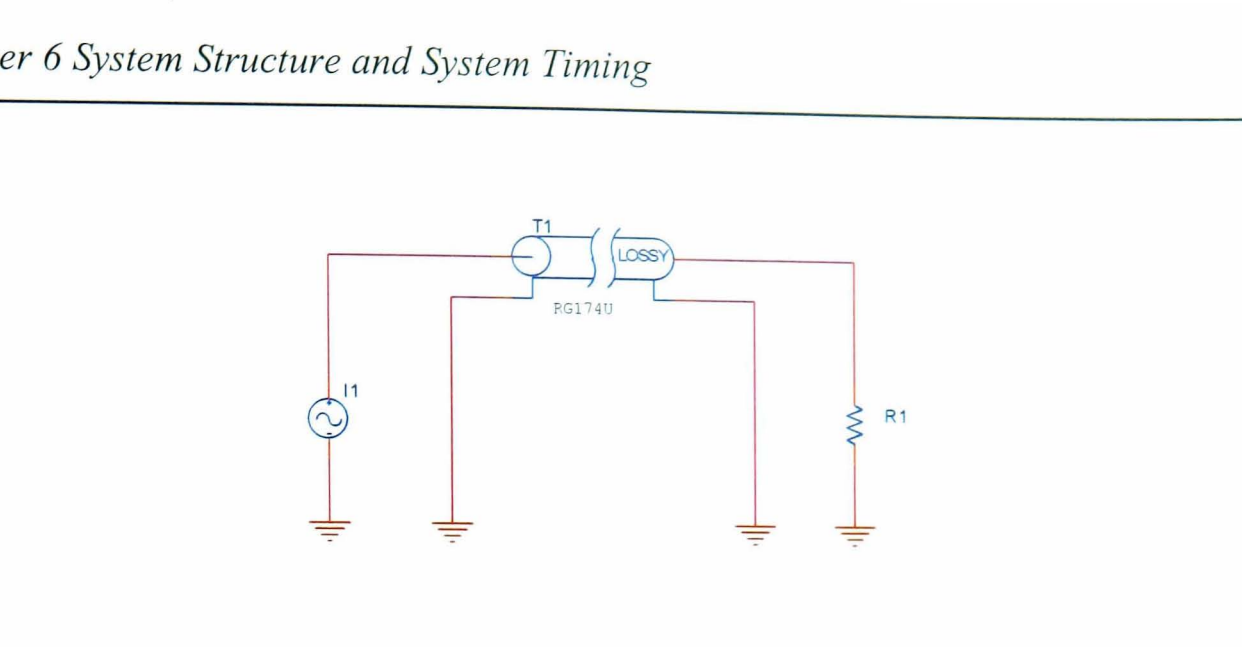

Figure 6.8 The simulation result of coaxial cable (loading is changed from 200Ω □ to 2000Ω ◦ by a step of 200Ω)

impedance is at the designed maximum 2000Ω. Figure 6.8 shows the shunt effect as the cable capacitance increases with frequency increasing. It can be seen that for 1%

accuracy of constant current transmission, the highest frequency of current passing through a 1 meter length of cable is 127.8 kHz. Furthermore, the capacitance of the cable also induces phase shift to the applied current. Any unmatched cable length over all configured channels will be an error source to the detected phase information. For these reasons, in practice, the length of cable should be kept as short as possible and must be matched and fixed.

Besides, when more electrodes are mounted on the surface of the imaged object, the situation is made worse and the four-electrode measurement method will not be achieved in it basic physical principle.

6.2.3.2 Guard shield of coaxial cable

The effect of the coaxial cable capacitance can be minimized by applying the same amplitude voltage to the shield conductor by means of shield driver amplifier, as shown in Figure 6.9. The performance is shown in Figure 6.10, as a simulation result using PSPICE. The models of electric devices in the simulation are RG174U coaxial cable and

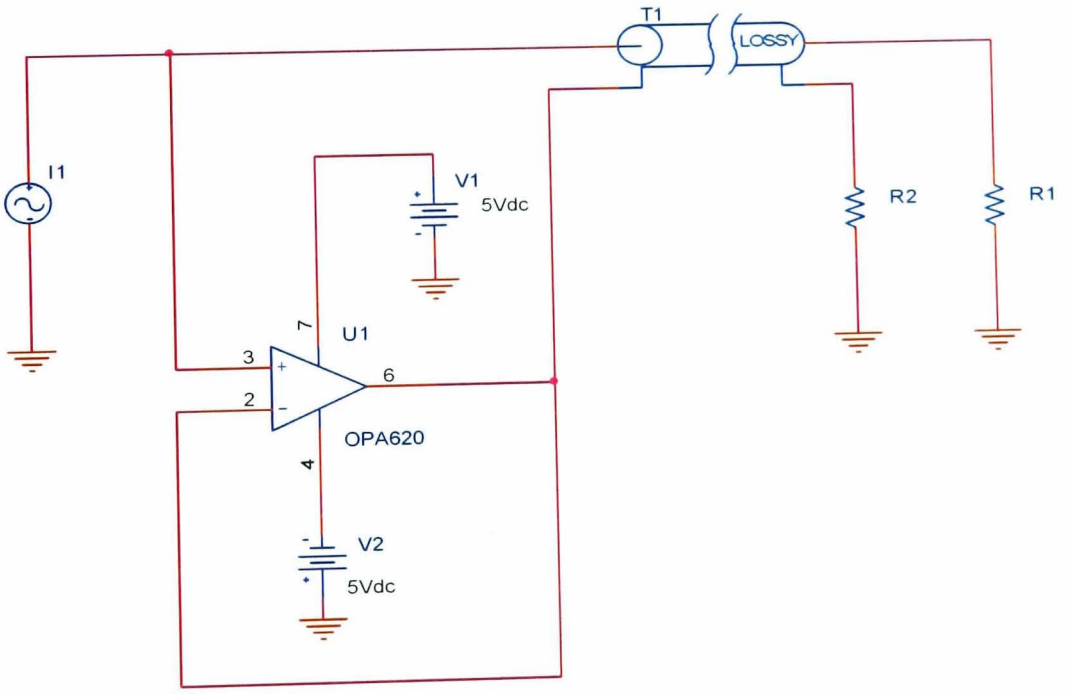

Figure 6.9 The coaxial cable with shield driver amplifier for PSPICE

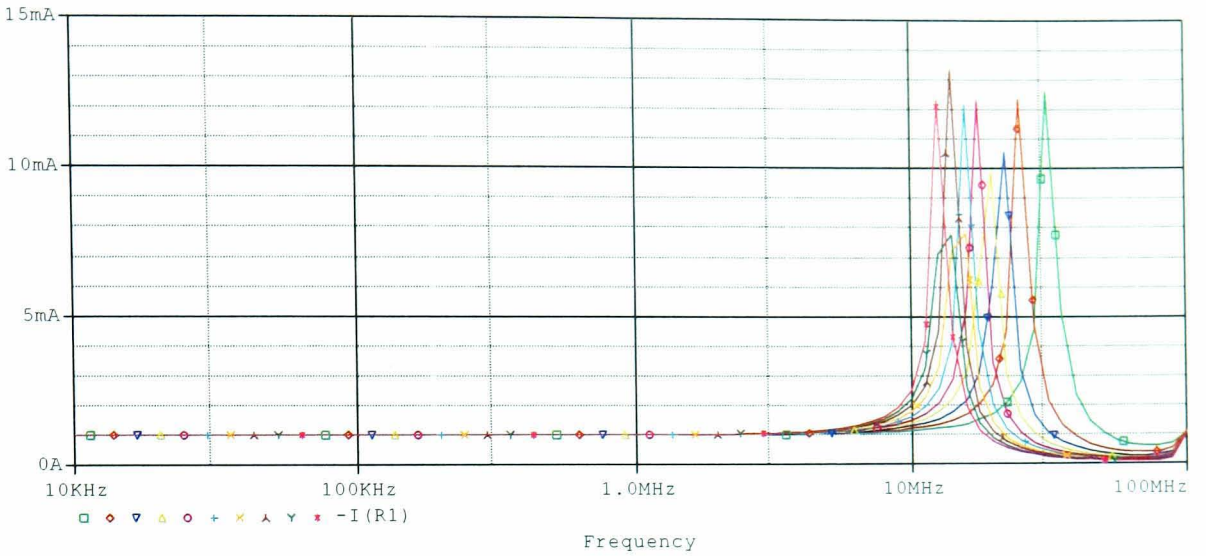

Figure 6.10 The simulation result of the coaxial cable with shield driver amplifier (loading is changed from 200Ω □ to 2000Ω ⋆ by a step of 200Ω)

OPA620 op-amp, which are from the Orcad simulation package. According to the simulation result, to achieve 1% accuracy constant current transmission to the load over one meter long coaxial cable, the highest frequency of current can extend to 1.316MHz. However, over this frequency range, the performance is degraded by the phase shift between the cable and the op-amp.

In the high-resolution EIT data acquisition system, the number of electrodes is large and the cost of guard shields to all cable goes up dramatically due to the double-shielded coaxial cable needed in practice.

The outer shield is grounded at the input end in the normal manner, and serves as an electromagnetic-interference suppression shield.

6.2.4 The performance of multiplexer and coaxial cable path

In EIT system design, the current is injected from the current source to the imaged object by means of multiplexer and coaxial cable path. The comprehensive effect is becoming even worse as simulation results shown in Figure 6.12. The simulation circuitry is displayed in Figure 6.11. The roll-off frequency at 1% accuracy constant current is just at 61.2 kHz. This simulation is taken on the multiplexer chip ADG406 and coaxial cable RG174U PSPICE mode. The length of coaxial cable is still set at 1 meter.

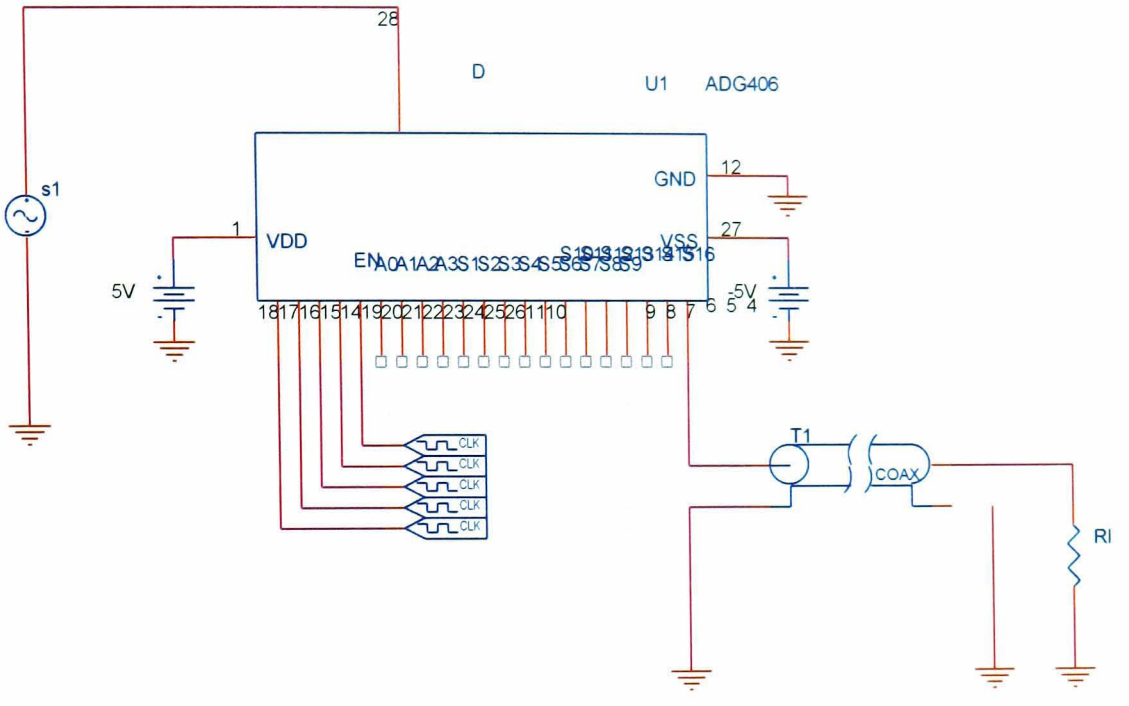

Figure 6.11 The simulation circuitry with the multiplexer and the coaxial cable

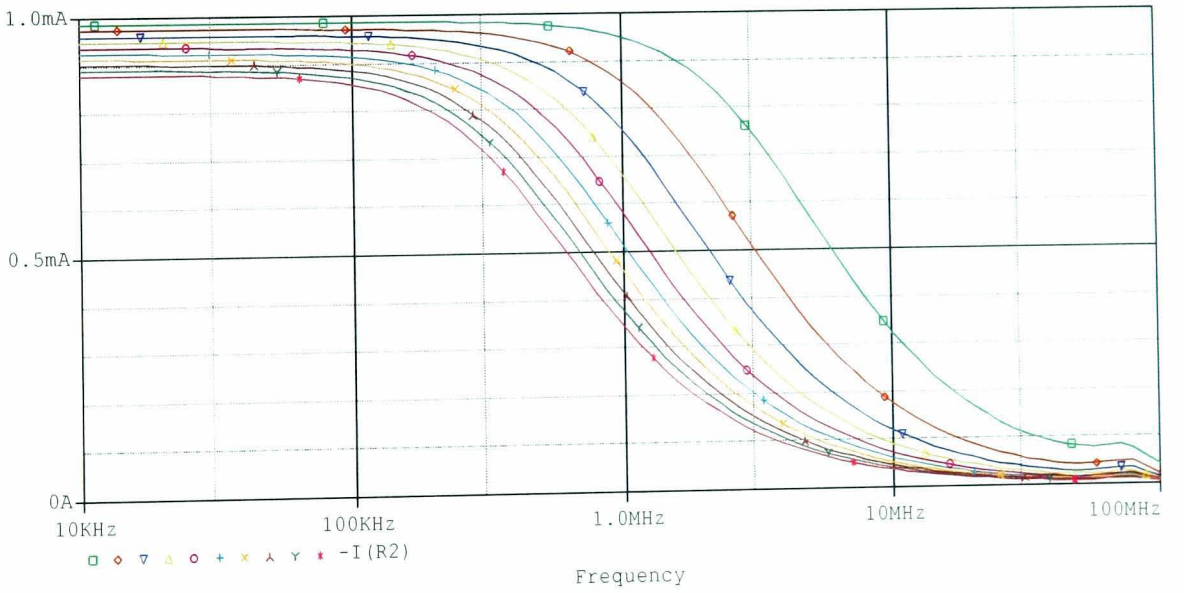

Figure 6.12 The performance of the multiplexer and the coaxial cable path (loading is changed from 200Ω □ to 2000Ω ◆ by a step of 200Ω)

6.2.5 Conclusion of signal transmission

Table 6.2 gives the roll-off point of performance of transmission that is abstracted from above simulations. It also provides the voltage signal bandwidth from the same simulation circuitry as of constant current transmission simulation. The bandwidth is given as the signal kept as 1% accuracy of its original value. Obviously, the voltage transmission has relatively large bandwidth than of the current signal transmission. This result reminds that in the EIT system design, it is necessary to avoid the constant current using multiplexer and long cable connection to the electrodes, or say, put the current source to the object to be imaged as near as it can.

Table 6.2 The non-attenuation frequency bandwidth (1% accuracy) of device in the signal transmission path

Device		Multiplex	Coaxial cable	Multiplex+cable	Cable with screen driving
Voltage signal transmission	RI=2KΩ	10.325M	4.4367M	2.2316M	>100M
	RI=2MΩ	10.000M	4.4367M	2.1168M	>100M
Current signal transmission	RI=2KΩ	100.00K	127.786K	61.240K	1.3160M

6.2.6 Active electrode

According to the previous discussion, the imaging frequency bandwidth of EIT data acquisition system is limited by the multiplexer and coaxial cable. The application of these devices reduces the output impedance of the current source and the input impedance of the front-end amplifier. Moreover, the situation becomes worse when more electrodes are applied, especially in the 3-dimenstional EIT measurement system proposed.

A suggested system for wide bandwidth multi-channel electrical impedance measurement has been shown in Figure 4.6, which overcomes the effect of cable and multiplexer. In the diagram, each electrode is connected to a current source and a voltage buffer amplifier so that it can be used to either applying constant current or sensing

voltage on the boundary. If these circuits are small enough to be built into the body of electrode, it forms the so-called active electrode as discussed in Chapter 3 and Chapter 4. As a current injection electrode, the output impedance is the value of output impedance of the current source originally designed. As a receiving electrode, the buffer amplifier on the electrode gives an impedance transformation from the high output impedance signal to the low output impedance signal.

Using discrete electronic components in the design, it is impossible to fit the active electrode into the space around the surface of the imaged object. In addition, from a high-density active electrode array manufacturing point of view, the mechanical difficulty is much higher than the electronic demand. Moreover, the power consumption is also a problem that needs to be considered. Advanced integrated circuit process technique appears to be the route to minimize the circuit outline and wiring connection. In chapter 3 and Chapter 4, the possibility of circuit implementation has already been discussed in detail.

6.3 Measurement strategy

The electrical impedance tomography data acquisition system adopts the four-electrode measurement method, which applies current to the object and collects boundary voltage on each electrode pair. The measurement should be able to provide enough independent data using the limited number of surface electrodes. In addition, the configuration of current injection and boundary voltage collection should reflect the change of current field to the internal impedance change efficiently and accurately. The hardware system design is prepared in the consideration of applying any suitable measurement strategy. In MK2 EIT system, the neighbouring method, cross method and opposite method are applied in the data acquisition research by means of software settings.

6.3.1 Neighbouring method

Figure 6.13 illustrates the application of this method for a cylindrical volume with 16 equally spaced electrodes, in which the current is applied through neighbouring electrodes and the voltage is measured successively from all other adjacent electrode pairs. The current is first injected through electrodes pair i, and definitely, the highest

current density is located in the area between these electrodes and then decreasing rapidly as a function of distance and internal conductivity. The boundary voltage measurements are achieved on all of the remaining neighbouring electrodes pairs, and there are 13 independently available on each current injection. With 16 current injection pairs, there are 208 measurements in total in a frame data set. With reference to two-port electric network theory, because of reciprocity of those measurements in which the current electrodes and voltage electrodes are interchanged yield identical measurement results. Therefore, for a 16 electrodes system, one frame data set can provide 104 independent measurements.

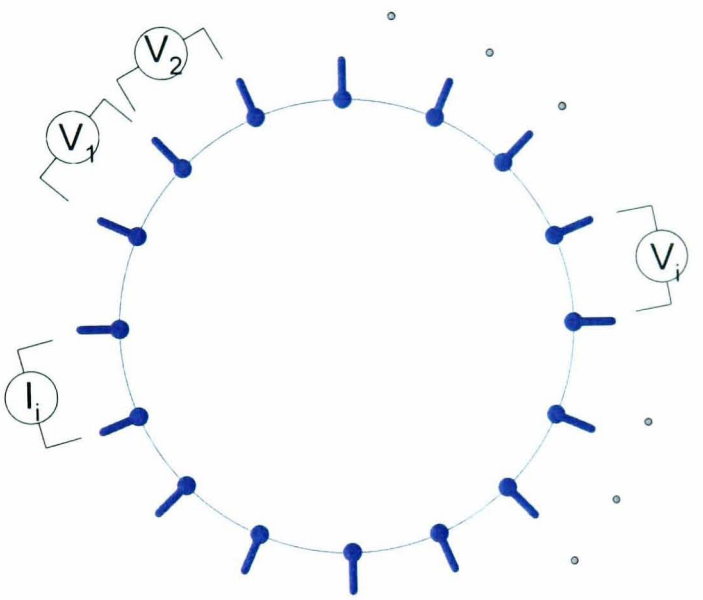

Figure 6.13 The neighbouring measurement method

In the neighbouring method, the measured voltage is at a maximum for adjacent electrode pairs. With opposite electrode pairs, the voltage is only about 2.5% of that. The neighbouring method is suitable for detection on the area located at 1/3 diameter place in the object.

6.3.2 Cross method

A uniform current distribution is obtained when the current is injected between a pair of more distant electrodes. The cross method is illustrated in Figure 6.14. In this method, the current injection mode is gradually changed from adjacent driving, and makes more measurements. With a 16-electrode 182 measurements are available. However, there are only 104 independent measurements among them.

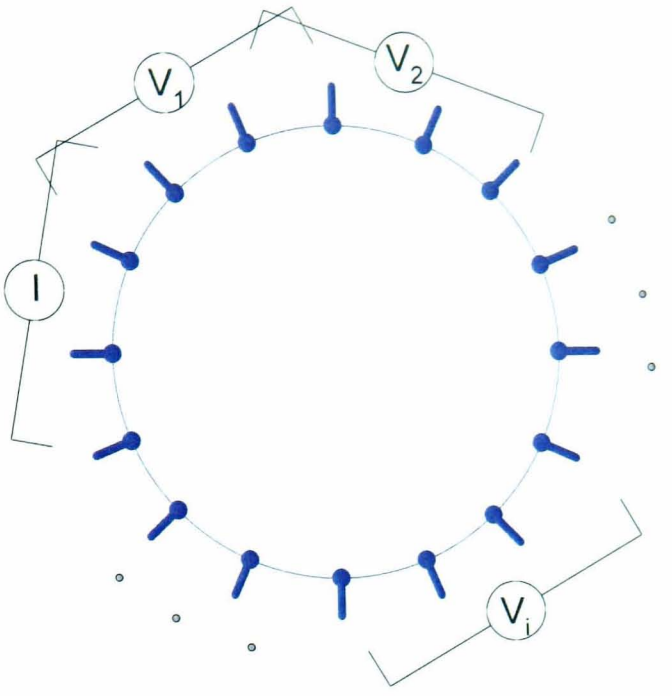

Figure 6.14 The cross measurement method

6.3.3 *Opposite method*

Another alternative impedance measurement is the opposite method, illustrated in Figure 6.15. In this method, current is injected through two diametrically opposed electrodes. The electrode adjacent to the current injecting electrode is used as the voltage reference. Voltage is measured from all other electrodes except from the current electrodes, yielding 13 voltage measurements. When 16 electrodes are used, the opposite method yields 104 data points.

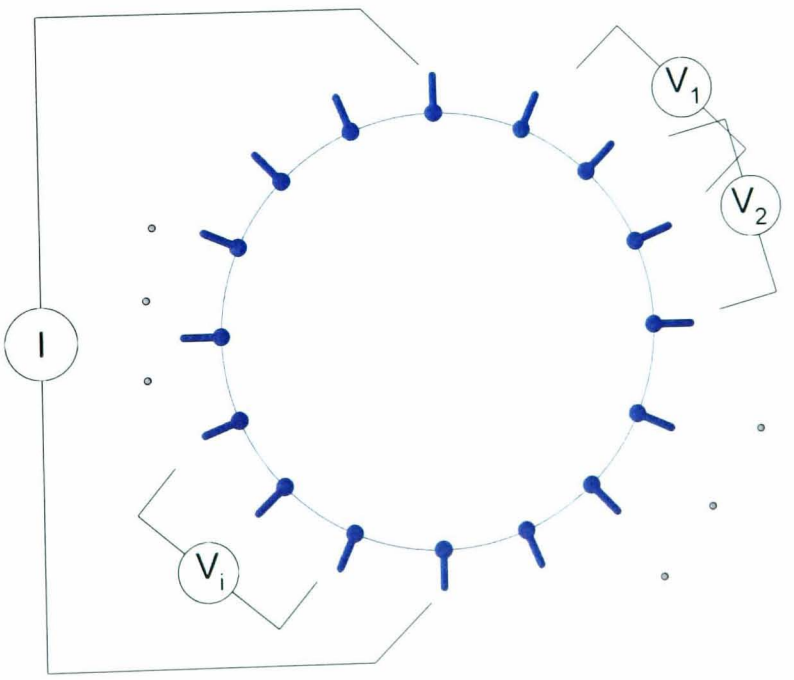

Figure 6.15 Opposite measurement method

6.3.4 Explanation of measurement on mathematics and physics

The measurement methods, based on the four-electrode measurement principle, are linear combinations of independent measurements. As it is assumed that the measured object is a linear system, the measured voltages using different current driving methods are linear-related, and one voltage set can be calculated from another voltage set in superposition. Therefore, in mathematics, the neighbouring method, the cross method or the opposite method does not add extra information for imaging reconstruction.

As Figure 6.16A illustrates, the measured voltage on one electrode pair *(m, n)* with current drive on an arbitrary electrode pair *(i, j)* is equal to the sum of voltages measured on same electrode pair, but with current injecting pair shift from *(i, i+1)* to *(j-1, j)*. In an equation, it can be described as

$$V_{(m,n)/I(i,j)} = \sum_{l=i}^{j-1} V_{(m,n)/I(l,l+1)} \qquad \text{Eq6.1}$$

where $I_{(l, l+1)}$ represents the current driving electrode pair position, l is an integer.

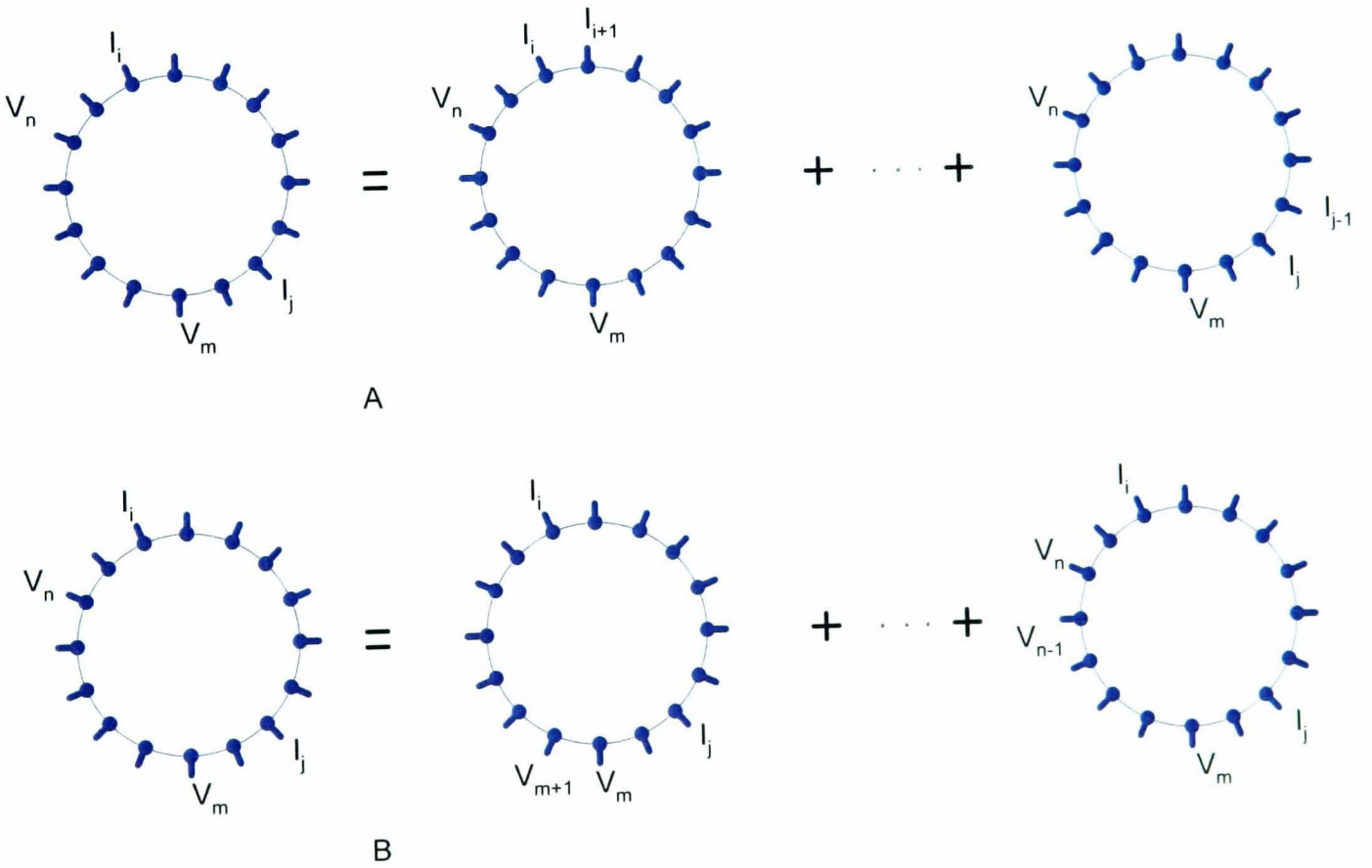

Figure 6.16 The boundary voltage measurement is satisfied superposition principle

It can also be described as the sum of measurements on electrode pair shifted from m to n, as Figure 6.16B shown

$$V_{(m,n)/I(i,j)} = \sum_{k=m}^{n-1} V_{(k,k+1)/I(i,j)} \qquad \text{Eq6.2}$$

where $V_{(k,\,k+1)}$ represents the measured voltage on the adjacent electrode pair, and k is an integer.

Combining equation Eq6.1 and Eq6.2, that is

$$V_{(m,n)/I(i,j)} = \sum_{l=i}^{j-1} \sum_{k=m}^{n-1} V_{(k,k+1)/I(l,l+1)} \qquad \text{Eq6.3}$$

It can be seen clearly that the superposition results of adjacent driving and adjacent receiving method forms other measurement methods.

Alternatively, from data processing point of view, the other measurement methods could be treated as smoothing filtering result of data set measured with neighbouring electrode current driving/receiving method. The cross method and opposite method can provide data set in less dynamic range. Therefore, the data set is more suitable for static image reconstruction, which reflects the absolute impedance distribution inside the object.

The neighbouring method is sensitive to the change in the local area where the measuring electrode pair is located. The more electrodes, the more detailed current field changes get. Moreover, with the application of a programmable gain amplifier, even small changes at the far side electrode pair can be accurately measured with high signal-to-noise ratio, which makes it possible to achieve high quality reconstructed image using back projection method.

The static image provides the absolute impedance distribution in the imaged object. The impedance change in the image represents shape change of body organ with physiological rhythm or abnormal change of the tissue under pathological conditions. However, in practice, due to the poor resolution of the reconstructed image, the obtained impedance information is distorted by the error and is difficult to be used in the desired applications.

The back projection image reconstruction algorithm based on differential changes on the boundary, emphasizes the impedance change inside the imaged object, and puts the position and amplitude information into second place. Therefore, this kind of image just indicates abnormal changes that happen without information of the property changes. Due to the sensitivity of the bioelectrical impedance, this dynamic image could be used in the early diagnosis of abnormal tissue and long term physiological trend monitoring.

In the electrical impedance mammography research, these measurement methods are all available by means of software setting. Therefore, the designed MK2 data acquisition system is suitable for static and dynamic image reconstruction research.

6.4 System configuration

The MK2 data acquisition system is configured as 16 current injection channels, which apply differential current injection mode to the desired driving electrode pair, and 16 differential voltage measurement channels, which multiplex the boundary voltage signal to the front-end amplifier.

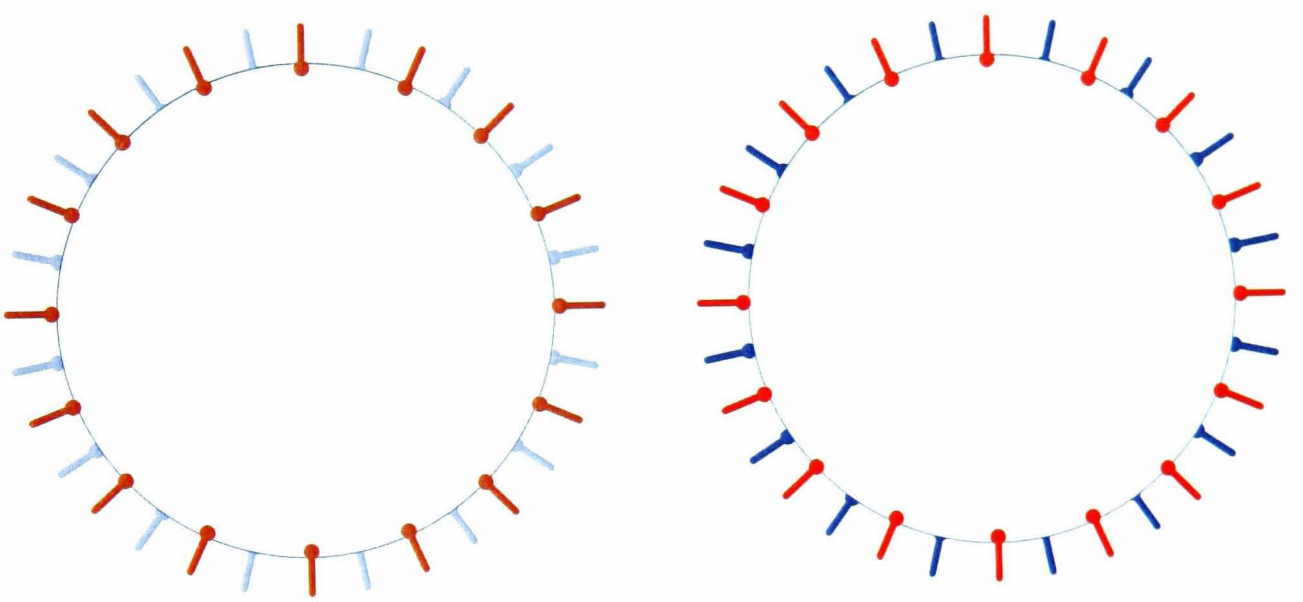

Figure 6.17 16 differential current channels and 16 differential voltage measurement channels in the MK2 system

A) 16 compound electrodes configuration B) 16 current electrodes and 16 voltage electrodes interlaced configuration

These 16 current injection channels and 16 voltage measurement channels can connect to compound electrode connections shown in Figure 6.17A. The compound electrodes inject current to the object or take voltage measurement from the object depending on the digital addressing. Using discussed measurement methods, all electrode combinations can provide 104 independent measurements, and the collected data set is

sent to computer system for image reconstruction using back projection algorithm. In practice, the dependent measurement data set can be used as calibration reference.

The current injection channels and voltage measurement channels can connect to the interlaced 32 electrodes configuration shown in Figure 6.17B. The electrodes just take one duty on either current injection or voltage measurement. With all possible electrode combinations, this electrode arrangement can provide 256 independent measurements, which can be used as a high resolution imaging reconstruction platform. However, due to the shift of current electrodes to voltage electrodes, the reconstructed image is distorted slightly.

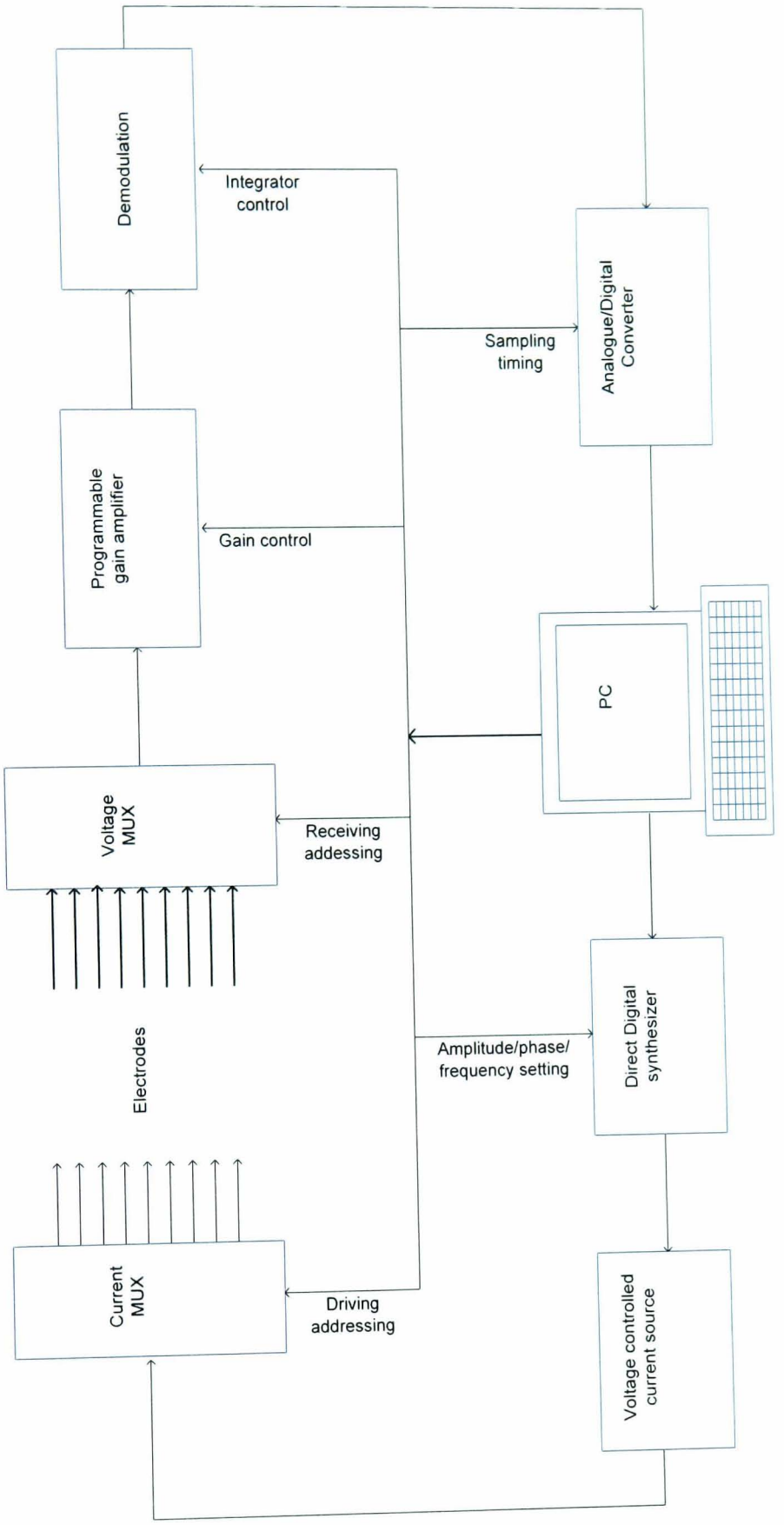

Figure 6.18 The whole system control timing and measurement sequence generated by digital control circuit

Figure 6.18 illustrates the control diagram of the system configuration. The measurement strategy is achieved with addressing the channel control multiplexers by digital logic combination.

The system can also be configured in electrode arrangements on arbitrary shape of phantom measurement for two-dimensional or three-dimensional imaging research. However, the forward problem has to be solved with the matching of the measured object and the appropriate mathematic model. Actually, the image reconstruction operation is a process to find a matched model for the imaged object. Alternatively, the matched model of the object is the desired image of the object.

6.5 System timing and implementation

The data acquisition system is controlled by system timing, which is stored in a programmable logic chip. All measurement process parameters including imaging frequency, driving and receiving electrode pattern, and delay time for signal settling, are set in a friendly software environment. Before the data acquisition task is taken, the timing logic is downloaded to the embedded hardware system.

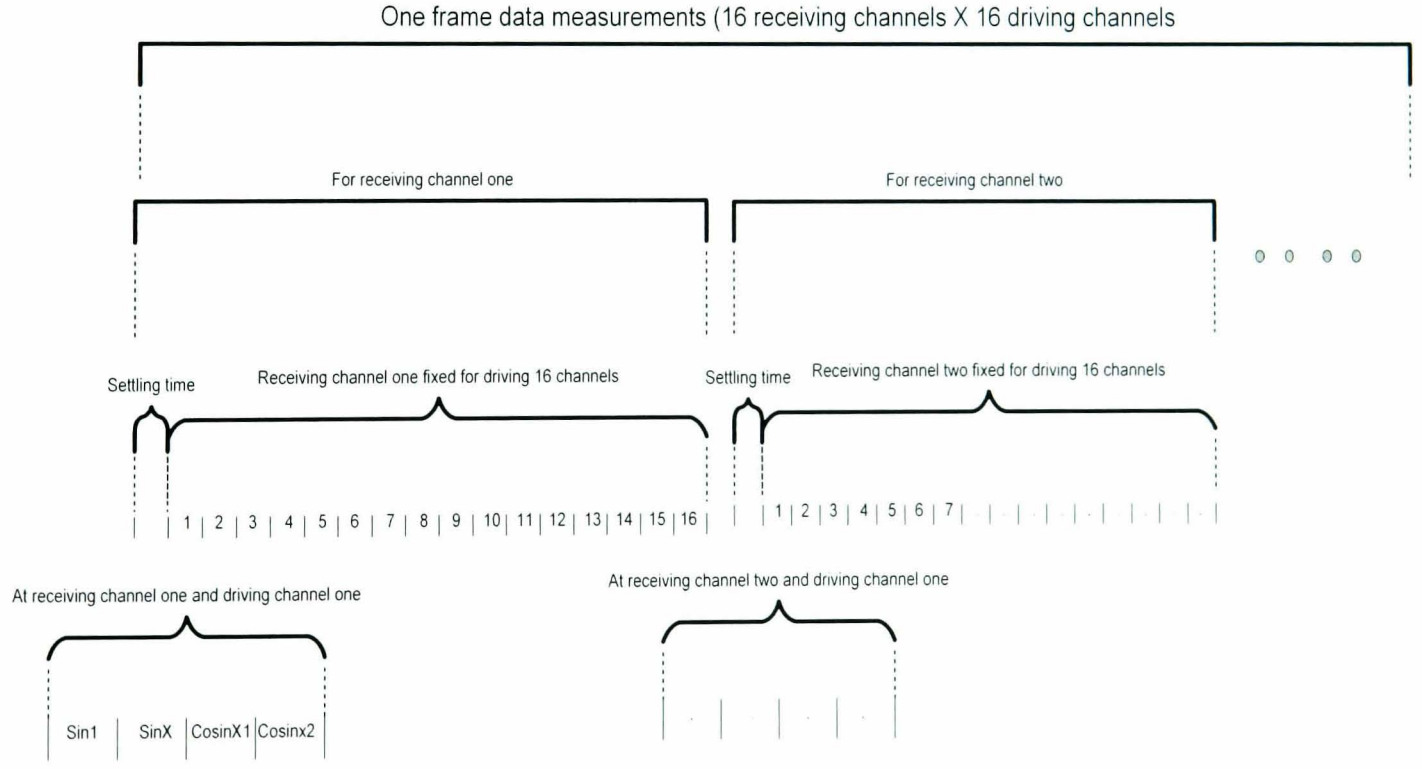

Figure 6.19 MK2 system data collection timing

The driving and receiving pattern starts at a selected receiving channel and then scanning all desired driving current channels, as illustrated in Figure 6.19. The system

then moves on to another receiving channel and the process is repeated and so on. A proper settling time is given before the shifted receiving channel starts because of the polarization potential effect. During all current drive electrodes combination scanning interval, the fixed receiving channel does not need settling time again.

When a driving current is injected into the object, the voltage measurement on the configured electrode pair is taken and demodulated to the real and imaginary component. To increase the signal-to-noise ratio, each channel measurement starts with basic signal path gain, and then with the confirmed amplitude of the signal, a programmed gain is set to the signal path by means of a programmable gain amplifier. In the MK2 data acquisition system, the real and imaginary part measurement is based on the proper PGA gain settings. This timing sequence is illustrated in Figure 4.15. The detailed description of digital timing demands on measurement has been given in Chapter 5 on demodulation method discussion.

The other control signals are also generated in the digital circuit for sample-and-hold and sampling trigger.

6.6 Safety design for medical application

The EIT data acquisition system must meet the necessary safety regulation before use in the clinical trial. With the electrodes directly mounted on the body skin, the machine has to be isolated from the earth. The isolation ensures that no electric loop is formed when the current leakage occurs.

In some medical applications, an isolation transformer is used for this purpose. However, in this case, the imaging frequency applied in the measurement is scanned over a wide bandwidth, which makes it extremely difficult to use a transformer in the current injection or voltage measurement side. Actually, it was used in single frequency EIT system design at very early age [33].

Another isolation technique is optical coupling, which uses electric-to-optical and optical-to-electric transform to achieve the isolation. The optical coupling devices normally have wide signal bandwidth, but lack enough accuracy on signal fidelity. Therefore, it is very difficult to be used in analogue signal path isolation. This technique is popularly used in digital signal isolation in the communication and data exchange fields.

Considering the data acquisition system power consumption and technique feasibility (wide bandwidth), the isolation is achieved in the design by a medical level isolation power supply and optical data isolation, shown in Figure 6.20.

Other safety regulations are also considered in the system design including casing and grounding. The whole machine has to acquire authority approval prior to in vivo tests and clinical trials.

The durability of body tissue to electric current increases as frequency increases. The bio-effect of the low frequency electromagnetic wave is mainly a heat effect, and the higher frequency wave can create a radiation effect for the living body tissue and cell. Some frequencies may also affect normal electro physiological activity in some special body parts. Therefore, the injected current energy must be limited to the safety level.

The amplitude of injected current to the body object in this design is set at 1mA over the whole measurement bandwidth. In the saline phantom test, the injected current can be higher than this value to increase the signal-to-noise ratio during the research and development period.

6.7 Summary

The electrical impedance tomography displays the anatomical image of the body, in which a grey level of pixel represents a bio-impedance property at that point. A high-speed data acquisition system can provide real time image that is significant when physiological monitoring is needed. Bio-impedance property changes also provide shape and status information about tissue or cell in physiological and pathological situation. In this application there is a need for a high sensitivity and high accuracy reconstructed image.

Using separate current source and voltage measurement circuit on each electrode combination, the parallel structure EIT data acquisition system definitely can provide higher speed data flow to image reconstruction and makes it suitable for physiological monitoring purpose. However, due to hardware cost and limited space, the parallel system cannot be used in high-density electrode array applications for either two-dimensional or three-dimensional EIT system implementation.

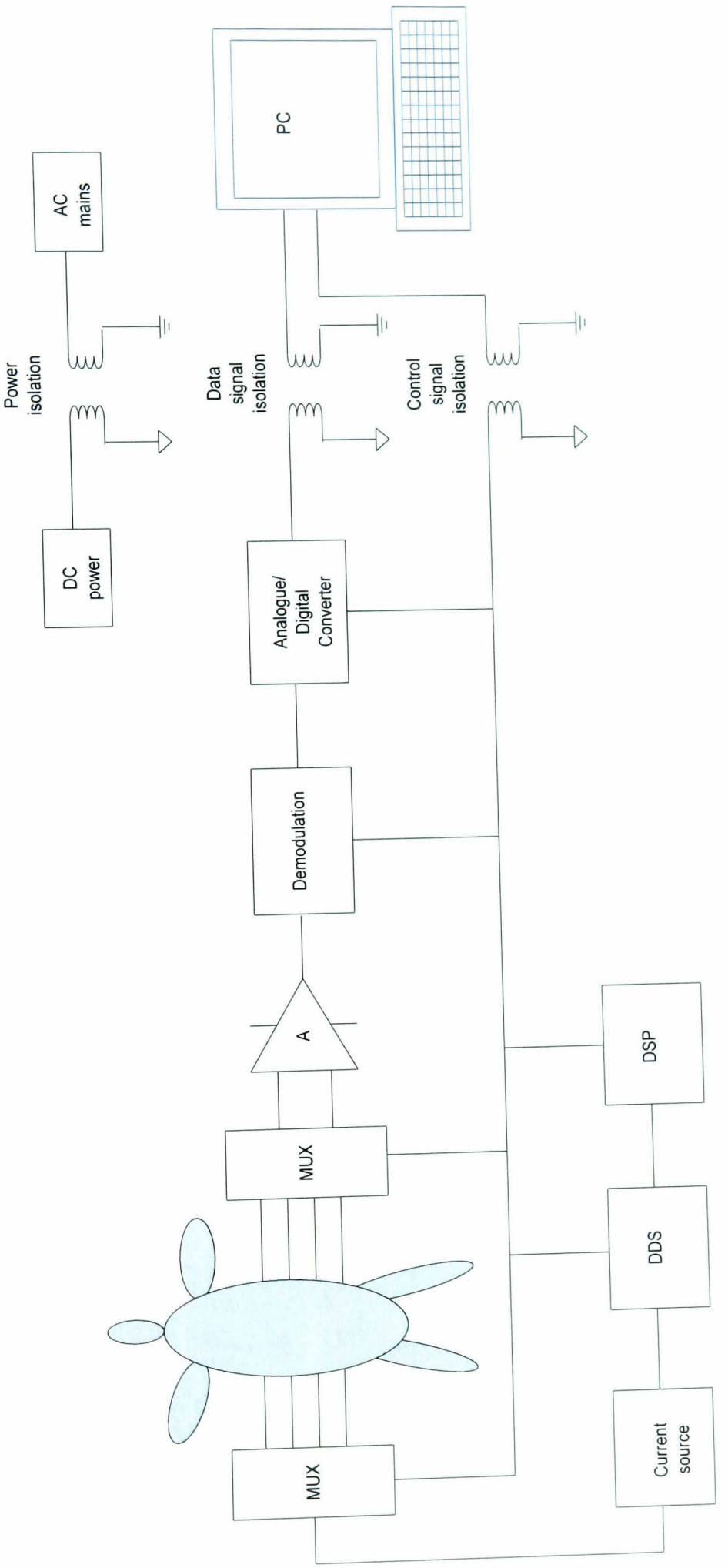

Figure 6.20 Electrical isolation in the EIT system design

The serial structure has a shared current source and a voltage measurement circuit, which is multiplexed to each electrode combination for data acquisition. It has the potential to easily be extended to an application using a massive number of electrodes.

In wide-band EIT system design, due to stray capacitance, the multiplexer reduces the output impedance of the current source and the input impedance of the front-end amplifier at high image frequency. The stray capacitance of the multiplexer mainly comes from the semiconductor material and the protection circuit used in the MOSFET manufacturing process. Some commercial products have improved parameters in recent years, and choosing the proper integrated circuit is necessary. In addition, using cascade multiplexers for a multi-channel application is another choice. It is always a trade-off between low capacitance and low on-resistance at multiplexer choosing. Coaxial cable affects the EIT system design and using a guard shield can improve the bandwidth to over 1MHz, but there is a huge manufacturing cost implication on using double shield coaxial cable. Therefore, there is a need to use shorter cabling connections.

The active electrode technique is an ideal solution for the EIT data acquisition system. It integrates current source and front-end amplifier into the electrode. Therefore, the bandwidth of the hardware circuit will not depend on the cable, or multiplexer. The number of applied electrode employed is extendable.

The measurement strategy for static or dynamic image reconstruction is discussed in this chapter. Combined with a flexibly system control timing, the complete firmware design is formed into the MK2 system.

Chapter 7 Electrodes System and Phantom

7.1 Introduction

The electrodes are used to inject current into the sample and sense the induced potential variations. In EIT data acquisition system, the electrodes are mounted on the surface of imaged object, and the reconstructed image resolution mainly relies on the number of applied electrodes. However, the number of electrodes cannot infinitely increase due to the contact problem with body tissue and space. The complex electrochemical reactions occur at the electrode-tissue interfaces that create polarization phenomena. These phenomena, which may induce large errors in the measurement. affect the contact area of electrode, output impedance of the signal source, and the performance of the measurement circuit from the current source to the front-end amplifier and complex parameter demodulation.

7.2 Electrode/tissue interface impedance

When a metal is placed in an electrolyte, two different current transport mechanisms are involved: a faradic current and a capacitive current. The faradic current results from the transfer of charges across the interface (direct neutralization reactions between electrons leaving the electrode and positively charged molecules off the electrolyte). The capacitive current originates from the formation of Helmotz "double-layer": the electrical charges are distributed across the interface into two layers of opposite polarity that act as a capacitance. A current across the electrode interface results in the charging of this capacitance and then in the polarization of the interface [61].

The electrical charge generates a voltage, which is the so-called half-cell potential. It is impossible to measure this voltage on one single electrode. Moreover, the potential of one interface, because of opposite signs, tends to be compensated by the other interfaces. Consequently, the measurement of this potential is usually made against an arbitrary reference, a hydrogen electrode most of time. Actual values range from –1.66 volts to +1.69 volts can be found in the literature for different electrode types and solutions [62]. Temperature significantly affects the value of half-cell potential, and its stability depends strongly on the metal and the electrolytic solution.

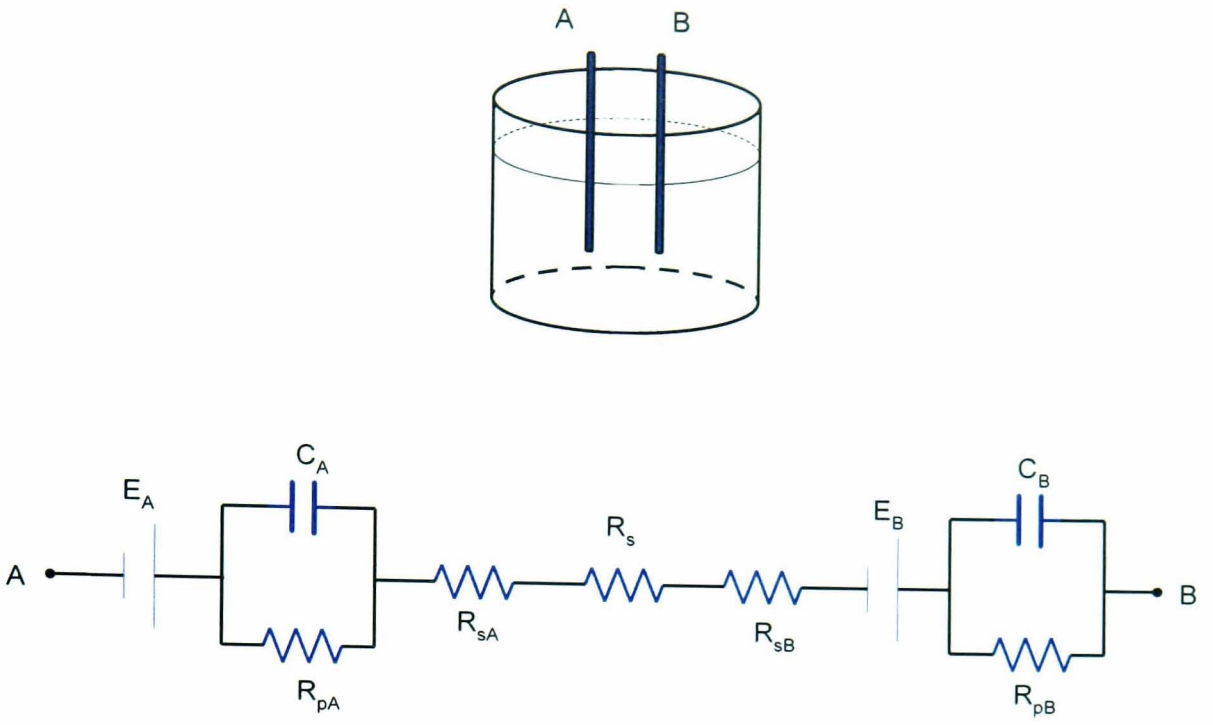

Figure 7.1 Possible metal electrode model in electrolytic solution

Figure 7.1 shows a possible model, where A and B stand for the input points. E_A and E_B represent the respective half-cell potentials (polarities are arbitrary because they depend on the particular metal/electrolyte combination); C_A and C_B correspond to the above mentioned capacitive components, and finally, R_{sA}, R_{sB}, R_{pA} and R_{pB} take into account the series and leak parallel ohmic pathways [63].

Some researches [64, 65] have revealed that, for small signals and relatively high frequencies, the interface impedance Z_p can be summarily modelled by a resistance R and a reactance X in series whose values decrease when the frequency increases

$$Z_p = R - jX = R + \frac{1}{j\omega C} \qquad \text{Eq7.1}$$

This impedance is also called polarization impedance, and it varies as a function of frequency and current density and depends not only on the electrode material but also on the nature of the electrolyte [66]. Figure 7.2 gives the plots, between 100Hz and 100 KHz, of resistance R and capacitive reactance X for stainless steel electrode [67].

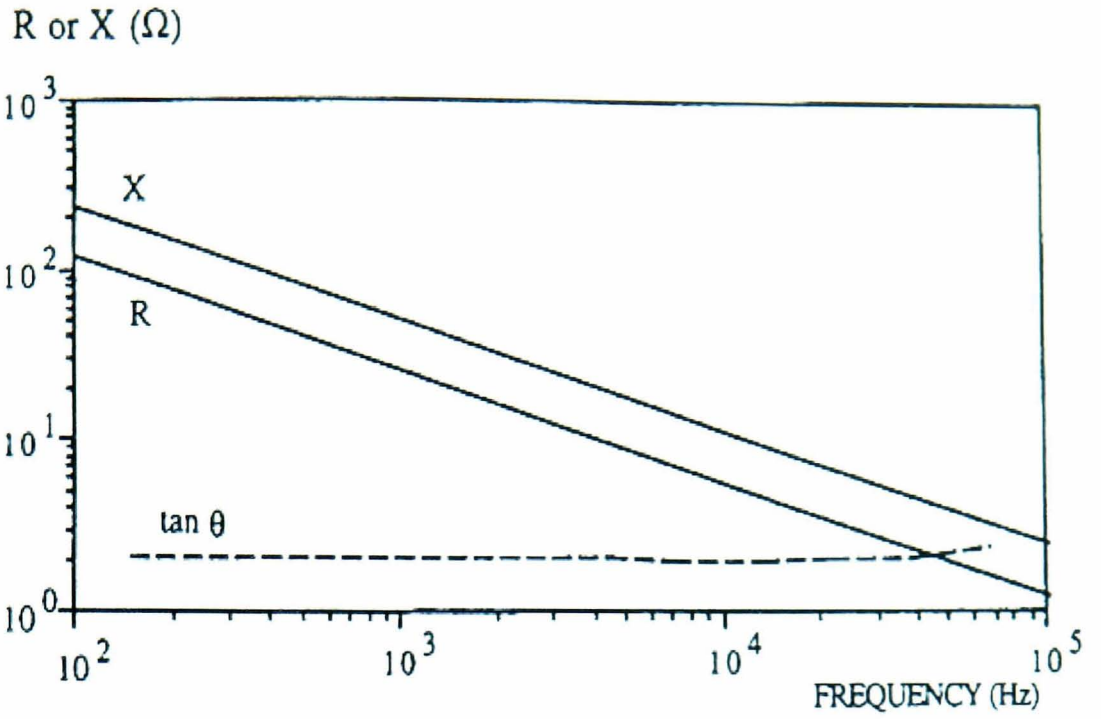

Figure 7.2 Resistance R and capacitive reactance X of the interface impedance for stainless steel electrodes with a cross-section 0.785cm^2 [55]

7.3 Electrode material

In the four-electrode measurement, the polarization effect on current electrodes is eliminated, but the polarization effect on the interface between the receiving electrodes and the electrolyte (tissue) can still affect the measurement result. The choice of the electrode material is important since it determines the dimension of the interface impedance for a given electrolyte, and enlarging the electrode surface area results in lowering the polarization potential.

Silver-silver chloride electrodes have been extensively used for electrophysiological measurements because they are easy to manufacture in any desired shape and exhibit stable potential.

Platinum electrodes have interesting features when an alternating signal is applied, since their polarization impedance is lower than that of other materials such as stainless steel or silver [67, 64]. Furthermore, platinum can be electrochemically coated with a porous layer of black platinum, which reduces the amplitude of the polarization impedance by a factor of four or more [68, 67 and 69].

One answer is to make the electrical contact with the sample by means of an intermediate coupling medium, which allows the sample to be handled without touching the porous layer. This medium can be a gel or a sodium chloride bridge [70].

Increasing the surface area of electrode is a promising method [71] to reduce the polarization voltage and high capacitance. This increasing of area is not an enlargement of absolute size of electrode, but the fractal contact area of electrode. With processing of sanding or sputtering, the stainless steel, which has high polarization impedance at low frequency, also improves its performance as shown in Figure 7.3.

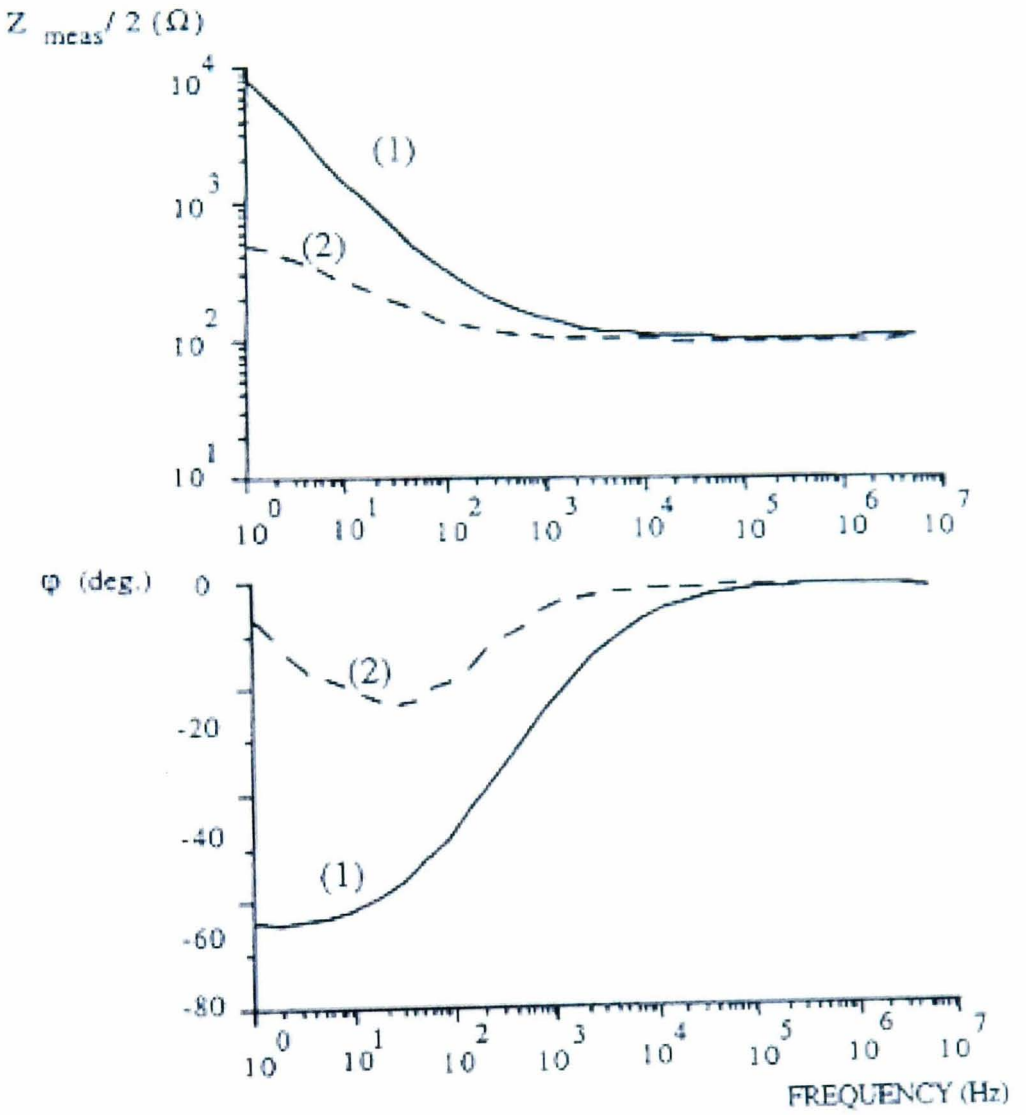

Figure 7.3 Contact impedance Zp=Zmeas/2 for stainless steel electrodes (1), and sanded stainless steel electrodes (2) of cross-section 0.785cm^2 for a current density of 0.35mA/cm^2

The use of ceramic material such as NASICON [72], which makes it possible to build non-polarizable dry electrodes, could perhaps help solve this problem. However, this type of electrode exhibits extremely high interface impedance. It will be a huge challenge to current source in electrical impedance measurement.

The toxic or catalytic effect of the electrode material on the tissue must also be taken into account. Prolonged contact between the electrode and a tissue or and

electrolyte can cause oxidation phenomena or pollution of the surface. The choice of biocompatible material is a proper consideration.

In the MK2 system design, comparing the performance and cost of different material on electrodes, the stainless steel is used in the measurement electrodes and saline tank phantom design. On *in vivo* study, silver-silver chloride electrodes are also used for body data acquisition, since it is commercially available.

7.4 Electrode leads connection

The electrodes for MK2 system are made of stainless steel A6, which is acid resistance material and can protect itself from rust and other corruptions. This property is essential as the application operates in an electrolyte environment. The contact surface of the electrode is roughened with sand paper to increase the actual area before measurements are taken. The tip of the electrode is a round area with a diameter of 3mm. The other end of the electrode is threaded for cabling and mounting.

The leads interfaced to the analogue boards are D37 connectors, which are connected by 32 cables for a 32 electrodes configuration. The cables are terminated with an eyelet, so it will also be easy to connect to commercial silver-silver chloride electrode on body image reconstruction.

7.5 Saline phantom design

In image reconstruction algorithm development, the boundary voltages being measured are dominated by the internal impedance of the object. The process using measured boundary voltages to work out the internal impedance distribution of object is called the inverse problem solving. Because the number of independent measurements for any boundary electrode combination is much less than the number of pixels on the image, the calculation to the impedance distribution is not sole and the reconstructed image may not truly reflect the internal impedance situation. Therefore, the possible way to limit these undesired results is to try to set a precise mathematical model for the internal impedance distribution. Obviously, the modelling provides certain restrict on reconstruction and this leads the iteration process convergence quickly. In practice, this process is achieved by comparing the boundary voltages calculated from modelling with

the measured voltages on the image object surface. It is also called as forward problem solving in the image reconstruction research.

A saline phantom is designed for solving the forward problem in the electrical impedance tomography image reconstruction. A tank with surrounded electrodes provides an ideal shape for modelling. All boundary conditions can be controlled in the simplest situation. The tank is transparent to the researcher and the mathematical model can be easily checked with the simulated internal impedance distribution inside it.

The saline tank is a cylinder container made of transparent material (Plexiglas). The internal content of the tank can be arranged to cope with the modelling assumption. The spatial position of the internal content can be measured for image resolution and fidelity calculation. The picture of the tank is shown in Figure 7.4. 32 stainless steel electrodes are mounted on the wall of the tank with equal distance, and the electrode surfaces are sanded to maximise contact area. The cable is fixed on the electrode with a nut and can easily be changed to configure a desired physical electrodes layout. The other end of the cable is connected to the D37 connectors mounted on the base of the phantom. This makes the tank convenient to move and clean. The tank has a special electrode near the bottom of tank cylinder, which is used for floating measurement as ground reference point to reduce the common mode voltage.

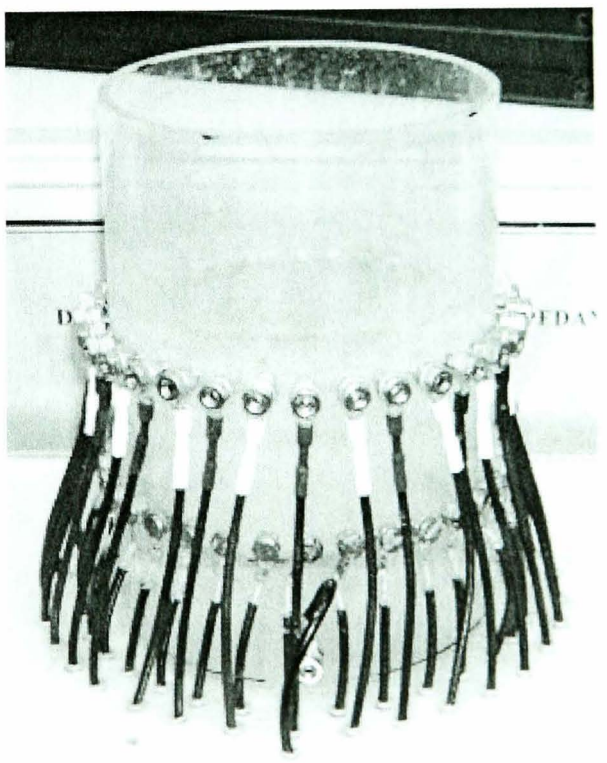

Figure 7.4 The saline tank

The electrolyte in the tank normally is a solution of sodium chloride and its conductivity is monitored by conductivity meter. The level of the liquid has to be controlled to a proper height to reflect the mathematical model. Each time after data acquisition, the tank must be emptied and then rinsed by clean water. It protects the electrodes from corroding. In addition, before the electrolyte is put into the tank, all the electrodes need to be carefully checked and cleaned to avoid any contact problems.

The tank is designed for 2-dimensional image reconstruction research and is not suitable for 3-dimensional imaging. However, the current field formed by the injected current is a 3-dimensional distribution and the modelling should reflect this situation. 32 electrodes can be used as an interlaced arrangement configuration with 16 current electrodes and 16 voltage electrodes, or can be used as compound electrodes for 16 or 32 electrodes configuration.

7.6 Electronic network calibration device design

Each working system needs a device for routine self-test before the data acquisition is taken. However, the saline tank is a real physical object with all the problems met in body impedance data acquisition, such as contact impedance and polarization potential. It cannot be used in the electronic circuit system test due to these uncertainties.

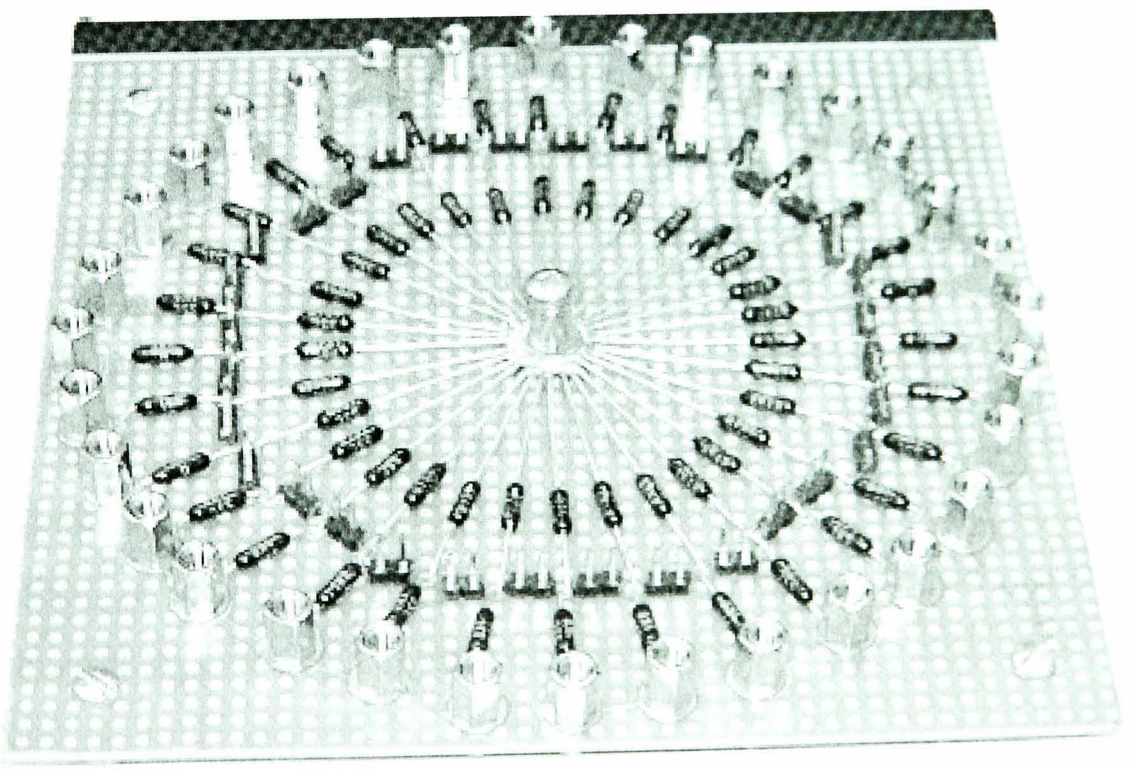

Figure 7.5 The electronic phantom

For electronic circuit test purposes, an electronic network is designed using high precision (0.5%) passive resistors, and this ensures the measurements made on it are relatively accurate. The network device is pictured in Figure 7.5 with 32 electrode connectors.

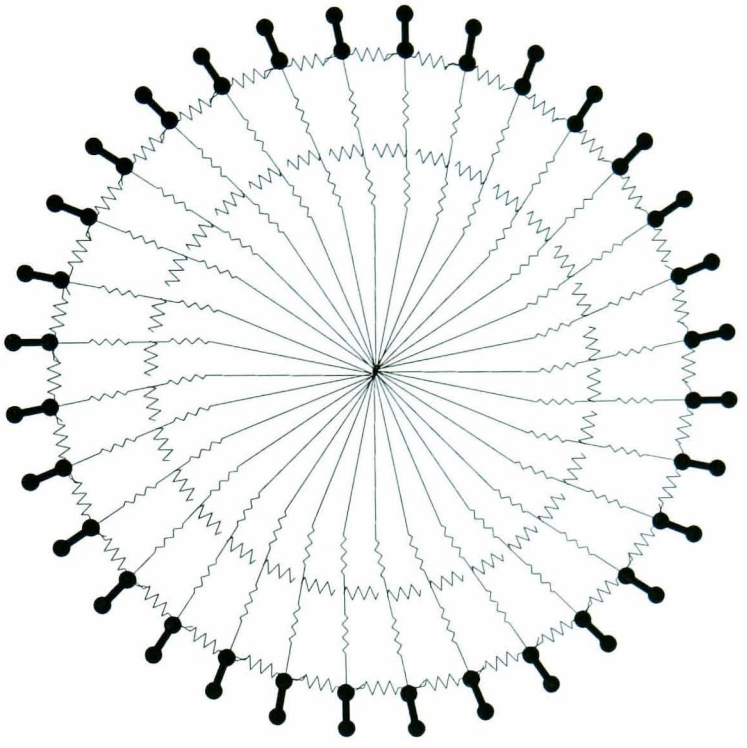

Figure 7.6 Electronics phantom with 32 electrodes connection for EIT system calibration

The network layout is shown in Figure 7.6. The voltage ratio between the maximum and minimum values occurring on the electrode pair, which is opposite the current electrode pair, and the electrode pair near the current electrode pair is about 1:80. It can be seen that the resistor network satisfies the test of an electronic circuit designed for 16/32 electrodes configuration EIT system, which has a 1:40 dynamic voltage range.

It must be clear that this resistor network is not a simulation phantom of any physical object. It can just be simply used for circuit test purpose. The data set acquired from this device can give a position-identified image using a developed image reconstruction algorithm but the image has no physical meaning.

The electrode and cable connection on the resistor network maintains the same design as the connection on the saline tank. Therefore, the electrode leads can be easily swapped between data acquisition and electronic circuit test.

7.7 Summary

When metal electrode contacts electrolyte, the polarization phenomena occurs. This brings polarization impedance and polarization potential to the measurement circuit. The choice of the electrode material is important since it determines the dimension of the interface impedance for a given electrolyte. Obviously, enlarging the fractal area of electrode to reduce the interface impedance is a promising method.

In the MK2 electrode system designed, stainless steel material is used to build the electrodes. This makes the electrodes easy to maintain and clean for repeat use.

A saline tank phantom is designed for the EIT system to enable simulation for image reconstruction algorithm development, especially for forward problem solving. For convenience to test and debug the system, an electronic network is built.

Chapter 8 EIT System Integration and Implementation

8.1 Introduction

The electrical impedance imaging technology has made great progress since 1980s. The data acquisition system has been developed from single frequency measurement in the early stage to multi-frequency wide band measurement. The configured number of electrodes is expanded from 8, 16 to 32 and even more to meet the demand on the 2D or 3D high resolution image reconstruction. As it has been introduced in Chapter 1, the quality of reconstructed image does not only rely on the number of electrodes, but also rely on the data measurement accuracy and the image reconstruction algorithm.

Most of real time image systems adopt parallel structure to enhance the data acquisition speed. Because the parallel measurement does not need multiplexing channels, the measurement bandwidth is mainly affected by the coaxial cable, which is used to connect the front-end amplifier and current source to the electrodes. Due to the expense increasing with increasing of applied number of electrodes, the systems with this structure are normally designed with very limited number of electrodes.

The measurement bandwidth of a serial structure system is limited by the coaxial cable and the multiplexer, as discussed in Chapter 6. However, it has the ability to extend more electrodes with little hardware expenditure. Because the measurement channels share one current source and one front-end amplifier, a serial system is obviously suitable for high resolute or 3D imaging implementation, which normally needs a large number of independent data for image reconstruction.

The problems in a serial structure system can be solved by means of distributed system, as discussed from Chapter 3 to Chapter 6. Using the method developed in the thesis, a high impedance current source and a front-end amplifier can be embedded into the electrode to form the active electrode. Thereafter, the measurement bandwidth and data acquisition speed can be improved to meet the demand.

De Montfort MK2 system is based on the serial structure design with configured as 16 current injection channels and 16 measurement channels. The machine is implemented as modularized functional block circuits, so that it can be upgraded easily by new research and development results

8.2 De Montfort MK2 System Description

The block diagram of the MK2 data acquisition system is shown in Figure 8.1. The system consists of a voltage controlled current source, a front-end amplifier and a programmable gain amplifier, a demodulation circuit, an analogue-to-digital converter, a digital timing generation circuit, an electrode system, and a PC as imaging reconstruction and image display terminal. The MK2 is a serial structure system, which uses the multiplexers to take all the driving and receiving electrode measurement combination for a frame data set acquisition.

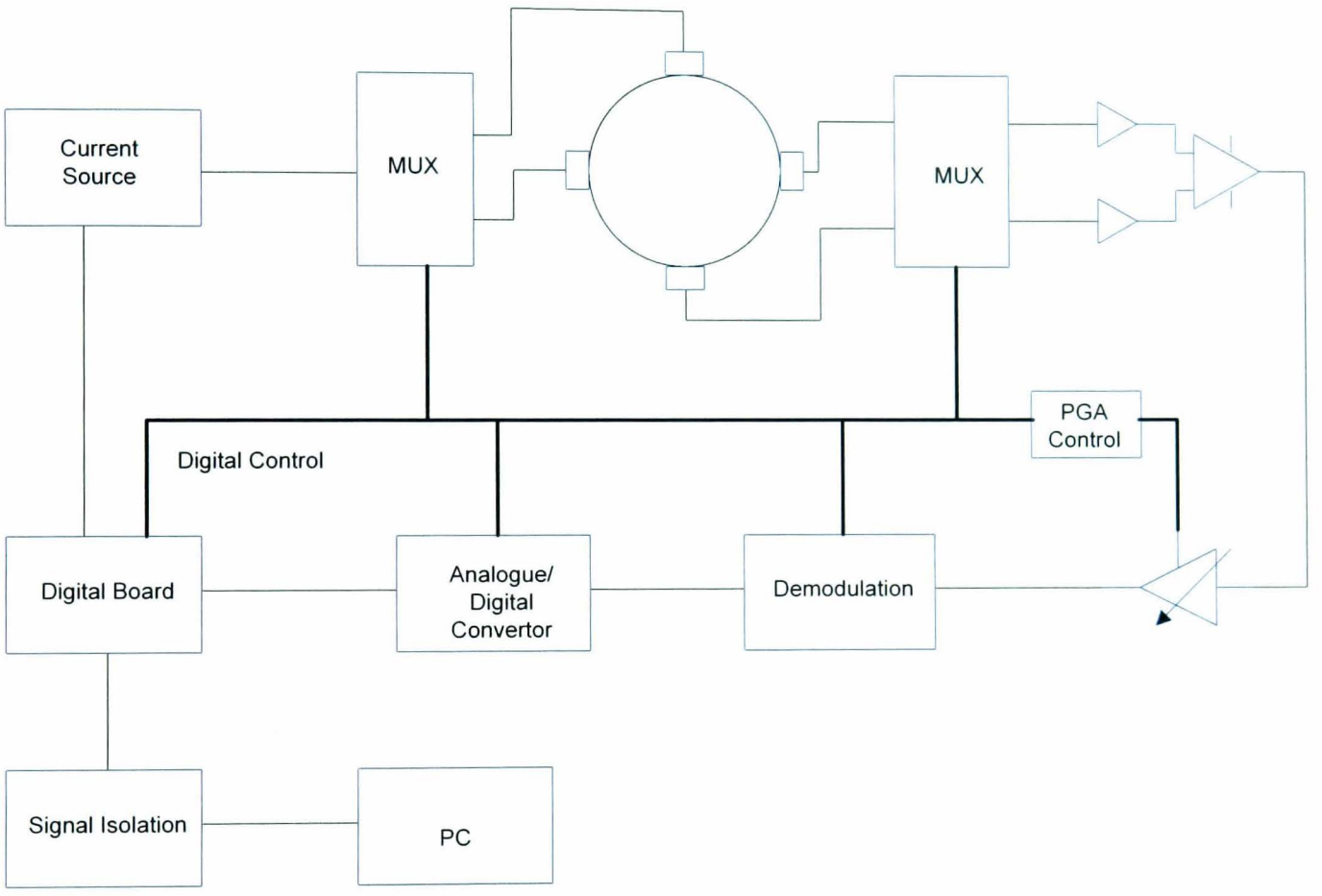

Figure 8.1 The block diagram of the MK2 data acquisition system

The voltage controlled current source injects constant current into the object to be imaged. The control voltage is synthesized directly by the digital circuit in the mainframe machine, and then sent to the current source by proper terminated transmission lines. The frequency, the phase and the amplitude of the current can be set simply in the PC software. The conversion from voltage to current is achieved by the Howland circuit that has been discussed in Chapter 3. Then, the constant current is multiplexed to each of 16

driving channels. The current generator is on a separate board with minimized physical size, so that it can be mounted on a place near the electrode system to reduce the length of coaxial cable.

The front-end amplifier and PGA board provides 16 channels voltage measurement by means of multiplexing. The function block is packed in a separated metal case near the electrodes system. The voltage signals are introduced into the amplifier board by two D37 connecters, and then the amplified signal is sent out to the demodulation board. All the analogue operations are synchronized by the data acquisition and PGA control timing signals, which are formed in a digital circuit in the mainframe machine. For system development convenience, the PGA gain setting is feedback to the data acquisition stage and used for offline data calibration.

The demodulation of the amplified signals is achieved by the phase coherent demodulation method. The core circuit is a high-speed analogue quadrature multiplier and two timing-controlled broadband precise integrators, which work in turn to avoid waiting for the discharge. After demodulation, the signal is digitalized in the quantization process. In this system, a commercial high-speed analogue-to-digital conversion product is adopted to provide data sampling function (Databook 200), which has 100K sampling per second with 16bit resolution. This data acquisition board also has flexible sampling trigger modes to match the control timing. After data acquisition is finished, the data set is sent to a computer for data storage and image reconstruction.

The mainframe machine includes demodulation circuit, sine wave synthesizer, digital timing generation and communication interface to master PC. The digital timing is generated by a field programmable gate array (FPGA) chip, and at each time of data acquisition, the electrode configuration and measurement strategy is downloaded into it by the parallel port. The power rails for analogue and digital circuits are generated in a DC-DC switch mode conversion type power supply, which is specially designed for medical uses. The care has to be taken in the way of the analogue and digital grounding to avoid forming a noise path in the ground loop.

The PC system is used as a human-machine interface for data acquisition strategy setting, data processing and final electrical impedance image reconstruction. The user can set the parameters for the image frequency combination, electrode driving and receiving configuration, the number of data frames to be collected, and signal-processing algorithm.

The electrode system can be connected to the patient with normal physiological measurement electrode. In the laboratory, the machine is mainly used in the saline phantom measurement for imaging reconstruction algorithm development.

8.3 System performance

The system is pictured in Figure 8.2, and the system specifications are listed in Table 8.1

Table 8.1 De Montfort MK2 EIT system main parameters

VCCS frequency range:	10K-2MHz
Output impedance of the current source:	>100kΩ as f<200KHz, >20kΩ as f<1M
Output current value	<2mA (peak-to-peak)
Preamplifier CMRR:	>60 dB @ imaging frequency <1MHz
Channel CMRR:	>50 dB
Measurement range:	±5V
Measurement accuracy:	<0.5%
Image frequency:	10 k-2MHz
Maxim driving electrode number:	16
Maxim receiving electrode number:	16
Image reconstruction algorithm:	Back-projection

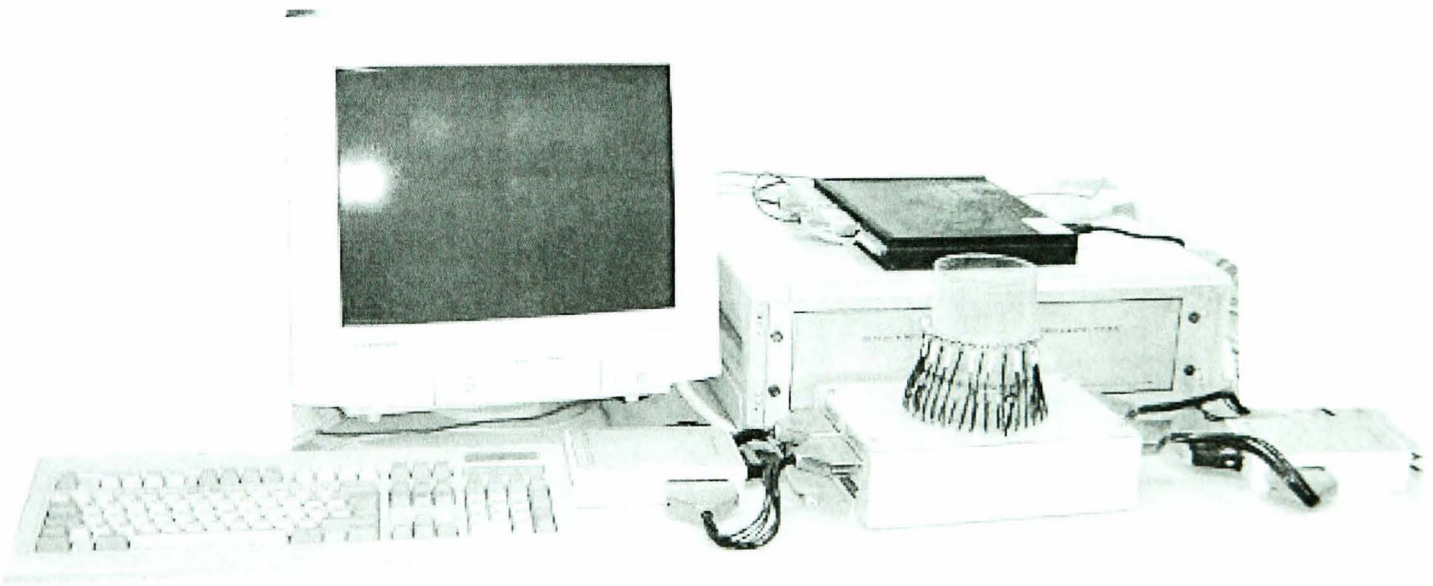

Figure 8.2 The De Montfort MK2 electrical impedance imaging system

8.3.1 System self-test and calibration

The MK2 electrical impedance data acquisition system is designed with self-test and calibration function that runs at each time before the machine starting measurement. The self-test function includes calibration test and electrode connection test, which is critical to detect that all the electrodes and cable connectors have been properly connected. Whole procedure flowchart is shown in Figure 8.3.

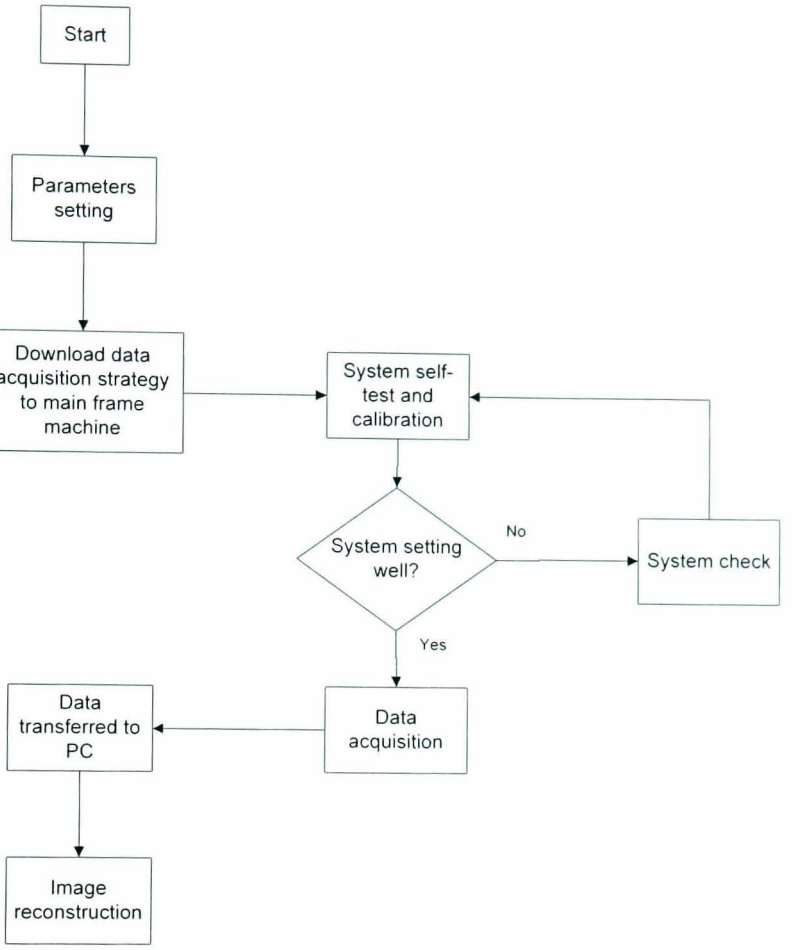

Figure 8.3 The executive flowchart of the system software functions

The machine can be tested and calibrated on the electronic phantom to ensure all the test conditions are fit. In practice, the self-test runs at the first step of the measurement and alert the measurement operators on any potential problems. Even in saline tank measurements, the electrodes are very often corrupted by the saline. If the proper cleaning is not given to all metal electrodes, the abnormal contact impedance of electrode will bring unexpected error to the data. The system calibration parameters include DC offset, integration constant, phase shift, and PGA gains. The calibration is taken on the electronic phantom and measurements results are compared with the values already stored in the machine.

8.3.1.1 DC offset

The DC voltage level shift is caused by the voltage draft and bias current of electronics devices. Most of DC offset has been removed by manual trims in the electronics assembly and test process. Some of DC offset is related to temperature changing. In addition, to temperature related drift, the offset voltage of a physical device changes as time passes. This aging effect is generally specified as long-term stability in μV/month. If all these DC drifts are summed together, in some occasions. it will play an error source to the data measurements.

The DC offset is mainly introduced at the demodulation stage. Before the signal is demodulated into its real part or imagination part, the signal is riding on the imaging frequency that is applied from injected current. This ac mode signal is immune to any dc mode error source. After demodulation, the signal is in the dc mode, and is easily corrupted by dc voltage, especially the dc offset from demodulation circuit itself. The dc offset can be either positive or negative value.

In the data acquisition period, once the driving electrode pair is fixed, the sum of adjacent electrode pair measurements on all surround boundary electrodes should be zero. This is used as criteria to check the performance of data acquisition process.

8.3.1.2 Demodulation integrators calibration

To improve the data acquisition speed, the EIT system uses two integrators in the signal demodulation operation, as discussed in chapter 6. The integrator's integration result is dominated by its RC constant. However, in the circuit implementation, it is difficult to match these two integrators with same RC values. Therefore, the calibration procedure is required to correct the difference of the integration results.

In MK2 system, the machine is controlled to acquire certain number of these two integrators' integration results with same amplitude of voltage signal, and then average the data to move the noise and calculate the relative difference of these two final values as calibration parameters.

8.3.1.3 PGA gains calibration

When the data acquisition system finds the voltage signals are small comparing to the system's dynamic range, the PGA will automatically switch the signal path to a proper higher gain amplifier. With this higher gain amplifier, the quality of final measured data is obviously improved in terms of signal to noise ratio, as discussed in chapter 4. The gain that is automatically applied to the signal path can be found in two different ways. One is using the ratio of acquired SINX to SIN1. Due to the error of measurement, this ratio is not exact value of gain applied in PGA. Therefore, in MK2 system the machine has to compare this ratio to the stored real PGA gain values to find which gain is applied. Another way is that the machine directly reads the gain control signals from the PGA circuit.

8.3.2 Electronic phantom test

The electronic phantom designed for the EIT data acquisition system test has been introduced in Chapter 7, which is made of resistor network. The electrodes configuration is shown in Figure 6.16. In MK2 system, 16 current injection electrodes and 16 voltage measurement electrodes can provide 256 data (interlaced electrode configuration and adjacent measurement). In the data collection strategy, the data are measured in the sequence of fixing receiving electrode pair first and then driving all neighbouring current pairs from 1 to 15 in turn. Figure 8.4 shows that the data set is displayed in the above manner.

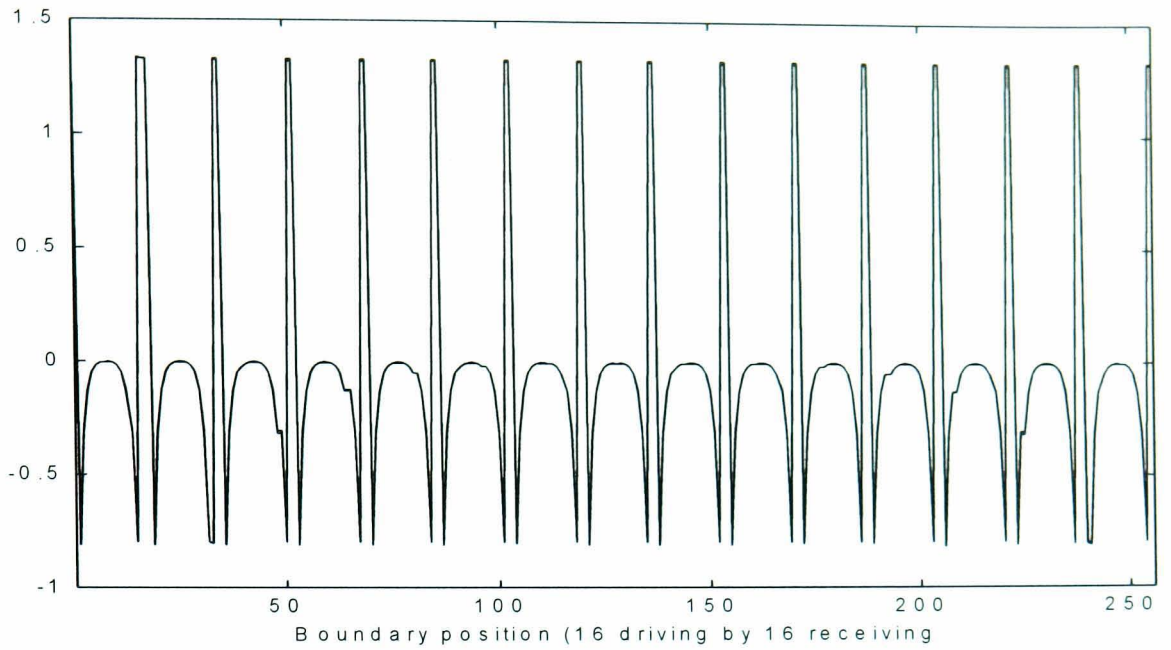

Figure 8.4 The data set collected from the electric phantom test (16 driving channels by 16 measurement channels)

The standard deviation of continually acquired 50 frames of data on the electrodes is used as a measure of the noise level of signals, which is shown in Figure 8.6. The noise level on Sin1 is in the range from 1.5mV to 2.5mV (Figure 8.6a), but it is improved on SinX after PGA gain calibration (Figure 8.6b). As the signal-to-noise ratio shown in the Figure 8.5, it can be seen after with PGA amplification, that the noise mixed in the small signal has been reduced dramatically.

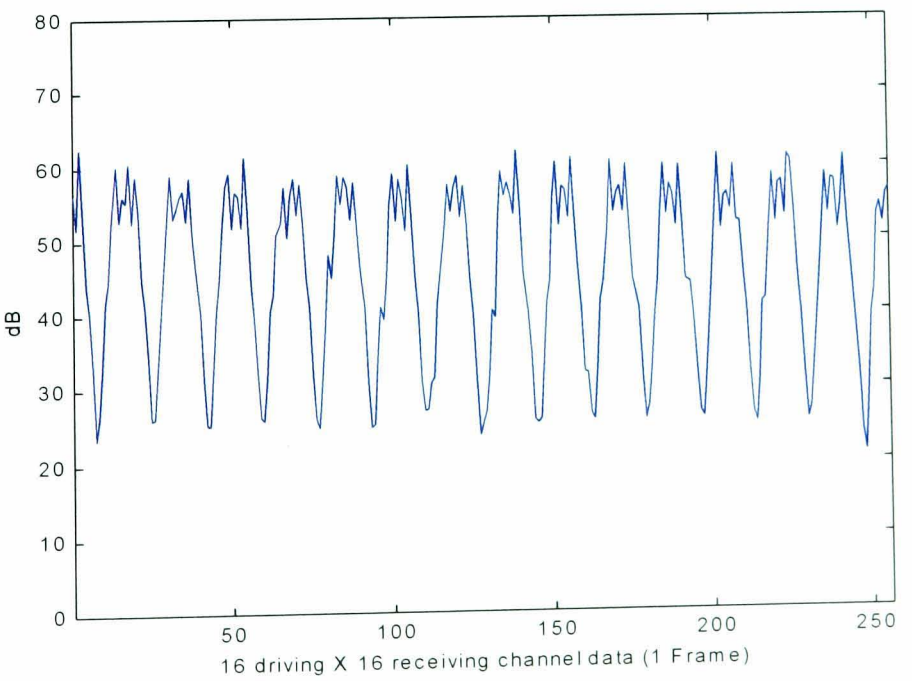

Figure 8.5 The Signal-to-Noise ratios on the electronics phantom

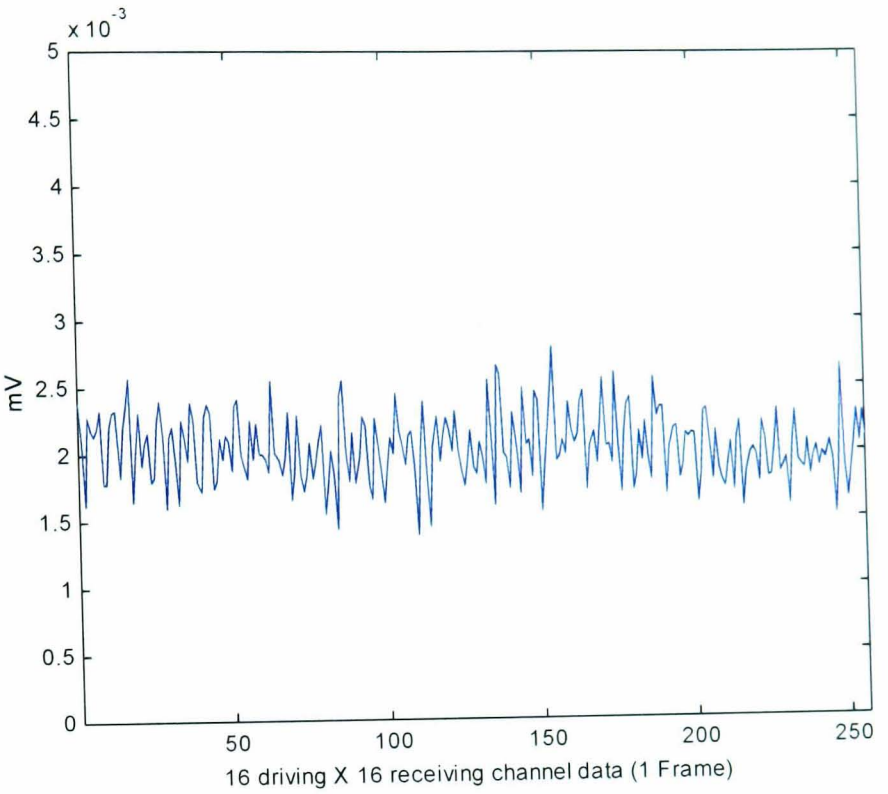

(a)

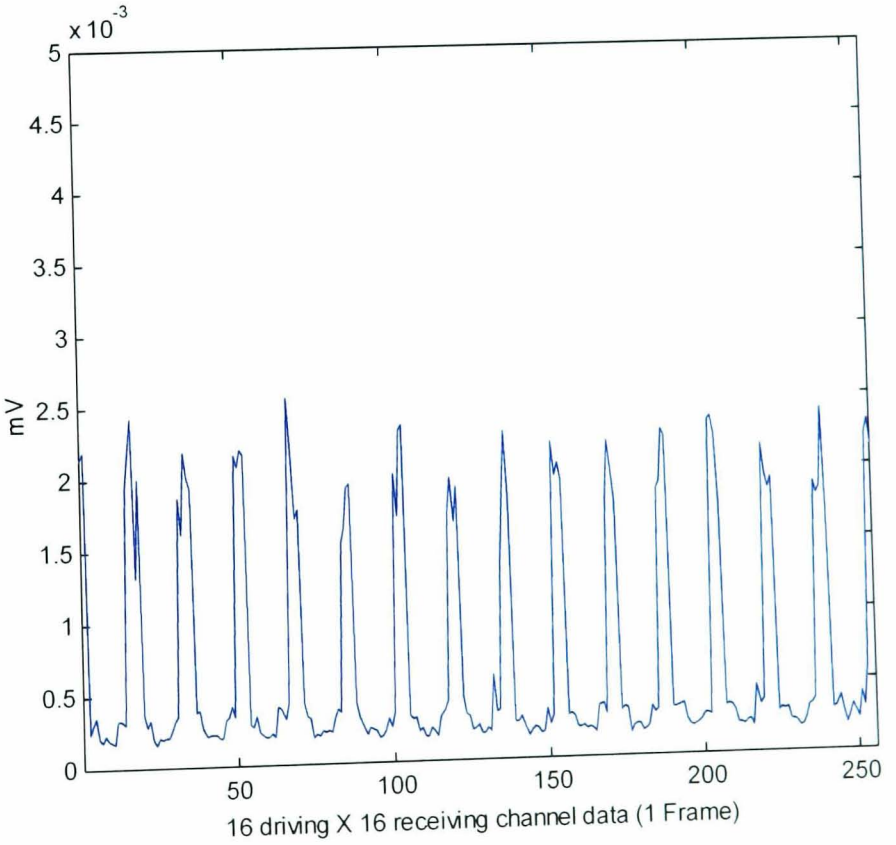

(b)

Figure 8.6 The measured data noise level on the electronics phantom

(a) the noise level on Sin1
(b) the noise level on SinX

8.3.3 Saline tank data collection

The saline tank is made of transparent material Plexiglas, and 32 electrodes are mounted on its cylinder surface. In the image reconstruction algorithm development, the saline tank is used as a physical phantom to simulate the real body structure. For back projection image reconstruction, the image shows the different part of saline with object from its original static background. Therefore, in practice, the background data frame has to be taken before the objective data is collected over all electrodes configuration on saline tank. The uniform saline tank background data are shown in Figure 8.7. The noise level calculated by standard deviation of 50 frames data is shown in Figure 8.8. It can be seen that, when measurement channel switched from one channel to another, the different polarization potential on the electrodes cause large error to measurement results, as shown in Figure 8.8a. However, after longer time delay, the SinX data measured have no this effect displayed in Figure 8.8b. In addition, after PGA gains calibration, the noise level is decreased even further (Figure 8.8c).

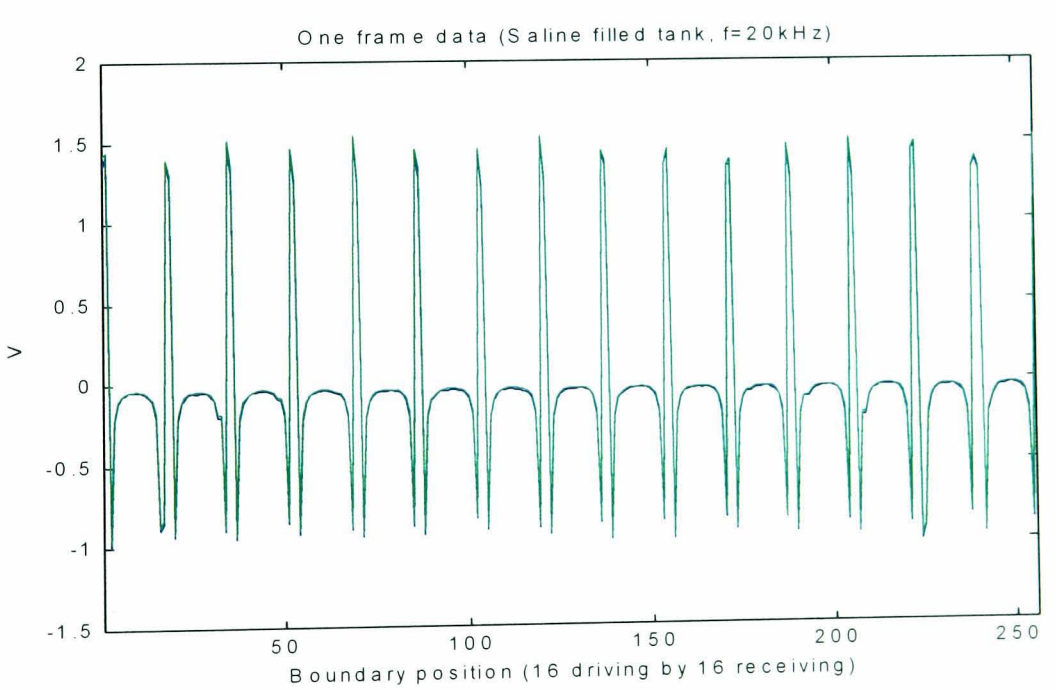

Figure 8.7 The collected data set on saline tank

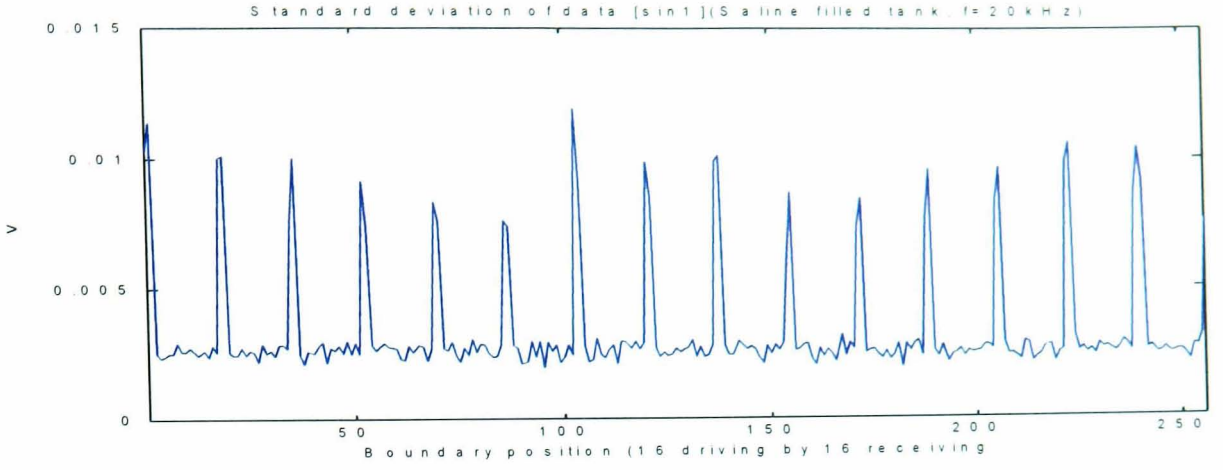

(a)

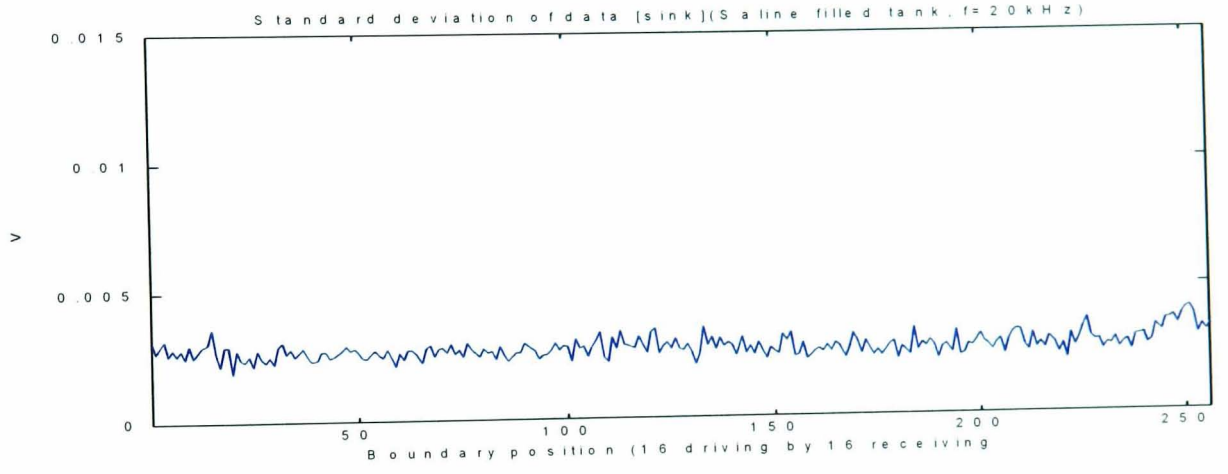

(b)

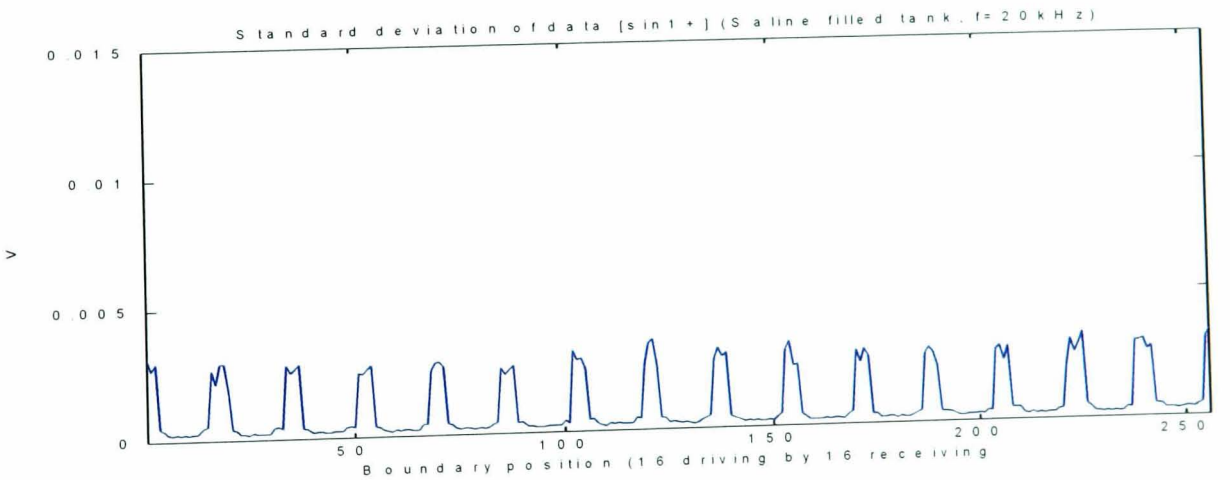

(c)

Figure 8.8 The noise level of collected saline tank data set

(a) the noise level on Sin1 data set

(b) the noise level on SinX data set

(c) the noise level on SinX data set after PGA calibration

Comparing with the 2D FE simulation data, as shown in Figure 8.9, it can be seen the measured saline data set has larger dynamic range. The reason is that in the saline tank the current is distributed in whole saline volume, or say in 3D distribution. Due to this, the image reconstructed has certain distortion from its real structure.

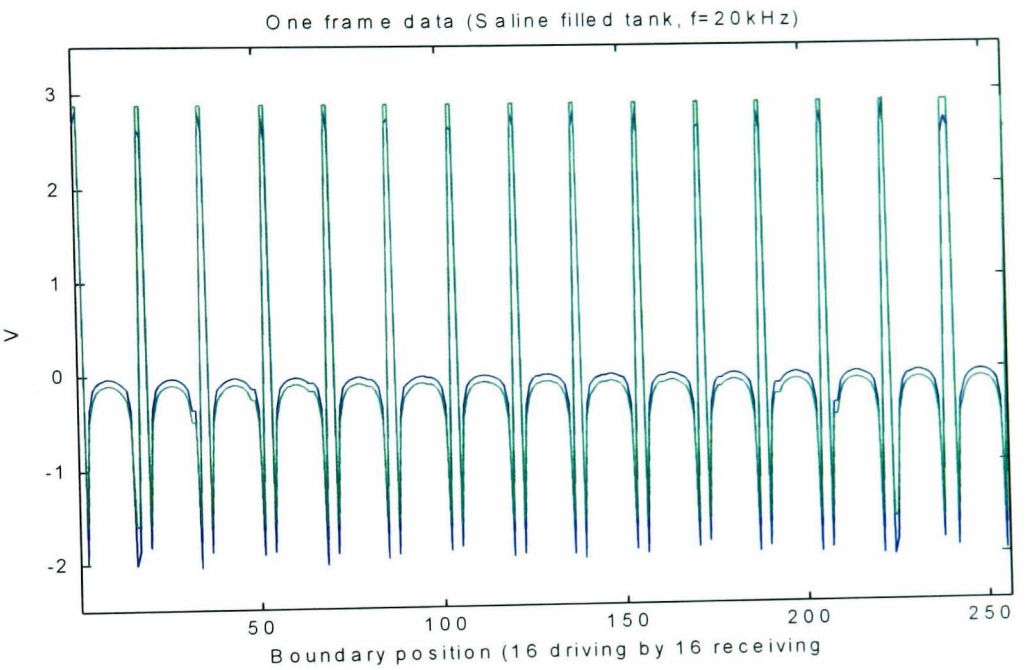

Figure 8.9 The collected saline tank data set (blue colour) and simulated data set from FE model (green colour)

8.3.4 Human body image reconstruction

The MK2 EIT system has been used in the monitoring of lung respiration activity. The Figure 8.10 shows reconstructed human chest slice image. In the body data collection, the system is also configured with 32 electrodes interlaced as 16 current electrodes and 16 voltage electrodes. The electrodes are normal ECG electrodes. Before the electrodes are mounted, the body skin is given certain shaving and cleaning to ensure good contact.

As using the back projection algorithm, the background data set is essential for the image reconstruction. In practice, the different image is reconstructed between two data set of breath-in and breath-out. The test is operated on a healthy volunteer, so that his breath can be controlled by a timing signal. For clinical usage, the breath monitoring and

synchronization has to be introduced to an automatic control of the data collection process.

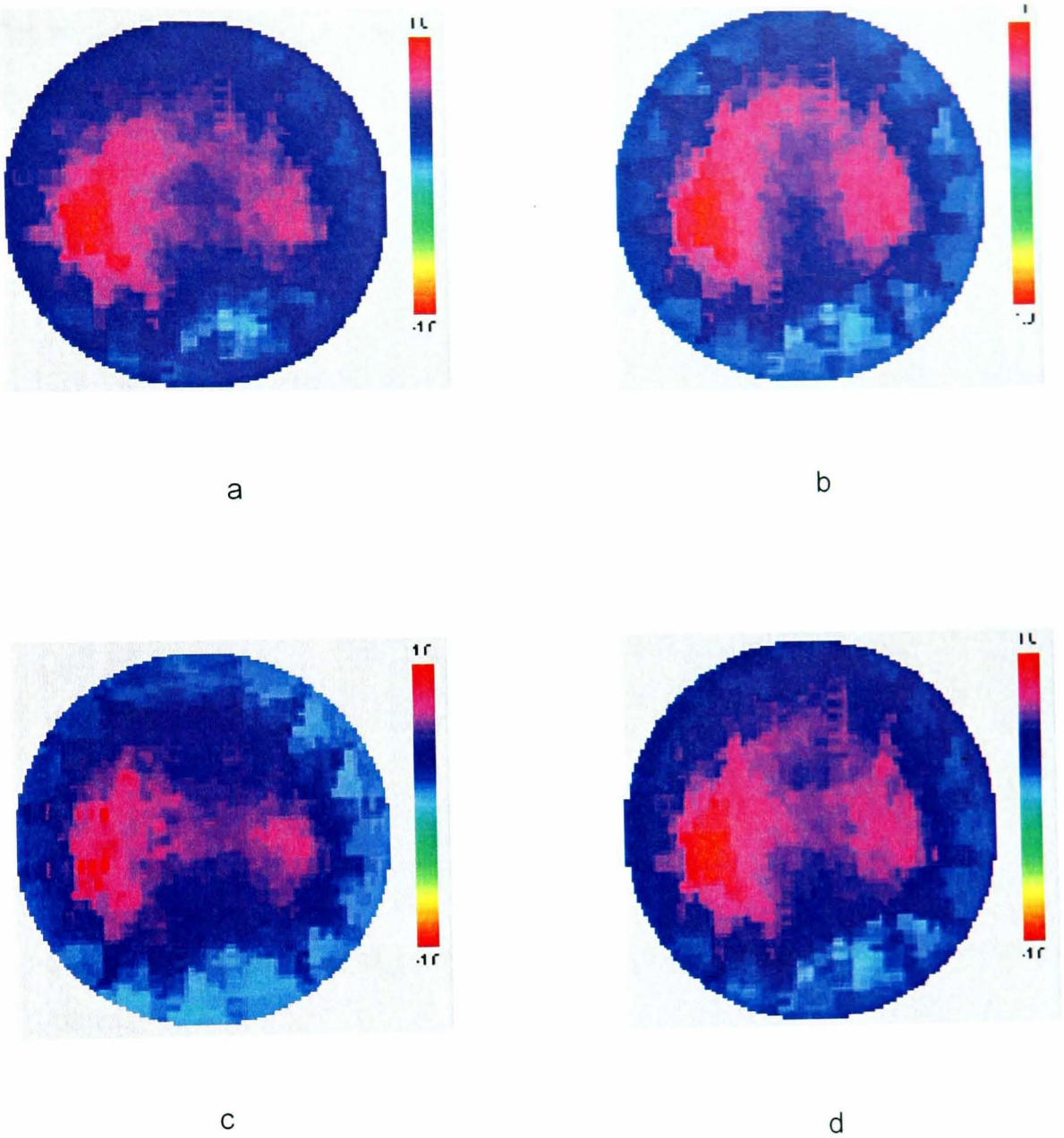

a b c d

Figure 8.10 The dynamic images of a lung in the respiration reconstructed by the De Montfort MK2 EIT system

8.4 Noise sources and analysis

The noise from the measurement system includes the heat noise from both signal source and electronic components. Because this kind of noise is proportional to the root square of bandwidth of signal path, the broad imaging frequency definitely causes large thermal noise. In additional, some digital circuit would also give interference to the signal measurement path, even though it has been improved by proper grounding and shielding.

However, from the above analysis on the collected data, it can be seen that the first data set Sin1 has much larger noise from the unsettled electronic circuit after each channel switching, comparing with SinX data, which is shown in the Figure 8.11 for detail. The main data distortion comes from the polarization potential due to the electrical chemistry reactions.

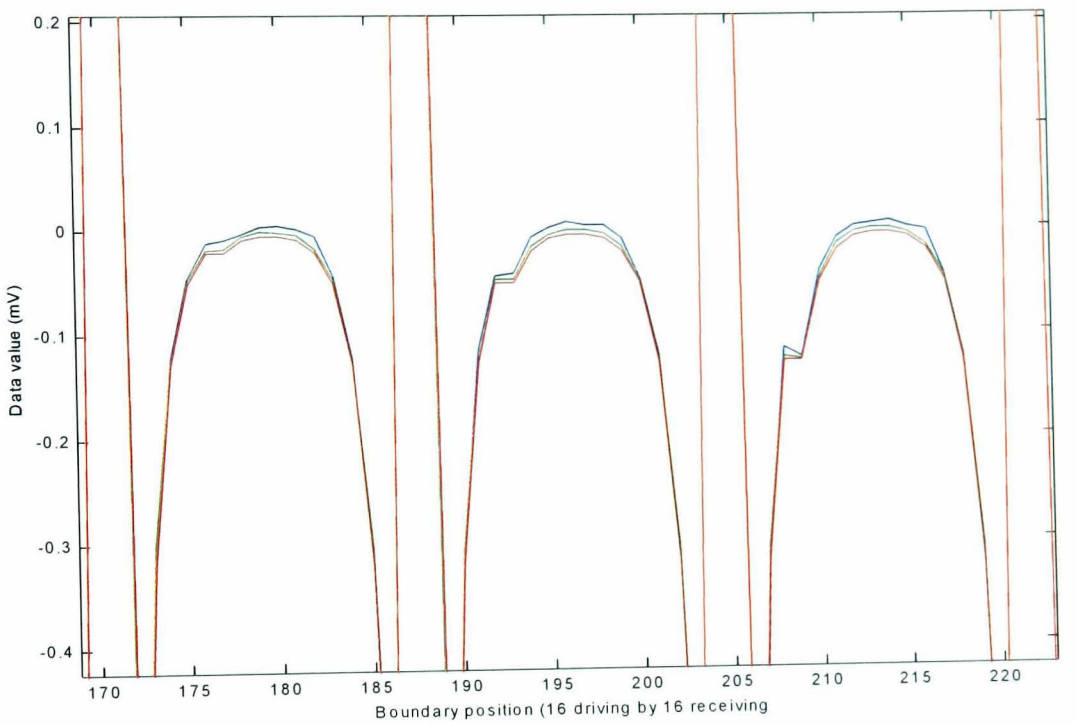

Figure 8.11 Measured signals (blue curve is Sin1, green is SinX and red is simulated data.

8.5 Summary

The MK2 system is implemented in the serial structure with 16 current injection channels and 16 voltage measurement channels. It has been tested on the phantoms and clinical volunteers for the image reconstruction.

The system is also used as a hardware platform for taking further research and development activity. With proper electrode array design, the machine can be expanded to fit even more electrodes measurement for high-resolution reconstruction imaging and 3D reconstruction imaging.

The system has to be allowed enough settling time to cope with the measurement multiplexing due to the effect of polarization voltage on the receiving electrodes. In the

MK 2 system, the Sin1 measurement is used for PGA gain selection, and this measurement period is necessary for circuit settling.

The PGA is applied for small signal measurement. From the collected data set, it can be seen that the signal-to-noise ratio has been obviously improved. Using Sin 1 and SinX two-step measurement did slow down the data collection speed. It is the price paid for the precise measurement.

The MK2 system has also been used continually on saline tank and human body image reconstruction for software development. It satisfied the design demands on further EIT research and development work.

Chapter 9 Conclusions and Future Works

9.1 Conclusions

Using the developing technology of bio-impedance measurement the electrical impedance characteristics of biological tissue can be measured which may yield internal information about its structure and shape inside the living body. Using computer-aid image reconstruction techniques, electrical impedance tomography has become a new clinical diagnosis method. However, the current quality of acquired EIT images is still not of sufficient quality to satisfy the clinical demands comparing with other imaging technologies. This is directly limited by the number of surface electrodes for the impedance measurement used to provide independent measurement data for image reconstruction. This means that the number of pixels in the reconstructed image is dominated by the number of independent measurements in one frame data set acquired from data collection system. The improvement of EIT system requires even more electrodes applied to the measurement increasing the complexity and expense of the electronic system dramatically. In practice, the performance of an image system is not proportional to increasing of number of electrodes after the number of electrodes reaches a certain level.

Many factors including injecting constant current, the input impedance and common mode rejection of a front-end amplifier, the material of electrodes and the contact impedance to an objective surface, all play important roles in the electronics system design. In addition, it has to be emphasized that the quality of reconstructed 2D EIT image would be degraded due to so-called "3D field effect" since the current field distribution in the objective of imaging plane is always in 3-dimensional space. To overcome this effect, the ideal EIT image reconstruction must be carried out on the real 3D objective, not on 2D slice. In summary, the current 2D EIT imaging introduces the systematic errors for any 2D image reconstruction algorithm due to the nature of current distribution in volumetric fields.

This thesis has comprehensively investigated number of key points of an EIT hardware system in the design issues, including measurement mode. current source, front-end amplification and signal demodulation, the signal transmission carried by coaxial cable and multiplexers. This research work is carried out, mainly based on the De Montfort MK1 EIT system, which is a single channel, serial data measurement system designed for bio-impedance analysis.

Design of high quality current source with wide bandwidth and high output impedance is the key point to make a breakthrough to the new development of EIT system. The current source injects constant current into an object by a pair of electrodes based on four-electrode measurement principle. The equivalent electric circuit of a current generator is an ideal current source with parallel-connected output impedance. For a precision current design, the output impedance should be large enough comparing with the load impedance. The Howland current generator is a typical circuit used in the wide bandwidth EIT system design, which consists of a high-speed operational amplifier and a matched resistor network. In ideal situation, the equivalent output impedance of the Howland circuit is only dominated by the matching of resistance value of its resistor network.

In this thesis, the detailed analysis has been given from the basic type to the modified Howland circuit design, which is based on the physical model of internal circuits of the selected operational amplifier. The open-loop gain and the input impedance of the operational amplifier have been investigated as main factors in the equivalent circuit modeling and analysis. Based on the mathematic analysis with the approved physical model, it has been indicated that the output impedance of the current source is affected mainly by the open-loop gain of the operational amplifier that is the core of Howland circuit, as described in equation Eq3.22. Especially at radio frequency, the open-loop gain of op-amp decreases with the frequency increasing, so that the matching of resistors in Eq3.5 could not be reached in the practical circuit implementation. A compensation method to improve this situation has been given in the thesis, as shown in formula Eq3.26. Therefore, the developed current source can provide a highly constant current in a wide frequency bandwidth.

This new compensation method can be achieved by using laser-trimming techniques in modern integrated circuit process. It means the Howland circuit can be

made to a small package, and then embedded into the electrode body to form so-called active electrode. The active electrode can inject current into the object to be imaged without the effects of cables and multiplexers.

This thesis also provides a method for achieving very high output impedance Howland current source design by using given precision commercial available resistors. At low frequency, the output impedance of the current source is dominated by the precision of resistors being used.

The measured voltage signal is collected on the receiving electrode surround the boundary of object to be imaged. As the current is injected into the object in ac mode. the received signal is modulated on the imaging frequency carrier. The object to be measured is equivalent to a high impedance signal source due to the relatively higher tissue impedance and possible contact impedance. For wide bandwidth EIT system design. the front-end amplifier should have sufficient high input-impedance and common mode rejection ability in the interested bandwidth.

In this thesis, the front-end amplifier is designed on the three-op-amp structure instrumentation amplifier, with consideration of integration of embedded active-electrode. The analysis on the matching of resistor network is given for identification of the effect of common mode rejection. It makes manufacturing process become relatively simple.

To improve the quality of reconstructed images, particularly in the central areas, the high precision amplification with large dynamic range is critical to collect very tiny signals. However, these measured tiny signals are usually contaminated by the noise and interference generated from electronic circuit and environments. In addition, the system errors are also generated from bias current and drift voltage introduced by the both electronic system and the temperature effect. To overcome these problems, full investigation and careful design of the programmable gain amplifier (PGA) have been carried out with adaptive amplification gain setting mechanism to improve the quality of small signal measurement. It has been achieved that the PGA with two-stage amplifier array would be able to provide 8-step amplification gains from 1 to 255 with wide bandwidth. From the saline phantom test result, it can be seen that the measurement is comfortable to achieve a 20dB signal-to-noise ratio improvement if the gain 10 is set.

In EIT system design, the real-time imaging needs high-speed data acquisition on the object boundary with all possible electrode combination. However, the signal

measurement and the signal demodulation process needs sufficient time for analogue circuit settling. In the coherent demodulation, using an integrator instead of a low-pass filter reduces the data acquisition time of each data to several periods of carrier signal. In the MK2 system, the integration time is controlled in the consideration of settling time of signal channel multiplexing. It can provide one frame data acquisition with 256 (16 by 16 channels) measurement in 0.1 second at 100 kHz image frequency.

The effect of polarization potential is a main issue that is discussed in this thesis. Using proper calculated integration starting time (Eq5.24 and Eq5.27) can minimize this impact on the measurement reading.

In this thesis, the studies of the signal transmission path in the serial EIT hardware, especially the key components such as multiplexer and cable has been comprehensively investigated. It is found that the input and output capacitance of FET analogue multiplexer damages the quality of well designed Howland current source and using coaxial cable makes this situation even worse. The parasitic capacitance of these devices also affects the performance of input impedance of front-end amplifier. This problem becomes worse at high image frequency.

The final part of the thesis, author gives a distribution structure layout with applying new active electrode. The main contents and contributions of this research have been directly used in the De Montfort MK2 EIT system implementation.

9.2 Contributions of the thesis

The contributions of this thesis to the EIT research work are mainly in the hardware design and implementation of the data collection system, from its electric circuit analysis to measurement methodology study.

(1) The high quality current source for EIT technology

A main function block of EIT system is the constant current source. As a popular used current generator, the Howland circuit is simple and easy achievable comparing with other electronic circuits. However, its output impedance is measured at the level of hundreds of thousand ohms and goes down dramatically with increasing of measurement frequency. This thesis gives a complete analysis result based on the op-amp electric circuit model and found that the constraints of output impedance of Howland is due to the

limited open-loop gain of op-amp, especially at radio frequency. According to this finding, the thesis provides a compensation method for improvement of output impedance on Howland circuit. This result is especially crucial to further active electrode implementation.

(2) The extra high gain-bandwidth amplification system

Another difficulty in the EIT data acquisition system is the signal-to-noise ratio improvement with wide frequency bandwidth. Because the dynamic range is much larger in some measurement configuration, it is necessary to introduce programmable gain amplifier (PGA) that can provide individual gain setting for each measurement. This has been implemented in the MK2 system, and from the test results, it can be seen that the small signal's quality is improved at least 20dB.

(3) The analysis of the electrode system configuration

The polarization potential gives the main effect on the analogue circuit settling. This thesis also gives a mathematically analysis on its impact. In addition, a comprehensive solution on system timing planning is given to limit this effect.

(4) The overall design of the MK2 EIT system

All these achievement of this thesis to EIT research and development have been applied in the design of the MK2 system. The MK2 system has been used in the research work in 3D and Imaging Group in De Montfort University.

9.3 Future works

The De Montfort MK2 data acquisition system is development in serial structure. The main problems are the measurement bandwidth and data acquisition speed. The solution relies on the application of active electrodes and distributed system design. Due to the expense of integrated circuit manufacturing, the improved Howland circuit has not been embedded into the electrode body for testing. Obviously, it will be the important work in the De Montfort MK2 system research and development.

Because the digital circuit is based on the FPGA logic chip, the system configuration and control timing have to be downloaded from the PC by means of the

parallel port. The system timing lacks flexibility for some precise adjustment. especially for settling time setting. This part of the system can be implemented using digital signal processor with high-speed universe serial bus (USB) connection to PC master. so that the developed method for settling time setting to minimize the impact of polarization potential can be achieved easily.

Digital signal processor can achieve the signal demodulation in digital format so that it can further improve the measurement quality, as discussed in the chapter 6. It also provides flexibility for on-line data processing and calibration work.

All these are expected in the De Montfort MK3 system design and implementation.

BIBLIOGRAPHY

1. Ferlay J, Bray F, and Pisani P, et al. Globocan 2002: Cancer Incidence, Mortality and Prevalence Worldwide, *Version 2.0: IARC CancerBase no.5, Lyon, IARCPress, 2004*
2. How Breast Cancer happens, *http://www.breastcancer.org/cmn_und_idx.html.*
3. Jung H, Assessment of usefulness and risk of mammographic screening with exclusive attention to radiation risk, *Radiology*, 41:385-95, 2001
4. Plevritis SK, Kurian A, Sigal Bronislava, Daniel B, Ikeda D, Stockdale F, Garber AM, Cost-effectiveness of Screening for Breast Cancer with Magnetic Resonance Imaging in BRCA1/2 Mutation Carriers, JAMA 24;295(20):2374-84, 2006.
5. Hall FM, Clinical breast examination for detecting breast cancer. Comment on: JAMA. 1999 Oct 6; 282 (13):1270-80, JAMA 283:1687, discussion 1688-9, 2000.
6. Fricke H, Morse S, The electric capacity of tumours of the breast. *J Cancer Res* 16:310-376, 1926.
7. Surowiec AJ, Stuchly SS, Barr JR, Swarup A, Dielectric properties of breast carcinoma and the surrounding tissues, *IEEE Transactions on Biomedical Engineering*, 35/4:257-263, 1988.
8. B. Tuntstall, W. Wang, Z, Cheng, An analysis of systematic errors in the electrical impedance measurements of tissue characteristics during an in-vitro study in the frequency range 1 kHz to 4MHz, *IEEE 19th Annual International Conference*, 1997.
9. Stojadinovic A, Nissan A, Electrical impedance scanning for the early detection of breast cancer in young women: preliminary results of a multicenter prospective clinical trial, *Journal Of clinical Oncology*, Vol. 23, No 12, 2005: pp. 2703-2715.
10. Yang J, Wang W *et al*, The design of data acquisition measurement system for detection of breast abnormalities, *2nd EPSRC Engineering Network meeting, Biomedical applications of EIT*, April, 2000
11. Cherepenin V *et al,* A 3D electrical impedance tomography (EIT) system for breast cancer detection, *Physiol. Meas.* 22: 9-18, 2001
12. Tang M, Wang W and Wheeler J, Incorporating more compatible prior information into the image in electrical impedance tomography, *3rd EPSRC Engineering Network meeting, Biomedical applications of EIT*, April, 2001

13. Valentinuzzi M., Bioelectrical impedance techniques in medicine, part I: bioimpedance measurement, *critical reviews in biomedical engineering*. 24(4-6): 223-255 1996
14. Cole S, Cole H, Dispersion and absorption in dielectrics. *J. Chem. Physics* 9: 341-51 1941
15. Foster, K. R. and Schwan, H. P., Dielectric properties of tissues and biological material, *critical reviews in biomedical engineering* 17(1): 25-104 1989
16. Gersing, E., measurement of electrical impedance in organs – measuring equipment for research and clinical applications. *Biomedizinische technik* 36(4), 6_11, 1991.
17. Ackmann, J., Complex bioelectrical impedance measurement system for the frequency range from 5Hz to 1MHz, *Annual biomedical engineering* 21, 135-146,1993.
18. Ackmann, J., Instrumentation considerations for complex impedance measurements, *Proc. 11th Annul. Int. Conf. IEEE-EMBS, Seattle*, 11, 1233-1234. 1989.
19. Hype, P., J., Wide frequency range dielectric spectrometer, *proc. IEEE*, 17(9) 1891-1901, 1970.
20. Gersing, E., Skin effect - a possible implication in multifrequency EIT? *Second EPSRC engineering network meeting, Biomedical applications of EIT*, 2000.
21. Rigaud, B., Hamzaoui, L., Chauveau, N., Granie, M., Scotto Di Rinaldi J. P., and Morucci, J. P., In vitro tissue characterization and modeling using impedance: in the 100Hz – 10MHz frequency range, *Physiol. Meas.*, 16(suppl. 3A), A15-A28, 1995.
22. Riu, P., Rosell, J., and Pallas-Areny, R., In vivo static imaging for the real and reactive parts in electrical impedance tomography using multifrequency techniques, *Proc. 14th Ann. Int. conf. IEEE-EMBS, Paris*, 14(5), 1706-1707, 1992.
23. Lu, L., Hamzaoui, L., Brown, B. H., Rigaud, B., Smallwood, R. H., Barber, D. C., and Morucci, J. P., Parametric modeling for electrical impedance spectroscopy system. *Med. Biol. Eng. Comput.*, 34(2), 122-126, 1996.
24. Chauveau, N., Dumont, P., Aligne, C., Rigaud, B., Cros, S., and Mocucci, J. P., In vivo and ex vivo impedance spectrometry of MCF-7 tumors on nude mice: Measurement problems, *Innov. Tech. Biol. Med.*, 16(6), 679-687, 1995.
25. Barber D. C. and Brown B. H., Applied potential tomography, *J. Phys. E: Sci. Instrum.*, 17, 723-732, 1884.

26. Barber D C, A sensitivity method for electrical impedance tomography. Clin. Phys. Physiol. Meas. 10 368-371 1989.
27. Barber D C and Seager A D Fast reconstruction of resistance images Clins. Phys. Physiol. Meas. 8(Suppl. A) 47-54, 1987.
28. Barber D C, and Brown B. H, Reconstruction of impedance images using filtered back-projections, Proc. CAIT Meeting on Eelectrical impeance Tomography (Copenhagen 1990) 1-8 1990
29. Barber D C and Brown B H Pregrass in electrical impedance tomography Inverse Problems in Partial differential Equations ed D Colton, R Ewing and W Rundell (Philadelphia, PA: SIAM) 151-164 1990.
30. Griffiths, H and Ahmed, A., A dual-frequency applied potential tomography technique: computer simulations, *Clin. Phys. Physiol. Meas.*, 8(Suppl. A), 103-107, 1987.
31. Yorkey, T. J. Comparing Reconstruction Algorithms for Electrical Impedance Tomography, *IEEE Transactions on Biomedical Engineering* BME-34, 843-852, 1987.
32. Brown B. H. and Seagar A. D., The Sheffield data collection system, *Clin. Phys. Physiol. Meas.*, 8(suppl. A), 91-97, 1987.
33. Smith R. W., Design of a real-time imaging system for medical application, PhD thesis, University of Sheffield, 1990.
34. Lu, L. and Brown, B. H., The electrode and electronic interface in an EIT spectroscopy system, *Innov. Tech. Biol. Med.*, 15(No. Special 1), 97-103, 1994.
35. Metherall P., Three Dimensional Electrical Impedance Tomography of the Human Thorax, *PhD thesis, Sheffield University,* January 1998
36. Seagar, A. D. and Brown, B. H., Limitations in hardware design in impedance imaging, *Clin. Phys. Physiol. Meas.*, 8(suppl. A), 85-90, 1987.
37. Newell, J. C., Isaacson, D., and Gisser, D. G., An electric current tomograph, *IEEE Trans. Biomed. Eng.*, 35(10), 823-833, 1988.
38. Brown, B. H. and Seagar, A. D., Applied potential tomography – data collection problems, *Proc. Electric & Magnetic Fields in Medicine & Biology Int. Conf., IEE Conf. Publ.*, 257, 79-82, 1987.

39. Kim, Y. and Woo, H. W., A prototype system and reconstruction algorithm for electrical impedance technique in medical body imaging, *Clin. Phys. Physiol. Meas.*, 8(Suppl. A), 63-70, 1987.
40. Smith, R. W., Freeston, I. L., and Brown, B. H., A real-time electrical impedance tomography system for clinical use – design and preliminary results, *IEEE Trans. Biomed. Eng.*, 42(3), 133-140, 1995.
41. Jossinet, J. Tourtel, C. and Jarry, R., Active current electrodes for in vivo electrical impedance tomography, *Physiol. Meas.*, 15(Suppl. 2A), 83-90, 1994.
42. Cook, R. D., Saulnier, G. J., Gisser, D. G., Goble, J. C., and Newell, J. C., ACT3: A high speed high-precision electrical impedance tomograph, *IEEE Trans. Biomed. Eng.*, 41(8), 713-722, 1994.
43. Edic, P. M., Saulnier, G. J., Newell, J. C., and Isaacson, D., A real-time electrical impedance tomograph, *IEEE Trans. Biomed. Eng.*, 42(9), 849-859, 1995.
44. Franco, S., Design with operational amplifiers and analog integrated circuits, New York: McGraw-Hill, 1988, 58-65.
45. Nowicki, D. J., Current generators. In: Webster, J. G., Ed., Electrical Impedance Tomography, Bristol: Adam Hilger, 1990, 29-42.
46. Bragos, R., Rosell, J., and Riu, P., A wide-band AC-coupled current source for electrical impedance tomography, *Physiol. Meas.*, 15(Suppl. 2A), A91-A99, 1994.
47. Rosell, J., Murphy, D., Pallas, R., and Rolfe, P., Analysis and assessment of errors in a parallel-data acquisition system for electrical impedance tomography, *Clin. Phys. Physiol. Meas.*, 9(Suppl. A), 93-99, 1988.
48. Guardo, R., Boulay, C., Provost, B., Boshina, D., and Malette, S., Micro-controller based active electrodes for impedance tomography, *Proc. 16th Annu. Int. Conf. IEEE-EMBS*, Baltimore, 16(1), 545-546, 1994.
49. Rosell, J., Riu, P., and Pallas-Areny, R., A parallel data acquisition system for electrical impedance tomography, *Proc. 11th Annu. Int. Conf. IEEE-EMBS*, Seattle, 11, 459-460. 1989.
50. Pallas-Areny, R. and Webster, J. G. AC instrumentation amplifier for bioimpedance measurements, *IEEE Trans. Biomed. Eng.*, 40(8), 824-829. 1993.
51. Zhu, Q. Lidgey, J. F, and Vere Hunt, M. A., Improved wideband, high CMRR instrumentation amplifier, *Clin. Phys. Physiol. Meas.*, 13(Suppl. A), 51-55. 1992.

52. Pallas-Areny, R. and Webster, J. G., Bioelectrical impedance measurements using synchronous sampling, *IEEE Trans. Biomed. Eng.*, 40(8), 824-829, 1993.

53. Sansen, W., Geeraerts, B., Van Petegem, W., and Steyaert, M., Electrical impedance tomography systems based on voltage drive, *Clin, Phys. Physiol. Meas.*, 13(Suppl. A). 39-42, 1992.

54. Nowicki, D. J., Voltage measurement and signal demodulation. In: Webster, J. G., Ed., Electrical impedance tomography, Bristol: Adam Hilger, 1990, 43-57.

55. Murphy, D and Rolfe, P., Aspects of instrumentation design for impedance imaging, *Clin. Phys. Physiol. Meas.*, 9(Suppl. A), 5-14, 1988.

56. Riu, P. J., Bragos, R., and Rosell, J., Broadband quasi-differential multifrequency electrical impedance imaging system, *Proc. IX ICEBI, Heidelberg, Germany*, Heidelberg: University of Heidelberg, 1995, 446-447.

57. Osypka, M., Schmerbeck, A., Gersing, E., and Meyer-Waarden, K., Determination of electrical impedances of tissue at a frequency range of 5 Hz to 20 kHz by digital correlation techniques. In: Nikiforidis, G., Pallifarakis, N., and Proimos, B., Eds., *Proc. V Mediterranean Conf. On Medical and Biol. Eng. MEDICON 89*, Patras, Greece, 1989, 168-169.

58. Chauveau, N., Rigaud, B., Shi, Y., and Morucci, J. P., Digital demodulation in electrical impedance tomography, *Proc. 14th Annu. Int. Conf. IEEE-EMBS*, Paris, 14(4), 1701-1702, 1992.

59. Skidmore R, Evans J M, Jenkins D and Wells P N T, A data collection system for gathering electrical impedance measurements from human breast. *Clin. Phys. Physiol. Meas.*, 8(Suppl. A), 99-102, 1987.

60. Henderson, R P and Webster J G, An impedance camera for spatially specific measurements of the thorax, *IEEE Trans. Biomed. Eng.*, BME-25(3), 250-254, 1987.

61. Schwan H P and Foster K R, RF-field interactions with biological systems: Electrical properties and biophysical mechanisms, *Proc. IEEE*, 68(1), 104-113,1980.

62. Gheorgiu E and Fugaru V, Characterizing cellular effects of different stimuli by means of dielectric spectroscopy, *Proc. IX ICEBI*, Heidelberg, Germany, Heidelberg: University of Heidelberg, 55-58, 1995.

63. Geddes L A, Foster K S, Reilly J, Voorhees W D, Bourland J D, Ragheb T and Fearnot N E, The rectification properties of an electrode-electrolyte interface operated at high sinusoidal current density, *IEEE Trans. Biomed. Eng.*, 34(9), 669-672, 1987.
64. Ragheb T and Geddes L A, The polarization impedance of common electrode metals operated at low current density, *Ann. Biomed. Eng.*, 19(2), 151-163, 1991.
65. Ragheb T and Geddes L A, Electrical properties of metallic electrodes, *Med. Biol. Eng. Comput.*, 28, 182-186, 1990.
66. Schwan H P, Determination of biological impedances., *Physical Techniques in Biological Research*, Vol 6, New York: Academy Press, 323-417, 1963.
67. Schwan H P, Alternating current electrode polarization, *Biophysics*, 3, 181-201, 1966.
68. Schmukler R, Bao J and Davis C, Measurement of the electrical impedance of biologic materials, *Proc 12th Annu Int Conf. IEEE-EMBS*, Seattle, 12(4), 1509-1510, 1990.
69. Tsuei T W, Henderson R H and Massoud H Z, Optimum preparation and storage of Ag/AgCl and Pt black microelectrodes for transmural cardiac recording application, *Proc. 13th Annu. Int. Conf. IEEE-EMBS*, Orlando, 13(4), 1585-1586, 1991.
70. Epstein B R, and Foster K R, Anisotropy in the dielectric properties of skeletal muscle, *Med. Biol. Eng. Comput*, 21, 51-55, 1983.
71. Schmidt K, Frolich R, Bolz A and Schaldach M, Effect of surface morphology on electrode impedance. A new approach to a low polarisation electrode, *Proc. IX ICEBI*, Heidelberg, Germany, Heidelberg: University of Heilderberg, 36-39, 1995.
72. Gondran C, Seibert E, Fabry P, Novakov E and Gumery P Y, Non-polarisable dry electrode based on NASICON ceramic, *Med. Biol. Eng. Comput.*, 33, 452-457, 1995.
73. CMOS DDS Modulator AD7008 Data Sheet *Rev.B Analog Devices, Inc.* 1995
74. Griffiths H, A phantom for electrical impedance tomography, *Clin. Phys. Physiol. Meas.*, Vol. 9, Suppl. A, 15-20, 1988.
75. W Wang, Z. Cheng and M McCormick, A design of programmable wide bandwidth current source for an impedance tomography system, *IEEE. 19th Annual International Conference*, 1997.
76. A S Ross, G J Saulnier, J C Newell and D Isaacson, Current source design for electrical impedance tomography, *Physiol. Meas.* 24 (2003) 509-51.

77. Singh B, Smith CW Hughes R, In vivo dielectric spectrometer, *Medical and Biol. Eng and Computing,* 17:45-60, 1979.

ABBREVIATION

AC	**A**lternating **C**urrent
CMOS	**C**omplementary **M**etal **O**xide **S**emiconductor
CMRR	**C**ommon **M**ode **R**ejection **R**atio
DC	**D**irect **C**urrent
DDS	**D**irect **D**igital **S**ynthesizer
DSP	**D**igital **S**ignal **P**rocessor
EIM	**E**lectrical **I**mpedance **M**ammography
EIT	**E**lectrical **I**mpedance **T**omography
FEM	**F**inite **E**lement **M**ethod
FET	**F**ield **E**ffect **T**ransistor
GIC	**G**eneral **I**mpedance **C**onverter
IC	**I**ntegrated **C**ircuit
JFET	**J** type **F**ield **E**ffect **T**ransistor
MUX	**M**ultiplexer
PCB	**P**rinted **C**ircuit **B**oard
PGA	**P**rogrammable **G**ain **A**mplifier
PSD	**P**hase **S**ensitive **D**emodulation
PSPICE	**P**c version **S**imulation **P**rogram for **I**ntegrated **C**ircuits **E**mphasis
PSRR	**P**ower **S**upply **R**ejection **R**atio
RMS	**R**oot **M**ean **S**quare
VCCS	**V**oltage **C**ontrolled **C**urrent **S**ources